CORN STOVER STEAM GASIFICATION

A DISSERTATION
SUBMITTED TO THE FACULTY OF THE GRADUATE SCHOOL
OF THE UNIVERSITY OF MINNESOTA
BY

HUIXIAO ZHENG

IN PARTIAL FULFILLMENT OF THE REQUIREMENTS
FOR THE DEGREE OF
DOCTOR OF PHILOSOPHY

ADVISOR: R. VANCE MOREY, PHD

May, 2013

Acknowledgements

First, I would like to thank my advisor R. Vance Morey. He is always patient, generous, inspiring, and helpful. He provides me enough financial support so that I can concentrate on my thesis very well. He is a great advisor, and he taught me how to think deeply while capturing the whole picture. He trusts and encourages me to try any new ideas and to do whatever I want. He is a very nice person and respects his students, which makes my PhD life quite pleasant.

Second, I would like to thank Prof. Thomas E. Schwartzentruber from Dept. of Aerospace and Engineering and Mechanics who provided me very useful advice on how to solve nonlinear equation systems. In addition, I would like to thank Prof. Roger Ruan who provided me with generous help on fitting into the study life here and selecting the thesis topic, and Prof. David Pui and Prof. Kevin Janni who are always nice and willing to be my committee members.

At last, I would like to thank people who have ever helped me during my study at the University of Minnesota-twin cities: Nalladurai Kaliyan, and my friends from Dept. of Mechanical Engineering and Dept. of Bioproducts and Biosystems Engineering.

Dedication

I dedicate my dissertation to my family who has been supporting me all the time.

Abstract

Biomass corn stover is a promising renewable energy resource. One of the most widely used technologies of utilizing biomass is fluidized bed steam gasification due to its flexibility of handling fuels and the high-energy-content gas produced. In this study a complex unsteady-state two-phase kinetic model including fluid dynamics and reaction kinetics is developed. An un-reacted core shrinking model is employed to describe chemical reactions, and particle entrainment is considered. In addition, a pyrolysis model including the effect of particle size and temperature is developed and incorporated in the gasification model. This model is able to reflect the effect of particle size, temperature, pressure, the steam/biomass ratio, mass flow rate, and superficial gas velocity on gasifier performance. In addition, this model can provide detailed information on the evolution of gas, char, and particle size in the bed, and percentages of particles consumed during reactions, turned to fines by friction, or entrained out of the bed.

There are many models with difference levels of complexity and modeling concepts for a fluidized bed but there are few studies available on comparing these models. Therefore, six other widely used models are also developed and compared to study the importance of modeling complexity on model selection. These models are the zero-dimensional non-stoichiometric equilibrium model, zero-dimensional stoichiometric equilibrium model, zero-dimensional kinetic model, one-dimensional one-phase kinetic model, one-dimensional two-phase kinetic model-all char in bed

with particle size, and one-dimensional two-phase kinetic model-all char in bed without particle size. Gasification results show that the one-dimension two-phase kinetic model and the one-dimensional one-phase kinetic model are equivalent, and both predict the same gasification results in terms of the gas volumetric fraction, yields of char and dry tar-free gas, the history of the evolution of particles, and higher heating values (HHVs). Therefore, it can be concluded that the number of phases in the fluidized bed does not affect the simulation results. Since it takes less time to finish a run for the one-phase kinetic model than for the two-phase kinetic model, the one-dimensional one-phase kinetic model is better than the two-phase kinetic model. In addition, the one-dimensional two-phase kinetic models-all char in the bed predict the same gas volumetric fractions and the yields of char and dry tar-free gas at steady state, but predict different amounts of time for the bed to reach steady state and different amounts of char in the bed at steady state. The main reason is because different methods are used to calculate the reactive surface area for reaction rates. Through model comparison, it is found that models with similar modeling concepts tend to have similar results.

Gasification models developed in this study are incorporated into a biomass integrated gasification combined cycle (BIGCC) system to provide heat and power for a corn ethanol plant. The effect of different gasification models on the overall BIGCC system performance is evaluated. Results show that BIGCC systems using different gasification models have similar but not identical overall system performances.

Table of Contents

List of Tables

List of Figures

1 Background

1.1 Biomass Energy for corn ethanol plants

Energy plays an important role in economic growth, and fossil fuels are the most widely used fuel. However, fossil fuels are non-renewable, and the combustion of fossil fuels is the main source of greenhouse gas emission, raising severe environmental issues. Considering sustainable development, people are putting more and more attention on renewable energy such as wind power, solar power, hydro power, geothermal power, and biofuels to meet electricity and heat demand. Compared to other renewable energies, biomass energy is less constrained by location and weather, and thus has received extensive attention. There are several generations of biofuels (Kumar, et al., 2008). First-generation biofuels are produced from food or feed-based feedstocks. Because of feedstock restrictions and the limitations of technologies of utilizing these feedstocks, research has switched to second-generation biofuels produced from renewable and non-food biomass sources such as wood waste, agricultural residues, sugar mill residues, paper mill sludge, and municipal waste.

Process energy in the form of heat and electricity is the largest energy input into the corn ethanol production process (Shapouri, Duffield and Wang, 2002). The most common fuel used to provide process heat is natural gas, although some plants burn coal (Mueller and Cuttica, 2007). Electricity purchased by ethanol plants is often generated with coal. Analyses of second generation, cellulosic biofuels suggest

improved energy balances and reduced greenhouse gas (GHG) emissions compared to corn ethanol (Farrell, et al., 2006). Some of the technologies proposed for the production of cellulosic biofuels can also be applied to the current corn ethanol production process, specifically the production of heat and power from biomass, an alternative renewable source of energy for ethanol plants. Dry-grind corn ethanol plants produce biomass co-products which contain a significant amount of energy when used as a fuel. These corn ethanol plants also are usually located in corn growing areas where corn stover could be available for fuel. Biomass powered dry-grind fuel ethanol plants could generate the electricity they need for their own use as well as electricity to sell to the grid. Using biomass replaces a large fossil fuel input with a renewable source which will significantly improve the renewable energy balance for dry grind corn ethanol (Morey, Tiffany and Hatfield, 2006; Wang, Wu and Huo, 2007). Several technology options using biomass were simulated to produce heat and power at dry-grind fuel ethanol plants (De Kam, Morey and Tiffany, 2009a). They showed significant improvements in the renewable energy balance by using biomass fuels with increasing improvements as the amount of electricity produced increased. The results suggested that even greater amounts of electricity could be produced while satisfying the process heat needs if Biomass Integrated Gasification Combined Cycle (BIGCC) technology were applied.

Extensive studies have been conducted on BIGCC systems for a 190 million liter (50 million gallon) per year dry-grind corn ethanol plant through Aspen Plus simulations

(Zheng, Morey and Kaliyan, 2010). The results showed that systems fueled with corn stover have good system performance.

1.2 Problem statement

The gasifier where synas is generated from feedstock plays a very important role in the overall BIGCC system. It determines the higher heating value (HHV) and flow rate of syngas, and thus determines the syngas distribution between power generation and heat generation and the size of downstream equipment. Therefore, an accurate gasification model is of vital importance for technical and economical analysis.

Despite its importance, gasification has not been fully understood due to the complex process affected by both chemical reaction kinetics and fluid dynamics. This is especially true for corn stover fluidized bed steam gasification used in previous studies of BIGCC systems. Few experimental studies have been conducted (Beck, Wang and Hightower, 1981; Perkins, et al. 2008; Carpenter, et al., 2010), and only two papers mentioned the simulation of corn stover fluidized bed gasification (De Kam, Morey and Tiffany, 2009b; Wang, Shahbazi and Hanna, 2011). De Kam, Morey and Tiffany (2009b) modeled the corn stover steam gasification process by minimizing system Gibbs free energy using Aspen Plus, and the yields of several products are fixed according to experimental data. Wang, Shahbazi and Hanna (2011) calculated the gasification products directly using atom balance equations and equilibrium constants. Many problems exist in the current studies on simulation of corn stover steam

gasification process. First, although the models used in these two papers are equilibrium models, the results using these two models are different in terms of yields of gasification products, higher heating value (HHV), and gas volumetric flow rate. Second, both models are based on an assumption that the whole system is in a chemical and thermal equilibrium state. Although this kind of model is very easy to understand and use, sometimes a system cannot reach an equilibrium sate, and equilibrium models cannot give inaccurate results (Jarungthammachote and Dutta, 2008). Third, the results provided by equilibrium models are very limited. They can give a maximum estimation of the amount of gases produced, but cannot reflect the effect of residence time and gasifier structure on the outlet syngas compositions, char produced, and temperature and mass distribution across the gasifier that are needed for reactor design and optimization.

In addition, it is found that there are many different models with different levels of complexity and modeling concepts. However, there are few studies available in comparing these different models and there is lack of guidance on model selection. Given the importance of corn stover steam gasification and the current problems with modeling, the objectives of this study are as follows:

1) Develop a model which includes both chemical reaction kinetics and fluidized bed hydrodynamics to investigate the effect of temperature, syngas residence time, the steam/biomass ratio on yields of syngas, the energy content of the syngas, and the amount of char produced.

2) Develop several other kinds of widely used models and compare these models to study the importance of modeling complexity on model selection.

3) Incorporate gasification models developed into BIGCC systems and investigate their effect on overall BIGCC system performance.

2. Literature Review

2.1 Thermal conversion of biomass

Generally, there are two kinds of methods of utilizing biomass: one is biochemical conversion, and the other is thermochemical conversion, and the major difference between these two technology options is the primary catalysis system (Kumar, et al., 2008). Of the two kinds of methods, thermochemical conversion has received extensive attention for biomass thermal treatment, and the most prevalent methods are combustion, pyrolysis, and gasification, the latter two of which can convert biomass to biofuels.

2.1.1Combustion

Combustion is an exothermic thermal conversion process during which biomass fuel reacts with enough oxidizing agent oxygen or air accompanied by the release of heat. The main products of combustion are carbon dioxide and steam, and the whole process could be expressed by equation (2.1):

$$\text{Biomass} + \text{oxygen} \rightarrow \text{products} + \text{heat} \qquad (2.1)$$

Combustion is the easiest thermal conversion method, and has been fully developed.

2.1.2 Pyrolysis

Pyrolysis is also called devolatilization during the gasification process. It is a thermal decomposing process that converts solids to char, gases (non-condensable gases), and

liquids (condensable gases) in the absence of oxidizing agent and other gases. The main components of the non-condensable gas are carbon monoxide, hydrogen, and methane which can be combusted in an engine or used in a fuel cell. The condensable vapors are known as bio-oil and are usually combusted in boilers, turbines, and engines to generate heat. The relative yield of char, liquids, and gases can be adjusted by changing operating conditions according to different applications (Basu and Kaushal, 2009). The temperature range of pyrolysis is 400 – 800 ^{o}C. A temperature that is lower than 450 °C favors the production of char, and when the temperature is between 450 to 550 °C, bio-oil could reach its maximum output. When the temperature is above 600 °C the majority of the products are non-condensable gas (Enviro News & Business, 2009). Pyrolysis is an endothermic process, and sufficient heat needs to be provided from an external heat source. The whole process could be expressed by the equation below:

$$\text{Biomass} + \text{heat} \rightarrow \text{char} + \text{non-condensable gas} + \text{condensable vapors} \qquad (2.2)$$

2.1.3 Gasification

Gasification is an endothermic conversion process during which fuel reacts with gasifying agents at relatively high temperature (usually higher than that of pyrolysis). The products of gasification are called syngas, and contain alkali compounds, tar, char, CO, CO_2, H_2O, CH_4, H_2, and other hydrocarbons (Basu and Kaushal, 2009). The main products of gasification are CO, CO_2, H_2O, CH_4, and H_2. The energy content of syngas depends on the components of the syngas. The gasifying agent can be air, oxygen,

steam, or a mixture of these compounds. When the gasifying agent is air, gasification is called air gasification, and the components of syngas are mainly CO, N_2, H_2, CH_4, and minor quantities of other hydrocarbons with a low heating value (LHV 4-7 MJ/m^3 against 38 MJ/m^3 of natural gas) (Blasi, n.d.; Basu and Kaushal, 2009). The heating value of syngas can be increased (LHV 10 to 18 MJ/m3) by using pure oxygen and steam instead of air, which is called oxygen or steam gasification (Blasi, n.d.; Basu and Kaushal, 2009). Syngas produced from air gasification can be used in engines, turbines, boilers, and that from oxygen or steam gasification can be used for conversion to methanol and gasoline (Basu and Kaushal, 2009). Some heat is required to complete the gasification process, and based on the type of heat source gasification could be divided into direct and indirect gasification. When the heat needed for gasification process is provided by an external heat source, it is referred to as indirect gasification. When the heat needed for gasification is provided by partial combustion of the gasification fuel, it is referred to as direct gasification.

The primary purpose of gasification is to convert chemical energy in the feedstocks to chemical energy in the syngas. Gasification is a successful option for waste treatment, chemical production, and energy production from non-conventional feedstocks such as municipal waste, agricultural waste, and other biomass (Basu and Kaushal, 2009). Normally, once feedstock is sent to the gasifier, it goes through several sequential steps as temperature increases: drying, devolatilization/pyrolysis, and char gasification. However, there is no sharp boundary dividing these steps, and they often overlap

(Basu and Kaushal, 2009). At relatively low temperature (between 100 – 200 ^{o}C), feedstock is dried and loosely bounded water is released from the feedstock. When the temperature of the feedstock increases further, pyrolysis begins to take place. Low molecular weight gases first are released from the feedstock, and then high molecular weight gases are released. Since biomass contains 75 – 80% volatiles compared to 50% or less than this level with coal, pyrolysis is very important input for biomass gasification (Gabra, et al., 2001). In the real process, the product distribution resulting from pyrolysis may vary significantly from that obtained from proximate analysis due to the extent of pyrolysis, and speed of heating up (Higman and Maarten, 2003). The extent of pyrolysis depends on its final temperature. When temperature is high enough, pyrolysis products react with char to produce syngas, which is called char gasification. At the same time, some pyrolysis products also react with the gasifying agent, and some high molecular weight gases are decomposed into low molecular weight gases. Methane and hydrocarbons are mainly produced through break-up of volatiles, and some methane is formed by reactions between hydrogen and carbon or hydrogen and carbon monoxide (Gabra, et al., 2001). The water-gas shift reaction becomes important when the amount of steam or the moisture content of feedstock is high, which is unfavorable since it reduces the heating value of syngas. The relative yields of syngas components depend on the geometry of the reactor, the fuel type and form, the gasifying agent, the residence time, the operating conditions, etc (Blasi, n.d.). During the gasification process, a fraction of alkali metals (K, Na, M, and so on) in the ash may be volatilized and released to the gas phase, and some alkali metals may serve as

catalyst for some reactions.

Gasification is influenced by heating rate and particle size. When the heating rate is slow, gasification reaction of both volatiles and char with steam are slow, and char gasification only sets in after pyrolysis is complete. Under this condition, lots of volatiles produced stay around the char as un-reacted, and then un-reacted volatiles are removed by the syngas. When the heating rate is high, both pyrolysis and char gasification happen simultaneously, and most volatiles produced from pyrolysis react with steam, and the syngas is clean (Higman and Maarten, 2003). When particle size is small, pyrolysis happens before char gasification. This is because volatiles continuously released from char particles at fast rates prevent oxidizing agent from reaching the char particle surface, and since the particle size is small, pyrolysis is completed before the temperature of the char particles is high enough for heterogeneous char-oxidizing reactions to be active (Blasi, n.d.).

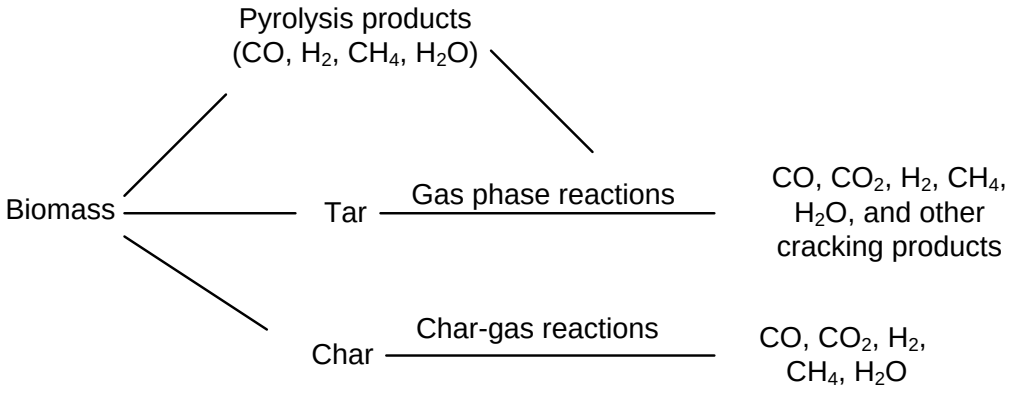

Figure 2. 1 Gasification of coal or biomass

The entire gasification process can be illustrated through the schematic diagram in Fig

2.1 (Basu and Kaushal, 2009). The gasification process is much more complex than combustion. During gasification a large number of overall and intermediate reactions take place. The possible reactions taking place during the gasification process are as follows (Rezaiyan and Cheremisinoff, 2005; Basu and Kaushal, 2009):

$$C + O_2 \rightarrow CO_2 \quad (2.3)$$

$$C + 1/2O_2 \rightarrow CO \quad (2.4)$$

$$H2 + 1/2O_2 \rightarrow H_2O \quad (2.5)$$

$$C + H_2O \rightarrow CO + H_2 \quad (2.6)$$

$$C + 2H_2O \rightarrow CO_2 + 2H_2 \quad (2.7)$$

$$C + CO_2 \rightarrow 2CO \quad (2.8)$$

$$C + 2H_2 \rightarrow CH_4 \quad (2.9)$$

$$CO + H_2O \rightarrow CO_2 + H_2 \quad (2.10)$$

$$CO + 3H_2 \rightarrow CH_4 + H_2O \quad (2.11)$$

$$C + H_2O \rightarrow 1/2CH_4 + 1/2CO_2 \quad (2.12)$$

$$CO_2 + 4H_2 \rightarrow CH_4 + 2H_2O \quad (2.13)$$

$$CH_4 + 0.5O_2 \rightarrow CO + 2H_2 \quad (2.14)$$

$$CH_4 + H_2O \rightarrow CO + 3H_2 \quad (2.15)$$

$$2CO + 2H_2 \rightarrow CH_4 + CO_2 \quad (2.16)$$

Reactions (2.3) through (2.5) happen when oxygen or air is sent to the gasifier to generate heat for the entire gasification process which includes reactions (2.6) through (2.11). Reactions (2.6) through (2.8) are water-gas reactions, among which (2.6) and (2.7) are the principle gasification reactions, and proceed quickly at high temperature

but low pressure. Reaction (2.8) proceeds quickly with the help of a catalyst at low temperatures. Reactions (2.9), (3.11), and (2.12) proceed very slowly without a catalyst, and reaction (2.10) is very slow at high pressure.

The reactor used for gasification is called the gasifier. There are several kinds of gasifiers: fixed bed gasifier (updraft, downdraft, side draft), fluidized bed gasifier (bubbling bed, circulating bed, fluidized bed, spout fluidized bed), and entrained bed (Basu and Kaushal, 2009). Although a lot of gasification processes are available, fluidized bed is attractive due to its ability of handling a wide range of feedstocks, and rapid heat and mass transfer (Pepiot, Dibble and Foust, 2010). In addition, since steam gasification can produce syngas with a higher HHV than air gasification, fluidized bed steam gasification is selected in this study.

2.2 Models for fluidized bed gasification

A wide variety of models are available for the fluidized bed gasification process with different levels of complexity and assumptions. Based on the approaches used, they can be divided into three groups: equilibrium models, kinetic models, and computational fluid dynamics (CFD) models (Lu, et al. 2008; Basu and Kaushal, 2009).

2.2.1 Equilibrium model

Equilibrium models are relatively simple compared with the other kinds of models. Equilibrium models are based on the assumption that the residence time is long enough so that the whole system can reach an equilibrium state. When using equilibrium models, researchers always assume that drying, pyrolysis, and gasification processes are lumped together in a single zone (Sharma, 2008). Generally, based on the ways of calculating the yields of gasification products equilibrium models can be categorized into stoichiometric model and non-stoichiometric model (Li, et al., 2001; Jarungthammachote and Dutta, 2008; Basu and Kaushal, 2009). The stoichiometric model employs equilibrium constants to determine the yields of products with element balance equations. The equilibrium constant for each reaction can be calculated using the partial pressure of products and reactants as shown in equation (2.17), and also can be determined through Gibbs free energy of reactants and products shown in equation (2.18). Since the pressure of gas is related to the mole of gas, equation (2.19) can be finally turned into equations of function of mole of gas. Together with atom balance equations, the yield of products can be determined. For stoichiometric equilibrium models, most researchers use the water-gas shift reaction (Eqn. (2.10)) and the methane carbon reaction (Eqn. (2.9)) to describe the reduction reactions (Sharma, 2008).

$$K_e = \frac{\sum P_{products}}{\sum P_{reactants}} \tag{2.17}$$

$$K_e = \exp\left(-\frac{\Delta G}{RT}\right) \tag{2.18}$$

$$\frac{\sum P_{products}}{\sum P_{reactants}} = \exp\left(-\frac{\Delta G}{RT}\right) \tag{2.19}$$

K_e---- Equilibrium constant

R---- Universal gas constant, 8.314 kJ/(kmol.K)

T---- Temperature, K

ΔG---- Standard Gibbs function of reaction, kJ/kmol

Non-stoichiometric models determine products distributions based on minimization of Gibbs free energy of the whole system, which is a constrained problem and generally solved using the Lagrange multiplier method. Basically, these two approaches are essentially of the same concept (Li, et al., 2001; Jarungthammachote and Dutta, 2008).

Equilibrium models are suitable for high temperature gasification which is usually above 1200 ^{o}C, and these kinds of models are very easy to use and understand. However, according to some researchers high residence time is required for the system to reach equilibrium state (Melgar, et al. 2007; Sharma, 2008), and thermodynamic equilibrium may not be achieved in many cases especially when the temperature of the reactor is less than 800 ^{o}C (Herguido, Corella and Gonzalez-Saiz, 1992; Jarungthammachote and Dutta, 2008; Basu and Kaushal, 2009; Kuznetsov and Shchipko, 2009; Wei, et al., 2007). Therefore, equilibrium models cannot give accurate results when used in systems that fail to reach an equilibrium state. In

addition, equilibrium models can only give a maximum yield of syngas compositions leaving the gasifier, and always over predict the production of carbon monoxide and hydrogen and under predict the formation of hydrocarbons. Moreover, equilibrium models cannot provide any information on yields of product across the gasifier (Lu, et al. 2008), and thus are not able to help reactor design and improvement.

2.2.2 Kinetic model

For kinetic models, both gasification rate and yields of gasification products are determined by reaction kinetics of chemical reactions occurring during gasification process. In the real process, fluid dynamics also affect the gasification process through solid and gas movements and reaction kinetics, thus most kinetic models have considered the effect of fluid dynamics on reaction rate and yields of final products.

Most researchers divide the entire reactor into the fluidized bed and the freeboard parts, while a few researchers divide the reactor into three main sections based on the rate of chemical reaction and mass transfer (Yang, 2003; Nemtsov and Zabaniotou, 2008): (1) the fluidizing gas entry or distributor section at the bottom, where the rate of inter mass transfer and chemical reaction is very high; (2) the fluidized-bed itself; (3) the freeboard section above the bed, where solid particle segmentation occurs. Since freeboard and the fluidized bed have different fluid dynamics and the fluidized bed is much more complex than the freeboard, the following section is focused on the fluidized bed.

Generally, there are two kinds of modeling approaches for kinetic models: one focuses on a single particle as it goes through pyrolysis and gasification process in the gasifier (Srinivas and Amundson, 1980; Porteiro, et al., 2006; Xu, Pang and Levi, 2011), and the other widely used approach focuses on the whole reactor (Nemtsov and Zabaniotou, 2008; Basu and Kaushal, 2009). In this study, effort was put on the second approach. Various models are available on gas-solid fluidized bed system, and their differences lie on how reaction rates and fluid dynamics are simulated. While some kinetic models only consider reaction kinetics (Wang and Kinoshita, 1993), most kinetic models consider both reaction kinetics and fluid dynamics. Models that include both reaction kinetics and fluid dynamics can be classified into three main categories based on the number of phases accounted: single-phase, two-phase, and three-phase models (Yang, 2003; Nemtsov and Zabaniotou, 2008; Basu and Kaushal, 2009). Because single-phase models are too simple, and three-phase models are too complicated, two-phase models are widely used by most researchers (Nemtsov and Zabaniotou, 2008). The two-phase fluidization theory was first proposed by Toomey and Johnstone (1952), and it assumes that: (1) the whole reactor is divided into two phases: bubble or dilute phase which is mainly gas, and emulsion or dense phase which consists of almost all solids and a little gas, and the bed voidage in emulsion phase is equal to that at minimum fluidization state (Yang, 2003); (2) the gas velocity in emulsion phase is equal to that at minimum fluidization state, and any gas in excess of minimum fluidization flow rate is in bubble phase.

$$\frac{G_B}{A} = U - U_{mf} \tag{2.20}$$

G_B---- Average volumetric gas flow in bubble phase across a given section of the bed

A---- Cross section area of the bed

U---- Gas superfical velocity

U_{mf} ---- Minimum fluidization velocity

Among various two-phase models the bubbling bed model proposed by Kunii and Levenspiel (1969) and the bubble assemblage model proposed by Kato and Wen (1969) have received the most attention (Yang, 2003; Nemtsov and Zabaniotou, 2008). Bubbling bed model assumes: (1) the bubble size is constant and bubbles are evenly distributed in the bed; (2) bubble gas stays with the bubble, recirculating and penetrating at a small distance into the emulsion; (3) each bubble drags along with it a wake of solids; (4) the emulsion stays at minimum fluidization conditions, while the relative velocity of gas and solids remain unchanged. State equations for the bubbling bed model are presented.

The bubble assemblage mode considers the change of the bubble size with height in the bed: (1) a fluidized bed may be represented by n compartments in a seies. The height of each compartment is equal to the size of each bubble at the corresponding bed height; (2) each compartment is considered to consist of a bubble phase and an emulsion phase. The gas flows through the bubble phase, and the emulsion phase is

considered to be completely mixed within the phase; the void space within the emulsion phase is considered to be equal to that of the bed at the minimum fluidization state. The upward velocity of the gas in the emulsion phase is U_e; (3) the bubbles are considered to grow continuously while passing through the bed until they reach the maximum stable size, or reach the diameter of the bed column; (4) the bed is assumed to be operating under isothermal conditions since the effective thermal diffusivity and the heat transfer coefficient are large. Through comparisons done by Chavarie and Grace (1975), the bubbling bed model of Kunii and Levenspiel (1969) gives the better overall representation of the experiments done in terms of phase profile and overall conversion.

The most important differences between different two-phase kinetic models are the different methods used to describe gas and solid behavior in the bed due to different assumptions. For gases in bubble phase and emulsion phase, they can be modeled as plug flow or well-mixed flow. When modeled as a plug flow, there is no gas diffusion in the axial direction and when modeled as mixed flow the gas diffusion is so large that there is no gas concentration gradient in the radial direction in each phase. For solid particles in the bed, there are three kinds of treatments: (1) the bed is well-mixed and solids are homogeneously distributed in the emulsion phase in the entire reactor; mass balance for solids is global (Raman, 1981; Souza-Santos 1989; Yan, Heidenreich and Zhang, 1998; Chejne and Hernandez, 2002); (2) solid particles have two phases: ascending and descending phases (Lavoie, Chaouki and Drouin, n.d.; Krambeck, et al.,

1987; Sett and Bhattacharya, 1988; Loffler, et al., 2003; Radmanesh, Chaouki and Guy, 2006); (3) solids moves in plug flow pattern from inlet to outlet (Jiang, 1991; Gordillo and Belghit, 2011a; b). In addition, some researchers assumed the solid remains in the bed all the time (Raman, 1981; Tojo, Chang and Fan, 1981; Sadaka, Ghaly and Sabbah, 2002; Lü, et al., 2008) and some researchers assumed solids leave the bed and enter the freeboard (Lavoie, Chaouki and Drouin, n.d.; Souza-Santos 1989; Jiang, 1991; Yan, Heidenreich and Zhang, 1998; Radmanesh, Chaouki and Guy, 2006). These different assumptions, especially the assumptions related to solid particles, significantly affect the concept of the model and the amount of char produced. There are also many other different assumptions related to mass transfer between phases, bubble and emulsion phase calculation, and effect of fluid dynamics on reaction kinetics, so there are various kinetic models with different levels of complexity.

The kinetic model is suitable for gasification simulation under 800 ^{o}C when thermodynamic equilibrium cannot be achieved and gasification is kinetics limited (Blasi, n.d.). Kinetic models are able to provide information of final products at any time during the entire process. In addition, a kinetic model including fluid dynamics can provide information on product distribution across the height of the reactor, and it is of great use and importance for reactor design, sizing, and operation parameter optimization (Blasi, n.d.; Mansaray, et al., 2000; Fiaschi and Michelini 2001; Nemtsov and Zabaniotou, 2008).

2.2.3 CFD model

Computational fluid dynamics (CFD) models are the most complex models. These models are based on conservation of mass, energy, species, and momentum in each computing elemnet in the entire reactor (Basu and Kaushal, 2009). Commercial software such as FLUENT, and ANSYS is always used by researchers to facilitate their research.

2.2.4 Pyrolysis

Pyrolysis is very complicated, during which various decomposition reactions happen instantaneously. There are two major modeling methods for pyrolysis: one is a one-step single reaction model which uses a first order decomposition reaction to approximate pyrolysis process, and the other is a multi-reactions model which has two sub-groups: models based on total volatiles and models based on individual volatile constituents (Basu and Kaushal, 2009). Many factors such as temperature, pressure, particle size, and heating rate affect pyrolysis products and the amount of time needed for pyrolysis (Gaston, et al., 2011). Generally, pyrolysis products increase with increased reactor temperature and decreased particle size. However, when the particle size is below certain value (on the order of 100 μm), pyrolysis time will not change as the particle size decreases. A correlation shown below is used by some researchers to study the effect of particle size on pyrolysis time (Gaston, et al., 2011).

$$\tau = e^{1013.2/T^{1.076}} d_o^{1.414} \tag{2.21}$$

τ---- Pyrolysis time, s

T---- Reactor temperature, K

d_o---- Particle initial diameter before pyrolysis, mm

There are few results available on the relationship between particle size and pyrolysis products. Because time needed for pyrolysis is always one order of magnitude shorter than that for char gasification (Basu and Kaushal, 2009), and because the pyrolysis process is complex, a large pool of gasification models consider pyrolysis as instantaneous. Therefore, pyrolysis is usually not modeled specifically, and instead products from pyrolysis based on experimental results are used as inputs for the following char gasification process (Basu and Kaushal, 2009; Fiaschi and Michelini 2001).

2.3 Char reaction kinetics

2.3.1 Char reactivity

During the process of gasification, external gas phase reactions, surface char reactions, and internal pyrolysis reactions at the surface of virgin solid are coupled together, and the coupling degree depends on the size of the particle, the condition of reaction environment, diffusion rate, reaction rate, initial moisture, and so on (Blasi, n.d.). In most cases, due to mass transfer limits, the slowest step during gasification process is the heterogeneous reactions between gases with char, which dominates the overall

gasification rate and gasification efficiency (Higman and Maarten, 2003; Basu and Kaushal, 2009). Therefore, char gasification is the most critical step during the entire gasification process, and a model of gasification often turns out to be a char gasification model (Basu and Kaushal, 2009).

The reactivity of char (conversion rate per remaining mass) is defined by Eqn. (2.22) below for a batch of particles when the driving force for the gasification is proportional to its mass (Blasi, n.d.; Blasi, 2009; Basu and Kaushal, 2009):

$$r = -\frac{1}{m}\frac{\partial m}{\partial t} = \frac{1}{1-X}\frac{\partial X}{\partial t} \tag{2.22}$$

Where r is the reaction rate, m is the mass of the sample at time t, and X is the degree of conversion defined by

$$X = \frac{m - m_o}{m_o - m_\infty} \tag{2.23}$$

Where m_o and m_∞ are the initial and final values of the sample mass, respectively.

When the driving force for gasification is proportional to surface area the reactivity is expressed as (Basu and Kaushal, 2009):

$$\mathrm{r} = -\frac{1}{\mathrm{m}^{2/3}}\frac{\partial \mathrm{m}}{\partial \mathrm{t}} \tag{2.24}$$

The rate of heterogeneous char reactions depends on the reactivity of chars (Blasi, n.d.). Char reactivity relies on various factors, such as the porosity of the char (its inner structure, surface area, and active sites), size of char, pore size distribution, catalytic effect of inorganic constituents of char, pretreatment of char, heating and

origin of char, temperature, pressure, gasifying agent, mass transfer of gases to char particles, etc (Blasi, n.d.; Basu and Kaushal, 2009). Because char structure varies with operating conditions, conversion, and time, char reactivity also changes with time, which results in a varied reactivity - conversion curves.

Char reactivity and properties are also affected by the conditions of pyrolysis greatly (Blasi, n.d.). The reactivity of resulting char from pyrolysis decreases as the temperature, retention time, and pressure of pyrolysis increase for both reducing and oxidizing environments. The reason is that increased temperature and retention time increase the structural ordering of the carbon matrix, which will lower the concentration of the active sites. Increased pyrolysis pressure reduces the char surface area, and increases the graphitization level in the char structure, which will results in lower reactivity.

In addition, fast heating rate results in a more reactive char due to increased active surface area, and the metallic constituents in the char can also increase the reactivity of char. Reactivity of char is also influenced by the type of gasifying agent (O_2, H_2, CO_2, H_2O) (Basu and Kaushal, 2009). O_2 is the most reactive gasifying agent out of the four gases. Compared to the reaction rate of the char-oxygen reaction, rates of the char-steam reaction and the char-carbon dioxide reaction are 3 to 5, and 6 to 7 order magnitude slower, respectively. Reaction rate of the char-hydrogen is the slowest one. Reaction rate also relies on the water-gas shift reaction, reaction temperature, and the

partial pressure of steam (Higman and Maarten, 2003).

Most of the studies on char reactivity are focused on coal char, and there are just a small number of studies available on biomass char. Distinguishing differences exist between biomass char and coal char (Blasi, n.d.; Basu and Kaushal, 2009). The reactivity of fossil fuel char such as coal char, lignit char, peat char decreases with time, while that of biomass char generally increases with time. In addition, the ash content of biomass is much lower than that of coal, and the pore structure of biomass is highly directional, which means biomass pyrolyzes and gasifies much faster than coal. Since many reactivity models have been developed for coal-based chars, it has been a common practice to use coal char data for modeling biomass gasification with little or no change (Liu and Gibbs, 2003; Basu and Kaushal, 2009). Due to the fact that reactivity of biomass char is much higher than that of coal char, researchers usually multiply reactivity of coal char with an empirical factor (Babu and Sheth, 2006; Gao and Li, 2008; Basu and Kaushal, 2009).

2.3.2 Models for char reaction rate

Kinetics of gasification has not yet been well developed as its thermodynamics. While homogeneous reactions in the gas phase can be described by a simple equation, heterogeneous reactions between solid and gases are intrinsically more complicated. The overall reaction rate depends not only on the intrinsic reaction rate in and on the surface of particles, but also on the rate of heat and mass transfer of fluids through the

solid as well as across the fluid-film surrounding the solid (Wen, 1968). A successful design of a reactor requires a good knowledge of the overall reaction rate which varies greatly under different operating conditions due to the different heat and mass transfer rates.

Gas-solid reactions take place in and on the surface of char particles, and the whole reaction process contains the following several steps (Wen, 1968): (1) gas reactants diffuse through the fluid film surrounding the solid from the bulk fluid to the solid particle surface; (2) gas reactants diffuse through the porous solid layer; (3) gas reactants are adsorbed to the solid particle surface; (4) gas reactants react with solid particle on the particle surface; (5) reaction products desorbe from the solid particle surface; (6) reaction products diffuse through the porous solid and the fluid film surrounding the particle from the solid particle surface to the bulk fluid. These steps take place consecutively, and the step with slowest rate becomes the rate-determining step. When the kinetic rate of reactions is slower than the diffusion rate of gases, the overall reaction is in kinetically controlled regime. On the other hand, if the diffusion rate is much slower than the kinetic rate of reactions, then the overall reaction is in the diffusion controlled regime. According to Wen (1968), solid-gas reactions can be classified to four classes based on the manner by which the reaction progresses: (1) heterogeneous reactions, when the reaction rate is relatively rapid compared to the diffusion rate and the porosity of the un-reacted solid is so small that the solid is impervious to gas reactants. Heterogeneous reactions usually happen on the surface of

the particles; (2) homogeneous reactions, when the porosity of the solid particles is so large that gas reactants and products can pass freely inside the particles and solid reactants are distributed homogeneously throughout the solid phase in the molecular scale; (3) reactants accompanying phase changes of solid components; (4) intermediate cases between heterogeneous reactions and homogeneous reactions, when solid reactants are small lumps of reactant distributed throughout the solid phase and the overall reaction rate is affected by intrinsic reaction rate, distribution of lumps, structure of solid, and mass and heat transfer in the solid. Of the four classes heterogeneous reactions and homogeneous reactions are special cases.

There are different kinds of models available to calculate the overall reaction rates of char gasification reactions. Based on the reaction expression, there are surface reaction rate models which require the information about the solid surface area and gas concentration, and volume reaction rate models which require only information about gas concentration or pressure (Prabir, 2011). Based on whether particle structure is considered, there are structural reaction rate models and reaction rate models without considering char structure. Based on whether the diameter or density of char change during the reaction process, there are shrinking core models and shrinking particle models. Of all the available models, three kinds of models are most widely used to simulate gas-solid reactions: the un-reacted core shrinking model, the random pore model, and the pseudo-homogeneous or volumetric model (De Souza-Santos, 2004; Wu, Wu and Gao, 2009; Seo, et al., 2010; Malekshahian and Hill, 2011).

2.3.2.1 Un-reacted core shrinking model

The un-reacted core shrinking model is widely used for gas-solid reactions that belong to the heterogeneous reaction class. A schematic diagram of the particle in the un-reacted core shrinking model is shown in Fig. 2.2. Based on whether the ash layer formed during the reaction stays on the surface of the un-reacted particle, the un-reacted core shrinking model can be furthered divided into exposed core (or ash segregation) model and un-exposed core model. For the former model, the ash layer formed on the surface of the un-reacted portion of the particle disintegrates from the particle immediately once it is formed due to severe collision between particles in the bed. For the exposed core model, it assumes that the ash layer exists during the whole reaction process, thus before gas reacts with solids it must diffuse through the ash layer surrounding the un-reacted core and the diffusion resistance is considered when developing correlations for reaction rates. The other assumptions for these two models are: the solid particles are nonporous and spherical; as reactions proceed, the residue after reactions forms an ash layer outside the un-reacted portion of the particle which is called the un-reacted core; reactions only take place on the un-reacted core's external surface.

For the un-reacted core shrinking model, for reactant gases in the bulk fluid reacting with solid particles, they must overcome two or three resistances: the gas film/gas boundary layer, the ash layer (exposed core model does not have this resistance), and

chemical reactions. Based on the magnitude of the resistances in different steps, it can be determined which regime the reaction rate is in. There are many different correlations available to describe the un-reacted core shrinking model, and many of them are in one of the forms shown below (Okuga, n.d.; Toomey and Johnstone, 1952; De Souza-Santos, 2004; Slezak, 2008; Wu, et al., 2010).

$$Rate = \frac{2}{d_p}\frac{1}{\sum_{k=1}^{3} U_{U,k}}(\rho_i - \rho_i^*) \tag{2.25}$$

$U_{U,1}$---- Resistance for the gas boundary layer

$U_{U,2}$---- Resistance for the shell, which surrounds the core

$U_{U,3}$---- Resistance for the core

d_p---- Particle diameter

ρ_i---- Mass concentration of gas reactant i

ρ_i^*---- The back reaction equilibrium mass concentration of gas reactant i

$$Rate = v_s M A_p C_{i,g}/(\frac{1}{\zeta k_r} + \frac{1}{k_{diff}} + 1/k_{dash}) \tag{2.26}$$

$C_{i,g}$---- Molar concentration of oxidizer or gasification agent in the bulk gas phase, kmole/m^3

v_s---- The number of moles of product gas per mole of oxidant

M---- Molecular weight of gas

$$Rate = \frac{1}{\frac{1}{k_{diff}} + \frac{1}{k_r Y^2} + \frac{1}{k_{dash}(\frac{1}{Y} - 1)}}(P_i - P_i^*) \tag{2.27}$$

k_{diff}---- Gas film mass diffusion coefficient

k_r---- Arrhenius rate constant

k_{dash}---- Ash layer diffusion coefficient

Y---- Char conversion factor defined as the ratio of the un-reacted core radius to the initial radius of the particle.

P_i---- Partial pressure of reactant i

P_i^*---- The back reaction equilibrium pressure of reactant i

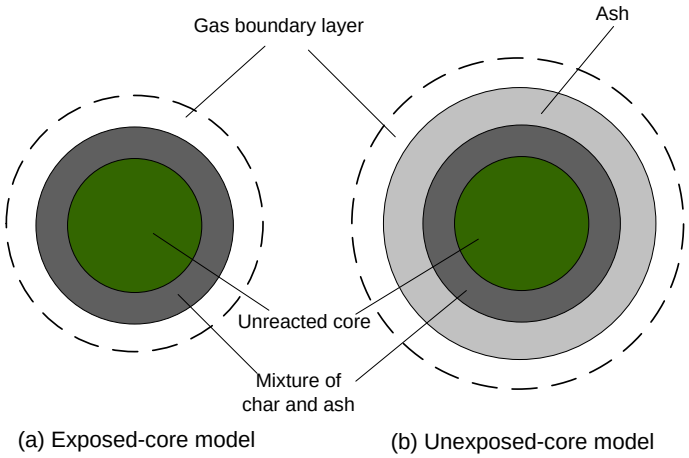

Figure 2. 2 Schematic diagram of un-reacted core shrinking model

2.3.2.2 Random-pore model

Char gasification reactions usually take place on the exterior and interior surfaces of char particles. When the char particle is highly porous, the surface area of the inner pores is several orders of magnitude higher than the external surface area (Prabir, 2011). Char particles with the same diameter may have different overall reaction kinetics due to the difference in their char reactive area. Therefore, it is wise to consider the internal char pore surfaces for highly porous particles, and the reaction

rate model should be carefully selected according to char characteristics. When the porosity of the solid particle is big enough so that little resistance exists and gas reactant can diffuse freely into the interior of the solid, the homogeneous model can be applied. When solid particles have very small porosity, un-reacted core (either exposed core model or unexposed core model) is suitable for that condition. In fact, gas-solid reactions cannot be completely described by the un-reacted core shrinking model or by the homogeneous model, and an intermediate model is suitable to describe the majority of gas-solid reactions (De Souza-Santos, 2004).

The random-pore model is another common structural model which considers the change of pore structure during chemical reactions. It assumes that: reaction occurs on the pore surfaces of the solid particles; pore volume and surface area increase until the neighboring pores intersect one another as the reaction progresses. The original equation for the random-pore model is shown in equation (Wurzenberger, et al., 2002):

$$\frac{dX}{dt} = k_r(1-X)[1-\psi \ln(1-X)]^{1/2} \quad (2.28)$$

ψ---- A parameter related to the pore structure of the un-reacted sample (X=0) and calculated as $\psi = \frac{4\pi L_o}{\rho_c S_o^2}$

L_o---- Original pore length

ρ_c---- Char true density

S_o ---- Original pore surface area

Due to the complex nature of internal particle diffusion, it is difficult to describe it mathematically. In addition, because developing core structure is difficult to describe, it has been a common practice to relate the char reaction rate to the external surface area as expressed by the following equation below (Hobbs, Radulovic and Smoot, 1993):

$$r_i = \upsilon_s M k_r \zeta A_p C_{i,s} \quad (2.29)$$

r_i---- Reaction rate for single particle, kg/s

υ_s---- Stoichiometric coefficient of char when that of reactant i is 1 (moles of char per mole gas)

M---- Molecular weight of char

k_r---- Rate constant

ζ---- Particle surface area factor to account for internal surface burning (effective burning area of the entire particle/external area of the equivalent spherical particle)

A_p---- Effective external surface area of the equivalent sphere, m2

$C_{i,s}$---- Molar concentration of the reactant in the gas phase at the surface of the particle (kmole/m3)

2.3.2.3 Pseudo homogeneous model

Although the majority of gas-solid reactions are not only influenced by the rate-determining step, due to the complex nature of mass and heat transfer from bulk fluid to the solid reactant, in many cases the pseudo homogeneous model is preferred (Wen, 1968; Holder, 2008). The volume or pseudo homogeneous model belongs to the

homogeneous reaction class, and it assumes that the active sites where gas-solid reactions take place are uniformly distributed in the whole particle; gas diffuses freely inside the particle and reactions between gas and solid are occurring homogeneously throughout the whole particle. Actually the pseudo homogeneous model is a special case of the unreacted-core shrinking model when the resistance of the film boundary laryer and ash layer is neglected and only the intrinsic gas-solid reaction is considered. The pseudo homogeneous model is usually described by a global reaction rate, and the two widely used global reaction rates are: 1) the n-order power law rate equation, and 2) Langmuir-Hinselwood mechanism (Blasi, n.d.; Blasi, 2009; Basu and Kaushal, 2009).

The Langmuir-Hinselwood mechanism accounts for the intrinsic conversion of reactants and the surface adsorption and desorption, and the reaction rate is usually in the following form.

$$r = \frac{(\text{kinetic term})(\text{driving force})}{\text{adsorption term}} \tag{2.30}$$

According to the Langmuir-Hinselwood mechanism, the heterogeneous char carbon dioxide reaction occurs through several steps, which include the inhibiting effect of some compounds:

$$C_f + CO_2 \overset{k_1}{\rightarrow} C(O) + CO \tag{2.31}$$

$$C(O) + CO \overset{k_2}{\rightarrow} C_f + CO_2 \tag{2.32}$$

$$C(O) \overset{k_3}{\rightarrow} CO + C_f \tag{2.33}$$

Where $k_1 - k_3$ are Arrhenius rate constants. C_f represents the number of active or available sites, and $C(O)$ represents a carbon-oxygen complex which occupies the site. The reaction rate, in accordance with reactions (3.6) – (3.8) and applying the steady-state assumption for the $C(O)$ complex, could be expressed as:

$$r_c = \frac{k_1 p_{co2}}{1 + \left(\frac{k_2}{k_3}\right) p_{co} + (k_1/k_3) p_{co2}} \tag{2.34}$$

Where p_{co2} and p_{co} are the partial pressure of CO_2 and CO. When the CO concentrations are small and/or the inhibiting effect exerted by this species is not taken into account, a simple global model can be applied (Blasi, 2009):

$$C + CO_2 \rightarrow 2CO \tag{2.35}$$

$$r_c = Aexp(-\tfrac{E}{RT}) p_{CO2}^n \tag{2.36}$$

A is the pre-exponential factor, E the activation energy, R the universal gas constant and n is an empirical parameter.

With the Langmuir-Hinselwood mechanism, the heterogeneous char steam reaction occurs through the following steps (Blasi, n.d.; Barrio, et al. 2008):

$$C_f + HO_2 \overset{k_1}{\rightarrow} C(O) + H_2 \tag{2.37}$$

$$C(O) + H_2 \overset{k_2}{\rightarrow} C_f + HO_2 \tag{2.38}$$

$$C(O) \overset{k_3}{\rightarrow} CO + C_f \tag{2.39}$$

$$C_f + H_2 \overset{k_4}{\rightarrow} C(H)_2 \tag{2.40}$$

$$C(H)_2 \overset{k_5}{\rightarrow} C_f + H_2 \tag{2.41}$$

$$C_f + \frac{1}{2}H_2 \overset{k_6}{\rightarrow} C(H) \tag{2.42}$$

$$C(H) \overset{k_7}{\rightarrow} C_f + \frac{1}{2}H_2 \tag{2.43}$$

Where $k_1 - k_7$ are Arrhenius rate constants. The surface rate reaction could be expressed as:

$$r_w = \frac{k_1 p_{H2O}}{1 + \left(\frac{k_1}{k_3}\right) p_{H2O} + f(p_{H2})} \tag{2.44}$$

Where r_w represents the reaction rate for char-steam gasification.

The following expression is obtained for the oxygen exchange:

$$f(p_{H2}) = \left(\frac{k_2}{k_3}\right) p_{H2} \tag{2.45}$$

The hydrogen inhibition by formation of the $\mathrm{C(H)_2}$ complex

$$f(p_{H2}) = \left(\frac{k_4}{k_5}\right) p_{H2} \tag{2.46}$$

And the hydrogen inhibition by formation of $\mathrm{C(H)}$ complex

$$f(p_{H2}) = \left(\frac{k_6}{k_7}\right) p_{H2}^{0.5} \tag{2.47}$$

Reaction rates for char gasification are summarized well by Blasi (2009).

The n-order power law rate reaction is the simplest approach to describe the char reaction kinetics. It needs less experimental data and fits experiments well. It is decided with the following formula:

$$r = k_c C_i^{n_i} \tag{2.48}$$

$$r = k_p p_i^{n_i} \tag{2.49}$$

Where r is the reaction rate, $\frac{\text{kmole}}{\text{m}^3\text{s}}$, C is molar concentration of component i, $\frac{\text{kmole}}{\text{m}^3}$, p is the partial pressure component i, and k is the reaction rate constant which follow the Arrhenius equations

$$k = Aexp(-\frac{E}{RT}) \tag{2.50}$$

A is the pre-exponential factor, E is activation energy, J/kmole. Activation energy is the minimum energy that the free energy of the system needs to overcome in order to get a reaction to occur. Pre-exponential factor represents the frequency of collisions between reactant molecules, and it is also dependent on temperature (UC Davis Chem WiKi, 2010).

2.4 Fluidized bed hydrodynamics

Hydrodynamics is the study of fluids in motion based upon the physical conservation laws of mass, momentum, and energy. Hydrodynamics affects the whole fluidized bed system through: (a) chemical reactions; (b) heat transfer; (c) mass transfer; (d) size reduction of particles; and (e) attrition and fragmentation of particles (Nemtsov and Zabaniotou, 2008).

2.4.1 Fluidization

When sending a gas flow to a bed with a certain amount of solid particles, the bed has different states as the velocity of gas increases shown in Fig. 2.3. When the velocity of gas entering the bed is small, particles in the bed remain immobilized, and the bed is called a fixed bed (Jiang, 1991). Increasing the velocity of the gas until the total upward forces on the particles equals the sum of solid weight and wall force, the particles are suspended in the gas flow, and the minimum fluidization state has been reached. If the velocity of gas is increased further, small bubbles which are mainly gas appear in the bed, and the bed is called a bubbling fluidized bed. Keep on increasing the velocity of the gas flow, and when the diameter of bubbles is close to that of the reactor the bed is called a slugging bed (Yang, 2003). At this state, if increase the velocity of gas flow further, solids will be entrained out of the bed and the bed is called an entrained bed.

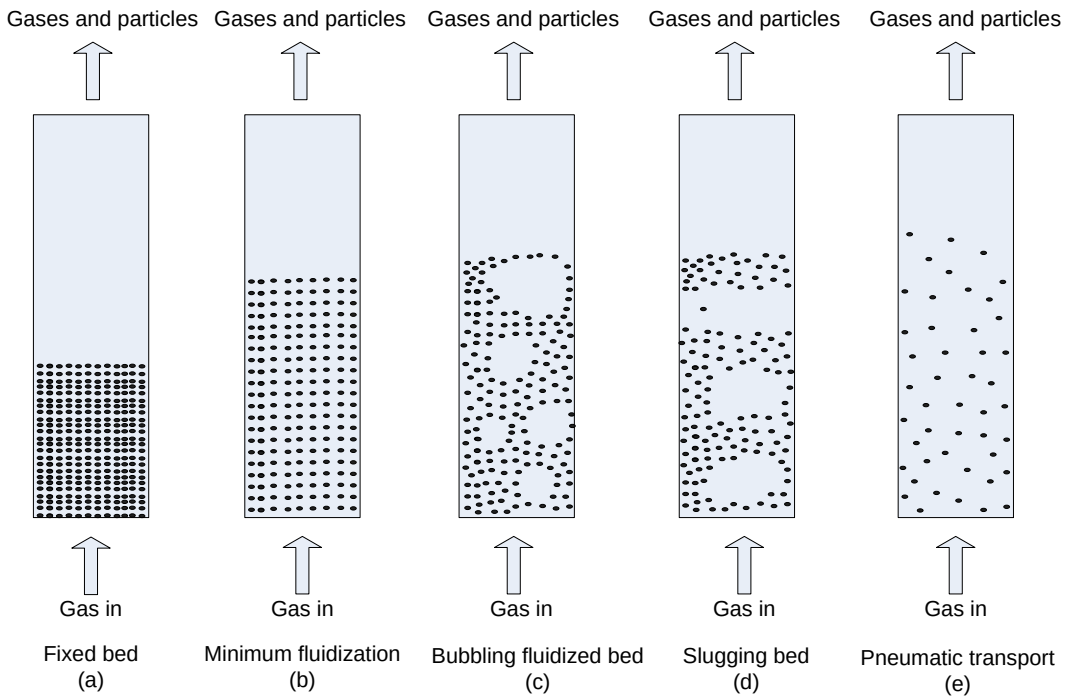

Figure 2. 3 Different fluidization states of gas-solid bed (De Souza-Santos, 2004)

2.4.2 Minimum fluidization velocity

The gas flow in the bed is limited by minimum fluidization velocity and terminal velocity. For a fluidized bed, the superficial velocity should be larger than the minimum fluidization velocity but smaller than the terminal velocity, otherwise the particles will either remain fixed or be entrained out of the bed. The velocity of gas at which the bed begins to fluidize is called minimum fluidization velocity (Yang, 2003). At minimum fluidization velocity, the upward drag force of particles equals the downward gravitational force of particles. Minimum fluidization velocity can be obtained either by pressure drop – gas velocity plot, or related equations (Yang, 2003).

When using the first method, the relationship between the bed pressure drop and gas velocity is used to determine the minimum fluidization velocity, which is plotted in Fig. 2.4. When increasing the gas velocity from 0, the pressure drop of the bed increases with an increased gas velocity until the gas velocity reaches a critical value. When the gas velocity is larger than that critical value, the bed pressure drop first decreases and then remains constant rapidly with increased gas velocity. The critical gas velocity is the minimum fluidization velocity.

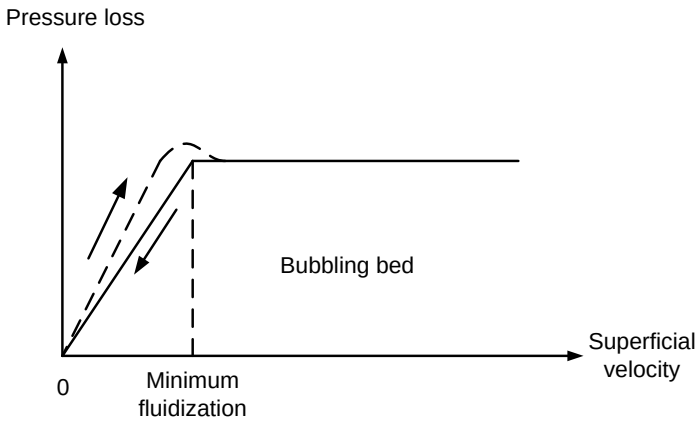

Figure 2. 4 Relationship between pressure drop and superficial gas velocity (De Souza-Santos, 2004)

For the second method, assume the bed to be loosely packed. At minimum fluidization state, the pressure drop of the bed equals the gravitational force of the bed particles (Yang, 2003).

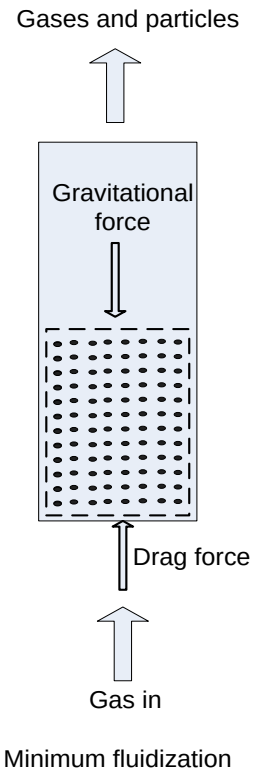

Figure 2. 5 Bed force balance

Therefore for force balance, we can get the following relationship neglecting friction force

$$\Delta PA = W = (\rho_p - \rho_f) g V_p = (\rho_p - \rho_f) g L (1 - \varepsilon_{mf}) \tag{2.51}$$

$$\frac{\Delta P}{L} = (\rho_p - \rho_f) g (1 - \varepsilon_{mf}) \tag{2.52}$$

$\frac{\Delta P}{L}$ can also be calculated through direct calculation with equations such as the Ergun equation or the carman equation.

Ergun equation:

$$\frac{\Delta P}{L} = 150 \frac{(1-\varepsilon)^2}{\varepsilon^3} \frac{\mu U}{(\emptyset_s d_p)^2} + 1.75 \frac{1-\varepsilon}{\varepsilon^3} \frac{\rho_f U^2}{\emptyset_s d_p} \tag{2.53}$$

$\emptyset_s$---- Particle sphericity

Carman equation:

$$\frac{\Delta P}{L} = -\frac{180\mu U(1-\varepsilon)^2}{d_s^2 \varepsilon^3} \tag{2.54}$$

Combining the initial pressure drop equation (equation (2.52)) with Ergun equation, we get

$$Ar = 150\frac{(1-\varepsilon_{mf})}{\emptyset^2 \varepsilon_{mf}^3}(Re)_{mf} + 1.75\frac{1}{\emptyset \varepsilon_{mf}^3}(Re)_{mf}^2 \tag{2.55}$$

Ar---- Archimedes number, and can be calculated using equation (2.56).

$$Ar = \frac{d_p^3 \rho_f (\rho_p - \rho_f) g}{\mu^2} \tag{2.56}$$

Equation (2.55) can be simplied by using approximations made by Wen, and the simplified equation (equation (2.58)) is called the Wen correlation which is most widely used to predict the minimum fluidization velocity.

$$\frac{1}{\emptyset \varepsilon_{mf}^3} \cong 14 \quad \frac{(1-\varepsilon_{mf})}{\emptyset^2 \varepsilon_{mf}^3} \cong 11 \tag{2.57}$$

$$(Re)_{mf} = \sqrt{C_1^2 + C_2 Ar} - C_1 \tag{2.58}$$

Table 2. 1 Values of C_1 and C_2

Researchers	C_1	C_2
Wen and Yu	33.7	0.0408
Richardson	25.7	0.0365
Saxena and Vogel	25.3	0.0571
Grace	27.2	0.0408
Chitester	28.7	0.0494
Babu	25.25	0.0651

Different researchers have suggested different values for C_1 and C_2 as shown in Table 2.1 (Yang, 2003).

Using the carman equation, we get

$$U_{mf} = 0.00114 \frac{g d_p^2}{\mu} (\rho_p - \rho_f) \tag{2.59}$$

2.4.3 Particle terminal velocity

In a fluid-particle system, particle termincal velocity is defined as the velocity of particle that is constant. When particles are at their terminal velocity, the sum of forces acting on each particle (drag force and gravitational force) is zero. The drag force on a single particle is defined as the area projected by the particle times the ratio of the force acting on the particle to the fluid dynamics pressure (Yang, 2003) :

$$F = \frac{1}{2} C_D \rho_f U_t^2 A_p = \frac{\pi}{8} C_D \rho_f U_t^2 d_p^2 \tag{2.60}$$

C_D---- Drag force coefficient

ρ_f----- Fluid density

U_t---- Terminal velocity of a single particle

A_p---- Projected area of particle

d_p---- Particle diameter

Equating the drag force and gravitational force on a single particle (equation (2.61)), an expression of terminal velocity can be obtained as shown in equation (2.62).

$$F_s = \frac{\pi}{8} C_D \rho_f U_t^2 d_p^2 = \frac{\pi d_p^3}{6} (\rho_p - \rho_f) g \tag{2.61}$$

$$U_t = \sqrt{\frac{4}{3} \frac{d_p (\rho_p - \rho_f) g}{\rho_f C_D}} \tag{2.62}$$

To get the value of terminal velcotiy U_t, the value of drag force coefficient C_D must

be known. C_D is a function of the particle's Renolds number Re_p. Based on the magnitude of Re_p, particles are in different regimes, so C_D has different expressions (Yang, 2003). Different literature has different values for the division between Stokes Regime and the Intermediate Regime (Fueyo and Dopazo, 1995; Yang, 2003; Nemtsov and Zabaniotou, 2008) and here only one value is used (Yang, 2003).

When $Re_p < 0.2$, particle is in the Stokes Regime, and C_D can be expressed as:

$$C_D = \frac{24}{Re_p} \tag{2.63}$$

When $Re_p > 500$, particle is in the Newton's Law Regime, and $C_D = 0.44$.

When $0.2 < Re_p < 500$, particle is in the Intermediate Regime, and C_D can be expressed as:

$$C_D = f(Re_p) \tag{2.64}$$

Accordingly, different correlations exist for particle terminal velocity in different regimes.

In Stokes Regimes (Fueyo and Dopazo, 1995; Yang, 2003)

$$U_t = \frac{d_p^2(\rho_p - \rho_g)g}{18\mu},\ Re \leq 0.2 \tag{2.65}$$

In the Intermediate Regime (Fueyo and Dopazo, 1995; Nemtsov and Zabaniotou, 2008)

$$U_t = d_p\left[\frac{4(p_p - p_g)^2 g^2}{225\mu\rho_g}\right]^{1/3},\ 0.2 < Re \leq 500 \tag{2.66}$$

$$U_t = \left[\frac{d_p^{1.6}(p_p - p_g)g}{13.9\rho_g^{0.5}\mu^{0.6}}\right]^{0.71},\ 2 < Re \leq 500 \tag{2.67}$$

In the Newton's Law Regime (Fueyo and Dopazo, 1995; Nemtsov and Zabaniotou,

2008)

$$U_t = [\frac{3.1 d_p g(\rho_p - \rho_g)}{\rho_g}]^{1/2},\ 500 < Re < 2 \times 10^5 \quad (2.68)$$

Instead of having three correlations for C_D in different regimes, Turton and Levenspiel proposed a single correlation for C_D for the whole range of Renolds numbers (Turton and Levenspiel, 1986) as shown by equation (2.69).

$$C_D = \frac{24}{(Re)_p}\left[1 + 0.173(Re)_p^{0.657}\right] + \frac{0.413}{1 + 16.3(Re)_p^{-1.09}} \quad (2.69)$$

In order to include nonspherical particles, Haider and Levenspiel (1989) subsequently improved the above equation by using two equations (equation (2.70) and equation (2.71)) (Turton and Levenspiel, 1986).

$$C_D = \frac{24}{(Re)_p}\left[1 + (8.1716e^{-4.0655\emptyset})(Re)_p^{0.0964+0.5565\emptyset}\right] + \frac{73.69(e^{-5.0748\emptyset})(Re)_p}{(Re)_p + 5.378e^{6.2122\emptyset}} \quad (2.70)$$

$$C_D = \frac{24}{(Re)_p} + 3.3643(Re)_p^{0.3471} + \frac{0.4607(Re)_p}{(Re)_p + 2682.5}, \text{ for spherical particles.} \quad (2.71)$$

$\emptyset$--- particle sphericity

Two other approximate correlations for calculating particle terminal velocity are also introduced which are shown in Table 2.2 (Yang, 2003).

Table 2. 2 Expressions for terminal velocity

$u_t = [\frac{18}{(d_p^*)^2} + \frac{2.335-1.744\emptyset}{(d_p^*)^{0.5}}]^{-1} \;\; 0.5 < \emptyset < 1$ $u_t = [\frac{18}{(d_p^*)^2} + \frac{0.591}{(d_p^*)^{0.5}}]^{-1} \;\; \emptyset = 1$ $d_p^* = d_p[\frac{\rho_f(\rho_p - \rho_f)g}{\mu^2}]^{1/3}$ $U^* = U[\frac{\rho_f^2}{\mu(\rho_p - \rho_f)g}]^{1/3} = [\frac{4}{3}\frac{Re_p}{C_D}]^{1/3}$
$log_{(Re)_t}(Y, \emptyset) = log_{(Re)_t}(Y, 1) + P(Y, \emptyset)$ $log_{(Re)_t}(Y, 1) = 0.77481 - 0.56032logY + 0.024246(logY)^2 - 0.0038056(logY)^3$ $Y = \frac{4}{3}\frac{g(\rho_p-\rho_f)\mu}{u_t^3\rho_f^2}$, $log_{10}(\frac{u_t}{Q}) = \sum_{n=0}^{5} a_n\,(log_{10}(Pd_t))^n$ $C_D Re^2 = \frac{4}{3}\frac{g(\rho_p-\rho_f)\rho_f d_t^3}{\mu^2} = P^3 d_t^3,\; \frac{Re}{C_D} = \frac{3}{4}\frac{\rho_f^2 U_t^3}{g(\rho_p-\rho_f)\mu} = \frac{U_t^3}{Q^3}$ $a_0 = -1.37323,\; a_1 = 2.06962,\; a_2 = -0.453219,\; a_3 = -0.0334612$ $a_4 = -0.745901 \times 10^{-2},\; a_5 = -0.24958 \times 10^{-2}$

2.4.4 Bed voidage

Bed voidage is defined as the fraction of total bed volume that is occupied by fluid (Nemtsov and Zabaniotou, 2008). The bed voidage under minimum fluidization condition is ε_{mf}, and its value is about 0.44 (Yang, 2003).

$$\varepsilon = \frac{V_f}{V} \tag{2.72}$$

Bed voidage is dependent on temperature and pressure. Researchers have developed many correlations to calculate the bed voidage, and some of the correlations are put in Table 2.3.

Table 2. 3 Expressions for bed voidage

No.	Correlations
1	$\varepsilon_d = \frac{(18Re_p+2.7Re_p^{1.687})^{0.209}}{Ga^{0.209}}$ void fraction in the dense phase (Smith, Arkun and Littman, 1982)
2	$\varepsilon_{mf} = (\frac{1}{14\emptyset A})^{1/3}$ void fraction at minimum fluidization (Wen and Yu, 1966)
3	$\varepsilon_E = \varepsilon_{mf}(\frac{U_E}{U_{mf}})^{1/6.7}$ void fraction in the emulsion phase (Delvosalle and Vanderschuren, 1985) $\varepsilon = 1 - \frac{1-\varepsilon_{mf}}{f_{bexp}}$ the bed expansion factor
4	$\varepsilon_{mf} = 1.424 - 0.2686\ln\underline{d} + 1.342 \times 10^{-2}\underline{u}_{mf} + 0.1845\ln\underline{u}_{mf} + 8.14 \times 10^{-3}(\ln\underline{u}_{mf})^2$ (Jiang, 1991) $\underline{u}_{mf} = U_{mf}\{\rho_f^2/[g\mu(\rho_p - \rho_f)]\}^{1/3}$ dimensionless minimum fluidization velocity $\underline{d} = Ar^{1/3} = d_p\{[g(\rho_p - \rho_f)\rho_f]/\mu^2\}^{1/3}$ dimensionless particle size
5	$\varepsilon_b = (U - U_{mf})/U_{bA} = U_b/U_{bA}$ bubble fraction (Jiang, 1991)
6	$\varepsilon_w = \left[1 + 0.6(\frac{d_p}{D})\right]\varepsilon - 0.6(\frac{d_p}{D})$ bed voidage near wall (Furnas, 1929) $\varepsilon_c = [\varepsilon + 0.3(1-\varepsilon)]\left[1 + 0.6(\frac{d_p}{D})\right] - 0.6(\frac{d_p}{D})$ bed voidage near core

2.4.5 Expanded Bed height

Due to bubble forming and breaking through the fluidized bed, the bed height and voidage are time-average values (Yang, 2003). Generally, the bed height of fluidized bed can be calcualted through the expression below:

$$\frac{L}{L_{mf}} = \frac{(1-\varepsilon_{mf})}{(1-\varepsilon)} \tag{2.73}$$

Where ε is the bed voidage, L is bed height, L_{mf} is bed height at minimum fluidization state, and ε_{mf} is bed voidage at minimum fluidization state.

Since ε is not easy to get directly, bed height is always expressed in terms of velocity.

Based on whether the bubble size is constant or not, there are two different expressions to calculate the bed height. When the bubble has a constant size,

$$(H_{max} - H_{mf})A = (U - U_{mf})At \tag{2.74}$$

t---- Time needed for bubble travel through the bed

$$t = \frac{H_{max}}{U_A} \tag{2.75}$$

U_A---- Absolute bubble velocity

$$U_A = (U - U_{mf}) + U_B \tag{2.76}$$

So we can get the value of H_{max} through the equation below

$$\frac{(H_{max} - H_{mf})}{H_{mf}} = \frac{(U - U_{mf})}{U_B} \tag{2.77}$$

When bubble size increases due to coalescence, suggested bed expansion formula is

$$H = H_{mf} + \left(\frac{5b}{3}\right)[(H+B)^{0.6} - B^{0.6}] - 5b^2[(H+B)^{0.2} - B^{0.2}] + 5b^{2.5}\{\tan^{-1}\left[\frac{(H+B)^{0.2}}{b^{0.5}}\right] - \tan^{-1}[\frac{B^{0.2}}{b^{0.5}}]\} \tag{2.78}$$

Where $b = 1.917\frac{(U-U_{mf})^{0.8}}{g^{0.4}}$, and $B = 4\sqrt{A_o}$

A_o---- The so-called catchment area for a bubble stream at the distributor plate. It is usually the area of distributor plate per orifice.

Geldart also developed an equation for bed expansion in freely bubbling beds with ‘‘sandlike’’ powders shown in equation (2.89) (Geldart 1975, p.237-244).

$$\frac{H}{H_{mf}} - 1 = \frac{2}{d}\sqrt{\frac{2}{g}}Y(U - U_{mf})[\frac{(c+dH)^{1/2} - c^{1/2}}{H_{mf}}] \tag{2.79}$$

Where $d = 0.027(U - U_{mf})^{0.94}$, and $c = 0.915(U - U_{mf})^{0.4}$

Y ---- A correction for deviation from the two-phase theory.

For a distributor with N holes per cm 2, c can be calculated by

$$c = \frac{1.43}{g^{0.2}} \left(\frac{U - U_{mf}}{N}\right)^{0.4} \tag{2.80}$$

Some researchers calculate the bed height through equation (2.91) (Raman, 1981; Jiang, 1991).

$$H - H_{mf} = \int_0^H \varepsilon_b \, (Z) dZ \tag{2.81}$$

2.4.6 Bubble diameter and velocity

When a bubble rises in the fluidized bed, it usually grows in size due to effective hydrostatic pressure decrease or bubble coalesce in vertical and horizontal directions (Yang, 2003). According to Geldart, for Group B powders the mean bubble size is dependent only on the type of the distributor, the distance above the distributor plate, and the excess gas velocity above that required at the minimum fluidization condit ion U – Umf (Geldart, 1972).

$$D_B = D_{Bo} + KH^n (U - H_{mf})^m \tag{2.82}$$

Through experiments, it has been found that (Yang, 2003):

$$D_B = 0.9(U - U_{mf})^{0.4} + 0.027H(U - U_{mf})^{0.94} \text{ , for the porous plates} \tag{2.83}$$

$$D_B = 1.43 \frac{[(U - U_{mf})/N_o]^{0.4}}{g^{0.2}} + 0.027H(U - U_{mf})^{0.94}, \text{ for the orifice plates} \tag{2.84}$$

The principal effect of adding fines to a fluidized bed of group B powders is the reduction of the mean particle size. At equal values of excess $U - U_{mf}$, adding fines to bed results in increased bed expansion and solid circulation rates but has little effect

on mean bubble size. Rowe suggested the following equation to estimate the bubble size in a fluidized bed (Rowe, 1976):

$$D_B = \frac{(U-U_{mf})^{1/2}(H+h_o)^{3/4}}{g^{1/4}} \quad (2.85)$$

h_o---- An emperical constant and is a characteritics of the distributor plate. h_o is effectively zero for a porous plate buy may be more than a meter for large tuyeres.

Mori and Wen (1975) developed expressions for calcualting bubble diameter assuming that all gas above the minimum fluidizing velocity went to form a single train of bubbles rising along the center line of the bed.

$$D_{BM} = 0.652[A(U - U_{mf})]^{2/5} \quad (2.86)$$

$$\frac{D_{BM}-D_B}{D_{BM}-D_{Bo}} = \exp(-0.3\frac{H}{D}) \quad (2.87)$$

When $30 < D < 130\ cm$, $0.5 < U_{mf} < 20\ cm/s$, $0.006 < d_p < 0.045\ cm$, $U - U_{mf} < 48\ cm/s$

D_{Bo}---- The initial bubble diameter

$D_{Bo} = 0.347[\frac{A(U-U_{mf})}{N_o}]^{2/5}$, for perforated plates

A---- The area of the bed

No---- The total number of orifices.

$D_{Bo} = 0.00376(U - U_{mf})^2$, for porous plates

Darton's correlation is as follows (Krishna, 1988):

$$d_b = 0.54(U - U_{mf})^{2/5}(Z + 4{A_o}^{1/2})^{4/5}g^{-1/5} \text{ for } Z < Z^* \quad (2.88)$$

$$d_b = 0.54(U - U_{mf})^{2/5}(Z^* + 4{A_o}^{1/2})^{4/5}g^{-1/5}, \text{ for } Z > Z^* \quad (2.89)$$

$$Z^* = 3.5D_T(1 - \sqrt{A_O/A}) \quad (2.90)$$

Where Z is height above the distributor plate; Z^* is the slugging limit; D_T is the diameter of the bed; A_o and A are areas of the orifice and the entire distributor plate, respectively.

Froment and Bischoff (1990) proposed a new procedure for the bubble size based a nonideal-flow reactor model.

$$s = h^{\frac{2}{5}}/({D_T}^{\frac{1}{2}} - {d_{bo}}^{1/2}) \quad (2.91)$$

Where $d_{bo} = 0.00376(U - U_{mf})^2$ for a porous plate; $d_{bo} = 0.347[A_o\big(U -$ *Umf]2/5* for a perforated plate

Then

$$d_b = ({d_{bo}}^{1/2} + 0.37Z^{2/5})^2, \text{ for } s \leq 0.9 \quad (2.92)$$

$$d_b = [{d_{bo}}^{\frac{1}{2}} + (0.406 - 0.04212s)Z^{\frac{2}{5}}]^2, \text{ for } s > 0.9 \quad (2.93)$$

Choi, Son and Kim (1988) presented an implicit equation for bubble size.

$$\big(U - U_{mf}\big)(d_b - d_{bo}) + 0.474g^{\frac{1}{2}}\Big({d_b}^{\frac{3}{2}} - {d_{bo}}^{\frac{3}{2}}\Big) = 1.132(U - U_{mf})Z \quad (2.94)$$

Bubble velocity can be calculated by correlations in Table 2.4 .

Table 2. 4 Correlations for bubble velocity

No	Correlations
1	$U_B = 0.711\sqrt{gD_e}$ (Yasui and Johanson, 1958)
2	$U_A = 1.2\frac{G}{A} + 0.35\sqrt{gD}$ the absolute bubble velocity (Nicklin, Wilkes and Davidson, 1962)
3	$U_{b\infty} = \beta\sqrt{\mathrm{gd_b}}$ (Werther, 1978) $\beta = 0.64,\ D_T \leq 0.1\ m$ $\beta = 1.6\mathrm{D_T}^{0.4},\ 0.1 < D_T \leq 1\ m$ $\beta = 1.6,\ D_T > 1\ m$
4	${U_{b\infty}}^{w} = 1.13\mathrm{U_{b\infty}}\exp\left[-(\mathrm{d_b/D_T})\right],\ 0.125 < \frac{d_b}{D_T} < 0.6$ (Clift, Grace and Weber, 1978)) ${U_{b\infty}}^{s} = 0.35\sqrt{\mathrm{gD_T}},\ \frac{d_b}{D_T} > 0.6$ $U_{bA} = U_{b\infty} + U_b$ $U_{b\infty}$ the velocity of rising for a single bubble U_b is the superficial velocity of the bubble phase
5	$U_b/U_{mf} = 0.48[(\mathrm{U - U_{mf}})/U_{mf}]^{1.15} U_{bA} = 0.48U_{mf}[(\mathrm{U - U_{mf}})/U_{mf}]^{1.15} + U_{b\infty}$ (Van den Aarsen, Beenackers and van Swaaij, 1986)

2.4.7 Particle entrainment and attrition

During the process of fluidized bed gasification, particle size decreases due to chemical reactions, attrition and segmentation, and attrition accounts for the generation of most critical particles. Fine particles generated through attrition are entrained out of the bed immediately under most operating conditions. The rate of production of fines through attrition can be calculated by the equation below (Merrick and Highley, 1974):

$$R_a = K(U_o - U_{mf})M_b \quad (2.95)$$

R_a---- The rate of production of fines by abrasion and K is the abrasion rate constant

M_b---- Mass of particles in the bed, kg

The rate of production of fines of size x is calculated by the equation below:

$$\frac{dM_x}{dt} = -R_{ax} = -K(U_o - U_{mf})M_x \quad (2.96)$$

M_x---- Mass of particles of size x in the bed, kg

When the particle size is small enough, particles with a certain momentum which is obtained from bubble eruption will be entrained out of the fluidized bed to the freeboard. There are two important mechanisms for the projection of particles from the fluidized bed to the freeboard (Yang, 2003). One is the eruption of bubbles on the surface of the fluidized bed and the other is the interstitial velocity in the dense bed. Based on the first entrainment mechanism, solids are projected to the freeboard either from the bubble roof or from the bubble wake with a momentum caused by the bubble eruption due to different particle sizes and gas velocities. Based on the other mechanism, particle entrainment is significant for fluidized bed with coarse particles and with a wide particle size distribution. Particle entrainment due to the later mechanism is much lower than that due to the first mechanism.

One important parameter of particle entrainment is the transport disengaging height (TDH) (Yang, 2003). The whole bed is divided into two different vertical zones: the dense phase fluidized bed, and the freeboard. At high gas velocity, the surface of the

fluidized bed becomes more and more fuzzy, and some particles are projected to the freeboard. Not all the particles projected to the freeboard can be entrained out of the freeboard. Most particles having a terminal velocity smaller than the gas velocity are entrained out of the freeboard, and solid particles that have a terminal velocity larger than the gas velocity return to the fluidized bed. Solids holdup decays with height from the fluidized bed surface and finally becomes constant. The height from the bed surface to the point beyond which solid entrainment remains constant is called the Transport Disengaging Height (TDH). The characteristics of TDH that solid entrainment decays with is very important to design the height of the freeboard. If the fluidized bed is designed to be a reactor for gas-solid reaction, solid entrainment should be reduced as much as possible, thus the freeboard must have a height of at least TDH, otherwise, the height of freeboard can be decreased. However, although there are many studies on TDH, there is no widely accepted method to calculate the TDH, and the value calculated through different correlations is different (Yang, 2003).

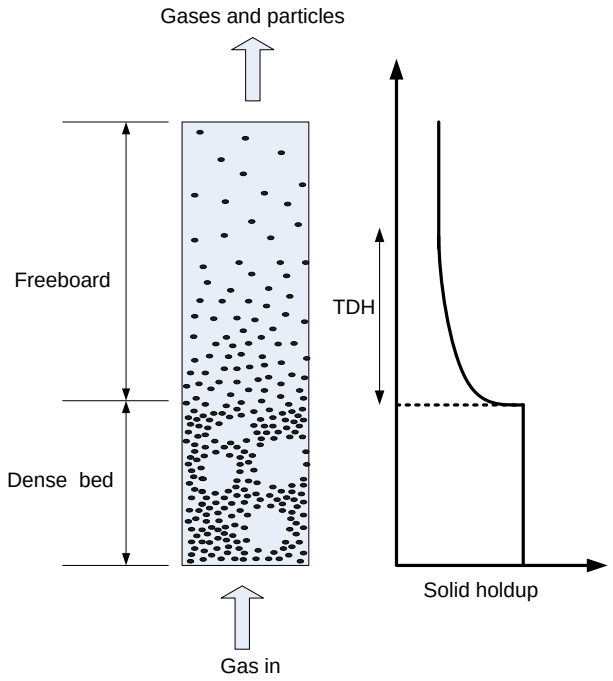

Figure 2. 6 Particle distribution in the bed (Yang, 2003)

Particle entrainment is affected by gas superficial velocity, diameter of the fluidized bed, diameter of the freeboard, the height of freeboard, temperature, pressure, and particle size. Generally, for particles whose terminal velocity is below the gas superficial velocity in the freeboard, solid entrainment increases with decreased particle size (Yang, 2003). However, for group A particles, once the particle size is below a critical value solid entrainment above the TDH decreases with decreased particle size due to particle agglomeration resulting from the cohesive force between particles which is large compared to the gradational force.

Solid entrainment can be expressed through total entrainment flux E_h in kg/(m^2.s) at the height h above the distributor or through an elutriation rate constant K_{ih}^* which is

shown in the equation below (Yang, 2003). The entrainment flux and elutriation rate constants above TDH are indicated with the index ∞ as E_∞ or K_∞.

$$K_{ih}^{*} = \frac{E_{ih}(t)}{x_i(t)} = \frac{\frac{1}{Area}\frac{d}{dt}[x_i(t)m_s]}{x_i(t)} \tag{2.97}$$

$Area$---- Bed cross-section, m^2

$E_{ih}(t)$---- Entrainment flux of particles of diameter $d_{p,i}$ at height h at time t

The total entrainment for particles of all size at height h is (Yang, 2003)

$$E_h(t) = \sum_i E_{ih}(t) \tag{2.98}$$

The entrainment rate of solids in the freeboard can be represented by the following equation.

$$F = F_\infty + (F_o - F_\infty)exp(-ah) \tag{2.99}$$

F---- Entrainment rate of particles in the freeboard at a height h above the bed surface

F_∞---- Entrainment rate above the TDH

F_o---- The entrainment rate at the bed surface

a---- A constant representing the characteristics of the fluidized bed entrainment system

TDH---- The height of freeboard above which rate of solids entrainment does not change appreciably

Although a lot of correlations for particle entrainment are available, because they are either unreliable or unsatisfactory to calculate the entrainment in the freeboard due to

the difficulty of measuring entrainment rate and the limited range of experimental operations, there is still lack of good correlations (Wen and Chen, 2004). One correlation that has attracted a lot of attention is shown here (Wen and Chen, 2004):

$$E_{i\infty} = \frac{1}{Area}\frac{d(x_i m_s)}{dt} \tag{2.100}$$

$$E_{i\infty} = \rho_p(1-\epsilon_f)U_{st} \tag{2.101}$$

$$U_{st} = U_o - u_t \tag{2.102}$$

$$\epsilon_f = \{1 + \frac{\lambda(U_o-u_t)^2}{2gD}\}^{-1/4.7} \tag{2.103}$$

$E_{i\infty}$---- Entrainment flux of particles of diameter $d_{p,i}$ above TDH

m_s---- Total mass of solid particles in the fluidized bed

x_i---- Mass fraction of particles of diameter $d_{p,i}$

U_{st}---- Particle velocity

D---- Bed diameter

λ---- Friction coefficient due to the collision between particles and particles and the wall, and it meets the following equation

$$\frac{\lambda\rho_p}{d_p^2}(\frac{\mu}{\rho_g})^{2.5} = \begin{cases} 5.17Rep^{-1.5}D^2, \text{for } Rep \le Rep_c \\ 12.3Rep^{-2.5}D, \text{for} Rep \ge Rep_c \end{cases} \tag{2.104}$$

$$Rep_c = 2.38/D \tag{2.105}$$

$$Rep = \rho_g(U_o - u_t)d_p/\mu \tag{2.106}$$

3 Model development

3.0 Overview

Since gasification is a very complex process, comprehensive modeling of the corn stover steam gasification process requires a good knowledge of both reaction kinetics and fluid dynamics (Abdollahi, Guy and Chaouki, 2010). The kinetic part describes the most important chemical changes that take place in the reactor, and fluid dynamics account for transport processes. In this study, a complex kinetic model including both chemical reaction kinetics and bed fluid dynamics was developed. In addition, because with different assumptions and simplifications there are models with different levels of complexity and different treatments of gas and solids, and because little literature is available on comparing these models, it is difficult to choose between different models. Therefore, in order to investigate the importance of modeling complexity and concept in model selection criteria, a total of seven gasification models with different levels of complexity and different treatments of gas and solids which are widely used by researchers were developed and compared in this study. These are summarized below starting with the pyrolysis sub-model which is an important component of several gasification models.

Pyrolysis Model

Since the pyrolysis model is a very important sub-model used in four of the seven gasification models it is introduced first in section 3.1.

Zero-Dimensional gasification models

Zero dimensional means that there is no sense of bed fluid dynamics**.** These models are discussed in section 3.2. There are two groups of zero dimensional models.

- Equilibrium models (section 3.2.1) in which there is no sense of time and pyrolysis is assumed to be instantaneous. There are two types of equilibrium models a) non-stoichiometric (referred to as **model 1**) and b) stoichiometric (**model 2)**.
- Kinetic model (section 3.2.2) which involves time and includes a separate pyrolysis sub-model (**model 3**).

One-Dimensional gasification models

One dimensional means that the bed depth and bed fluid dynamics are included in addition to time and a pyrolysis sub-model. The system modeled includes a fluidized bed and freeboard and is describe in section 3.3. There are three groups of one-dimensional models.

- One phase kinetic model (section 3.3.1) – the one phase is an emulsion phase which includes gases and solids. The concept of char particle entrainment is also introduced (**model 4**).
- Two phase kinetic model (section 3.3.2) – the two phases include an emulsion phase containing both gases and solids, and a bubble phase which includes only gases. Char particle entrainment is also included (**model 5**).
- Two phase kinetic models – all char in bed (section 3.3.3) – This is a special case of the two phase model in which all char stays in the bed. Two approaches

are modeled: 1) char particles modeled as particles (**model 6**) and 2) char treated as a single solid – not particles (**model 7**).

3.1 Pyrolysis model

During the gasification process, once feedstock is heated to a certain temperature pyrolysis takes place, during which the feedstock breaks down to solid char, condensable gases, and non condensable gas. Pyrolysis is usually followed by char-gasification. In real process, there is no distinct edge between pyrolysis and char gasification, and most of the time they overlap together.

When researchers were developing gasification models, in order to simplify their study many researchers made an assumption that the whole gasification process was divided into two stages: devolatilization/pyrolysis and gasification, and pyrolysis happens instantaneously (Neogi, et al., 1986; Solomon, et al., 1988; Fletcher, et al., 1990; Graham, Bergougnou and Freel, 1994; Olazar, et al., 2001; Sadaka, Ghaly and Sabbah, 2002; Radmanesh, Chaouki and Guy, 2006; Ranzi, et al., 2008; Nikooa and Mahinpey, 2008). Therefore, pyrolysis was not included in their study, and pyrolysis products which were represented by char, ash, H_2, CO, CO_2, CH_4, C_2H_x, tar, and H_2O were used as starting reactants for the following gasification process. In addition, in order to get the pyrolysis products distribution, some researchers did calculation based on minimum Gibbs free energy (Sadaka, Ghaly and Sabbah, 2002), while other researchers either used results obtained from TGA experiments or bench scale

experiments (Raman, 1981; Neogi, et al., 1986; Jiang, 1991). However, the treatments toward pyrolysis mentioned above have some problems. First, the assumption that pyrolysis happens instantaneously can only be used under very strict conditions (small particle size and high temperature). For particles whose size is not small enough, it takes a relatively long time for pyrolysis process to complete (Gaston, et al., 2011). Since particles with a wide range of sizes will be covered in this study and relatively long time is needed for pyrolysis of large particles, pyrolysis and char gasification will happen simultaneously during a relatively long time, thus the assumption that pyrolysis happens instantaneously cannot be used here.

In addition, yields of pyrolysis products and their distribution are affected by temperature and particle size greatly (Gaston, et al., 2011), thus pyrolysis products obtained from TGA experiments, bench-scale experiments, or equilibrium models for one particle size and temperature may be different from those under different operating conditions and fuel condition, which will ultimately affect gasification products distribution. Therefore, in order to reflect the real process a pyrolysis model which includes the effect of particle size and operating conditions on pyrolysis time and pyrolysis products distribution was developed.

3.1.1 Pyrolysis time and products distribution

Pyrolysis time varies with particle size. According to the size of original particles pyrolysis goes through two regions: kinetic-controlled regime where the pyrolysis

time is independent of the particle size and heat and mass transfer-controlled regime where the rate of pyrolysis is controlled by heat and mass transfer. The heat and mass transfer-controlled regime is further categorized to internal heat and mass transfer controlled regime (for large particles with a size larger than 10 mm) and external transfer controlled regime (Gaston, et al., 2011). When the initial particle size is larger than 0.7 mm, pyrolysis is in heat and mass transfer-controlled regime. For particles with a size larger than 6 mm the total pyrolysis time can be described by a power law model which is a function of temperature and initial particle size (De Diego, et al., 2002; Jand and Foscolo, 2005; Rapagnà and Mazziotti di Celso, 2008; Gaston, et al., 2011).

$$\tau = Ad_0^n \tag{3.1}$$

τ---- Pyrolysis time, a function of the initial particle size, s

d_0---- Initial particle size, mm

A---- A parameter determined through experiments

If particles have a size smaller than 6 mm but larger than 0.7 mm, the equation used to calculate pyrolysis time is different from that for particles with a size larger than 6 mm (Gaston, et al., 2011). When particle size is no larger than 0.7 mm, the heat and mass transfer limitation is negligible, and pyrolysis time remains constant (around 17 second (800 ^{o}C)), which is consistent to results obtained by some researchers (Pyle and Zaror, 1984; Kersten, et al., 2005; Radmanesh, Chaouki and Guy, 2006) and from which it can be seen that pyrolysis does not happen instantaneously. However, some

researchers also showed that the yields of pyrolysis products of biomass in fluidized bed were independent of particle size in the range of 4 um to 2 mm (Pyle and Zaror, 1984; Kersten, et al., 2005). Therefore, it can be seen that there are some discrepancies between the pyrolysis time obtained, and the current research failed to cover the whole range of particle sizes. In order to simplify the pyrolysis model, here it is assumed that when the particle size is smaller than 0.7 mm, pyrolysis takes place instantaneously; when particle size is larger than 0.7 mm, pyrolysis time is calculated using the same equation (Equation (3.1)).

Table 3. 1 Properties of corn stover (You, et al.; De Kam, Morey and Tiffany, 2009b)

Moisture (wt %, wet)	8.0
HHV (MJ kg^{-1}, dry)*	17.93
Ultimate (wt %, dry)	
Carbon	45.44
Hydrogen	5.52
Nitrogen	0.69
Oxygen	41.49
Sulfur	0.04
Chlorine	0.1
Ash	6.72

* HHV: higher heating value

The biomass fuel used in this study is corn stover, and its relevant properties are shown in Table 3.1. Since the relationship between particle size and pyrolysis time is different from one kind of biomass to another, values of the parameters used in equation (3-1) need to be decided for corn stover. However, we are not able to conduct experiments, and literature on pyrolysis of corn stover becomes the information source for this study. Although some experiments have been done on corn stover pyrolysis, most of them were at low temperature and low heating rate, and only one paper is

suitable to use (You, et al., nd). However, that paper did not cover the effect of particle size on pyrolysis time and pyrolysis products distribution. Therefore, although this may introduce errors, in order to establish a relationship between particle size and pyrolysis time for corn stover, the relationship for wood was used and two assumptions were made: 1) the relationship between particle size and pyrolysis time for wood is the same as that for corn stover; and 2) the ratio of yields of pyrolysis products for one particle size to that for another particle size for corn stover is the same as the ratio for wood. Therefore, with the first assumption, the pyrolysis time for different particle sizes for corn stover, which is the same as that for wood, can be calculated through equation (3.2) for particles with a size larger than 0.7 mm (Gaston, et al., 2011):

$$\tau = e^{1013.2/T^{1.076}} d_0^{1.414} \quad (3.2)$$

T---- Temperature, K

In addition, since the yields of pyrolysis products for different particle sizes for wood are known, with the second assumption those for corn stover can be calculated. The whole procedure is described below. First based on the pyrolysis products for wood provided in the literature (Gaston, et al., 2011), relationships between yield of product and particle size were established at each temperature:

$$y = a(T) * x + b(T) \quad (3.3)$$

Where x and y represent particle diameter in mm and yield of product in kg/kg fuel, respectively. A relationship also exists for corn stover:

$$y_{corn\ stover} = a(T)_{corn\ stover} * x + b(T)_{corn\ stover} \quad (3.4)$$

Table 3. 2 Value of $a(T)_{corn\ stover}$ at different temperature

T,K	750	850	950	1050	1150
Char	0.0022	0.002	0.0014	0.0014	0.0038
Total gas	-0.001	-0.004	-0.006	-0.005	-0.004
CO	0	-0.003	-0.003	-0.003	-0.003
CO_2	-0.001	-0.001	-0.001	-0.001	-0.001
H_2	-0.00012	-0.00013	-0.00009	-0.00017	0
CH_4	-0.0001	-0.0001	-0.0005	-0.0005	-0.0005
H_2	-0.00012	-0.00013	-0.00009	-0.00017	0
CH_4	-0.0001	-0.0001	-0.0005	-0.0005	-0.0005

Table 3. 3 Value of $b(T)_{corn\ stover}$ at different temperature

T,K	750	850	950	1050	1150
Char	0.26978	0.2198	0.19986	0.19986	0.17962
Total gas	0.2301	0.4004	0.6106	0.6405	0.7204
CO	0.068923	0.125013	0.22253	0.243589	0.289552
CO_2	0.125331	0.208721	0.279475	0.27318	0.261804
H_2	0.001397	0.004036	0.006812	0.008458	0.015026
CH_4	0.017241	0.034493	0.050846	0.059631	0.07518

Based on the second assumption, the value of $a(T)_{corn\ stover}$ is the same with $a(T)$ at the same temperature, and since $y_{corn\ stover}$ is known for given a given particle size for corn stover the value of $b(T)$ can be calculated by equation (3.5):

$$b(T)_{corn\ stover} = y_{corn\ stover} - a(T)_{corn\ stover} * x \quad (3.5)$$

Substituting equation (3.5) to equation (3.4), pyrolysis products distribution for other particle sizes for corn stover can be obtained through equation (3.4). The values of $a(T)_{corn\ stover}$ and $b(T)_{corn\ stover}$ for corn stover are shown in Tables 3.2 and 3.3.

3.1.2 Reaction kinetics

Besides the relationship between the pyrolysis time and the particle size, the relationship between pyrolysis time and distribution and yield of pyrolysis products is also needed. Since multiple reactions take place during the pyrolysis process and it is very difficult to study each pyrolysis reaction separately, kinetic models suggested are based on the weight of the residue (Tran, and Rai, 1978). Many studies show that the pyrolysis step follows the kinetics of a first-order or pseudo first-order reaction, and one of the most widely used model for the pyrolysis process is shown below (Tran, and Rai, 1978; Hajaligol, et al., 1982; Nunn, et al., 1985; Manyà, Velo and Puigjaner, 2003; Ji, Feng and Chen, 2009):

$$\frac{dm}{dt} = ke^{-\frac{E}{RT}}(m^* - m) \tag{3.6}$$

m---- Instantaneous yield, kg/kg fuel

m^*---- Ultimate yield, kg/kg fuel

k---- Pre-exponential factor

E---- Activation energy, kJ/kmol

R---- Universal gas constant, 8.314 kJ/(kmol.K)

The main disadvantage of the current pyrolysis models is that there are few models available which provide the relationship between particle size and pyrolysis time and pyrolysis products, and most models which show the evolution of pyrolysis products with time failed to consider the effect of particle size. Therefore, a pyrolysis model

which can show the evolution of pyrolysis products at different time for different particle sizes was derived by incorporating the relationship between particle size and pyrolysis time to general pyrolysis model (through combining equations (3.2) and (3.6) together) as shown in equations (3.7) and (3.8). The pyrolysis time calculated by this model is close to that given by equation (3.2) for the same particle size, and the instantaneous yields of pyrolysis products calculated by this pyrolysis model are close to those given by equation (3.6).

$$\frac{dm}{dt} = factor * \frac{1}{\tau}(m^* - m) \tag{3.7}$$

$$\frac{dm}{dt} = 5 * d_p^{-1.414} e^{-1013.2/T^{1.076}}(m^* - m) \tag{3.8}$$

$factor$---- A factor used to adjust the pyrolysis time so that pyrolysis time calculated by this model is close to that calculated by equation (3.2)

3.1.3 Model validation

Pyrolysis time is defined as the time taken for the yields of pyrolysis products to reach a constant value. The pyrolysis time for different particle sizes at different temperature calculated by equation (3.2) is shown in Table 3.4. The evolution of pyrolysis products with time predicted by the pyrolysis model developed in this study is shown in Fig. 3.1 when the temperature is 870 ^{o}C. It can be found that the pyrolysis time predicted by the model is close to that calculated by equation (3.2) at 870 ^{o}C. The pyrolysis time predicted by the model developed at other temperatures is also close to the values in Table 3.4, but due to limited space those figures will not be shown here. Therefore, it

can be concluded that the pyrolysis model developed in this study can give reasonable results.

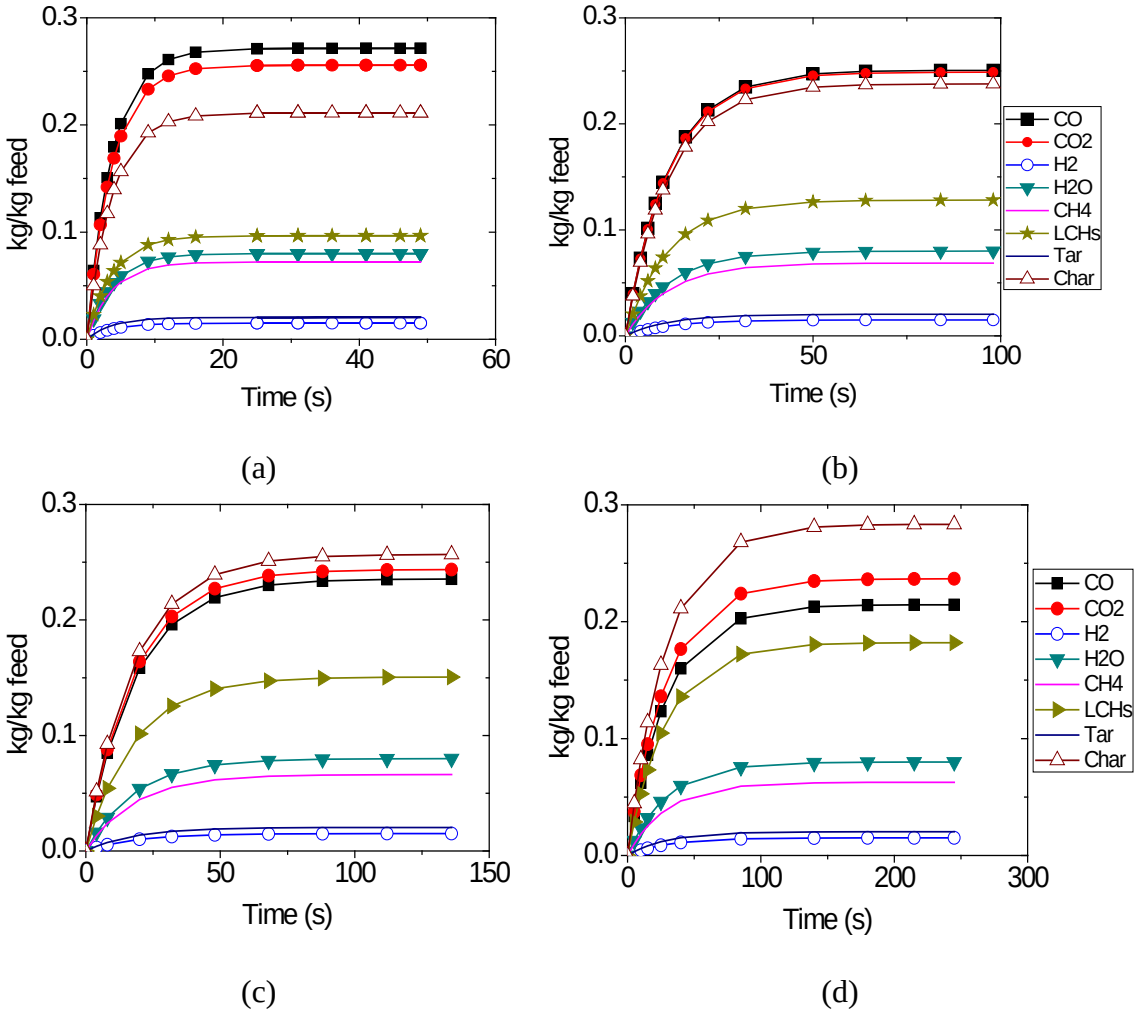

Figure 3. 1 Evolution of pyrolysis products with time at 870 ^{o}C for different particle sizes. Particle size is (a) 6 mm, (b) 13 mm; (c) 18 mm; (d) 25 mm

Table 3. 4 Pyrolysis time (s) calculated based on equation (3.2)

Particle size, mm	6	13	18	25
870 ^{o}C	21.2	63.2	100.1	159.3

800 ^{o}C	22.0	65.5	103.8	165.2
700 ^{o}C	23.4	69.7	110.4	175.7
600 ^{o}C	25.2	75.2	119.2	189.6

3.2 Zero-dimensional models

Zero-dimensional models are the simpler level of simulation for equipment or a set of equipment (De Souza-Santos, 2004). They are based on the fundamental equations of mass and energy balance over the whole or part of the system. This kind of model is very useful to get a first estimate of the performance characteristics of the equipment or the system without requiring much information about the equipment or the system.

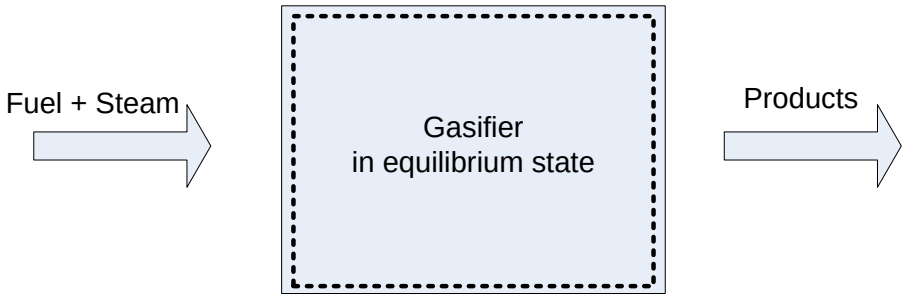

Figure 3. 2 Schematic diagram of the zero-dimensional models modeled as control volume

Zero-dimensional models can be modeled as control volume and control mass. When they are modeled as control volume, the system or equipment is an open system, and mass can transfer through its control surface that envelopes it as shown in Fig. 3.2. Mass accumulation in the system during unit time equals mass entering the system minus the mass leaving the system during that time:

$$\frac{dm}{dt} = \sum_{i}^{n} m_{in,i} - \sum_{j}^{m} m_{out,j} \tag{3.9}$$

m---- Mass in the control volume

$m_{in,i}$--- Mass of stream i entering the control volume

$m_{out,j}$---- Mass of stream j leaving the control volume

When zero-dimensional models are modeled as control mass, the biomass and gasifying agent fed to the equipment or system are a control mass. During the following reaction time volume and shape of the control mass may change, but mass cannot transfer through the control surface that envelopes it, and the overall mass does not change in the control mass. Mass change in the system during unit time equals mass consumed or generated through chemical reactions during that time:

$$\frac{dm_{total}}{dt} = 0 \tag{3.10}$$

$$m_{total} = \sum_{i=1}^{n} m_i \tag{3.11}$$

$$\frac{dm_i}{dt} = \sum_{j=1}^{m} m_{i,reaction\ j} \tag{3.12}$$

m_{total}---- Total mass in the control mass system

m_i---- Mass of species i in the control mass system

$m_{i,reaction\ j}$---- Mass of species i consumed or generated through chemical reaction

t---- Time, s

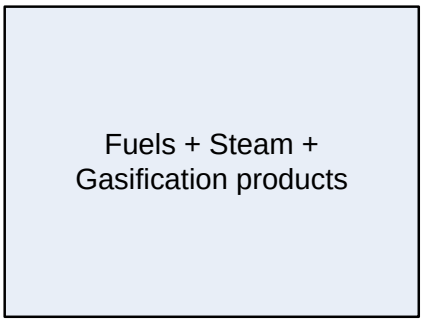

Figure 3. 3 Schematic diagram of zero-dimensional model modeled as control mass

In this study, two kinds of zero-dimensional models were developed: zero-dimensional equilibrium models and zero-dimensional kinetic model. The former was modeled as a control volume, and the other model was modeled as a control mass.

3.2.1 Zero-dimensional equilibrium models

The zero-dimensional equilibrium model does not consider chemical reactions or fluid dynamics for the gasification process and it predicts the gasification products distribution using the characteristics of systems at chemical equilibrium state. For any system, its Gibbs free energy can be calculated according to the equation below subject to atom balance (White III and Seider, 1981):

$$G = \sum_{j=1}^{S} G_j^o n_j^C + \sum_{j=S+1}^{C} \sum_{l=1}^{P} G_{jl} n_{jl} \tag{3.13}$$

The atom balance can be expressed as:

$$b_k = \sum_{j=1}^{S} m_{jk} n_j^C + \sum_{j=S+1}^{C} \sum_{l=1}^{P} m_{jk} n_{jl},\ k=1,\ldots,\ E \tag{3.14}$$

C---- The number of chemical species

P---- The number of mixed species (vapor, solid, and liquid)

S ---- The number of condensed species (which does not distribute among other phases and appears in only one pure phase, are normally solid)

n_{jl}---- The moles of compound j in phase l

G_{jl}---- The chemical potential of compound j in phase l

b_k---- Gram-atoms of element k

m_{jk}---- The number of atoms of element k in compound j

E---- The number of elements

According to related theory, when compositions of a system are in chemical and phase equilibrium, the system Gibbs free energy is minimum. Therefore, the compositions of a system in chemical and phase equilibrium can be calculated based on this characteristic, and models using this characteristic are called equilibrium models. Generally, there are two kinds of equilibrium models based on minimum Gibbs free energy theory: one is non-stoichiometric model, and the other is stoichiometric model. Non-stoichiometric models minimize system Gibbs free energy through adjusting n_j^c and n_{jl} in equation (3.13) under the constraints of atom balance in equation (3.14) without requiring additional information.

Stoichiometric models calculate the yields of product species through solving an independent set of reactions the number of which equals the number of chemical

species C. Through the atom balance relationship, k equations are obtained, and the moles of compound j in equation (3.14) can be expressed as in the equations below including reaction extents:

$$n_j = \begin{cases} n_j^C = n_j^{C0} + \sum_{i=1}^{Q} \upsilon_{ij}\varepsilon_i \,, j = 1, \dots, S \\ \sum_{l=1}^{P} n_{jl} = n_j^0 + \sum_{i=1}^{Q} \upsilon_{ij}\varepsilon_i \,, j = S+1, \dots, C \end{cases} \tag{3.15}$$

υ_{ij}---- The stoichiometric coefficients of compound j in reaction i

ε_i---- The extent of the reaction i

n_j^0---- The moles of compound j in the feed mixture

ρ---- Rank of atom matrix m_{jk}

Q---- The number of independent chemical reactions (normally C- ρ)

However, because the number of atoms k is usually smaller than the number of unknown chemical species C, additional equations are required to close the equation system, which is achieved by using the equilibrium constant of chemical reactions. For reaction i at equilibrium state, its equilibrium constant can be calculated as:

$$K_i = e^{-\Delta G_i^o/R/T}, \text{ i=1,…, Q} \tag{3.16}$$

R---- Universal gas constant, 8.314 kJ/(kmol.K)

In addition, the equilibrium constant also meets the relationship below:

$$\prod_{j=1}^{C} a_j^{\upsilon_{ij}} = K_i \tag{3.17}$$

a_j---- The activity of species j

Therefore we can establish such a relationship:

$$e^{-\Delta G_i^o/R/T} = \prod_{j=1}^{C} a_j^{\boldsymbol{v}_{ij}} \quad (3.18)$$

Since ΔG_i^o and activity are functions of moles of compositions taking part in the reaction i, relationship between moles of compositions taking part in reaction i is established and one equation is obtained. By following the same procedure, we can get the other equations needed by using the equilibrium constant of the other reaction. Equilibrium models using this kind of method are referred to as stoichiometric models. However, the stoichiometric and non-stoichiometric models are essentially of the same concept (Li, et al., 2001; Jarungthammachote and Dutta, 2007).

3.2.1.1 Non-stoichiometric equilibrium model

Non-stoichiometric equilibrium model was developed for the corn stover steam gasification process. Biomass and steam are sent to the gasifier at corresponding operating conditions, and gasification products leave the gasifier at the same temperature and pressure with those used during the gasification process. Assumptions made for this mode are:

1) In order to compare with stoichiometric model gasification products are the same as those of stoichiometric model, and they are char, ash, H_2, CO, CO_2, CH_4, and H_2O. The other high molecular weight hydrocarbons such as C_2H_2, C_2H_6 and tar are not included, and minor elements of the fuel are neglected.
2) Char only contains pure carbon.
3) Ash is inert, and does not take part in the reactions.
4) The whole system is at chemical equilibrium state.

5) The whole reactor is isothermal.

Non-stoichiometric equilibrium model was created with Aspen Plus. Aspen plus is a process modeling environment for conceptual design, optimization, and performance monitoring (Aspen Plus, 2012). It has built-in models for industrial process equipment and the world's largest database of pure component and phase equilibrium data for conventional chemicals, solids, and polymers. It can be used for design, simulation, and optimization. A very important block used for non-stoichiometric model is RGibbs which is based on the minimization of Gibbs free energy subject to atom balance constrains. It calculates phase and chemical equilibrium without requiring reaction stoichiometry. In addition, one can realize restrict equilibrium in RGibbs by specifying (Aspen Plus, n.d.): 1) fixed moles of any product; 2) percentage of a feed component that does not react; 3) temperature approach to equilibrium for the entire system; 4) temperature approaches for individual reactions; 5) fixed extents of reaction. When the method to restrict equilibrium is specified, a whole set of linearly independent chemical reactions must be specified as well even if only one reaction is restricted. The set of linearly independent reactions required equals the total number of products in the product list including solids minus the number of atoms present in the system. The reactions must involve all participating components. A component is participating if it satisfies these criteria: it is in the product list. However, RGibbs can only solve specified components (Sinnott and Towler, 2012). If a component which is actually formed is not listed in the product list, RGibbs is not able to predict its yield.

In addition, for species with high Gibbs free energy, RGibbs cannot predict their yield properly. Another thing needs to the pointed out is that RGibbs cannot predict the yield of char correctly, and that yield should be specified in the RGibbs block.

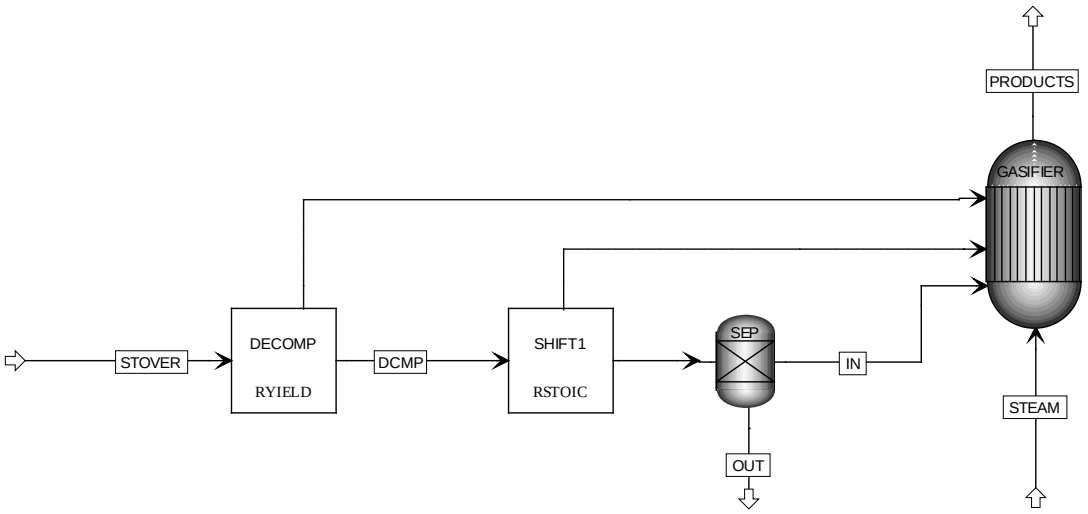

Figure 3. 4 Aspen Plus diagram of the non-stoichiometric equilibrium model

The flow diagram for equilibrium model using Aspen Plus is shown in Fig. 3.4. First nonconventional biomass is decomposed into elements N_2, O_2, H_2, ash, and C based on ultimate analysis in a DECOMP block, then these elements and moisture in the biomass are sent to a RSTOIC block where char is generated from C with a yield obtained from kinetic model. Later, char is separated from the remaining components through a SEP block. Finally the remaining components are sent to a RGIBBS block where gasification products are formed based on minimum Gibbs free energy.

3.2.1.2 Stoichiometric equilibrium model

Stoichiometric equilibrium model for the corn stover steam gasification process was created and programmed with MatLab software. Assumptions made for this mode are:

1) Gasification products include char, ash, H_2, CO, CO_2, CH_4, and H_2O. Tar and heavier hydrocarbons are not included, and minor elements of the fuel are neglected.

2) Char only contains pure carbon.

3) Ash is inert, and does not take part in the reactions.

4) The whole system is at chemical equilibrium state.

5) The whole reactor is isothermal.

Since the yield of char is not able to be predicted by the stoichiometric equilibrium model, it is set a fixed value. Given the fact that products have 5 species (H_2, CO, CO_2, CH_4, and H_2O) and 3 equations can be obtained based on 3 atom balance (C, H, O) equations, two more equations are needed to close the equation system. Since several reactions take place during the gasification process, different reaction combinations during which water-gas shift reaction is always one of them have been used by different researchers (Zainal, et al., 2001; Mountouris, Voutsas and Tassios, 2006; Jarungthammachote and Dutta, 2007; Vaezi, et al., 2008; Huang and Ramaswamy, 2009; Wang, Shahbazi and Hanna, 2011), and in this study the following two reactions were selected (Zainal, et al., 2001; Jarungthammachote and Dutta, 2007; Wang, Shahbazi and Hanna, 2011):

$$C + 2H_2 = CH_4 \tag{3.19}$$

$$CO + H_2O = CO_2 + H_2 \tag{3.20}$$

The equilibrium constants for these two reactions are:

$$K_1 = \frac{P_{CH4}}{P_{H2}P_{H2}} = \frac{x_{CH4}P}{(x_{H2}P)^2} = \frac{n_{CH4}n_t}{(n_{H2})^2} \quad (3.21)$$

$$K_2 = \frac{P_{CO2}P_{H2}}{P_{CO}P_{H2O}} = \frac{n_{CO2}n_{H2}}{n_{CO}n_{H2O}} \quad (3.22)$$

P_i---- Particle pressure, atm

P---- Total pressure of the system, atm

x_i---- Mole fraction of species i

n_t---- Total mole of gas, kmole

n_i---- Mole of species i, kmole

In addition, equilibrium constant can be expressed in terms of Gibbs energy:

$$\ln K = -\frac{\Delta G_T^o}{RT} \quad (3.23)$$

ΔG_T^o---- Standard Gibbs function of reaction, kJ/kmol

R---- Universal gas constant, 8.314 KJ/(kmol.K)

$$\Delta G_T^o = \sum_i v_i \Delta \bar{g}_{f,T,i}^o \quad (3.24)$$

$\Delta \bar{g}_{f,T,i}^o$---- Standard Gibbs function of formation at given temperature T of species i, kJ/kmol

$\bar{g}_{T,i}^o$---- Gibbs free energy of species i at standard state

Because the value of $\Delta \bar{g}_{f,T,i}^o$ can be obtained directly from thermodynamic database or empirical equations available (Jarungthammachote and Dutta, 2007), thus the value of $\ln K$ can be calculated. In addition, the value of K can be obtained from figure or table directly (Heiberg and Eichberg, 1982; Zainal, et al., 2001; Wang, Shahbazi and

Hanna, 2011). Therefore, substitute the value of K into equations (3.21) and (3.22), and the moles of the gas compositions can be obtained through solving the closed equations. In this study, empirical equations shown in equation (3.25) and (3.26) were used to calculate $\ln K$(Wang, Shahbazi and Hanna, 2011).

$$\ln K_1 = \exp\left(\frac{4000}{T} - 3.5\right) \tag{3.25}$$

$$\ln K_2 = \exp\left(\frac{10000}{T} - 12.2\right) \tag{3.26}$$

Since the gasification process is an endothermic process and additional heat needs to be provided, knowing the amount of heat needed is very important to reactor design. In this study the amount of heat needed was calculated based on energy balance of the whole system. Since the gasifier is an open system, based on the law of conservation of energy the energy balance in an open system is shown in equation (3.27):

$$(H_2 - H_1) + \left(E_{k,2} - E_{k,1}\right) + \left(E_{p,2} - E_{p,1}\right) = Q - W \tag{3.27}$$

H_i---- Enthalpy of inlet flow or outlet flow

$E_{k,i}$---- Kinetic energy of inlet flow or outlet flow

$E_{p,i}$---- Potential energy of inlet flow or outlet flow

Q---- Heat transfer between the system and outside heat source, + indicates heat transfer to the system, and – represents the opposite direction

W---- Work done by the fluid, + means work done by the fluid, and – represents work to the fluid

Neglecting kinetic energy, potential energy, and work, the above equation becomes

$$H_2 - H_1 = Q \tag{3.28}$$

$$\Delta H = \sum_i v_i \, \bar{h}_T^o = \sum_i v_i \left(\bar{h}_{f,i}^o + \Delta h_{T,i}^o\right) \tag{3.29}$$

H_i---- Enthalpy of flow, 1 represents inlet, and 2 represents outlet

$\bar{h}_{f,i}^o$---- Enthalpy of formation of species i at 1 atm and 25 ^{o}C

$\Delta h_{T,i}^o$----- Change of enthalpy of species i between any temperature T and 25 ^{o}C

v_i---- Stoichiometric number (+ for products and – for reactants)

$\bar{h}_T^o$---- Enthalpy of species at any given temperature T (in kelvin), kJ/kmol

The enthalpy for CO, CO_2, H_2, and H_2O is calculated using equation (3.30), and the values of coefficients in a temperature range of 1000 K – 5000 K used in equation (3.30) are shown in Table 3.5 (Bethie, 1996).

$$\bar{h}_T^o = RT(a_1 + \frac{a_2 T}{2} + \frac{a_3 T^2}{3} + \frac{a_4 T^3}{4} + \frac{a_5 T^4}{5} + \frac{a_6}{T}) \tag{3.30}$$

The enthalpy of fuel is calculated using the equation below (Aspen Plus, n.d.; Bethie, 1996):

$$HHV = \bar{h}_{f,fuel}^o - \sum_{products} v_i \left(\bar{h}_{f,i}^o\right) \tag{3.31}$$

$$\bar{h}_{f,fuel}^o = HHV + \sum_{products} v_i \left(\bar{h}_{f,i}^o\right) \tag{3.32}$$

HHV---- Higher heating value of fuel

Table 3. 5 Values of coefficients used in equation (3.30) (Bethie, 1996)

	CO	CO_2	H_2	H_2O
a_1	2.951	4.413	3.044	2.671
a_2	1.553*10^(-3)	3.192*10^(-3)	6.119*10^(-4)	3.032*10^(-3)
a_3	-6.191*10^(-7)	-1.298*10^(-6)	-7.399*10^(-9)	-8.535*10^(-7)
a_4	1.135*10^(-10)	2.415*10^(-10)	-2.033*10^(-11)	1.179*10^(-10)
a_5	-7.788*10^(-15)	-1.674*10^(-14)	2.459*10^(-15)	-6.197*10^(-15)
a_6	-1.423*10^4	-4.894*10^4	-8.549*100	-2.989*10^4

3.2.2 Zero-dimensional kinetic model

The zero-dimensional kinetic model only considers chemical reactions for the gasification process, and it is a simple model to get information of gasification products distribution with time (Wang and Kinoshita, 1993). Assumptions made for this model are described below.

1) Pyrolysis does not happen instantaneously, and pyrolysis model used in developing the two-phase kinetic model section is also used here. Pyrolysis products char, ash, H_2, CO, CO_2, CH_4, C_2H_4, tar, and H_2O take part in the following char gasification process once they are generated from pyrolysis. The other gases such as C_2H_2, C_2H_6, and the other heavier hydrocarbons are included in C_2H_4 in order to simplify simulation.
2) Char only contains pure carbon.
3) Ash, C_2H_4, and tar are inert, and do not take part in the reactions.
4) No particle attrition, entrainment and segmentation.
5) Gas behaves ideally, and gas concentration can be calculated following equation

(3.33):

$$C = \frac{P}{RT} \tag{3.33}$$

R---- Gas constant, 8.314 KJ/kmole/K

P---- Pressure, Pa

T---- Temperature, K

A general equation for the gasification process is:

$$CH_\alpha O_\beta + wH_2O = x_1C + x_2H_2 + x_3CO + x_4H_2O + x_5CO_2 + x_6CH_4 + x_7tar + x_8C_2H_4 \tag{3.34}$$

$CH_\alpha O_\beta$ is the chemical representative for corn stover, and the values of α and β were determined from the ultimate analysis of corn stover. x_i and w are moles of products and steam/biomass ratio, respectively.

After fuel enters the gasifier, it goes through pyrolysis, and pyrolysis products take part in the following char gasification. The reactions happening during char gasification process are the same as those used for the one-dimensional two-phase kinetic model.

$$C + H_2O \overset{k_1}{\rightarrow} CO + H_2 \tag{3.35}$$

$$C + CO_2 \overset{k_2}{\rightarrow} 2CO \tag{3.36}$$

$$C + 2H_2 \overset{k_3}{\rightarrow} CH_4 \tag{3.37}$$

$$CO + H_2O \overset{k_4}{\leftrightarrow} CO_2 + H_2 \tag{3.38}$$

According to equation (3.12), the evolution of CO with time can be calculated as:

$$\frac{dm_{co}}{dt} = VM_1(r_1 + 2r_2 - r_4) + m_{p,co} \tag{3.39}$$

$$\frac{dx_{co}}{dt} = V(Ak_1C_{H2O} + 2Ak_2C_{CO2} - k_4C_{CO}C_{H2O} + k_5C_{H2}C_{CO2}) + n_{p,co} \tag{3.40}$$

$$\frac{dx_{co}}{dt} = (A_tk_1x_{H2O} + 2A_tk_2x_{CO2} - k_4x_{CO}x_{H2O} + k_5x_{H2}x_{CO2})/V + n_{p,co} \tag{3.41}$$

A---- Particle surface area in unit volume, m^2 surface /m^3

A_t---- Total particle surface area in the system, m^2

$m_{p,co}$---- The amount of CO generated from pyrolysis, kg

$n_{p,co}$---- The amount of CO generated from pyrolysis, kmole

V---- Volume of gas at time t, m^3

M_1---- Molecular weight of CO, kg/kmol

m_1---- Mass of CO at time t, kg

r---- Reaction rate, kmole/(m^3.s)

k_i---- Intrinsic reaction rate of reaction i, 1/m

Similarly we can get the evolution of other species with time:

CO_2: $$\frac{dx_{CO2}}{dt} = -A_tk_2x_{CO2} + k_4x_{CO}x_{H2O} - k_5x_{H2}x_{CO2} + n_{p,co}/V \tag{3.42}$$

H_2: $$\frac{dC_{H2}}{dt} = A_tk_1x_{H2O} - 2A_tk_3x_{H2} + k_4x_{CO}x_{H2O} - k_5x_{H2}x_{CO2} + n_{p,co2}/V \tag{3.43}$$

H_2O: $$\frac{dC_{H2O}}{dt} = -A_tk_1x_{H2O} - k_4x_{CO}x_{H2O} + k_5x_{H2}x_{CO2} + n_{p,H2}/V \tag{3.44}$$

CH_4: $$\frac{dC_{CH4}}{dt} = A_tk_3x_{H2} + n_{p,CH4}/V \tag{3.45}$$

C_2H_4: $$\frac{dC_{C2H4}}{dt} = n_{p,C2H4}/V \tag{3.46}$$

Tar: $$\frac{dC_{Tar}}{dt} = n_{p,Tar}/V \quad (3.47)$$

C: $$\frac{dC_s}{dt} = -A_t k_1 x_{H2O} - A_t k_2 x_{CO2} - A_t k_3 x_{H2} + n_{p,c}/V \quad (3.48)$$

At $t = 0$ (when the fuel first enters the gasifier):

$$x_i = 0, i = 1, 2, 3, 5, 6 \quad (3.49)$$

$$x_4 = w \quad (3.50)$$

For the water-gas shift reaction, the equilibrium constant k_{eq} calculated by different equations is different (Bustamante, et al., n.d.). In addition, according to some researchers, the water-gas shift reaction cannot reach equilibrium state if the temperature is not high enough, and the value of k_{eq} is different from the theoretical value calculated (Herguido, Corella and Gonzalez-Saiz, 1992; Rapagnà, et al., 2000; Franco, et al., 2003; Wei, et al., 2007; Carpenter, et al., 2010). In this study, k_{eq} is calculated through the equation shown in Table 3.6 at 870 ^{o}C, and it is set a value obtained from the graph in the literature when the temperature is lower than 870 ^{o}C (Herguido, Corella and Gonzalez-Saiz, 1992), which is 0.25, 0.4, and 0.8 at 600, 670, and 770 ^{o}C, respectively.

A widely used un-reacted-core shrinking model is employed (Okuga, n.d.) for solid-gas reactions, as shown in Eqn. 3.51. This kind of models consider the effect of mass transfer on reaction kinetics, and the effect of particle size on the gasification process is realized through affecting the mass transfer process.

$$r_i = \frac{A_p C_i}{1/k_m + 1/k_i} \tag{3.51}$$

Where

$$k_m = \frac{2.06 U_{gas} Re^{-0.575} Sc^{-0.667}}{\varepsilon_{bed}} \tag{3.52}$$

$$Re = \frac{\rho U_{gas} d_p}{\mu_{gas}} \tag{3.53}$$

r_i---- Reaction rate of reaction i, $\frac{\text{kmol}}{\text{m}^3\text{s}}$

A_p---- Total particle surface area in unit emulsion volume, $\frac{\text{m}^2\text{surface area}}{\text{m}^3}$

C_i---- Gas concentration, $\frac{\text{kmol}}{\text{m}^3}$

k_m---- Mass transfer coefficient, $\frac{\text{m}}{\text{s}}$

k_i---- Reaction kinetics constant, $\frac{\text{m}}{\text{s}}$

ρ---- Gas density, $\frac{\text{kg}}{\text{m}^3}$

μ_{gas}---- Dynamic gas viscosity, $\frac{\text{kg}}{\text{ms}}$

$$\mu_{gas} = 1.98 \times 10^{-5} (\frac{T}{300})^{2/3} \tag{3.54}$$

U_{gas}---- Gas superficial velocity, $\frac{\text{m}}{\text{s}}$

Sc---- Schmidt number, a dimensionless ratio of momentum transport to mass transfer.

$$Sc = \frac{\mu_{gas}}{D_{gas}\rho} \tag{3.55}$$

D_{gas}---- Gas diffusivity (Okuga, n.d.)

$$D_{gas} = 8.677 \times 10^{-5} \frac{T^{1.75}}{P} \quad (3.56)$$

P---- Gas pressure in Pascal

Table 3. 6 Reaction rates for the gasification process

Chemical reaction	Reaction Kinetics	Reference
Heterogeneous reactions(kmole/(s.m^3))		
$C + H_2O \overset{k_1}{\rightarrow} CO + H_2$	$k_1 = 7.492 * 10^4 \exp\left(-\frac{22220}{T}\right)$	(Okuga, n.d.)
$C + CO_2 \overset{k_2}{\rightarrow} 2CO$	$k_2 = 7.92 * 10^4 \exp\left(-\frac{22220}{T}\right)$	(Okuga, n.d.)
$C + 2H_2 \overset{k_3}{\rightarrow} CH_4$	$k_3 = 79.2 \exp\left(-\frac{22220}{T}\right)$	(Okuga, n.d.)
Homogeneous reactions (kmole/(s.m^3))		
$CO + H_2O \overset{k_4}{\leftrightarrow} CO_2 + H_2$	$r_4 = k_4(C_{CO}C_{H2O} - \frac{C_{CO2}C_{H2}}{k_{eq}})$, $k_4 = 0.1 \times \frac{10^8}{3600} \exp\left(-\frac{12560}{RT}\right)$ $k_{eq} = 0.0265 \exp(\frac{3955.7}{T})$	(Okuga, n.d.)

Since reaction kinetics vary from one fuel to another and current studies on reaction kinetics of many fuels are limited, many researchers facilitated their research by adjusting reaction kinetics of others fuels to fit their own fuel (Neogi, et al., 1986; Giltrap, McKibbin and Barnes, 2003; Babu and Sheth, 2006; Gao and Li, 2008; Basu and Kaushal, 2009). In this study, since few studies have been found on reaction kinetics of corn stover char, following other researchers' methods, reaction kinetics of other chars were used. Because the reaction kinetics shown in Table 3.6 gave reasonable results through sensitivity analysis for the one-dimensional two-phase kinetic model, they are used in this study.

The explicit method is used for to solve the eight equations. The whole process is

programmed using Matlab, and the main calculation steps are as follows: (1) at each time step send in biomass and calculate the amount of particle pyrolyzed; (3) iterative process of solving the system of differential equations. The whole process is shown in Fig. 3.5.

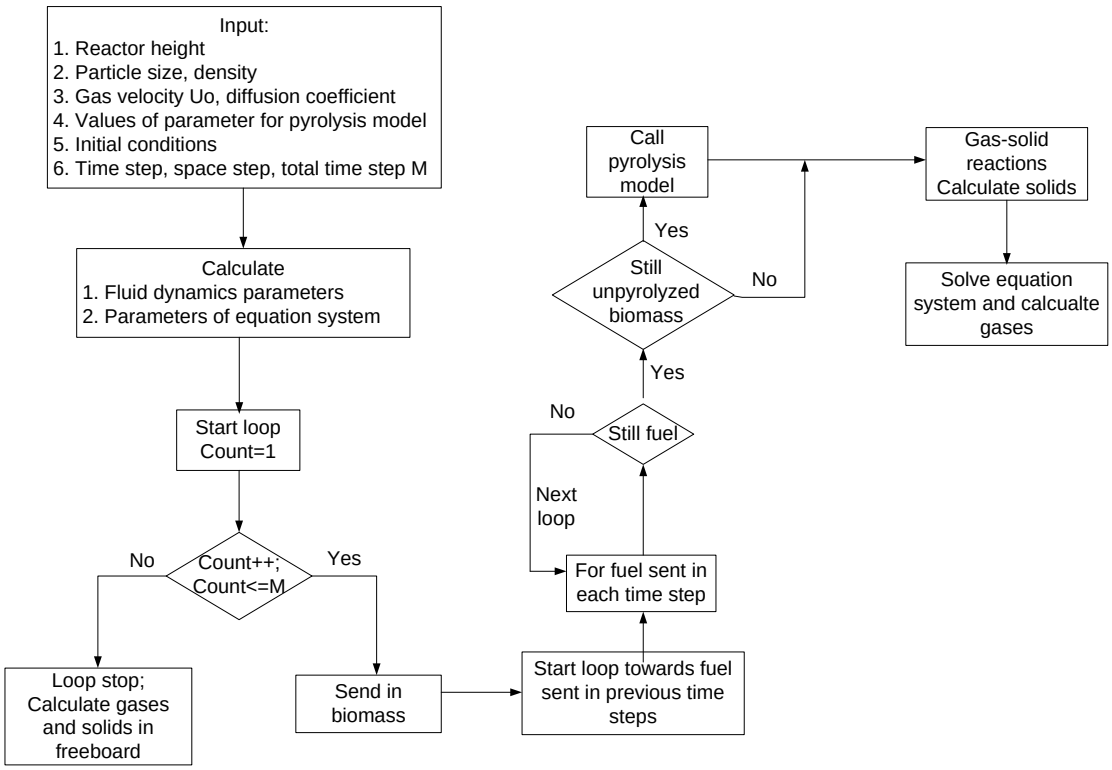

Figure 3. 5 Schematic diagram of the calculation procedure for the zero-dimensional kinetic model

3.3 One-dimensional models

3.3.1 One-dimensional one-phase kinetic model

3.3.1.1 Assumptions for the one-dimensional one-phase kinetic model

During the real gasification process, hundreds of reactions happen simultaneously and in sequence, and millions of particles with different ash and carbon contents move inside the reactors. Due to the complex characteristics of the fluidized bed gasification process, researchers usually simplify their study by making assumptions, and different assumptions are made by different researchers according to the research purpose. In this study, assumptions are also made based on this criterion: the simplification should not affect the results a lot thus this model can reflect the real process as closely as possible. Therefore, assumptions which have been widely used and proven to give better results according to literature available are chosen, and many features which were simplified in other studies are well kept here.

1) It is an unsteady state mathematical model, which includes both reaction kinetics and fluid dynamics. This gasification model includes several sub-models: pyrolysis, gasification, and solid entrainment.
2) The whole gasification process is divided into two stages: devolatilization/pyrolysis and gasification. The components of pyrolysis products are char, ash, H_2, CO, CO_2, CH_4, C_2H_x, tar, and H_2O. The other gases such as C_2H_2, C_2H_4, and C_2H_6 are included in C_2H_x in order to simplify simulation. Both

pyrolysis and char gasification are controlled by reaction kinetics.

3) The temperature of the whole reactor is uniform.

4) For many kinetic models, solids in the reactor contain carbon and sand (Sadaka et al 2002; Gordillo and Belghit, 2011a; b) Since the amount of char produced in this study is mainly determined by solid entrainment which is highly related to particle size, and since ash plays an important role in particle entrainment, solids in this study include sand, un-reacted biomass, mixture of un-reacted biomass, carbon and ash, and mixture of carbon and ash.

5) Char is pure carbon. Ash is inert, and does not take part in reactions. Due to the lack of related theories and experimental data, char deactivation and particle fragmentation are not considered. Therefore, particles keep taking part in chemical reactions as long as there is carbon in the particles, and the number of particles does not change.

6) Due to rapid mass transfer solids are well mixed and homogeneously distributed inside the fluidized bed, and mass balance for solid phase in the fluidized bed section is global (Chejne and Hernandez, 2002). Difference in gas concentration in radial direction is neglected, and gas concentration gradient only exists in axial direction for both bubble phase and emulsion phase. Gases in the system consist of CO, CO_2, H_2, CH_4, H_2O, tar, and C_2H_x.

7) Condition over the fluidized bed cross section is uniform.

8) The size of particles decreases due to chemical reactions. Once the particle velocity is less than its terminal velocity, particles are entrained out of the

fluidized bed to the freeboard immediately. All the particles entering the freeboard do not return to the fluidized bed.

9) Mass transfer influences gas-solid reactions, thus mass transfer is considered in the reaction kinetics. Particle is impervious, and no diffusion exists inside particles. Gas-solid reactions take place on the surface of un-reacted core. The ash layer formed on the surface of un-reacted core peels off immediately due to severe collisions in the bed. Particles are isothermal.
10) Based on different bed hydrodynamics the whole reactor is divided into two parts: fluidized bed and freeboard. Both the fluidized bed and the freeboard are modeled as a one-phase system. Both solid-gas and gas-gas reactions take place in the fluidized bed, while only the gas-gas reaction takes place in the freeboard.

The whole reactor is divided into a series of infinitely thin vertical elemental cylinders of dz thickness up to the gasifier outlet, and the gas concentration in each element is uniform. Governing equations are established for each species in each element in differential form. Because seven kinds of gases are involved in the system: CO, CO_2, H_2O, H_2, CH_4, tar, and C_2H_x, there are 8 governing equations in each element: 7 for gases and 1 for solid particles.

3.3.1.2 Model development for the fluidized bed

A schematic diagram of an element in the fluidized bed is shown in Fig. 3.6.

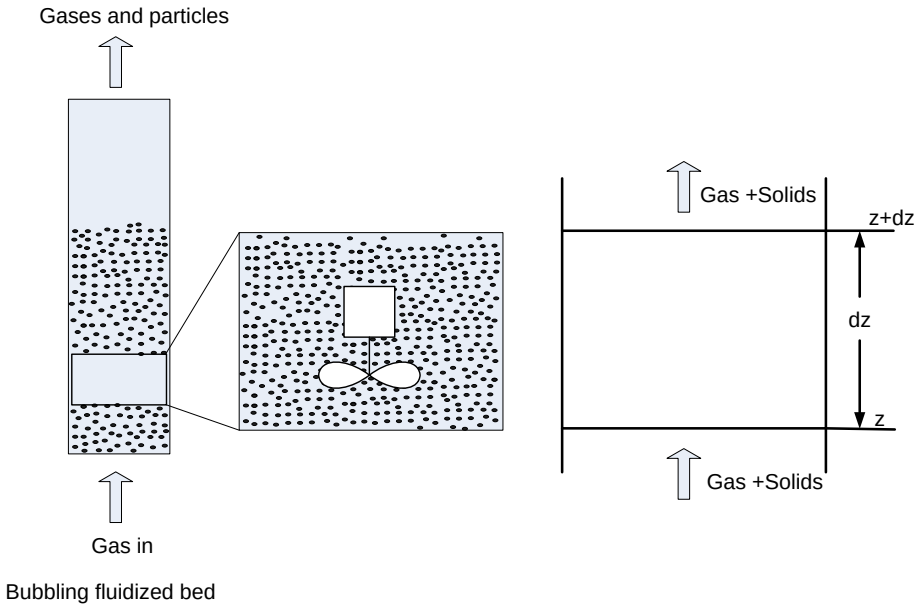

Figure 3. 6 Schematic representation of the one-dimensional one-phase model

For an element j with a height of ΔZ, the mass balance is shown below:

Accumulation of species i = rate of species i in by convection - rate of species i out by convection + rate of species i in by dispersion - rate of species i out by dispersion - rate of species i by exchange between bubble and emulsion phase + rate of species i by chemical reaction. (3.57)

The amount of species i entering element j from element j-1 by convection during unit time is

$$AC_{i,j-1}U_o \tag{3.58}$$

$C_{i,j-1}$---- Average molar concentration of species i in element j-1, $\frac{\text{kmole}}{\text{m}^3}$

U_o---- Gas superficial velocity neglecting velocity increase due to gas production, m/s

A---- cross area of the fluidized bed, m^2

The amount of species i leaving element j to element j+1 by convection during unit time is

$$AC_{i,j}U_o \tag{3.59}$$

$C_{i,j}$---- Average molar concentration of species i in element j, $\frac{\text{kmole}}{\text{m}^3}$

The amount of species i entering element j from element j-1 by diffusion during unit time is

$$-DA\frac{\partial C_{i,j-1}}{\partial z} \tag{3.60}$$

D---- Diffusion coefficient, $\frac{\text{m}^2}{\text{s}}$

The amount of species i leaving element j to element j+1 by diffusion during unit time is

$$-DA\frac{\partial C_{i,j}}{\partial z} \tag{3.61}$$

The amount of species i generated through chemical reactions during unit time is

$$R_{i,j}A\Delta Z \tag{3.62}$$

$R_{i,j}$---- Production rate of species i through chemical reactions, $\frac{\text{kmole}}{\text{m}^3\text{s}}$

The amount of species *i* generated through biomass pyrolysis during unit time is:

$$n_{i,j}A\Delta Z \tag{3.63}$$

$n_{i,j}$---- Production rate of species *i* through biomass pyrolysis, $\frac{\text{kmole}}{\text{m}^3\text{s}}$

The net amount of species i increased in element j during unit time is

$$\Delta(C_{i,j}A\Delta Z)/\Delta t \tag{3.64}$$

t---- Time, s

So the governing equation for species i in the bubble phase in element j during unit

time is

$$\frac{\partial(C_{i,j}A\Delta Z)}{\partial t} = \left(AC_{i,j-1}U_O - AD\frac{\partial C_{i,j-1}}{\partial z}\right) - \left(AC_{i,j}U_O - AD\frac{\partial C_{i,j}}{\partial z}\right) + R_{i,j}A\Delta Z + n_{i,j}A\Delta Z \tag{3.65}$$

$$\frac{\partial(C_{i,j})}{\partial t} = \left(\frac{U_O}{\Delta Z}C_{i,j-1} - \frac{D}{\Delta Z}\frac{\partial C_{i,j-1}}{\partial z}\right) - \left(\frac{U_O}{\Delta Z}C_{i,j} - \frac{D}{\Delta Z}\frac{\partial C_{i,j}}{\partial z}\right) + R_{i,j} + n_{i,j} \tag{3.66}$$

$$\left(1 + \frac{2Ddt}{dz^2} + \frac{U_o dt}{dz}\right)C_{i,j}^{n+1} - \left(\frac{Ddt}{dz^2} + \frac{U_o dt}{dz}\right)C_{i,j-1}^{n+1} - \frac{Ddt}{dz^2}C_{i,j+1}^{n+1} = C_{i,j}^{n} + dtR_{i,j} + dtn_{i,j} \tag{3.67}$$

The solid phase includes inert bed materials, ash and char. First of all, it is important to make clear the definition of char and ash. The term char and ash can be confusing since in some studies char is a mixture of carbon and ash, while in some other studies char is merely carbon (Reed and Das, 1988; Brewer, Unger and Brown, 2009; Carpenter, et al., 2010; Klinghoffer, Castaldi and Nzihou, 2011; Pan and Eberhardt, 2011). However, it is generally accepted that the byproduct of pyrolysis or gasification is a solid residue, and it contains both carbon and ash. Depending on the carbon content, the solid residue can be classified as char (high carbon content) or ash (low carbon content). In this study, char means pure carbon, and solid phase includes inert bed material, biomass, mixture of biomass, ash and char, and mixture of ash and char. During the real gasification process, the solid phase can be very complex due to the following phenomena:

1) Char accumulation During the real fluidized bed gasification process, once fuel particles are sent to the bed they go through a series of reactions, during which the size

of fuel particle decreases. The particles will be entrained out of the bed when the size of particles is small enough. Due to the reaction kinetics, char produced from pyrolysis cannot be gasified immediately, and it takes some time to reduce the particle size. Therefore, before the particles can be entrained out of the bed, they will stay and accumulate in the bed. Char accumulation is affected by operating conditions, ash content, and reaction kinetics, etc, and it varies with time. Here, the term accumulation merely means remaining in bed, and is not related with steady state or unsteady state, and it does not matter whether the bed can reach steady state or not. With this definition, since in every reactor there is always some amount of char in the bed there is char accumulation in each reactor. However, there is also another meaning of the term accumulation, which means the amount of char in the bed increases all the time (NETL, n.d.; Granatstein, n.d.; Scott, et al., n.d.; Miccio, 1999; Chattopadhyay, 2000; Bayarsaikhan, et al., 2006; Salam, Kumar and Siriwardhana, 2010), and with this meaning the bed cannot reach steady state. Therefore, the term accumulation can be confusing. In order to avoid confusion, in this study the second definition is used. Due to lack of both theoretical and experimental information on char accumulation, here it is assumed that the bed can reach steady state and there is no char accumulation in the bed. Here the term steady state means the amount of char and biomass in the bed remain constant.

2) Char deactivation. One assumption used for models developed is that char particles will keep taking part in reactions until their sizes are small enough to be entrained out of the bed, and the reaction kinetics remains the same during the entire

gasification as long as the temperature does not change. In the real situation, the reaction kinetics of char changes during the entire process, and char reactions slowdown or stops as reactions proceed due to char deactivation whose possible reasons may be thermal annealing, carbon dilution, and limited mass, especially for medium and high ash content fuels (Scott, et al., n.d.; Miccio, 1999; Stringel, 2011). Therefore, even though the bed can reach steady-state, the amount of char calculated in the bed is still different from that obtained in the real process. The extent to which char loses its reactivity is unknown due to lack of experimental information. In order to simplify the study, here it is assumed that reaction kinetics of char remains the same during the entire gasification process.

3) Char fragmentation During the process of pyrolysis and gasification, when carbon is consumed on both the surface and in the interior of the particle, pores inside the particle are enlarged and broken down and the particle losses its mechanical strength. At the same time, the particle swells. As the reaction proceeds at critical value of porosity, fragmentation happens caused by pressure buildup within the particle (Singer and Ghoniem, n.d.; Reed and Das, 1988; Basu 2006, p.116; Ammendola and Scala, 2012). Generally there are two types of fragmentation: primary, and secondary. During primary fragmentation, a particle is broken into several pieces that are smaller than but comparable to the size of the parent particle, while during secondary fragmentation, fragments produced are an order of magnitude larger than the attired fines in size. The fragments generated can be further reduced to smaller sizes due to attrition of bed materials. For wood, since its ash content is low, in the absence of a coherent ash

skeleton, fragmentation happens when the mechanical strength is week, increasing reactivity. For high ash content, due to the mechanical resistance of ash skeleton, the fuel does not go through fragmentation, and its shape and volume does not change a lot (Miccio, 1999). For high ash content fuel, the carbon is diluted by ash, and mass transfer is limited by ash, and the size is large, so its reactivity is low (Miccio, 1999).

In this model, both char deactivation and fragmentation are neglected due to lack of both theoretical and experimental information. Even without considering char deactivation and fragmentation, char still experiences a very complex process as shown in Fig. 3.7. After fuels are sent to the bed at each time step, fuel particles experience, pyrolysis, char gasification, and attrition at the same time (At the beginning attrition model was included. However, since the simulation time is very long, in order to use strategies to decrease the simulation time, attrition model was excluded later). Once the fuel particles are small enough they are entrained out of the fluidized bed. When the particles are entrained out of the bed, they may contain both char and unpyrolyzed biomass, or only contain char or unpyrolyzed biomass. In this model, the composition(s) of particles entrained out of the bed are predicted by the entrainment model, pyrolysis model, and char reaction model together.

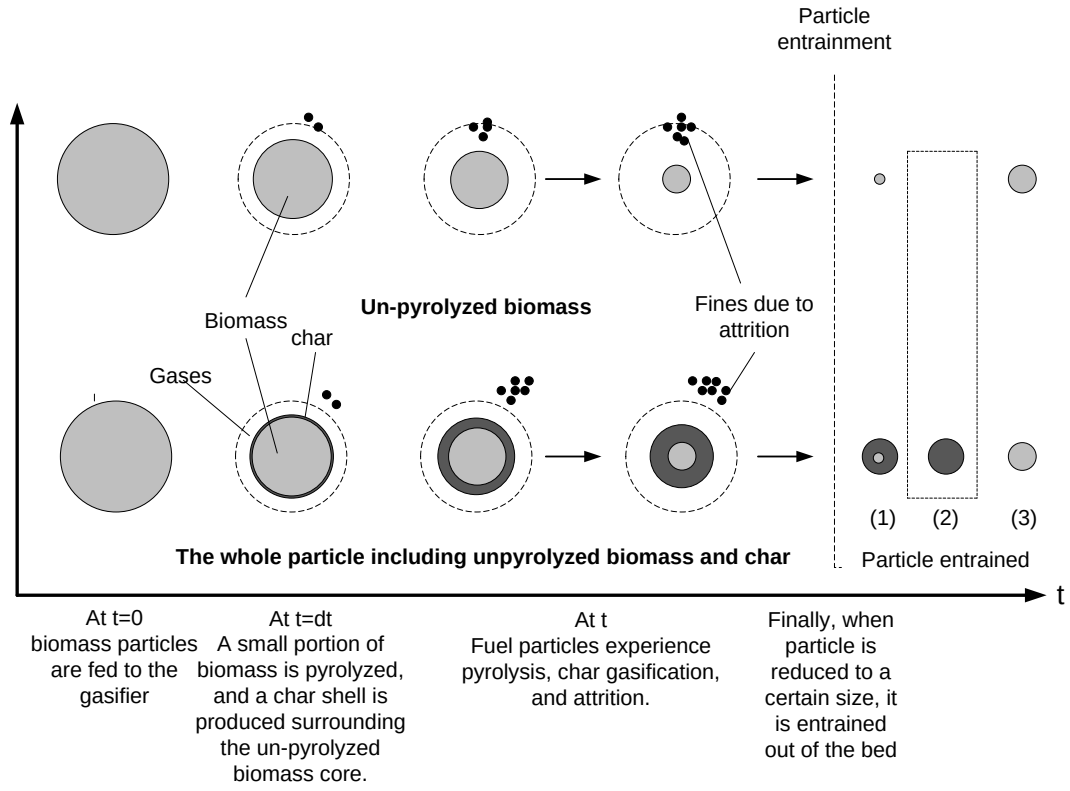

Figure 3. 7 Schematic diagram of the evolution of a single char particle in the bed

Before particles are entrained out of the fluidized bed, they stay in the bed and take part in reactions and particle attrition. The size of particles and the portion of ash and char in the total particle are different for particles sent to the bed at different time steps. Therefore, based on the value of reaction rates and superficial gas velocity, the number of particle sizes in the bed varies from hundreds to several thousands. Due to the well-mixed feature of the fluidized bed, it is assumed that particles of different sizes are distributed evenly in the fluidized bed. The amount of char consumed and gas generated/consumed through char-gas reactions is calculated in each element for each particle size, which will be used in the governing equations for gases.

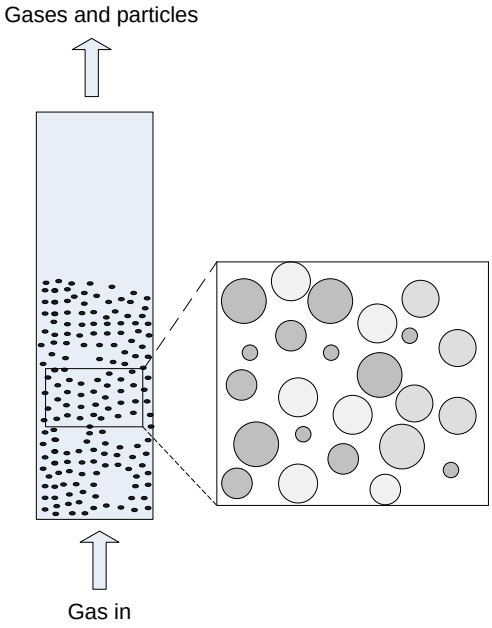

Figure 3. 8 Schematic diagram of particles in bed

The mass balance for char is global (De Souza-Santos, 1989; Milioli and Foster, 1995; Chejne and Hernandez, 2002):

Change of char in the bed = char generated through pyrolysis – char consumed through chemical reactions – char entrained out of the bed (3.68)

The change of mass of char in the bed during unit time: $\frac{\partial m_c}{\partial t}$

The amount of char generated through pyrolysis during unit time in the bed: m_p

The mass of char entrained out of the bed during unit time in the bed: m_E

Char consumed through chemical reactions in the whole bed: $\int_0^L \sum_{i=1}^{3} r_{i,j} A_{p,j}\, dz$

Therefore:

$$\frac{\partial m_c}{\partial t} = \int_0^L \sum_{i=1}^{3} r_{i,j} A_{p,j} M_c dz + m_p + m_E \tag{3.69}$$

m_c---- Total mass of char in the fluidized bed, kg

m_p---- The amount of char generated through fuel pyrolysis, kg/s

m_E---- The amount of char entrained out of the bed, kg/s

$r_{i,j}$---- Reaction rate of char reaction i in element j, $\frac{\text{kmole}}{\text{m}^2\text{surface area.s}}$

$A_{p,j}$---- Total particle surface area in unit volume in element j, $\frac{\text{m}^2}{\text{m}^3\text{.s}}$

M_c---- Molecular weight of carbon, kg/kmol

The expression of reaction rates used in the governing equations developed are shown below:

$$R_{g,j} = k_4 ({C_{1,j}}^{n+1} {C_{4,j}}^{n+1} - \frac{{C_{2,j}}^{n+1} {C_{3,j}}^{n+1}}{k_{eq}}) \tag{3.70}$$

$$R_{1,j} = M_c A_{p,j} \left(k_{t,1} {C_{4,j}}^{n-1} + 2k_{t,2} {C_{2,j}}^{n-1}\right) - R_{g,j} \tag{3.71}$$

$$R_{2,j} = -M_c A_{p,j} k_{t,2} {C_{2,j}}^{n-1} + R_{g,j} \tag{3.72}$$

$$R_{3,j} = M_c A_{p,j} (k_{t,1} {C_{4,j}}^{n-1} - 2k_{t,3} {C_{3,j}}^{n-1}) + R_{g,j} \tag{3.73}$$

$$R_{4,j} = -M_c A_{p,j} k_{t,1} {C_{4,j}}^{n-1} - R_{g,j} \tag{3.74}$$

$$R_{5,j} = -M_c A_{p,j} k_{t,3} {C_{3,j}}^{n-1} \tag{3.75}$$

$$R_{6,j} = 0 \tag{3.76}$$

$$R_{7,j} = 0 \tag{3.77}$$

$k_{t,i}$---- Total reaction rate constant including mass transfer, $\frac{\text{m}}{\text{s}}$

3.3.1.3 Model development process for the freeboard

A schematic diagram of an element j in the freeboard is shown in Fig. 3.9.

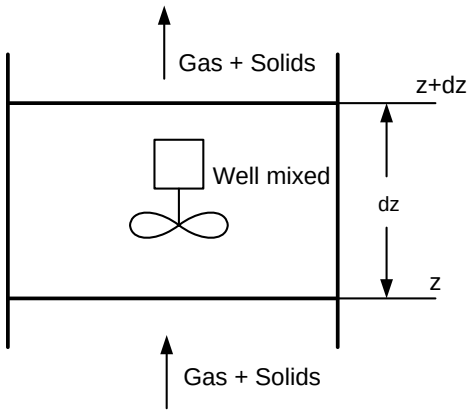

Figure 3. 9 Schematic of an element in the freeboard for the zero-dimensional one-phase kinetic model

There is only one phase in each element, and each species has one governing equation in each element. The amount of species i entering the element j from element j-1 by convection during unit time is

$$A_{f,j-1}C_{f,i,j-1}U_{f,j-1} \tag{3.78}$$

$A_{f,j-1}$---- Cross section area in element j, m^2

$C_{f,i,j-1}$---- Average gas concentration of species i in element j, $\frac{\mathrm{kmole}}{\mathrm{m}^3}$

$U_{f,j-1}$---- Average gas velocity in element j, $\mathrm{m/s}$

The amount of species i leaving the j element to j+1 element by convection during unit time is

$$A_{f,j}C_{f,i,j}U_{f,j} \tag{3.79}$$

The amount of species i generated through chemical reactions during unit time is

$$R_{f,i,j}A_{f,j}\Delta Z \tag{3.80}$$

Assume steady-state, so the governing equation of species i in element j is

$$A_{f,j-1}C_{f,i,j-1}U_{f,j-1} - A_{f,j}C_{f,i,j}U_{f,j} + R_{f,i,j}A_{f,j}\Delta Z = 0 \tag{3.81}$$

$$\frac{A_{f,j-1}U_{f,j-1}}{A_{f,j}\Delta Z}C_{f,i,j-1} - \frac{U_{f,j}}{\Delta Z}C_{f,i,j} + R_{f,i,j} = 0 \tag{3.82}$$

The governing equation of char in element j is

$$R_{f,j} = k_4({C_{f,1,j}}^{n-1}{C_{f,4,j}}^{n-1} - \frac{{C_{f,2,j}}^{n-1}{C_{f,3,j}}^{n-1}}{k_{eq}}) \tag{3.83}$$

$$R_{f,1,j} = -R_{f,j} \tag{3.84}$$

$$R_{f,2,j} = R_{f,j} \tag{3.85}$$

$$R_{f,3,j} = R_{f,j} \tag{3.86}$$

$$R_{f,4,j} = -R_{f,j} \tag{3.87}$$

$$R_{f,5,j} = 0 \tag{3.88}$$

$$R_{f,6,j} = 0 \tag{3.89}$$

$$R_{f,7,j} = 0 \tag{3.90}$$

3.3.1.4 Boundary and initial conditions

For element 1 in the fluidized bed

The amount of species i leaving from element 1to element 2 during unit time is

$$(C_{i,1}U_oA - AD\frac{\partial C_{i,1}}{\partial z})$$

(3.91)

The amount of species i generated through chemical reactions during unit time is

$$R_{i,1}Adz/2 \tag{3.92}$$

The amount of species *i* generated through biomass pyrolysis during unit time is:

$$n_{i,1}A\Delta Z/2 \tag{3.93}$$

The amount of species i entering element 1during unit time is n_o. So

$$\frac{\partial(C_{i,1}Adz/2)}{\partial t} = n_o - (C_{i,1}U_oA - AD\frac{\partial C_{i,1}}{\partial z}) + \frac{R_{i,1}Adz}{2} + n_{i,j}A\Delta Z/2 \tag{3.94}$$

$$\frac{\partial(C_{i,1})}{\partial t} = \frac{2n_o}{Adz} - \left(\frac{2U_o}{dz}C_{i,1} - \frac{2D}{dz}\frac{\partial C_{i,1}}{\partial z}\right) + R_{i,1} + n_{i,j} \tag{3.95}$$

$$\left(1 + \frac{2Ddt}{dz^2} + \frac{2U_odt}{dz}\right)C_{i,1}^{n+1} - \frac{2Ddt}{dz^2}C_{i,2}^{n+1} = C_{i,1}^{n} + \frac{2n_odt}{Adz} + dtR_{i,1} + dtn_{i,1} \tag{3.96}$$

For element NN in the fluidized bed

The amount of species i leaving from element NN-1 to element NN by convection during unit time is

$$C_{i,NN-1}U_oA \tag{3.97}$$

The amount of species i generated through chemical reactions during unit time is

$$\frac{R_{i,NN}Adz}{2} \tag{3.98}$$

The amount of species i leaving element NN during unit time is

$$C_{i,NN}U_oA \tag{3.99}$$

The amount of species i entering from element NN-1 to element NN by diffusion during unit time is

$$-AD\frac{\partial C_{i,NN-1}}{\partial z} \tag{3.100}$$

The amount of species *i* generated through biomass pyrolysis during unit time is:

$$n_{i,NN} A \Delta Z/2 \tag{3.101}$$

The net amount of species i generated during unit time is

$$\Delta(C_{i,NN} A dz/2)/\Delta t \tag{3.102}$$

So

$$\frac{\partial(C_{i,NN} A dz/2)}{\partial t} = (C_{i,NN-1} U_o A - AD \frac{\partial C_{i,NN-1}}{\partial z}) - C_{i,NN} U_o A + \frac{R_{i,NN} A dz}{2} + n_{i,j} A \Delta Z/2 \tag{3.103}$$

$$\frac{\partial(C_{i,NN})}{\partial t} = \left(\frac{2U_o}{dz} C_{i,NN-1} - \frac{2D}{dz} \frac{\partial C_{i,NN-1}}{\partial z}\right) - \frac{2U_o}{dz} C_{i,NN} + R_{i,NN} + n_{i,j} \tag{3.104}$$

$$\frac{\partial(C_{i,NN})}{\partial t} = \left(\frac{2U_o}{dz} C_{i,NN-1} - \frac{2D}{dz} \frac{\partial C_{i,NN-1}}{\partial z}\right) - \frac{2U_o}{dz} C_{i,NN} + R_{i,NN} + n_{i,j} \tag{3.105}$$

$$\left(1 + \frac{2Ddt}{dz^2} + \frac{2U_o dt}{dz}\right) C_{i,NN}^{n+1} - \left(\frac{2Ddt}{dz^2} + \frac{2U_o dt}{dz}\right) C_{i,NN-1}^{n+1} = C_{i,NN}^{n} + dt R_{i,NN} + dt n_{i,NN} \tag{3.106}$$

Initial conditions are as follows (Raman, 1981; Sadaka, Ghaly and Sabbah, 2002; Gordillo and Belghit, 2011a; b):

$$C_{b,i} = 0, \text{ at } t = 0 \tag{3.107}$$

$$C_{e,i} = 0, \text{ at } t = 0 \tag{3.108}$$

$$C_{f,i} = 0, \text{ at } t = 0 \tag{3.109}$$

3.3.1.5 Calculation procedure

The explicit method is used for the solid phase, and the implicit method is used to solve the nonlinear, time-dependent, partial differential equations for gases. The whole process is programmed using Matlab, and the main calculation steps are as follows: (1) input of gas superficial velocity and bed geometry, and calculate parameters for fluid

dynamics; (2) at each time step calculate the amount of particle pyrolyzed, and determine whether some particles can be entrained out of the bed or not; (3) calculate the amount of particles consumed and the amount of gases generated during the char gasification process; (4) iterative process of solving the system of differential equations. The schematic diagram for the whole process is shown in Fig. 3.10.

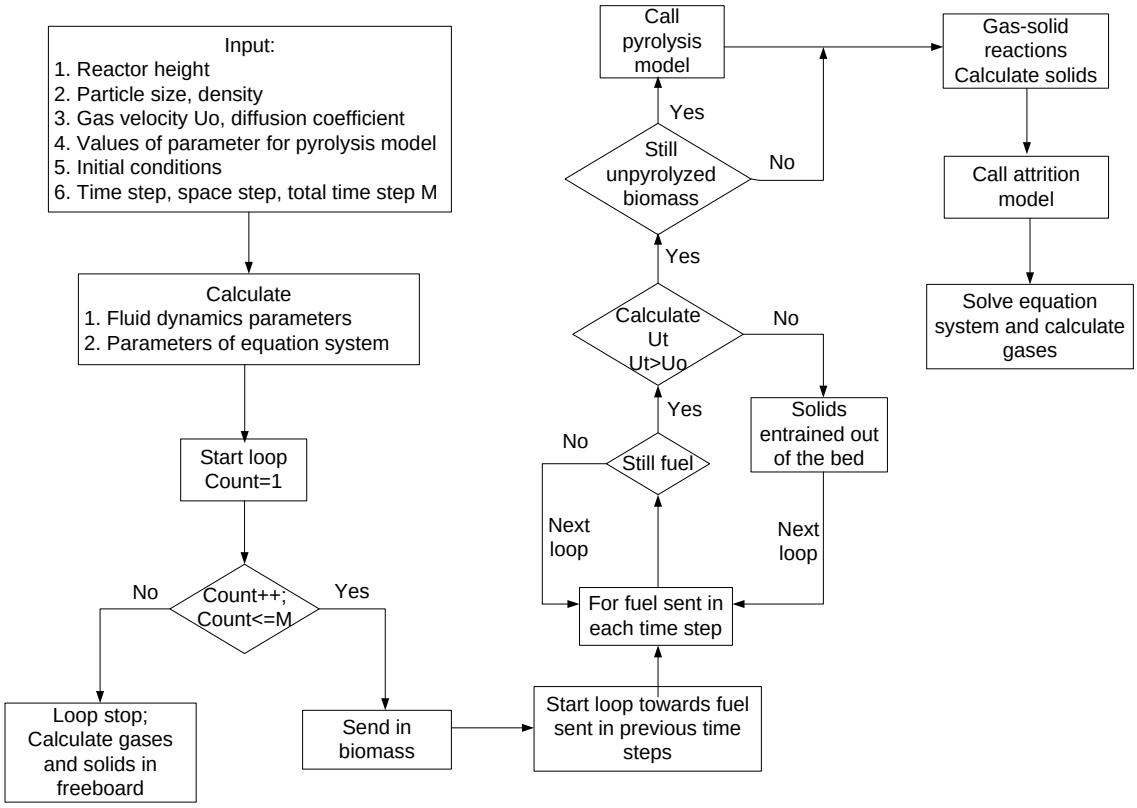

Figure 3. 10 Schematic diagram of calculation procedure for the one-dimensional one-phase kinetic model

3.3.2 One-dimensional two-phase kinetic model

The one-dimensional two-phase kinetic model is similar to the one-dimensional

one-phase kinetic model, and part of its model development process is the same as that of the one-dimensional one-phase kinetic model. In this section, the model development process that has been introduced in section 3.3.1 will not be repeated here.

3.3.2.1 Assumptions for the one-dimensional two-phase kinetic model

The assumptions through (1) to (9) used here are the same as those used for the one-dimensional one-phase kinetic model, and they are repeated here to for completeness.

1) It is an unsteady state mathematical model, which includes both reaction kinetics and fluid dynamics. This gasification model includes several sub-models: pyrolysis, gasification, and solid entrainment.
2) The whole gasification process is divided into two stages: devolatilization/pyrolysis and gasification. The components of pyrolysis products are char, ash, H_2, CO, CO_2, CH_4, C_2H_x, tar, and H_2O. The other gases such as C_2H_2, C_2H_4, and C_2H_6 are included in C_2H_x in order to simplify simulation. Both pyrolysis and char gasification are controlled by reaction kinetics.
3) The temperature of the whole reactor is uniform.
4) For many kinetic models, solids in the reactor contain carbon and sand (Sadaka et al 2002; Gordillo and Belghit, 2011a; b) Since the amount of char produced in this study is mainly determined by solid entrainment which is highly related to particle

size, and since ash plays an important role in particle entrainment, solids in this study include sand, un-reacted biomass, mixture of un-reacted biomass, carbon and ash, and mixture of carbon and ash.

5) Char is pure carbon. Ash is inert, and does not take part in reactions. Due to the lack of related theories and experimental data, char deactivation and particle fragmentation are not considered. Therefore, particles keep taking part in chemical reactions as long as there is carbon in the particles, and the number of particles does not change.
6) Due to rapid mass transfer solids are well mixed and homogeneously distributed inside the fluidized bed, and mass balance for solid phase in the fluidized bed section is global (Chejne and Hernandez, 2002). Difference in gas concentration in radial direction is neglected, and gas concentration gradient only exists in axial direction for both bubble phase and emulsion phase. Gases in the system consist of CO, CO_2, H_2, CH_4, H_2O, tar, and C_2H_x.
7) Condition over the fluidized bed cross section is uniform.
8) The size of particles decreases due to chemical reactions and bed material abrasion. Once particle velocity is less than its terminal velocity, particles are entrained out of the fluidized bed to the freeboard immediately. All the particles entering the freeboard do not return to the fluidized bed.
9) Mass transfer influences gas-solid reactions, thus mass transfer is considered in the reaction kinetics. Particle is impervious, and no diffusion exists inside particles. Gas-solid reactions take place on the surface of un-reacted core. The ash layer

formed on the surface of un-reacted core peels off immediately due to severe collisions in the bed. Particles are isothermal.

10) Based on different bed hydrodynamics the whole reactor is divided into two parts: fluidized bed and freeboard. Since bed material (sand) which is used to facilitate fluidization takes a relatively large part of the fluidized bed, the fluidized bed is modeled as a two-phase system (shown in Fig. 3.11). The rest part of the gasifier is called freeboard, and is modeled as a one-phase system. When the fluidized bed is used as a chemical reactor the freeboard is not only a place for disengagement of solids from gas, but also for addition reactions between gases and solids. For the reactions in the freeboard for the fluidized bed gasification, some researchers assumed only gas-gas reactions (Lavoie, Chaouki and Drouin, n.d.; Jiang, 1991), and some researchers assumed solid-gas reactions also happen (De Souza-Santos, 1989; Radmanesh, Chaouki and Guy, 2006). Here it is assumed that there are no solid-gas reactions in the freeboard.

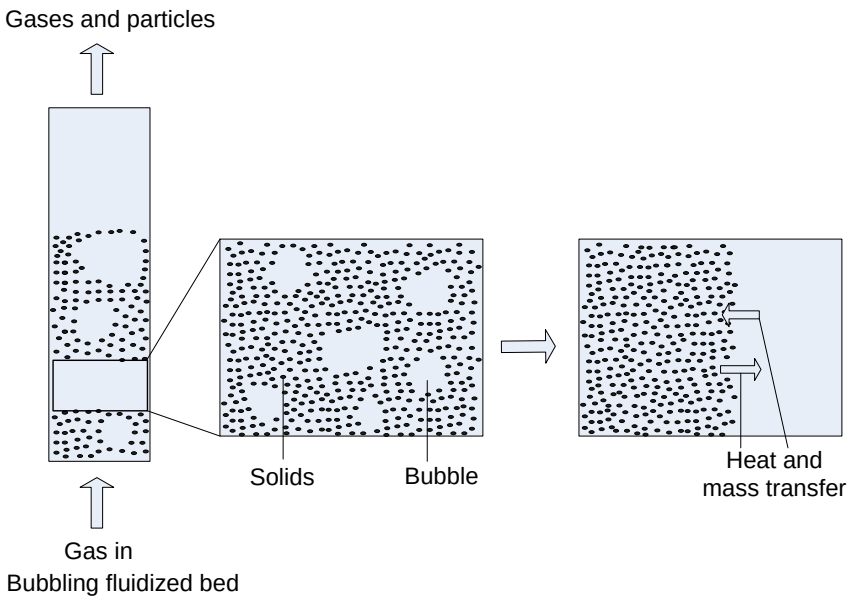

Figure 3. 11 Schematic diagram of the one-dimensional two-phase kinetic model

11) According to Lu et al., well-mixed model predicts a higher conversion rate than the real one due to the reason that both bubble and emulsion phases exist in the fluidized bed, and there is gas exchange between the bubble and the emulsion phase (Lu, et al. 2008). In this study the fluidized bed consists of a bubble phase and an emulsion phase. Emulsion phase consists of gases, char, and bed material (sand), and the bubble phase is free of solids. Mass exchange takes place between the bubble phase and the emulsion phase, and mass transfer considers both convection and dispersion.

12) Flow of gas in excess of the minimum fluidization velocity passes through the bed in the form of bubbles. The voidage of the emulsion remains constant, and is equal to that at incipient fluidization.

3.3.2.2 Model development

The whole reactor is divided into a series of infinitely thin vertical elemental cylinders of dz thickness up to the gasifier outlet as indicated by the figure below, and gas concentration of each phase in each element is uniform. Governing equations are established for each species of each phase in each element in differential form. Because seven kinds of gases are involved in the system: CO, CO_2, H_2O, H_2, CH_4, tar, and C_2H_x, there are 14 governing equations in each element: 7 for bubble phase and 7 for emulsion phase. The process of establishing governing equations in the fluidized bed and the freeboard will be introduced in the following sections, respectively.

For the fluidized bed

A schematic diagram of an element in the fluidized bed is shown in Fig. 3.12.

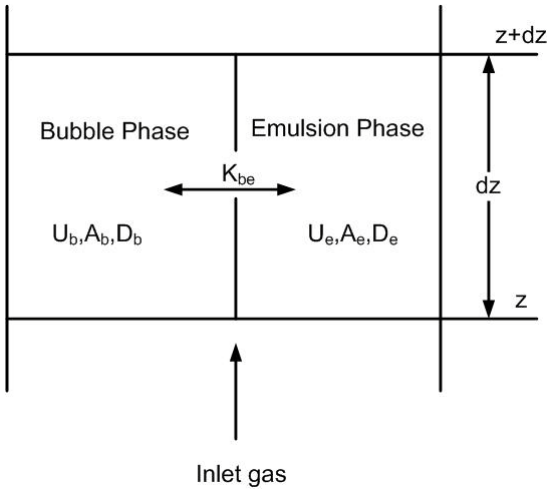

Figure 3. 12 Schematic representation of elements in the fluidized bed

There are two phases in each element, and each species has two governing equations:

one for the bubble phase, and the other for emulsion phase. For an element j with a height of ΔZ in the bubble phase, the mass balance is shown below:

Accumulation of species i= rate of species i in by convection- rate of species i out by convection+ rate of species i in by dispersion- rate of species i out by dispersion $_+$ rate of species i by exchange between bubble and emulsion phase + rate of species i by chemical reaction. (3.110)

The amount of species i entering element j from element j-1 by convection during unit time is

$$A_{b,j-1}C_{b,i,j-1}U_{b,j-1} \quad (3.111)$$

$C_{b,i,j-1}$---- Average molar concentration of species i of bubble phase in element j-1, $\frac{\text{kmole}}{\text{m}^3}$

$U_{b,j-1}$---- Average gas velocity of bubble phase in element j-1, m/s

$A_{b,j-1}$---- Average area of bubble phase in element j-1, m^2

The amount of species i leaving element j to element j+1 by convection during unit time is

$$A_{b,j}C_{b,i,j}U_{b,j} \quad (3.112)$$

$C_{b,i,j}$---- Average molar concentration of species i in bubble phase in element j, $\frac{\text{kmole}}{\text{m}^3}$

$U_{b,j}$---- Average gas velocity of bubble phase in element j, m/s

$A_{b,j}$---- Average area of bubble phase in element j, m^2

The amount of species i entering element j from element j-1 by diffusion during unit

time is

$$-D_b A_{b,j-1} \frac{\partial C_{b,i,j-1}}{\partial z} \tag{3.113}$$

The amount of species i leaving element j to element j+1 by diffusion during unit time is

$$-D_b A_{b,j} \frac{\partial C_{b,i,j}}{\partial z} \tag{3.114}$$

D_b---- Mass diffusion coefficient of the bubble phase, $\frac{\mathrm{m}^2}{\mathrm{s}}$

The amount of species i passing from the bubble phase to the emulsion phase in element j during unit time is

$$K_{be}\left(C_{b,i,j} - C_{e,i,j}\right) A_{b,j} \Delta Z \tag{3.115}$$

K_{be}---- Mass transfer coefficient between emulsion phase and bubble phase, $\frac{1}{\mathrm{s}}$

The amount of species i generated through chemical reactions during unit time is

$$R_{b,i,j} A_{b,j} \Delta Z \tag{3.116}$$

The net amount of species i increased in element j during unit time is

$$\Delta(C_{b,i,j} A_{b,j} \Delta Z)/\Delta t \tag{3.117}$$

So the governing equation for species i in the bubble phase in element j during unit time is

$$\begin{aligned} \frac{\partial(C_{b,i,j} A_{b,j} \Delta Z)}{\partial t} &= \left(A_{b,j-1} C_{b,i,j-1} U_{b,j-1} - A_{b,j-1} D_b \frac{\partial C_{b,i,j-1}}{\partial z}\right) \\ &- \left(A_{b,j} C_{b,i,j} U_{b,j} - A_{b,j} D_b \frac{\partial C_{b,i,j}}{\partial z}\right) \\ &- K_{be}\left(C_{b,i,j} - C_{e,i,j}\right) A_{b,j} \Delta Z + R_{b,i,j} A_{b,j} \Delta Z \end{aligned} \tag{3.118}$$

$$\frac{\partial C_{b,i,j}}{\partial t} = \left(\frac{A_{b,j-1}U_{b,j-1}}{A_{b,j}\Delta Z}C_{b,i,j-1} - \frac{A_{b,j-1}D_b}{A_{b,j}\Delta Z}\frac{\partial C_{b,i,j-1}}{\partial z}\right)$$

$$-\left(\frac{U_{b,j}}{\Delta Z}C_{b,i,j} - \frac{D_b}{\Delta Z}\frac{\partial C_{b,i,j}}{\partial z}\right) - K_{be}\left(C_{b,i,j} - C_{e,i,j}\right) + R_{b,i,j} \qquad (3.119)$$

t---- Time, s

$R_{b,i,j}$---- Production rate of species i in bubble phase through chemical reactions, $\frac{\text{kmole}}{\text{m}^3\text{s}}$

The procedure for developing governing equations for an element in the emulsion phase is similar to that for the bubble phase, and the only difference is that there is a source item for the emulsion phase due to fuel pyrolysis. The governing equation for species i in the emulsion phase in element j is:

$$\frac{\partial(C_{e,i,j}A_{e,j}\Delta Z E_{mf})}{\partial t} = \left(A_{e,j-1}C_{e,i,j-1}U_{e,j-1} - E_{mf}D_e A_{e,j-1}\frac{\partial C_{e,i,j-1}}{\partial z}\right) - \left(A_{e,j}C_{e,i,j}U_{e,j} - E_{mf}D_e A_{e,j}\frac{\partial C_{e,i,j}}{\partial z}\right) + K_{be}\left(C_{b,i,j} - C_{e,i,j}\right)A_{b,j}\Delta Z + R_{e,i,j}A_{e,j}\Delta Z E_{mf} + \frac{n_{p,i}}{V_e}A_{e,j}\Delta Z E_{mf} \qquad (3.120)$$

$$\frac{\partial C_{e,i,j}}{\partial t} = \left(\frac{A_{e,j-1}U_{e,j-1}}{A_{e,j}\Delta Z E_{mf}}C_{e,i,j-1} - \frac{D_e A_{e,j-1}}{A_{e,j}\Delta Z}\frac{\partial C_{e,i,j-1}}{\partial z}\right) - \left(\frac{U_{e,j}}{\Delta Z E_{mf}}C_{e,i,j} - \frac{D_e}{\Delta Z}\frac{\partial C_{e,i,j}}{\partial z}\right) + \frac{A_{b,j}K_{be}}{A_{e,j}E_{mf}}\left(C_{b,i,j} - C_{e,i,j}\right) + R_{e,i,j} + \frac{n_{p,i}}{V_e} \qquad (3.121)$$

$C_{e,i,j}$---- Average gas concentration of species i in emulsion phase in element j, $\frac{\text{kmole}}{\text{m}^3}$

$A_{e,j}$---- Average cross section area of emulsion phase in element j, m^2

$U_{e,j}$---- Average gas velocity of emulsion phase in element j, $\mathrm{m/s}$

D_e---- Mass diffusion coefficient in emulsion phase, $\frac{\mathrm{m}^2}{\mathrm{s}}$

E_{mf}---- Bed void fraction at minimum fluidization velocity in emulsion phase

$R_{e,i,j}$---- Production rate of species i in emulsion phase through chemical reactions, $\frac{\mathrm{kmole}}{\mathrm{m}^3\mathrm{s}}$

$n_{p,i}$---- Species i generated during unit time through pyrolysis in the bed, $\frac{\mathrm{kmole}}{\mathrm{s}}$

V_e---- Total volume of emulsion phase, m^3

Mass balance for fuel is global (De Souza-Santos, 1989; Milioli and Foster, 1995; Chejne and Hernandez, 2002):

Change of char in the bed = char generated through pyrolysis – char consumed through chemical reactions – char entrained out of the bed (3.122)

The change of mass of char in the bed during unit time: $\frac{\partial m_c}{\partial t}$

The amount of char generated through pyrolysis during unit time in the bed: m_p

The mass of char entrained out of the bed during unit time in the bed: m_E

Char consumed through chemical reactions in the whole bed: $\int_0^L \sum_{i=1}^{3} r_{i,j} A_{p,j}\, E_{mf}\, dz$

Therefore:

$$\frac{\partial m_c}{\partial t} = \int_0^L \sum_{i=1}^{3} r_{i,j} A_{p,j}\, M_c E_{mf}\, dz + m_p + m_E \tag{3.123}$$

m_c---- Total mass of char in the fluidized bed, kg

m_p---- The amount of char generated through fuel pyrolysis, kg/s

m_E---- The amount of char entrained out of the bed, kg/s

$r_{i,j}$---- Reaction rate of char reaction i in element j, $\frac{\text{kmole}}{\text{m}^2\text{surface area.s}}$

$A_{p,j}$ ---- Total particle surface area in unit emulsion phase in element j, $\frac{\text{m}^2}{\text{m}^3\text{emulsion phase.s}}$

M_c---- Molecular weight of carbon, kg/kmol

The expression of reaction rates used in the governing equations developed for the bubble phase and emulsion phase are shown below:

$$R_{b,j} = k_4\left({C_{b,1,j}}^{n+1} {C_{b,4,j}}^{n+1} - \frac{{C_{b,2,j}}^{n+1} {C_{b,3,j}}^{n+1}}{k_{eq}}\right) \tag{3.124}$$

$$R_{e,j} = k_4\left({C_{e,1,j}}^{n+1} {C_{e,4,j}}^{n+1} - \frac{{C_{e,2,j}}^{n+1} {C_{e,3,j}}^{n+1}}{k_{eq}}\right) \tag{3.125}$$

$$R_{b,1,j} = -R_{b,j} \tag{3.126}$$

$$R_{b,2,j} = R_{b,j} \tag{3.127}$$

$$R_{b,3,j} = R_{b,j} \tag{3.128}$$

$$R_{b,4,j} = -R_{b,j} \tag{3.129}$$

$$R_{b,5,j} = 0 \tag{3.130}$$

$$R_{b,6,j} = 0 \tag{3.131}$$

$$R_{b,7,j} = 0 \tag{3.132}$$

$$R_{e,1,j} = M_c A_{p,j}\left(k_{t,1} {C_{e,4,j}}^{n-1} + 2k_{t,2} {C_{e,2,j}}^{n-1}\right) - R_{e,j} \tag{3.133}$$

$$R_{e,2,j} = -M_c A_{p,j} k_{t,2} {C_{e,2,j}}^{n-1} + R_{e,j} \tag{3.134}$$

$$R_{e,3,j} = M_c A_{p,j}(k_{t,1} {C_{e,4,j}}^{n-1} - 2k_{t,3} {C_{e,3,j}}^{n-1}) + R_{e,j} \tag{3.135}$$

$$R_{e,4,j} = -M_c A_{p,j} k_{t,1} {C_{e,4,j}}^{n-1} - R_{e,j} \tag{3.136}$$

$$R_{e,5,j} = -M_c A_{p,j} k_{t,3} {C_{e,3,j}}^{n-1} \tag{3.137}$$

$$R_{e,6,j} = 0 \tag{3.138}$$

$$R_{e,7,j} = 0 \tag{3.139}$$

$k_{t,i}$---- Total reaction rate constant including mass transfer, $\frac{\mathrm{m}}{\mathrm{s}}$

The process of model development for the freeboard for the one-dimensional two-phase kinetic model is the same as that for the one-dimensional one-phase kinetic model, so it is not repeated here.

Boundary initial conditions

For element 1 in the fluidized bed

For bubble phase

The amount of species i leaving from element 1to element 2 during unit time is

$$(C_{b,i,1} U_{b,1} A_{b,1} - A_{b,1} D_b \frac{\partial C_{b,i,1}}{\partial z}) \tag{3.140}$$

The amount of species i transferring from bubble phase to emulsion phase during unit time is

$$K_{be}\left(C_{b,i,j} - C_{e,i,j}\right) A_{b,1} dz/2 \tag{3.141}$$

The amount of species i generated through chemical reactions during unit time is

$$R_{b,i,1}A_{b,1}dz/2 \tag{3.142}$$

The amount of species i entering element 1during unit time is n_b. So

$$\begin{aligned}\frac{\partial(C_{b,i,1}A_{b,1}dz/2)}{\partial t} &= n_b - (C_{b,i,1}U_{b,1}A_{b,1} - A_{b,1}D_b\frac{\partial C_{b,i,1}}{\partial z}) \\ &\quad - \frac{K_{be}\left(C_{b,i,j} - C_{e,i,j}\right)A_{b,1}dz}{2} + R_{b,i,1}A_{b,1}dz/2\end{aligned} \tag{3.143}$$

$$\frac{\partial C_{b,i,1}}{\partial t} = \frac{2n_b}{A_{b,1}dz} - (C_{b,i,1}\frac{2U_{b,1}}{dz} - \frac{2D_b}{dz}\frac{\partial C_{b,i,1}}{\partial z}) - K_{be}\left(C_{b,i,j} - C_{e,i,j}\right) + R_{b,i,1} \tag{3.144}$$

Similarly, for species i in the emulsion phase in element 1 the governing equation is

$$\begin{aligned}\frac{\partial(C_{e,i,1}A_{e,1}dz/2E_{mf})}{\partial t} &= n_e - (C_{e,i,1}U_{e,1}A_{e,1} - E_{mf}A_{e,1}D_e\frac{\partial C_{e,i,1}}{\partial z}) \\ &\quad + \frac{K_{be}\left(C_{b,i,j} - C_{e,i,j}\right)A_{b,1}dz}{2} + \frac{R_{e,i,1}A_{e,1}dz}{2E_{mf}} \\ &\quad + \frac{n_{p,i}}{V_e}A_{e,j}\Delta Z E_{mf}/2\end{aligned} \tag{3.145}$$

$$\begin{aligned}\frac{\partial C_{e,i,1}}{\partial t} &= \frac{2n_e}{A_{e,1}dzE_{mf}} - (C_{e,i,1}\frac{2U_{e,1}}{dzE_{mf}} - \frac{2D_e}{dz}\frac{\partial C_{e,i,1}}{\partial z}) \\ &\quad + \frac{K_{be}\left(C_{b,i,j} - C_{e,i,j}\right)A_{b,1}}{A_{e,1}E_{mf}} + R_{e,i,1} + \frac{n_{p,i}}{V_e}\end{aligned} \tag{3.146}$$

For element NN in the fluidized bed

The amount of species i in bubble phase leaving from element NN-1 to element NN by convection during unit time is

$$C_{b,i,NN-1}U_{b,NN-1}A_{b,NN-1} \tag{3.147}$$

The amount of species i passing from bubble phase to emulsion phase during unit time is

$$\frac{K_{be}\left(C_{b,i,NN}-C_{e,i,NN}\right)A_{b,NN}dz}{2} \tag{3.148}$$

The amount of species i in bubble phase generated through chemical reactions during unit time is

$$\frac{R_{b,i,NN}A_{b,NN}dz}{2} \tag{3.149}$$

The amount of species i in bubble phase leaving element NN during unit time is

$$C_{b,i,NN}U_{b,NN}A_{b,NN} \tag{3.150}$$

The amount of species i entering from element NN-1 to element NN by diffusion during unit time is

$$-A_{b,NN-1}D_b\frac{\partial C_{b,i,NN-1}}{\partial z} \tag{3.151}$$

The net amount of species i generated in bubble phase during unit time is

$$\Delta(C_{b,i,NN}A_{b,NN}dz/2)/\Delta t \tag{3.152}$$

So

$$\begin{aligned}\frac{\partial(C_{b,i,NN}A_{b,NN}dz/2)}{\partial t} &= (C_{b,i,NN-1}U_{b,NN-1}A_{b,NN-1}-A_{b,NN-1}D_b\frac{\partial C_{b,i,NN-1}}{\partial z})\\ &- C_{b,i,NN}U_{b,NN}A_{b,NN}-\frac{K_{be}\left(C_{b,i,NN}-C_{e,i,NN}\right)A_{b,NN}dz}{2}\\ &+ R_{b,i,NN}A_{b,NN}dz/2\end{aligned} \tag{3.153}$$

$$\begin{aligned}\frac{\partial C_{b,i,NN}}{\partial t} = (C_{b,i,NN-1}&\frac{2U_{b,NN-1}A_{b,NN-1}}{A_{b,NN}dz}-\frac{2A_{b,NN-1}D_b}{A_{b,NN}dz}\frac{\partial C_{b,i,NN-1}}{\partial z})\\ &-\frac{2C_{b,i,NN}U_{b,NN}}{dz}-K_{be}\left(C_{b,i,NN}-C_{e,i,NN}\right)+R_{b,i,NN}\end{aligned} \tag{3.154}$$

Similarly, for species i in the emulsion phase in element NN the governing equation is

$$\frac{\partial(C_{e,i,NN}A_{e,NN}dz/2E_{mf})}{\partial t} = (C_{e,i,NN-1}U_{e,NN-1}A_{e,NN-1} - E_{mf}A_{e,NN-1}D_e\frac{\partial C_{e,i,NN-1}}{\partial z}) - C_{e,i,NN}U_{e,NN}A_{e,NN} + \frac{K_{be}(C_{b,i,NN} - C_{e,i,NN})A_{b,NN}dz}{2} + \frac{R_{e,i,NN}A_{e,NN}dz}{2E_{mf}} \quad (3.155)$$

$$\frac{\partial C_{e,i,NN}}{\partial t} = (C_{e,i,NN-1}\frac{2U_{e,NN-1}A_{e,NN-1}}{A_{e,NN}dzE_{mf}} - \frac{2A_{e,NN-1}D_e}{A_{e,NN}dz}\frac{\partial C_{e,i,NN-1}}{\partial z}) - \frac{2C_{e,i,NN}U_{e,NN}}{dzE_{mf}} + \frac{K_{be}(C_{b,i,NN} - C_{e,i,NN})A_{b,NN}}{A_{e,NN}E_{mf}} + R_{e,i,NN} \quad (3.156)$$

3.3.2.3 Fluidized bed hydrodynamics parameters

Minimum fluidization voidage E_{mf}

$$E_{mf} = 0.42 \quad (3.157)$$

Minimum fluidization velocity U_{mf}

$$U_{mf} = \left(\frac{\mu}{\rho_g d_p}\right)[\sqrt{(1135.7 + 0.0408Ar} - 33.7] \quad (3.158)$$

Where

$$Ar = \frac{d_p^3\rho_g(\rho_s - \rho_g)g}{\mu^2} \quad (3.159)$$

Bubble velocity U_b

$$U_b = U_o - U_{mf} + 0.711\sqrt{(gd_b)} \quad (3.160)$$

Where U_o is the inlet gas velocity, and d_b is the bubble diameter defined by the following equation:

$$d_b = d_{bm} - (d_{bm} - d_{bo})\exp\left(-\frac{0.3Z}{D}\right) \tag{3.161}$$

$$d_{bm} = 1.64[A(U - U_{mf})]^{0.4} \tag{3.162}$$

$$d_{bo} = 0.872[\frac{A(U - U_{mf})}{N}]^{0.4} \tag{3.163}$$

Where D is bed diameter, m; d_{bm} is the maximum bubble diameter, m; d_{bo} is initial bubble diameter, m; and N is the number of holes (nozzles) in the distributor plate.

Emulsion phase gas velocity U_e

$$U_e = \frac{U_{mf}}{(1 - EDL)} \tag{3.164}$$

Volume fraction of the bubble phase

$$DEL = \frac{(U - U_{mf})}{U_b} \tag{3.165}$$

The height of the expanded bed H (Raman, 1981)

$$H = \frac{H_{mf}}{1 - DEL} \tag{3.166}$$

Where H_{mf} is the bed height at incipient fluidization

Viscosity of gases

$$\mu = a_1 + b_1T + c_1T^2 + d_1T^3 + e_1T^4 + f_1T^5 \tag{3.167}$$

Viscosity for steam

$$\mu_{H2O} = [80.4 + 0.407(T - 273.15) \times 10^{-7}] \quad 273 < T < 973(K) \tag{3.168}$$

Viscosity of the gas mixture

$$\mu_{ij} = \sum_{i=1}^{7} y_i\mu_i \tag{3.169}$$

3.3.2.4 Solutions

These equations are approximated using the finite difference method, and are turned into the following equations:

Bubble phase in the fluidized bed:

$$\frac{\partial C_{b,i,j}}{\partial t} = \left(\frac{A_{b,j-1}U_{b,j-1}}{A_{b,j}\Delta Z}C_{b,i,j-1} - \frac{A_{b,j-1}D_b}{A_{b,j}\Delta Z}\frac{\partial C_{b,i,j-1}}{\partial z}\right) - \left(\frac{U_{b,j}}{\Delta Z}C_{b,i,j} - \frac{D_b}{\Delta Z}\frac{\partial C_{b,i,j}}{\partial z}\right) - K_{be}\left(C_{b,i,j} - C_{e,i,j}\right) + R_{b,i,j} \tag{3.170}$$

$$\begin{aligned} {C_{b,i,j}}^{n+1} = {} & {C_{b,i,j}}^{n} \\ & + dt\left(\frac{A_{b,j-1}U_{b,j-1}}{A_{b,j}\Delta Z}{C_{b,i,j-1}}^{n+1} - \frac{A_{b,j-1}D_b}{A_{b,j}\Delta Z}\frac{{C_{b,i,j}}^{n+1} - {C_{b,i,j-1}}^{n+1}}{\Delta Z}\right) \\ & - dt\left(\frac{U_{b,j}}{\Delta Z}{C_{b,i,j}}^{n+1} - \frac{D_b}{\Delta Z}\frac{{C_{b,i,j+1}}^{n+1} - {C_{b,i,j}}^{n+1}}{\Delta Z}\right) \\ & - dtK_{be}\left({C_{b,i,j}}^{n+1} - {C_{e,i,j}}^{n+1}\right) + dtR_{b,i,j} \end{aligned} \tag{3.171}$$

$$\begin{aligned} & \left(1 + \frac{A_{b,j-1}D_b dt}{A_{b,j}\Delta Z^2} + \frac{U_{b,j}dt}{\Delta Z} + \frac{D_b dt}{\Delta Z^2} + dtK_{be}\right){C_{b,i,j}}^{n+1} \\ & - \left(\frac{A_{b,j-1}U_{b,j-1}dt}{A_{b,j}\Delta Z} + \frac{A_{b,j-1}D_b dt}{A_{b,j}\Delta Z^2}\right){C_{b,i,j-1}}^{n+1} \\ & - \frac{D_b dt}{\Delta Z^2}{C_{b,i,j+1}}^{n+1} - dtK_{be}{C_{e,i,j}}^{n+1} = {C_{b,i,j}}^{n} + dtR_{b,i,j} \end{aligned} \tag{3.172}$$

Emulsion phase in the fluidized bed:

$$\frac{\partial C_{e,i,j}}{\partial t} = \left(\frac{A_{e,j-1}U_{e,j-1}}{A_{e,j}\Delta Z E_{mf}}C_{e,i,j-1} - \frac{D_e A_{e,j-1}}{A_{e,j}\Delta Z}\frac{\partial C_{e,i,j-1}}{\partial z}\right) - \left(\frac{U_{e,j}}{\Delta Z E_{mf}}C_{e,i,j} - \frac{D_e}{\Delta Z}\frac{\partial C_{e,i,j}}{\partial z}\right) + \frac{A_{b,j}K_{be}}{A_{e,j}E_{mf}}\left(C_{b,i,j} - C_{e,i,j}\right) + R_{e,i,j} + \frac{n_{p,i}}{V_e} \tag{3.173}$$

$$
\begin{aligned}
{C_{e,i,j}}^{n+1} = {C_{e,i,j}}^{n} & \\
&+ dt\left(\frac{A_{e,j-1}U_{e,j-1}}{A_{e,j}\Delta Z E_{mf}}{C_{e,i,j-1}}^{n+1}\right. \\
&\left.-\frac{A_{e,j-1}D_e}{A_{e,j}\Delta Z}\frac{{C_{e,i,j}}^{n+1}-{C_{e,i,j-1}}^{n+1}}{\Delta Z}\right) \\
&- dt\left(\frac{U_{e,j}}{\Delta Z E_{mf}}{C_{e,i,j}}^{n+1}-\frac{D_e}{\Delta Z}\frac{{C_{e,i,j+1}}^{n+1}-{C_{e,i,j}}^{n+1}}{\Delta Z}\right) \\
&+ \frac{A_{b,j}K_{be}dt}{A_{e,j}E_{mf}}\left({C_{b,i,j}}^{n+1}-{C_{e,i,j}}^{n+1}\right)+dtR_{e,i,j}+\frac{n_{p,i}}{V_e}dt
\end{aligned}
\tag{3.174}
$$

$$
\begin{aligned}
&\left(1+\frac{A_{e,j-1}D_e dt}{A_{e,j}\Delta Z^2}+\frac{U_{e,j}dt}{\Delta Z E_{mf}}+\frac{D_e dt}{\Delta Z^2}+\frac{A_{b,j}K_{be}dt}{A_{e,j}E_{mf}}\right){C_{e,i,j}}^{n+1} \\
&\quad-\left(\frac{A_{e,j-1}U_{e,j-1}dt}{A_{e,j}\Delta Z E_{mf}}+\frac{A_{e,j-1}D_e dt}{A_{e,j}\Delta Z^2}\right){C_{e,i,j-1}}^{n+1} \\
&\quad-\frac{D_e dt}{\Delta Z^2}{C_{e,i,j+1}}^{n+1} \\
&\quad-\frac{A_{b,j}K_{be}dt}{A_{e,j}E_{mf}}{C_{b,i,j}}^{n+1}={C_{e,i,j}}^{n}+dtR_{e,i,j}+\frac{n_{p,i}}{V_e}dt
\end{aligned}
\tag{3.175}
$$

Char in the emulsion phase in the fluidized bed

$$
\frac{\partial C_{s,j}}{\partial t}=\frac{A_{e,j-1}U_{e,j-1}}{A_{e,j}\Delta Z E_{mf}}C_{s,j-1}-\frac{U_{e,j}}{\Delta Z E_{mf}}C_{s,j}+R_{s,j} \tag{3.176}
$$

$$
{C_{s,j}}^{n+1}={C_{s,j}}^{n}+\frac{A_{e,j-1}U_{e,j-1}dt}{A_{e,j}\Delta Z E_{mf}}{C_{s,j-1}}^{n+1}-\frac{U_{e,j}dt}{\Delta Z E_{mf}}{C_{s,j}}^{n+1}+R_{s,j}dt \tag{3.177}
$$

$$
\left(1+\frac{U_{e,j}dt}{\Delta Z E_{mf}}\right){C_{s,j}}^{n+1}-\frac{A_{e,j-1}U_{e,j-1}dt}{A_{e,j}\Delta Z E_{mf}}{C_{s,j-1}}^{n+1}={C_{s,j}}^{n}+R_{s,j}dt \tag{3.178}
$$

Due to the complexity of the solid phase, the explicit method is used for solid phase, and implicit method is used to solve time-dependent, partial differential equations for gases. The schematic diagram of the procedure of solving this model is the same as that for the one-dimensional one-phase kinetic model (Fig. 3.10).

3.3.3 One-dimensional two-phase kinetic models-all char in bed

3.3.3.1 Assumptions for the two-phase kinetic models-all char in bed

Assumptions used for the two-phase kinetic models without char entrainment are as follows:

1) Unsteady state mathematical model, which includes both reaction kinetics and fluid dynamics. The whole gasification process is divided into two stages: devolatilization/pyrolysis and gasification. The main components of pyrolysis products are char, ash, H_2, CO, CO_2, CH_4, C_2H_x, tar, and H_2O. The other gases such as C_2H_2, C_2H_4, and C_2H_6 are included in C_2H_x in order to simplify simulation.
2) Two-phase kinetic model-all char in bed with particle size: Both pyrolysis and char gasification are controlled by reaction kinetics.

   Two-phase kinetic model-all char in bed without particle size: Pyrolysis happens instantaneously, and pyrolysis products are used as input.
3) The temperature of the whole reactor is uniform.
4) Solid in bed is sand, un-reacted biomass, mixture of un-reacted biomass, carbon and ash, and mixture of carbon and ash. Char is pure carbon. Due to lack of related theories and experimental data, char deactivation and particle fragmentation are not considered. No particle attrition or entrainment.
5) Ash is inert, and does not take part in reactions.

6) The whole reactor is divided into two parts: fluidized bed and freeboard based on different bed hydrodynamics. The fluidized bed is modeled as a two-phase system, and the freeboard is modeled as a one-phase system. There are no solid-gas reactions in the freeboard.

7) The fluidized bed consists of a bubble phase and an emulsion phase. Emulsion phase consists of gases, char, and bed material (sand), and the bubble phase is free of solids. Mass exchange takes place between the bubble phase and the emulsion phase, and mass transfer considers both convection and dispersion.

8) Flow of gas in excess of the minimum fluidization velocity passes through the bed in the form of bubble. The voidage of the emulsion remains constant, and is equal to that at incipient fluidization.

9) Due to rapid mass transfer solids are well mixed and homogeneously distributed inside the fluidized bed, and mass balance for solid phase in the fluidized bed section is global (Chejne and Hernandez, 2002). Gas concentration difference in radial direction is neglected, and gas concentration gradient only exists in axial direction for both the bubble phase and the gases in emulsion phase. Gases in the system consist of CO, CO_2, H_2, CH_4, H_2O, tar, and C_2H_x.

10) Condition over the fluidized bed cross section is uniform.

11) Two-phase kinetic model-all char in bed with particle size: Particle is impervious, and no diffusion exists inside particles. Gas-solid reaction takes place on the surface of un-reacted core. The ash layer formed on the surface of un-reacted core peels off immediately due to severe collisions in the bed. Particles are isothermal.

3.3.3.2 Model development

The model development process for gases in the bubble phase and emulsion in the fluidized bed and the model development process in the freeboard are the same as those for the one-dimensional two-phase kinetic model in section 3.3.2, so they are not repeated here.

The mass balance for char in the bed is global:

Change of char in the bed = char generated through pyrolysis – char consumed through chemical reactions

(3.179)

The change of mass of char in the bed during unit time: $\frac{\partial m_c}{\partial t}$

The amount of char generated through pyrolysis during unit time in the bed: m_p

Char consumed through chemical reactions in the whole bed: $\int_0^L \sum_{i=1}^{3} r_{i,j} A_{p,j} E_{mf} dz$

Therefore:

$$\frac{\partial m_c}{\partial t} = \int_0^L \sum_{i=1}^{3} r_{i,j} A_{p,j} M_c E_{mf} dz + m_p \quad (3.180)$$

m_c---- Total mass of char in the fluidized bed, kg

m_p---- The amount of char generated through fuel pyrolysis, kg/s

m_E---- The amount of char entrained out of the bed, kg/s

$r_{i,j}$---- Reaction rate of char reaction i in element j, $\frac{\text{kmole}}{\text{m}^2\text{surface area.s}}$

$A_{p,j}$---- Particle surface area in unit emulsion phase in element j, $\frac{\mathrm{m}^2}{\mathrm{m}^3\,\mathrm{emulsion\ phase.s}}$

M_c---- Molecular weight of carbon, kg/kmol

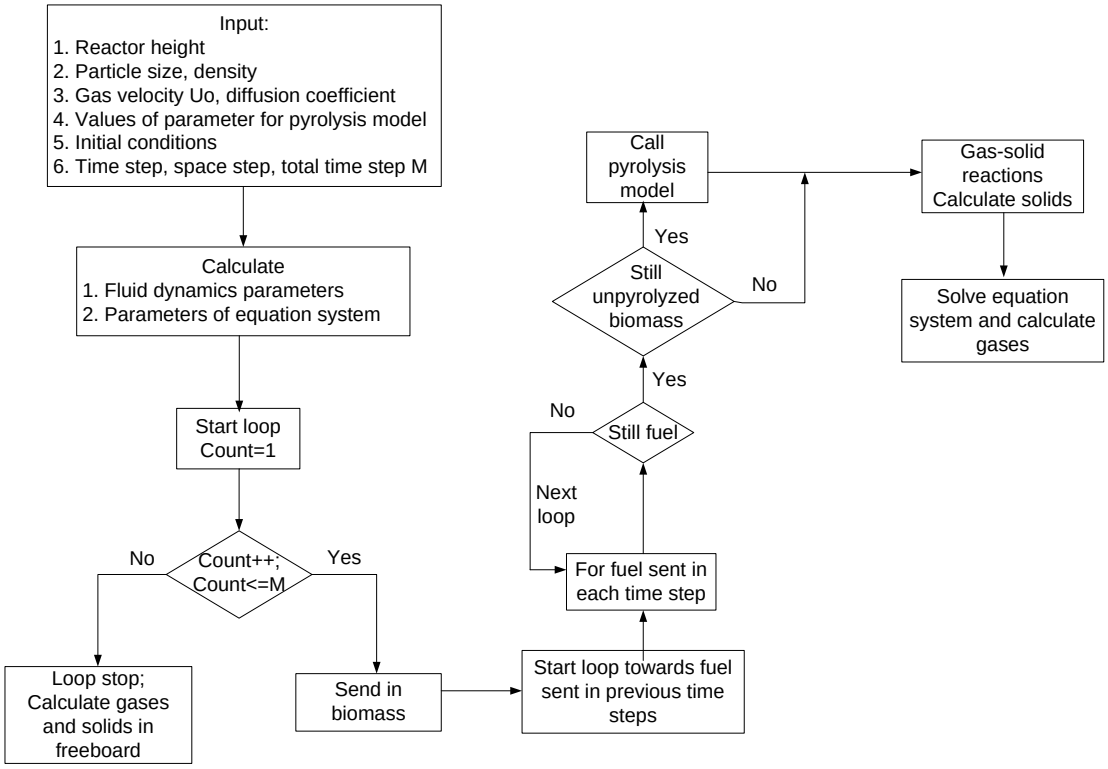

Figure 3. 13 Schematic diagram of calculation procedure for the one-dimensional two-phase kinetic model-all char in bed with particle size

3.3.3.3 Calculation procedure

The explicit method is used for solid phase, and the implicit is used for the nonlinear, time-dependent, partial differential equations for gases. The whole process is programmed using MatLab, and the calculation procedures for these two kinetic models without char entrainment are shown in Figs. 3.13 and 3.14.

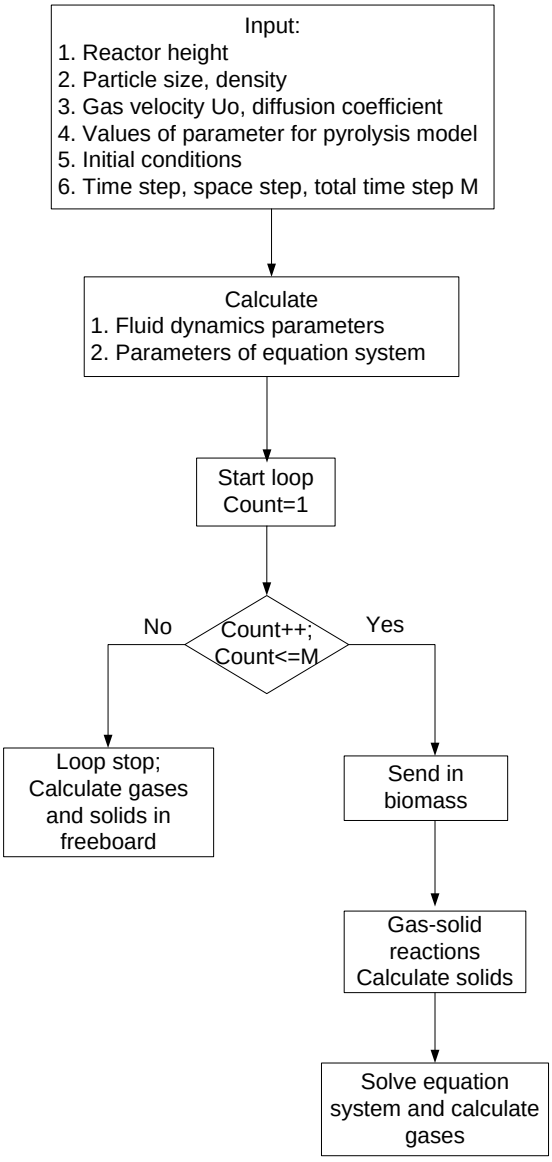

Figure 3. 14 Schematic diagram of calculation procedure for the one-dimensional two-phase kinetic model-all char in bed without particle size

3.4 Model validation for the one-dimensional two-phase kinetic model

Because we believe that the best model to represent the real gasification process is the the one-dimensional two-phase kinetic model, the model validation is conducted for

this model. Although biomass such as wood, grass, waste, and wheat straw has been widely studied, corn stover has not received as much attention, and just a few experimental studies are available on corn stover gasification (Beck, Wang and Hightower, 1981; Perkins, et al. 2008; Kumar, et al. 2009; Carpenter, et al., 2010), especially on corn stover steam gasification (Beck, Wang and Hightower, 1981; Perkins, et al. 2008; Carpenter, et al., 2010). In addition, the results available on corn stover steam gasification are not suitable for model validation because they either failed to present enough information on the gasification product distribution because of their different research purposes or they used gasifying agents other than steam. Therefore, the results of steam gasification of other fuels are used in this study for model validation, which is based on the assumption that if the model works well for other fuels it can also work well for corn stover.

The main information source for model validation is the literature available. Because yields of pyrolysis products are required for the kinetic models developed, fuels that can be used for model validation must meet two conditions: 1) gasification must be fluidized bed steam gasification; 2) yields of both pyrolysis products and gasification products must be available for the fuel used for gasification. However, most fuels fail to meet the above two requirements. First, experimental studies on fluidized bed steam gasification are limited, and due to different research purposes some literature does not provide the information needed. Second, for fuels whose fluidized bed steam gasification results are available and complete, many of them lack information on

pyrolysis product distribution at similar or corresponding temperatures. After an extensive literature review, cattle manure was selected because information on both pyrolysis and fluidized bed steam gasification was available (Raman, Walawender and Fan, 1980; Raman, 1981). Through preliminary study, it was found that the simulation results were different from the results in the literature in terms of the amount of char produced.

One possible reason lies in the different calculation methods for the amount of char produced. Based on the modeling concept used for this model, the amount of char produced is calculated by the equation below:

$$\eta_{c,1} = \frac{\dot{m}_{c,b} + \dot{m}_{c,E}}{\dot{m}_{fuel}} \tag{3.181}$$

$\dot{m}_{fuel}$---- Mass flow rate of fuel sent to the reactor, kg/s

$\dot{m}_{c,b}$---- Amount of char increased in the bed during unit time, kg/s

$\dot{m}_{c,E}$---- Amount of char entrained out of the bed during unit time, kg/s

$\eta_{c,1}$---- Percentage of char produced

When the bed reaches steady state, since char accumulation in the bed is not able to be modeled due to lack of theory and experimental data, equation (3.181) becomes:

$$\eta_{c,1} = \frac{\dot{m}_{c,E}}{\dot{m}_{fuel}} \tag{3.182}$$

Some researchers say it is impossible to calculate the amount of char produced because the bed can hardly reach a true steady state due to char accumulation (Hovland et al 1982; Neogi, et al., 1986; Hrdlicka, et al., 2008; Corella, Toledo and

Molina, 2008; Sakaguchi, Watkinson and Ellis, 2010). Most researchers who did experimental studies used equations to equation (3.176) to calculate the amount of char produced (Aznar, et al., 1993; Franco, et al., 2003; Bayarsaikhan, et al., 2006; Xiao, et al., 2010):

$$\eta_{c,2} = \frac{m_{c,b} + m_{c,E}}{m_{fuel}} \tag{3.183}$$

m_{fuel}---- Total amount of fuel sent to the bed during the whole time, kg

$m_{c,b}$---- Total amount of char in the bed, kg

$m_{c,E}$---- Total amount of char entrained out of the bed during the whole time, kg

$\eta_{c,2}$---- Percentage of char produced

Equation (3.183) gives different values for different operation time no matter whether the bed can reach a steady state or not. If the bed can finally reach a steady state, the amount of char and biomass in the bed remains constant and the amount of char collected in the cyclone increases with a constant rate at steady state, which means $m_{c,b}$ remains constant and $m_{c,E}$ increases as m_{fuel} increases. Therefore, the longer the operation time, the smaller the value of $\eta_{c,2}$. If the operation time is long enough, equation (3.183) becomes equation (3.184) which gives the same char yield as equation (3.182).

$$\eta_{c,2} = \frac{m_{c,E}}{m_{fuel}} \tag{3.184}$$

Because the operation time for the cattle experiments is no longer than 1 hour, it is highly possible that the amount of char calculated in the literature is different from

that when the experimental time is relatively long, and the difference in the char yield might be due to the different calculation equations. In addition, when the bed cannot reach the steady state, the values of $m_{c,E}$, $m_{c,b}$, and m_{fuel} vary with time, as does the value of $\eta_{c,2}$. Therefore, it is highly possible that $\eta_{c,1}$ calculated by the model is right, and the difference in the yield of char is because the different operation time selected.

The other possible reason for the difference between the model result and the literature value is char accumulation in the bed due to deactivation and high ash content. In the real process, char cannot be totally gasified especially for high-ash content char, and char is accumulating all the time in the bed, which is not included in the model.

The process of model validation is also a process of model calibration, and the model can be adjusted to fit the experimental results by increasing the amount of char entrained out of the bed to compensate the char accumulation in the bed. However, some experimental studies show a certain amount of char accumulated in the bed in unit time during gasification process (Raman, Walawender and Fan, 1980), but the amount of char in the bed remains constant at steady-state in the model, which indicates the solid behavior predicted by the model is different from the real process (char accumulation in the bed) due to the lack of related information on char deactivation. Therefore, before the model developed can be used to predict the gasification results of corn stover, several questions must be answered first: 1) when

can this model be used/ what kind of fuel can this model simulate? 2) which kind of fuels always lead to char accumulation in the bed, or when the fuel is corn stover will there be char accumulation in the bed? 3) how to model fuels that can lead to char accumulation in the bed or can this model be expanded to simulate fuels that can lead to char accumulation in the bed?

Because one of the assumptions used by the model is that the bed can reach steady state, the answer to the first question is that fuels that do not result in char accumulation and have a constant bed height can be simulated by this model. Because accumulation is always related to high ash content fuel (NETL, n.d.; Granatstein, n.d.; Scott, et al., n.d.; Barea and Ollero, n.d.; Flanigan and Padiscor, 1987; Miccio, 1999; Chattopadhyay, 2000; Bayarsaikhan, et al., 2006; Salam, Kumar and Siriwardhana, 2010; Gordillo and Belghit, 2011a; b], and there are some studies showing that low ash content fuel such as wood does not lead to char/ash accumulation (Miccio, 1999; Hrdlicka, et al., 2008), it can be inferred that low ash content fuels do not cause char accumulation and may be suitable for this model. In order to verify this conclusion, an effort was made to find a low ash content fuel. Through extensive literature reviews and comparisons, low-ash content pine sawdust was selected because complete information on fluidized bed steam gasification was available (Herguido, Corella and Gonzalez-Saiz, 1992). Because no satisfactory pyrolysis results were found for pine sawdust, pyrolysis results obtained for birch wood were used (Zanzi, Sjöström and Björnbom, 2002).

The properties of these two woods are shown in Table 3.7. In addition, because the mass closure for birch wood gasification is 88% and the maximum char produced after gasification is much more than that after pyrolysis, some modifications were made to close the mass balance and increase the amount of char after pyrolysis, as shown in Table 3.8. Since studies on reaction kinetics of fuels other than coal were not extensive, reaction kinetics in Table 3.6 were adjusted to fit the simulation results to experimental results.

Table 3. 7 Properties of wood for pyrolysis and gasification

	Pyrolysis	Gasification
Name	Birch wood (Zanzi, Sjöström and Björnbom, 2002)	Pine sawdust (Herguido, Corella and Gonzalez-Saiz, 1992)
Particle size, mm	0.5—0.8	0.5
Ultimate analysis		
C, wt% daf	48.4	42.5
H, wt% daf	5.6	6.3
N, wt% daf	0.2	0.2
O, wt% daf	45.8	51
sum	100	100
Proximate analysis		
Ash, wt%	0.3(daf)	1.2
Moisture, wt%	5	8.5
Volatiles, wt%		77.4
Fixed carbon, wt%		12.9
Bulk density, kg/m3		
Raw material	300	
char	90	

Through sensitivity analysis, a set of gasification results that are close to the experimental results were obtained and shown in Fig. 3.15, and the reaction kinetics used are shown in Table 3.9. The trend of gas composition over the entire range of S/B

is consistent with that of experiments, and the yields of gas, char, and tar are close to those obtained during experiments. Meanwhile, it is also noticed that the largest difference between the volumetric fraction predicted by the model and that obtained from experiments is 15%, 6.9%, and 6.1% for H_2, CO_2, and CO, respectively. This difference may be due to the inaccurate reaction kinetics used, and it may also be due to the different wood material used for modeling (birch wood) and experiments (pine wood). Another possible reason may be the experimental results for pine wood is not accurate.

Table 3. 8 Pyrolysis products of birch wood (Zanzi, Sjöström and Björnbom, 2002)

T, ^oC	800	After adjustment
gas, wt% daf	0.811	0.759
tar, wt% daf	0.011	0.011
char, wt% daf	0.058	0.23
sum	0.88	1
Compositions, vol%, N_2 and H_2O free		
CO	50.7	
CO_2	9.6	
H_2	17.3	
CH_4	15.7	
LCH_s	6.1	
Benzene	1.2	
sum	100.6	

From Table 3.10 we can see that even for the same kind of wood (pine wood), the gasification results in terms of the distribution of gas composition and yields of char and gas are different. For instance, although different steam/biomass ratios were used, the gas fractions obtained by two papers were almost the same (Herguido, Corella and Gonzalez-Saiz, 1992; Gil, et al. 1999) and the volumetric fraction of H_2 obtained in one study is in the range of 35 to 39 while in another study it is in the range of 40-56 under similar operating conditions. Therefore, it seems that experimental results are

sparse and inconsistent. Because the simulation results fall in the same range, it can be concluded that the simulation results are reasonable, thus the model developed is suitable for low ash content fuels.

Table 3. 9 Reaction rates used for the model validation

Chemical reaction	Reaction Kinetics
Heterogeneous reactions(kmole/(s.m^3))	
$C + H_2O \overset{k_1}{\rightarrow} CO + H_2$	$k_1 = 7.492 * 10^3 \exp\left(-\frac{22220}{T}\right)$
$C + CO_2 \overset{k_2}{\rightarrow} 2CO$	$k_2 = 7.92 * 10^4 \exp\left(-\frac{22220}{T}\right)$
$C + 2H_2 \overset{k_3}{\rightarrow} CH_4$	$k_3 = 792 \exp\left(-\frac{22220}{T}\right)$
Homogeneous reactions (kmole/(s.m^3))	
$CO + H_2O \overset{k_4}{\leftrightarrow} CO_2 + H_2$	$r_4 = k_4\left(C_{CO}C_{H2O} - \frac{C_{CO2}C_{H2}}{k_{eq}}\right)$ $k_4 = 0.1 \times \frac{10^8}{3600} \exp\left(-\frac{12560}{RT}\right)$ $k_{eq} = \frac{0.0265}{1.3} * \exp\left(\frac{3955.7}{T}\right)$

Table 3. 10 Results of steam gasification for pine wood from literature

Ref. No	(Franco, et al., 2003)	(Gil, et al. 1999)	(Herguido, Corella and Gonzalez-Saiz, 1992)	Wei, et al., 2007	(Hrdlicka, et al., 2008)
Fuel	Pine	Pine	Pine	Pine	Pine
Dp, mm	1.25—2	Small chips	0.5	0.3—0.45	2
Bed	Fluidized	Fluidized	Fluidized	Free fall	Fluidized
T, ^{o}C	800	750-780	750	800	750
S/B	0.5—0.8	0.53-1.1	0.5—2.5	0--1	0.81-2.0
CO	45-36-38	32-17	32-10	43--33	18.9-17.7-23.4
CO_2	12--14	13-17	13-27	15--20	24.3-24.1-22.1
H_2	21-35-28	38-56	40-56	28--35	35.6-39.1-35.3
CH_4	14-10-12	12-7	12-2	10--7	12.1-10.1-13.3
LCHs	7-4-5	2.3-2.1	2.5-2.3		3.8-3.4-4.7
Char		0.11-0.095	0.16-0.02	0.06—0.03	
Gas			0.90—1.18	0.75—1.00	

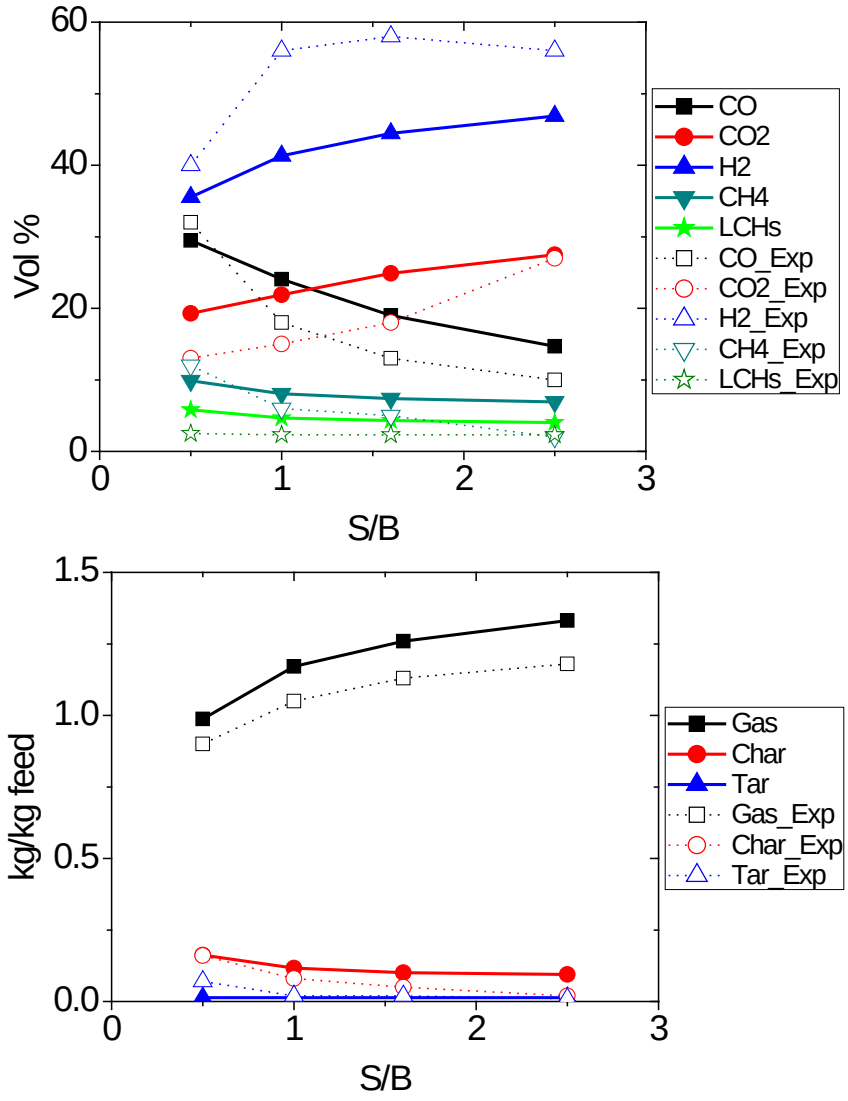

Figure 3. 15 Simulation results of the wood gasification for model validation, T=750 ^{o}C. Experimental results are obtained from the literature (Herguido, Corella and Gonzalez-Saiz, 1992)

Because the model developed in this study is not able to model char accumulation, the answer to the second question (which kind of fuels always lead to char accumulation in the bed, or when the fuel is corn stover will there be char accumulation in the bed) is that fuels that can result in char accumulation cannot be modeled by this model, and

if corn stover can lead to char accumulation it cannot be modeled by this model. It is generally accepted that high ash content fuel can lead to char/ash accumulation in the bed (NETL, n.d.; Granatstein, n.d.; Scott, et al., n.d.; Barea and Ollero, n.d.; Flanigan and Padiscor, 1987; Miccio, 1999; Chattopadhyay, 2000; Bayarsaikhan, et al., 2006; Hrdlicka, et al., 2008; Salam, Kumar and Siriwardhana, 2010; Gordillo and Belghit, 2011a; b). For medium ash content fuel such as coal, some literature says that after 30-40 minutes the bed height remains constant (Neogi, et al., 1986), while some literatures say that the char accumulated in the bed increases with time (NETL, n.d.; Granatstein, n.d.; Chattopadhyay, 2000; Bayarsaikhan, et al., 2006; Salam, Kumar and Siriwardhana, 2010).

Therefore, it may be concluded that medium and high ash content fuel can lead to char accumulation, and because corn stover has an ash content of around 8-10% (Carpenter, et al., 2010), it seems that corn stover cannot be modeled by this model. However, at the same time it should also be noticed that if high and medium ash content fuels have a small particle size which enables them to be entrained out of the bed and avoid char accumulation, it is possible that particles have been already entrained out of the bed before they become deactivated, and under this condition these fuels can be modeled by the model developed in this study. In addition, if low-ash content fuels have a large particle size, char deactivation may happen before they can be entrained out of the bed, and char accumulation will still happen. Through careful examine of the accumulation, two possible situations for char accumulation in the bed are: 1) only ash is

accumulated in the bed, and the initial size of particles is so large that even only the ash part cannot be entrained out of the bed; 2) the mixture of dead char and ash is accumulated in the bed, and the percentage of dead char in the whole solid residue is unknown. Therefore, it can be concluded that whether char accumulation happens or not mainly depends on whether the char becomes dead before it can be entrained out of the bed which is highly related to the initial particle size and the ash content.

The answer to the third question (how to model fuels that can lead to char accumulation in the bed or can this model be expanded to simulate fuels that can lead to char accumulation in the bed) is now it is unable to simulate char accumulation in the bed exactly due to lack of information on the rate of char accumulation in the bed and to what extent the char loses its reactivity and becomes dead char, but there are also some possible treatments. One method is to neglect the char accumulation in the bed and adjust the amount of char entrained out of the bed to fit experimental results since a large portion of solid removed from the bed is ash (NETL, n.d.; Granatstein, n.d.; Flanigan and Padiscor, 1987; Miccio, 1999; Chattopadhyay, 2000; Brown, et al., 2006; Salam, Kumar and Siriwardhana, 2010; Gordillo and Belghit, 2011a; b; Meijden, Drift and Vreugdenhil, 2012). The other method is to set a critical time and remove char and biomass whose residence time in the bed exceeds the critical time, which is more close to the real process in the industry. The third method is to remove a certain amount of char and ash out the bed to keep a constant bed depth, once the depth of the bed exceeds the desired depth. The only problem for these methods is that the

adjustment, the critical time or the certain amount of char and biomass removed need to be determined experimentally first.

4 Results and discussion

Various operating parameters can be used to characterize the gasification process. In this study, an investigation was carried out on 1) the steam/biomass (S/B) ratio which is defined as the ratio of the mass flow rate of steam to the mass flow rate of biomass (including moisture and ash); 2) gasification temperature; and 3) gas superficial velocity (for models considering fluid dynamics). In addition, the effect of particle size was studied for the zero-dimensional kinetic model and the one-dimensional two-phase kinetic model.

4.1 Zero-dimensional non-stoichiometric equilibrium model

Equilibrium models do not consider the effects of reactor geometry, gas velocity and particle size, and the variables studied for equilibrium models are temperature and steam/biomass ratio.

4.1.1 Effect of temperature

The effect of gasifier temperature on gasification product yields and gas distribution was studied for corn stover with a steam/biomass ratio of 1 shown in figures below. Four different values were taken for gasifier temperature: 600 ^{o}C, 677 ^{o}C, 777 ^{o}C and 870 ^{o}C. Since the equilibrium model is not related to fluid dynamics, the absolute mass flow rate and superficial gas velocity do not affect the gasification results. The yield of char at different temperatures obtained for the one-dimensional two-phase

kinetic model was used as input for the equilibrium model. The products of the equilibrium model are CO, CO_2, H_2, H_2O, and CH_4.

The yields of char and dry tar-free gas for cases with different temperatures are shown in Fig. 4.1 for the non-stoichiometric equilibrium model. The yield of char decreases with increased temperature. When the temperature increases from 600 ^oC to 870 ^oC, the amount of char produced after gasification decreases from 0.15 to 0.11 kg/kg feed. The yield of dry tar-free gas increases from 1.00 to 1.04 kg/kg feed when the temperature increases from 600 ^oC to 670 ^oC, then it decreases to 1.04 and 1.03 kg/kg feed with an increase of temperature from 670 to 770 and 870 ^oC. This may be due to the shortcomings of the non-stoichiometric equilibrium model itself. Because this kind of model predicts the yields of gases based on minimum Gibbs free energy, gases with a large Gibbs free energy such as CH_4 cannot be predicted correctly.

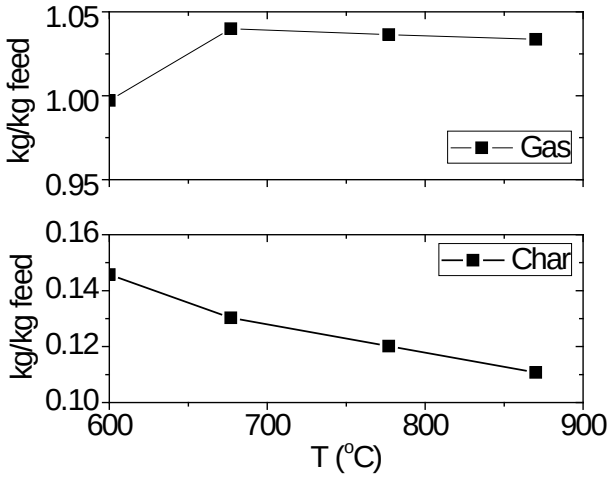

Figure 4. 1 Effect of gasifier temperature on yields of char and dry tar-free gas for the zero-dimensional non-stoichiometric equilibrium model, steam/biomass ratio=1

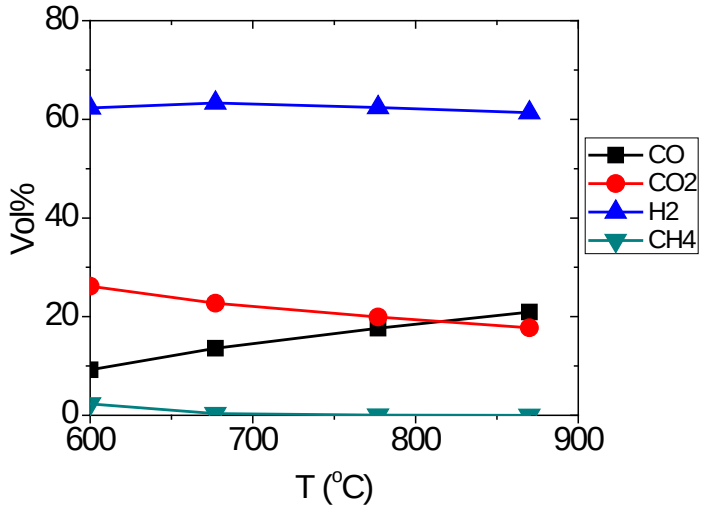

Figure 4. 2 Effect of temperature on the gas distribution on a dry tar-free basis for the zero-dimensional non-stoichiometric equilibrium model, steam/biomass ratio=1

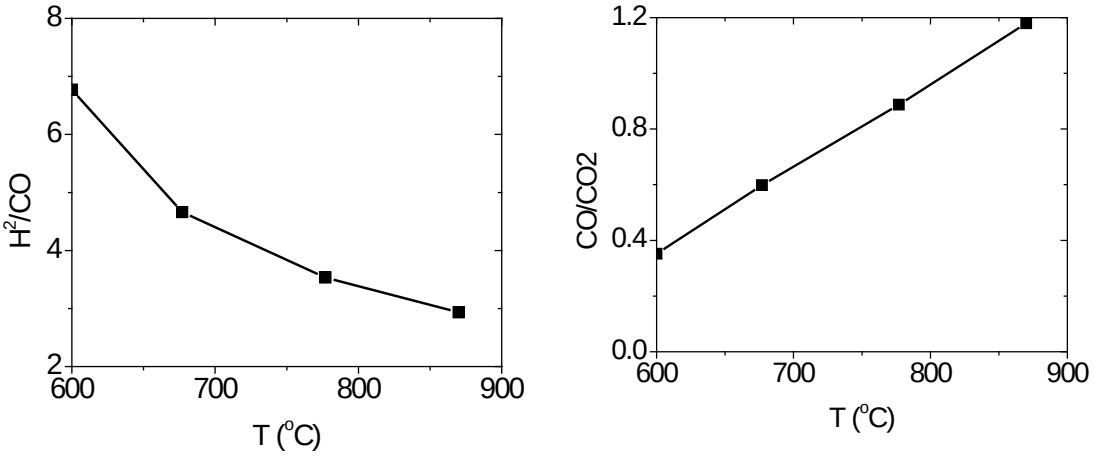

Figure 4. 3 Effect of temperature on the H2/CO ratio and the CO/CO2 ratio for the zero-dimensional non-stoichiometric equilibrium model

The effect of gasifier temperature on gas distribution is shown in Fig. 4.2. Over the range of temperatures studied, the volumetric fraction of H_2 does not change much and decreases about 1%. Meanwhile, the volumetric fraction of CO increases from 9.2% to 20.9%, while that of CO_2 and CH_4 decreases from 26.2% and 2.3% to 17.7% and 0

when the temperature increases from 600 to 870 ^{o}C. The increase of CO and decrease of CO2 and CH4 with increased temperatures are consistent with other studies (Rapagnà, et al., 2000; Loha, Chatterjee, and Chattopadhyay, 2011). The evolution of the H_2/CO ratio and the CO/CO_2 ratio with temperature is shown in Fig. 4.3. The H_2/CO ratio decreases with an elevated temperature, while the CO/CO_2 ratio increases with elevated temperature.

4.1.2 Effect of the steam/biomass ratio

Compared to models considering fluid dynamics, models equilibrium models do not consider fluid dynamics. The temperature of the reactor is 870 ^{o}C. Since equilibrium models are not able to predict the yield of char, the yield of char at different steam/biomass ratios is set in advance at the same value as that obtained for the one-dimensional two-phase kinetic model.

The effect of steam/biomass ratios on the yields of char and dry tar-free gas are shown in Fig. 4.4. The yield of dry tar-free gas increases with increased steam/biomass ratios. As the steam/biomass ratio increases from 0.2 to 1.6, the yield of gas after gasification increases from 0.88 to 1.29 kg/kg feed. In addition, the increase of dry tar-free gas decreases as the steam/biomass ratio increases. The yield of dry tar-free gas increases 0.31 kg/kg feed as the steam/biomass ratio increases from 0.2 to 1.0, while it increases 0.10 kg/kg feed when the steam/biomass ratio increases from 1.0 to 1.6. This is

because as the steam/biomass ratio increases the water-gas shift reaction approaches equilibrium state; thus, although more steam is provided, the rate of the increase of steam consumption decreases.

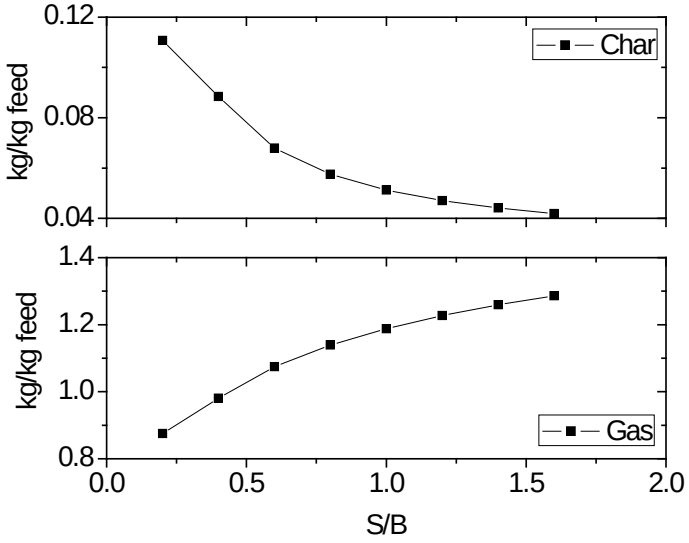

Figure 4. 4 Effect of steam/biomass ratio on the yields of char and dry tar-free gas for the zero-dimensional non-stoichiometric equilibrium model, T=870 ^{o}C

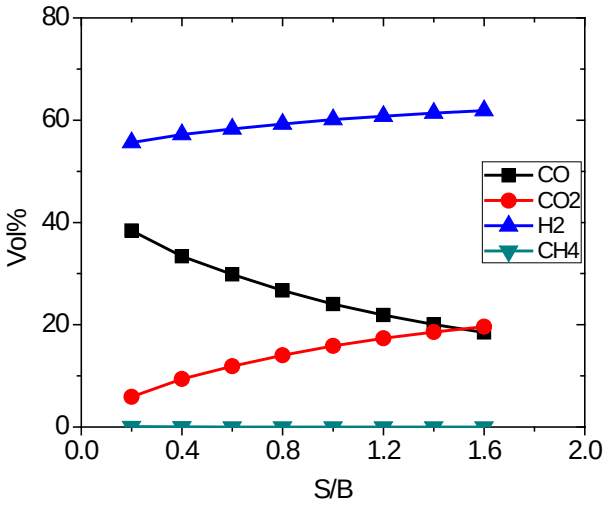

Figure 4. 5 Effects of steam/biomass ratio on gas volumetric fraction for the zero-dimensional non-stoichiometric equilibrium model, T=870 ^{o}C

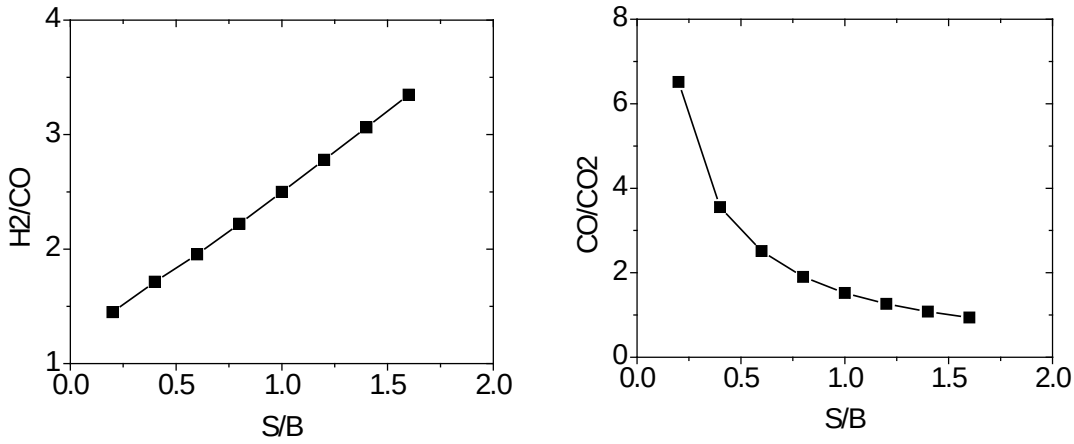

Figure 4. 6 Effect of steam/biomass ratio on the H2/CO ratio and the CO/CO2 ratio for the zero-dimensional non-stoichiometric equilibrium model, T=870 ^{o}C

The gas volumetric fractions at different steam/biomass ratios are shown in Fig. 4.5. As the steam/biomass ratio increases from 0.2 to 1.6, the gas volumetric fractions of CO_2 and H_2 increase from 5.8% and 55.6% to 19.6% and 61.9%, respectively, while those of CO and CH_4 decrease from 38.4% and 0.07% to 18.5% and 0, respectively. The change of gas volumetric fractions with increased steam/biomass ratios can be explained by the relatively rapid water-gas shift reaction and the relatively slow char-gas reactions, and the former reaction plays an important role in determining whether gas concentrations are increased or decreased. The volumetric fraction of CH_4 is almost 0 over the range of steam/biomass ratios studied, which indicates that the yield of CH_4 in the system is very small. This is because the equilibrium model is based on minimum Gibbs free energy, and because CH_4 has large a Gibbs free energy the model does not favor the generation of CH_4. Therefore, without adjusting the yield of gases with large Gibbs free energy, the results predicted by the equilibrium models are not accurate.

The effect of steam/biomass ratio on two important parameters, the hydrogen-to-carbon monoxide ratio and the carbon monoxide-to-carbon dioxide ratio, are shown in Fig. 4.6 for different steam/biomass ratios.

4.2 Zero-dimensional stoichiometric equilibrium model

4.2.1 Effect of temperature

The gasification results at different temperatures are shown in Figs.4.7-4.9. The steam/biomass ratio is 1, and four different temperatures are studied: 600 ^{o}C, 677 ^{o}C, 777 ^{o}C and 870 ^{o}C. As the non-stoichiometric equilibrium model, the stoichiometric equilibrium model also does not consider the effect of gas velocity and mass flow rate, and the yield of char obtained for one-dimensional two-phase kinetic model at different temperatures was used as an input for the stoichiometric equilibrium model at different temperatures.

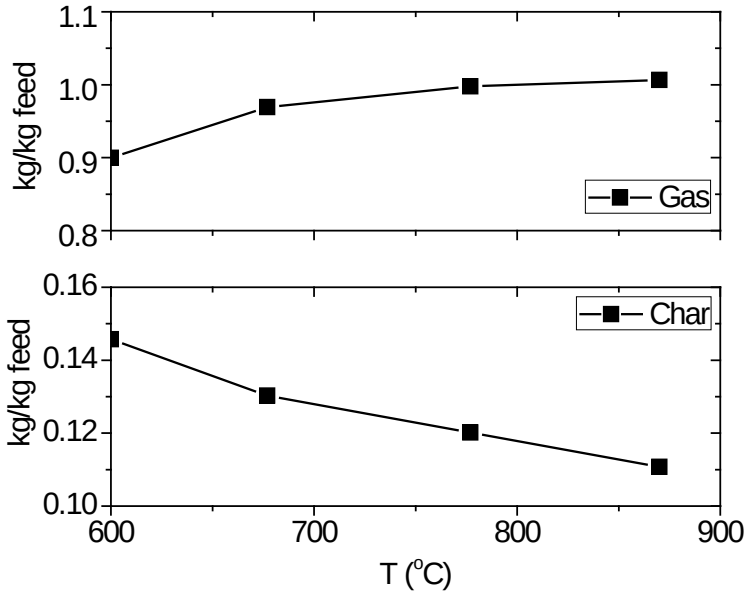

Figure 4. 7 Effect of gasifier temperature on yield of char and dry tar-free gas for the zero-dimensional stoichiometric equilibrium model, steam/biomass ratio=1

The yield of char and dry tar-free gas at different temperatures is available in Fig. 4.7. It can be seen that the yield of gas increases with increased temperature, while that of char decreases when the temperature is increased. With an increase of temperature from 600 to 870 ^{o}C, the yield of dry tar-free gas increases from 0.90 to 1.01 kg/kg feed, and that of char decreases from 0.15 to 0.11 kg/kg feed. This is because with increased temperature, the reaction rate of char-gas reactions becomes larger, and thus more gas is generated and less char is produced, which is consistent with the real process.

The volumetric fraction of gases and values of H_2/CO and CO/CO_2 ratios are shown in Fig 4.8 and Fig 4.9. The volumetric fraction of CO and H_2 increases while that of CO_2 and CH_4 decrease with increased temperature. At 600 ^{o}C the volumetric fractions of CO and H_2 are 6.0% and 55.5%, respectively, and they are increased by 12.0% and 4.9%

when the temperature is increased by 300 ^{o}C from 600 ^{o}C. Meanwhile, the volumetric fraction of CO_2 decreases from 31.0% to 20.9%, and that of CH_4 decreases from 7.4% to 0.7%. This is because with increased temperature, the equilibrium constants (ratios of the partial pressure of products to that of reactants) of the water-gas shift reaction and the C-H_2 reaction decrease. Therefore, due to the decreased equilibrium constant of the C-H_2 reaction with increased temperature, the volumetric fraction of CH_4 decreases, while that of H_2 increases. In addition, due to the decreased equilibrium constant of the water-gas shift reaction, the volumetric fractions of CO_2 and H_2 are decreased while those of CO and H_2O are increased. Because the increase of H_2 by the C-H_2 reaction overweighs the decrease of H_2 by the water-gas shift reaction, the volumetric fraction of H_2 increases with increased temperature.

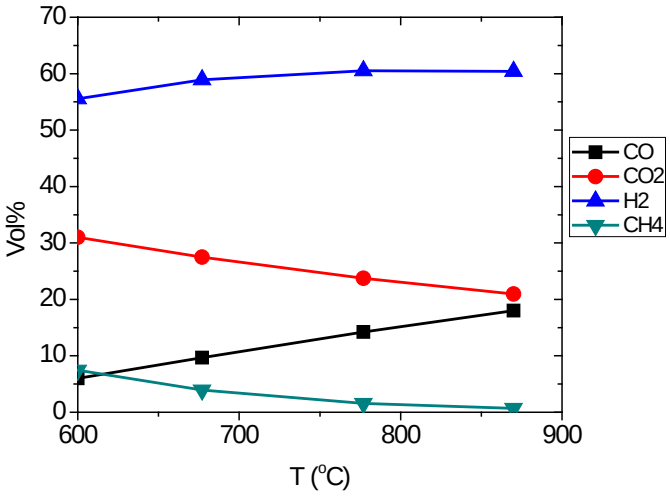

Figure 4. 8 Effect of temperature on gas distribution on dry and tar-free basis for the zero-dimensional stoichiometric equilibrium model, steam/biomass ratio=1

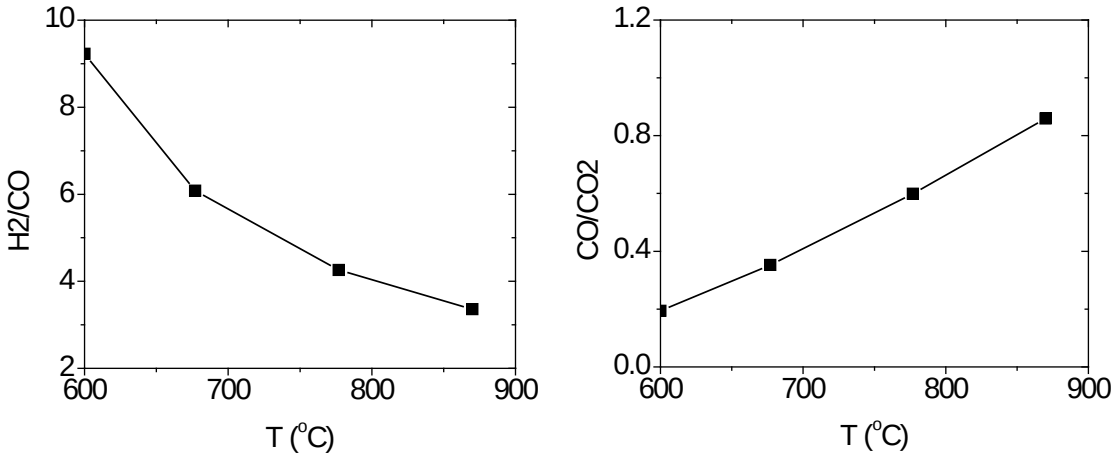

Figure 4. 9 Effects of temperature on H2/CO and CO/CO2 ratios for the zero-dimensional stoichiometric equilibrium model, steam/biomass ratio=1

The evolution of H_2/CO ratio and CO/CO_2 ratio with temperature is shown in Fig. 4.9. From this figure it can be also seen that the rate of increase of H_2 is slower than that of CO, so the H_2/CO ratio decreases with increased temperature. The increase of the CO/CO_2 ratio is mainly due to the increase of CO and decrease of CO_2 with elevated temperature.

4.2.2 Effect of steam/biomass ratio

The temperature of the reactor is 870 ^{o}C. The model does not provide any information on residence time. Since equilibrium models are not able to predict the yield of char, the yield of char at different steam/biomass ratios was set in advance at the same value as that obtained for the one-dimensional two-phase kinetic model.

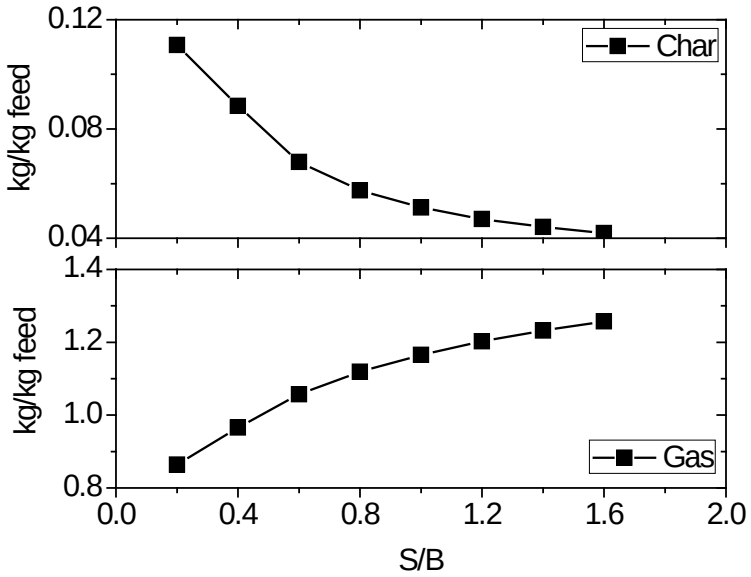

Figure 4. 10 Effects of steam/biomass ratio on gas and char yields for the zero-dimensional stoichiometric equilibrium model, T=870 ^{o}C

The influences of steam/biomass ratios on yields of gasification products using the equilibrium model are shown in Fig. 4.10. It can be seen that as the steam/biomass ratio increases from 0.2 to 1.6, the yield of gas after gasification increases from 0.86 to 1.26 kg/kg feed. In addition, it can also be noticed that as the steam/biomass ratio increases, the rate of the increase of gas yield decreases. The yield of gas increases greatly at low steam/biomass ratios, and as the steam/biomass ratio increases from 0.2 to 1.0, gas yield increases from 0.86 to 1.17 kg/kg fuel while gas yield increases from 1.17 to 1.26 kg/kg fuel with an increase of steam/biomass ratio from 1.0 to 1.6. This is because addition of steam favors the char-steam reaction and the water-gas shift reaction; thus, more char is consumed and more steam is converted to other gases with an increased steam/biomass ratio. However, as the steam/biomass ratio increases the water-gas shift reaction approaches equilibrium state; thus, although more steam is

provide the rate of increase of steam consumption decreases.

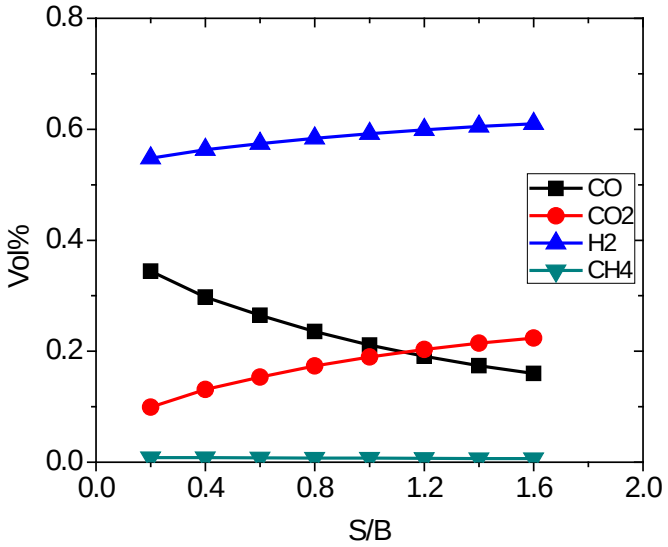

Figure 4. 11 Effects of steam/biomass ratio on gas volumetric fraction for the zero-dimensional stoichiometric equilibrium model, T=870 ^{o}C

The effect of steam/biomass ratios on the volumetric gas fraction is shown in Fig. 4.11. As the steam/biomass ratio increases from 0.2 to 1.6, concentrations of CO_2 and H_2 increase from 9.9% and 54.8% to 22.4% and 61.0%, respectively, while concentrations of CO, and CH_4 decrease from 34.44% and 0.8% to 16.0% and 0.6%, respectively. This is because the rates of production of CO_2 and consumption of CO through the water-gas shift reaction exceed the rates of consumption of CO_2 and the production of CO through the char-CO_2 reaction. Therefore, the concentration of CO_2 increases and that of CO decreases. In addition, because the rate of the char-H_2 reaction is very slow, more H_2 is produced than consumed by the char-H_2 reaction and the volumetric fraction of CH_4 decreases due to increases of the total gas. It can also be seen that the change of gas concentrations at low steam/biomass ratios is faster than at high

steam/biomass ratios, which is consistent with the change of yields of gasification products, and due to the fact that the system cannot turn the same percentage of H_2O to other gases at high steam/biomass ratios as it does at low steam/biomass ratios due to equilibrium state limit.

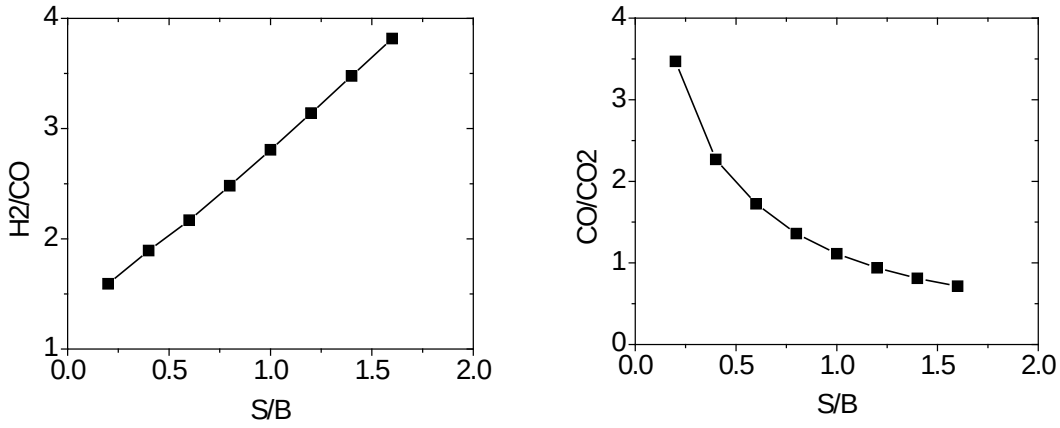

Figure 4. 12 Effect of steam/biomass ratio on H2/CO and CO/CO2 ratios for the zero-dimensional stoichiometric equilibrium model, T=870 ^{o}C

The effects of two important parameters, the hydrogen-to-carbon monoxide ratio and the carbon monoxide-to-carbon dioxide ratio, are shown in Fig. 4.12 for different steam/biomass ratios. The trend obtained for the equilibrium model is consistent with that obtained for the zero-dimensional non-stoichiometric equilibrium model.

4.3 Zero-dimensional kinetic model

Since the zero-dimensional kinetic model does not consider fluid dynamics and reactor geometry, the variables studied are the steam/biomass ratio, the temperature, and the particle size.

4.3.1 Evolution of gasification products with time

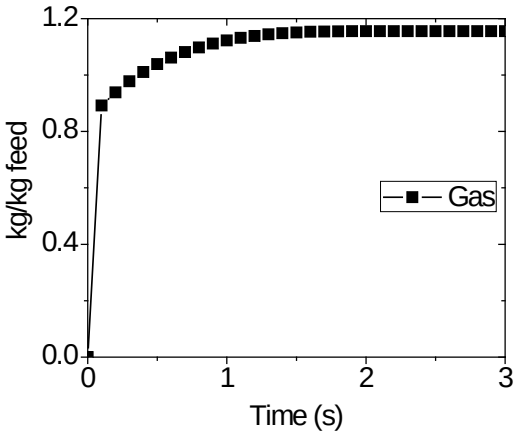

(a) Yield of dry tar-free gas

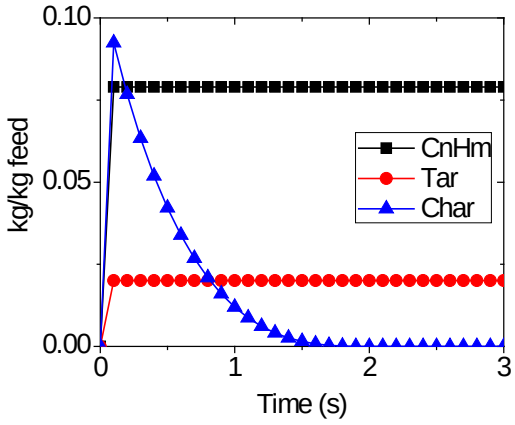

(b) Yield of char, tar and C_nH_m

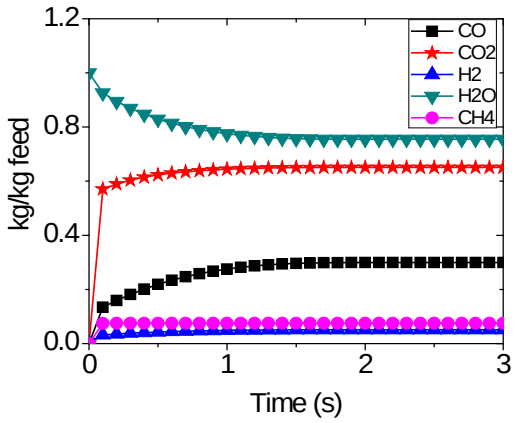

(c) Yields of gases

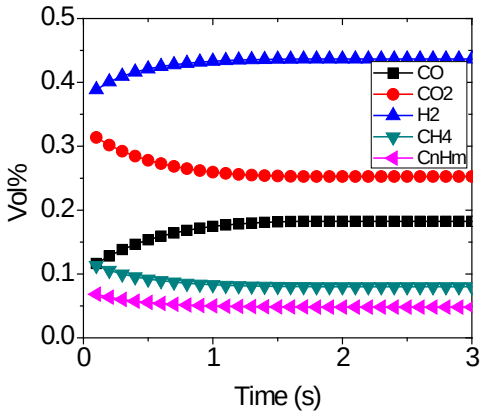

(d) Gas volumetric fraction

Figure 4. 13 Evolution of gasification products with time for the zero-dimensional kinetic model, T=870 ^{o}C, steam/biomass ratio=1, particle size=0.3mm

The evolution of gasification products with time was studied for corn stover at 870 ^{o}C. In order to compare with other models, the particle size of 0.3 mm used in the one-dimensional two-phase kinetic model is used in this model. The steam/biomass ratio is 1. The results predicted by the zero-dimensional kinetic model are shown in

Fig. 4.13. It can be seen that as reaction time increases the yields of dry tar-free gas, CO, and CO_2 increase, and the increase is relatively more significant than that of H_2 and CH_4. It can also be seen that the yields of C_nH_m and tar remain constant because they do not take part in any reactions except for the pyrolysis reaction. The amount of char in the reaction decreases rapidly in the first 1.5 seconds, which leads to the rapid change of the gas volumetric fraction and gas yields during that time. When the reaction time increases further, because there is no char in the reactor, the system reaches an equilibrium state, so there is no change in the gas yields or gas volumetric fractions as the time increases.

4.3.2 Effect of temperature

Four different temperatures are studied: 600 ^oC, 677 ^oC, 777 ^oC and 870 ^oC. The steam/biomass ratio used is 1. The particle size is 0.3 mm. The evolution of char in the bed with time is shown in Fig. 4.14. At time 0 there are only steam and unpyrolized fuel in the bed, and the mass of char and gases is zero. Then the unpyrolized fuel goes through the pyrolysis process which is controlled by the pyrolysis model, during which char and gases are generated. Meanwhile, the char generated during pyrolysis process takes part in the char-gas reactions, which leads to the decrease of char in the bed. The consumption of char is much faster at higher temperatures than at lower temperatures. It takes only 1.8 seconds and 10 seconds to consume all the char in the bed once the fuel is sent to the bed at 870 ^oC and 770 ^oC, respectively, while after 70 seconds two thirds of char is still left un-reacted at 600 ^oC.

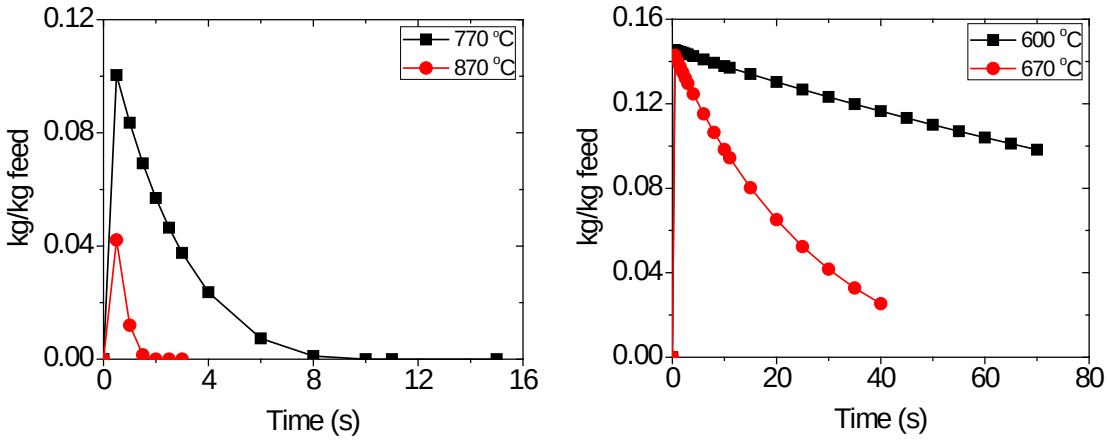

Figure 4. 14 Char in the bed for the zero-dimensional kinetic model, steam/biomass ratio=1, the particle size=0.3 mm

The gasification results at different temperatures are shown in Figs. 4.15-17. The gasification results obtained at 1 s and at 5 s are very close at 600 ^{o}C. Then, as the temperature increases, the difference between these results increases and reaches a maximum value at 770 ^{o}C. Afterwards, these results become close again and are almost the same at 870 ^{o}C. This is because at low temperatures, the reaction rate is very slow and the generation or consumption of material is very small during unit time. Therefore, there is little difference between the gasification products at 1 s and those at 5 s. As temperature increases, the reaction rate also increases and production and consumption become larger than they are at lower temperatures, which leads to significant change in unit time. However, when the temperature is high enough such as 870 ^{o}C used in this study, the reaction rate is so fast that most reactions are completed during a very short time, and after that there is little change in the gasification products, which can explain the similar results obtained at 1 s and 5 s.

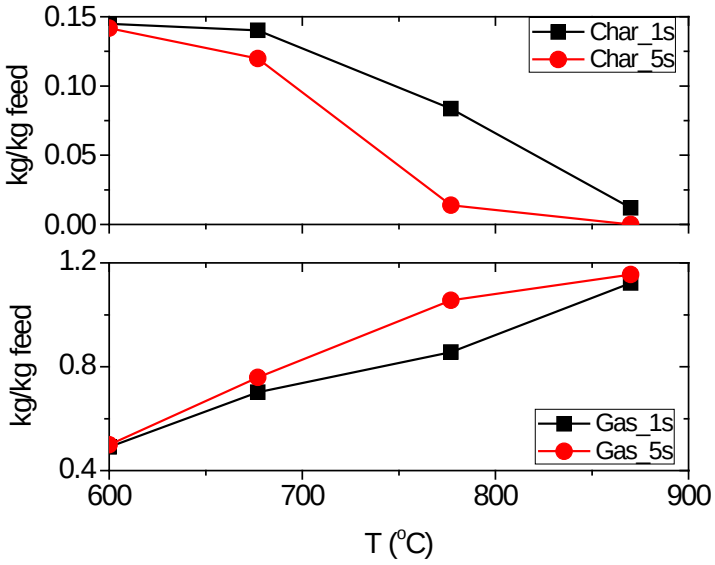

Figure 4. 15 Effect of gasifier temperature on yields of char and dry and tar-free gas for the zero-dimensional kinetic model, steam/biomass ratio=1, the particle size=0.3 mm

The yield of char and dry tar-free gas at different temperatures is shown in Fig. 4.15. It can be seen that the yield of char decreases with elevated temperatures while that of dry and tar-free gas increases with elevated temperatures. When the temperature increases from 600 ^{o}C to 870 ^{o}C , at 1 s the yield of dry tar-free gas increases from 0.49 to 1.12 kg/kg feed and that of char decreases from 0.15 to 0.01 kg/kg feed, while at 5 s the yield of dry tar-free gas increases from 0.50 to 1.16 kg/kg feed , and that of char decreases from 0.14 to 0 kg/kg feed.

The effect of gasifier temperature on the gas volumetric fractions is shown in Fig. 4.16. It can be seen that the volumetric fraction of H_2 increases greatly from about 25% to 43%, while that of CO only has a slight increase which is about 1.3-1.4% when the

temperature increases from 600 ^{o}C to 870 ^{o}C. Meanwhile, the volumetric fraction of CO_2, CH_4 and C_nH_m decreases, which is about 13%, 4.4% and 1.4% for CO_2, CH_4, and C_nH_m, respectively with an increase of temperature from 600 ^{o}C to 870 ^{o}C. The increase of H_2 and CO and decrease of CO_2 is mainly due to char-gas reactions during which H_2 and CO are produced and CO_2 is consumed. In addition, the decrease of CO_2 and the minor increase of CO indicate that the effect of char-gas reactions is larger than that of the water-gas shift reaction, and char-gas reactions take an important role in determining the gas compositions and their yields. The decrease of the volumetric fraction of CH_4 and C_nH_m proves the increase of gas with increased temperature.

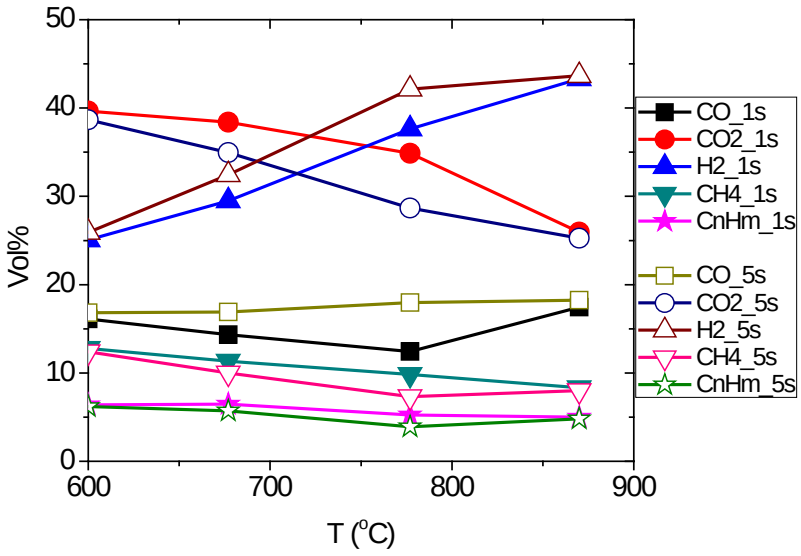

Figure 4. 16 Effect of temperature on the gas volumetric fraction on a dry and tar-free basis for the zero-dimensional kinetic model, steam/biomass ratio=1, the particle size=0.3 mm

The values of the H_2/CO and CO/CO_2 ratios with elevated temperature are shown in Fig. 4.17. It can be seen from these two figures that the H_2/CO ratio first increases

then decreases with increased temperature after reaching a maximum value, which indicates the rate of increase of H_2 and the decrease of CO. As for the CO/CO_2 ratio, it increases with increased temperature, and indicates an increase of CO and a decrease of CO_2.

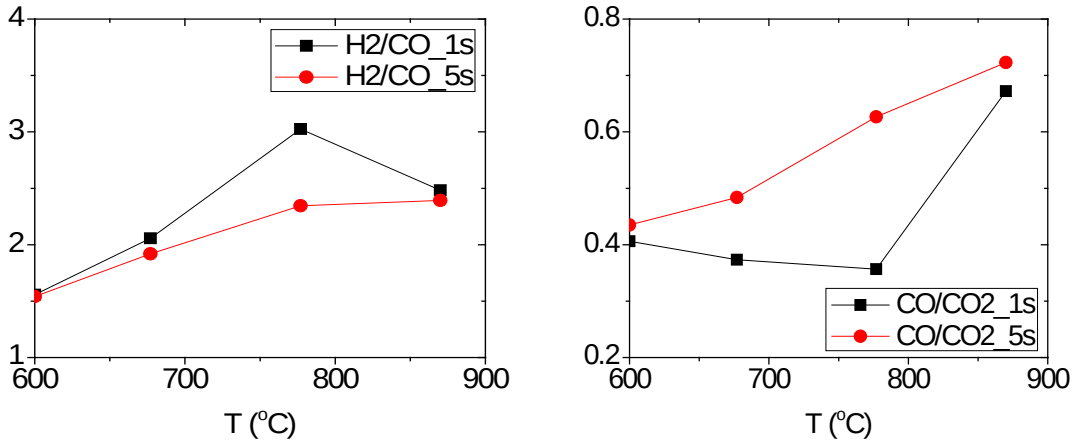

Figure 4. 17 Effects of temperature on the H2/CO and CO/CO2 ratios for the zero-dimensional kinetic model, steam/biomass ratio=1, the particle size=0.3 mm

4.3.3 Effect of steam/biomass ratio

From the evolution of gasification products with time, it can be seen that the reaction rate is fast and char is consumed in 2 seconds. Therefore, the effect of steam/biomass ratios on gasification products in the reactor is studied by using the gasification products at the 1st second. The temperature is 870 ^{o}C, and the particle size is 0.3mm.

As the steam/biomass ratio increases, the volumetric fraction of H_2 and CO_2 increases from 33.1% and 16.1% to 46.9% and 30.0%, respectively, while that of CO, CH_4, and C_nH_m decreases from 33.9%, 10.5% and 6.3% to 10.8%, 7.7% and 4.6%, respectively.

The change of H_2, CO, and CO_2 is mainly determined by the water-gas shift reactions, and the change of C_nH_m and CH_4 is mainly determined by the change of the total gas volume. In addition, with increased steam/biomass ratios, the reaction rate of char-gas reaction increases, which leads to the increase of dry tar-free gas from 0.92 kg/kg feed to 1.21 kg/kg feed and the decrease of char from 0.038 kg/kg feed to 0.0057 kg/kg feed.

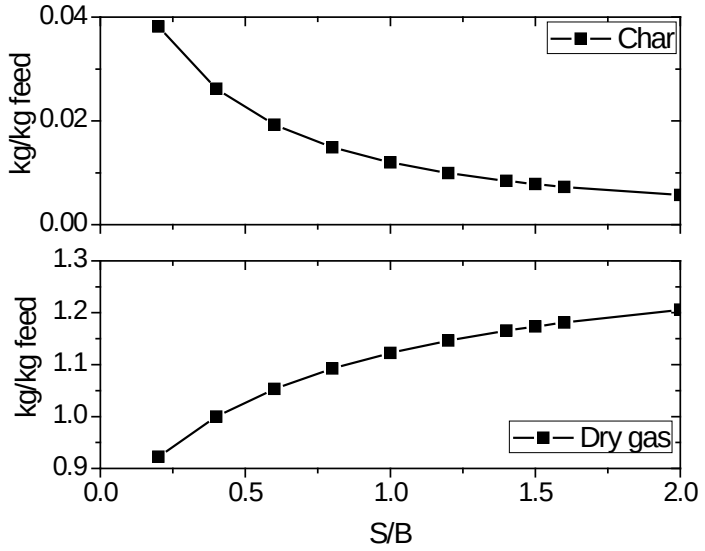

Figure 4. 18 Effect of steam/biomass ratio on yields of char and dry tar-free gas for the zero-dimensional kinetic model, T=870 ^oC, the particle size=0.3mm

The effects of steam/biomass ratios on H_2/CO and CO/CO_2 ratios are shown in Fig. 4.20. The change of H_2/CO and CO/CO_2 ratios reflects the change of gas volumetric fractions with increased steam/biomass ratios.

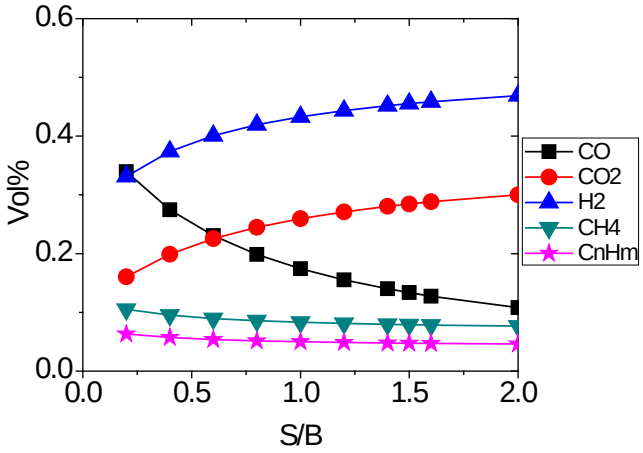

Figure 4. 19 The effect of steam/biomass ratio on gas volumetric fractions for the zero-dimensional kinetic model, T=870 ^{o}C, the particle size=0.3mm

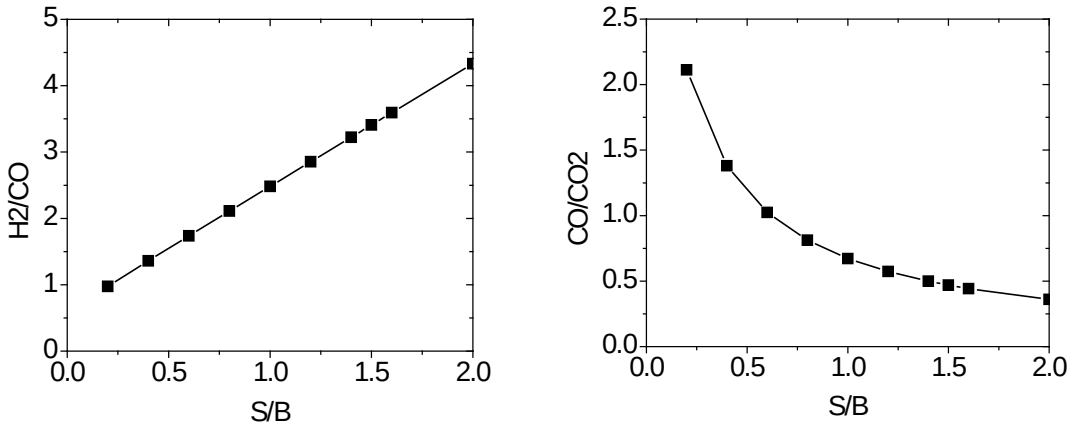

Figure 4. 20 Effect of steam/biomass ratio on H2/CO and CO/CO2 ratios for the zero-dimensional kinetic model, T=870 ^{o}C, the particle size=0.3mm

4.3.4 Effect of Particle size

The effect of particle size was studied for the zero-dimensional kinetic model, and the change of the yields of char and gas and the gas distribution with time is shown in Figs. 4.21 and 4.22. The temperature of the system is 870 ^{o}C, and the steam/biomass ratio is

1. It can be seen that the difference between the gasification results for cases with different particle sizes is relatively large in the first 8 seconds in terms of the yields of dry tar-free gas and char and gas composition distribution. Particles with a smaller size generate more gas and less char while particles with a larger size generate less gas and more char. The difference is mainly due to the pyrolysis model used in this study which predicts different yields of char and gases for different particle sizes. Therefore, if fuel stays in the bed for just a few seconds, the effect of particle size should be considered. However, when the reaction time exceeds 8 seconds, the difference between the gasification results for different particle sizes gets smaller, and finally approaches zero, which is mainly because particles are consumed and gases reach the equilibrium state at the end.

The effect of particle size on gasification products at different steam/biomass ratios is shown in Fig. 4.23. It can be seen that at 1 s the difference between the yields of char with different particle sizes during the whole range of steam/biomass ratios is as large as 0.063 kg/kg feed, and the maximum difference between the yields of gas for different particle sizes during the whole range of steam/biomass ratios studied is 0.19 kg/kg feed. At 5 s, the difference between the yields of char and dry tar-free gas for different particle sizes becomes smaller, and the maximum differences between the yields of char and dry tar-free gas are 0.051 and 0.094 kg/kg feed. In addition, it can be noticed that at 1 second the difference between the yields of char and dry tar-free

gas increases with increased steam/biomass ratios, while at 5 s it decreases with increased steam/biomass ratios.

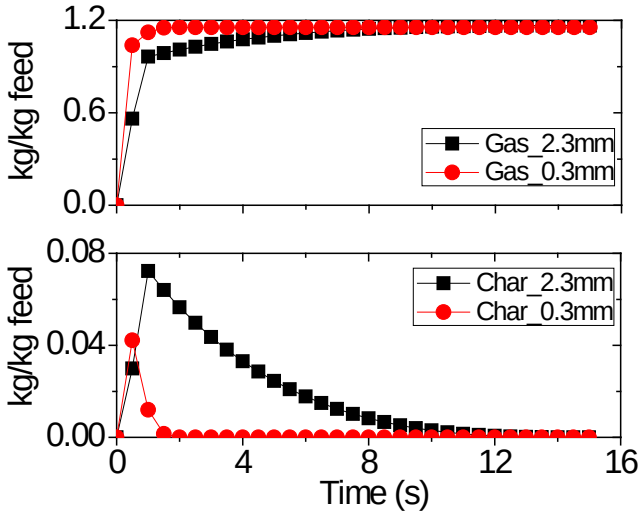

Figure 4. 21 Effect of particle size on yields of char and dry tar-free gas with time for the zero-dimensional kinetic model, T=870 ^{o}C, steam/biomass ratio=1

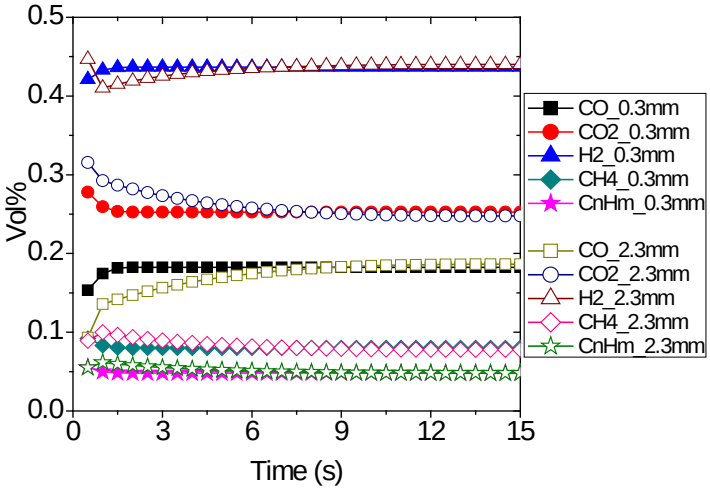

Figure 4. 22 Effect of particle size on gas distribution with time for the zero-dimensional kinetic model, T=870 ^{o}C, steam/biomass ratio=1

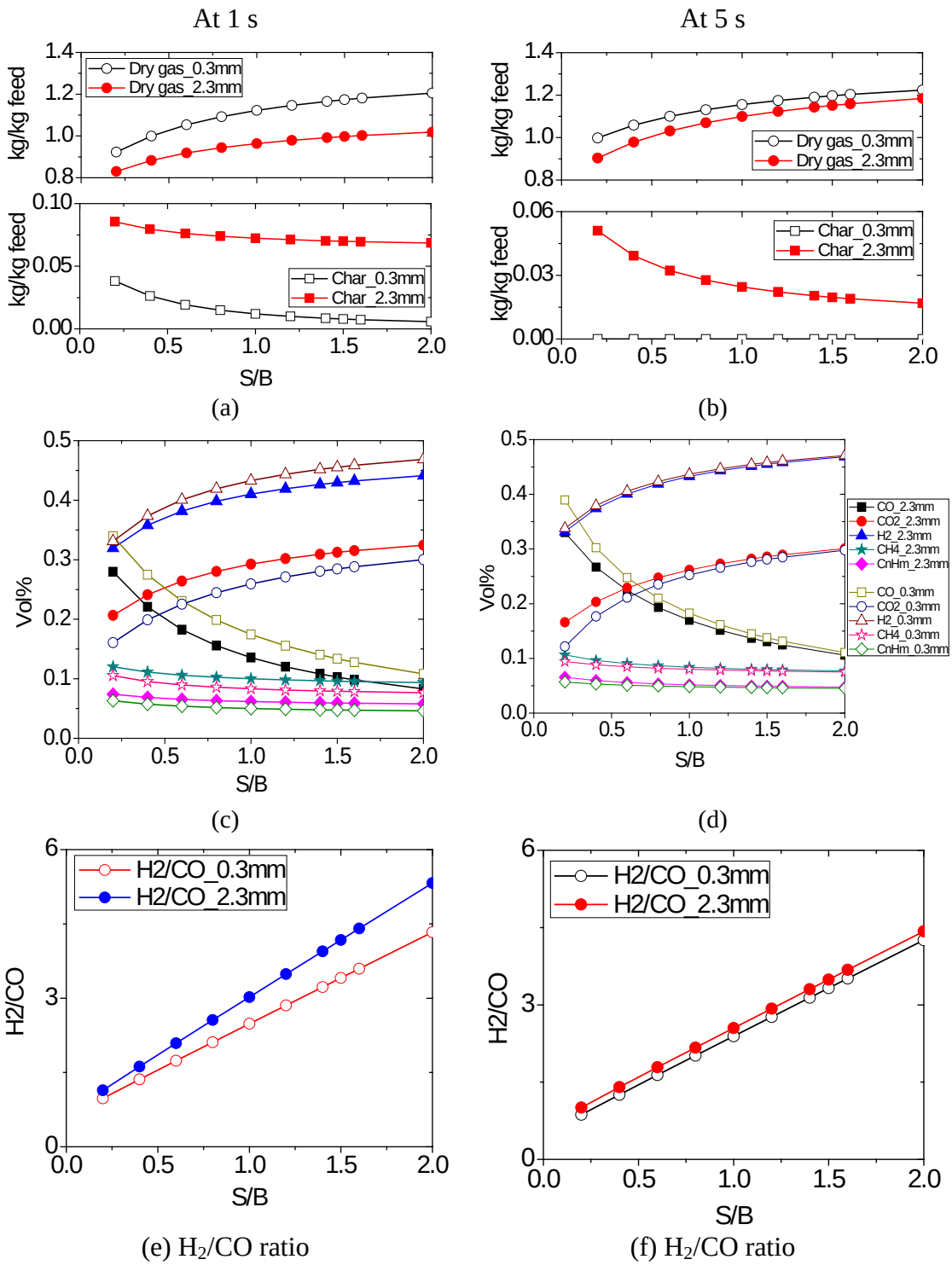
At 1 s
At 5 s
kg/kg feed
Dry gas_0.3mm
Dry gas_2.3mm
Char_0.3mm
Char_2.3mm
S/B
(a)
(b)
Vol%
CO_2.3mm
CO2_2.3mm
H2_2.3mm
CH4_2.3mm
CnHm_2.3mm
CO_0.3mm
CO2_0.3mm
H2_0.3mm
CH4_0.3mm
CnHm_0.3mm
(c)
(d)
H2/CO
H2/CO_0.3mm
H2/CO_2.3mm
(e) H2/CO ratio
(f) H2/CO ratio

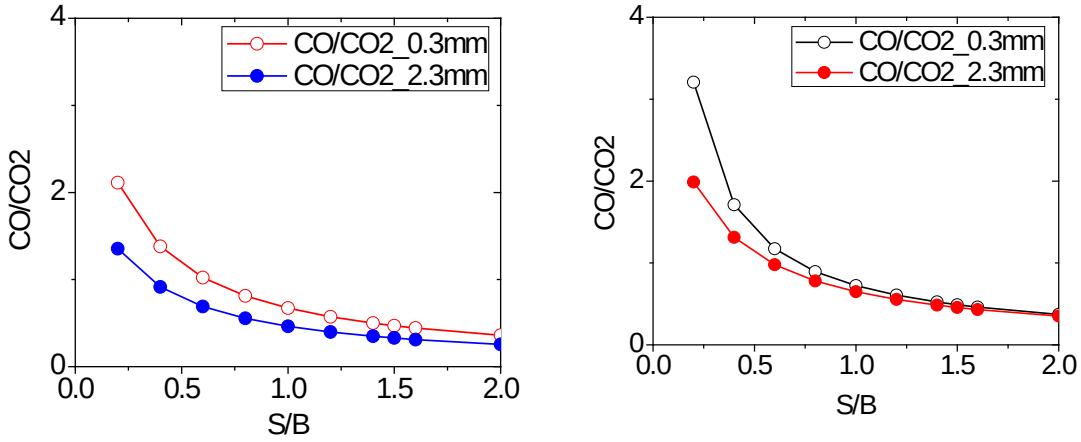

(g) CO/CO_2 ratio (h) CO/CO_2 ratio

Figure 4. 23 Effects of particle size, steam/biomass ratio, and reaction time for the zero-dimensional kinetic model, T=870 ^{o}C, steam/biomass ratio=1

Comparing the evolution of the H_2/CO ratio and the CO/CO_2 ratio with increased steam/biomass ratios in Fig. 4.23 (e-h), it can be seen that for different particle sizes there is little difference between the values of H_2/CO and CO/CO_2 at 5 s and the difference between the values of H_2/CO and CO/CO_2 at 1 s is relatively large, which is consistent with the results of other variables for different particle sizes. In addition, by comparing the values of H_2/CO and CO/CO_2 over the range of steam/biomass ratios with different amounts of time, the value of H_2/CO at 1 s is larger than that at the 5th second, while the value of CO/CO_2 at 1 s is smaller than that at 5 s, which indicates the increase of CO concentration with time.

4.4 One-dimensional one-phase kinetic model

4.4.1 Products distribution with time and height

The following results are presented under this operating condition: 1) The temperature is 870 ^{o}C; 2) the initial particle size is 0.3 mm; and 3) the steam/biomass ratio is 1, and superficial gas velocities are 0.3 and 0.4 m/s. The concentration of gases along the reactor height is shown in Fig. 4.24. As the height increases from the bottom to the top the change of yields of gases mainly happens under the height of 0.5 m, and beyond 0.5 m the yields of gases change little. This is mainly because char reactions only happen in the fluidized bed section which is no higher than 0.5m; thus, the yields of gases change significantly. Because there is only a water-gas shift reaction in the freeboard which is from 0.5 to 2.76 m, and because the water-gas shift reaction reaches equilibrium state rapidly, there is little change of the yields of gases when the height is higher than 0.5 m. Compared to the yields of gases, the gas volumetric fraction remains almost the same over the entire reactor.

The evolution of char and the size of a single particle in the bed with time is shown in Figs. 4.25 and 4.26. It can be seen that it takes about 200 s and 50 s for the bed to reach steady state at superficial velocities of 0.3 m/s and 0.4 m/s, respectively. The amount of time taken for the bed to reach steady state depends on the reaction rates and the superficial gas velocity. Since the absolute value of reaction rates for corn stover is unknown, the time obtained here may be different from that of the real

process.

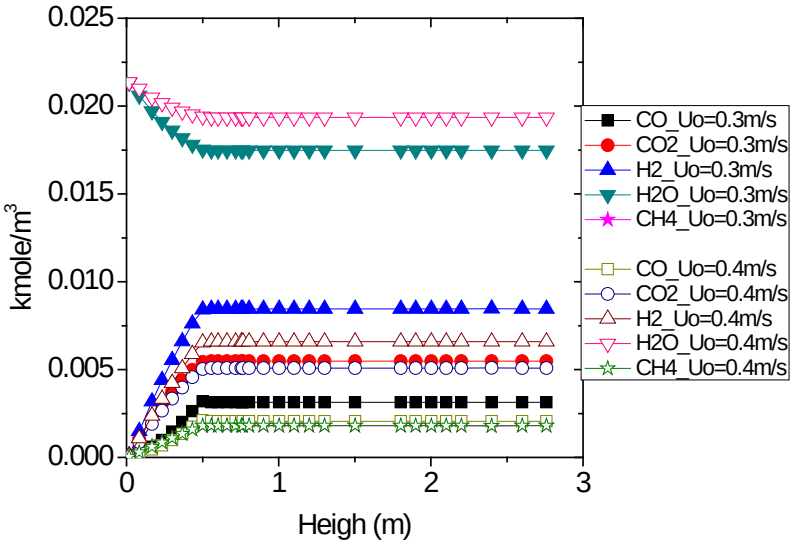

Figure 4. 24 Gasification products distribution with height for the one-dimensional one-phase kinetic model, T=870 ^{o}C, steam/biomass ratio=1, the particle size is 0.3 mm, and the superficial gas velocities (U_o) are 0.3 and 0.4 m/s

The evolution of the size of a single particle sent to the reactor at each time step is studied and shown in Fig. 4.26. After particles are sent to the reactor, particle size decreases significantly due to pyrolysis. Meanwhile, particle size also decreases due to chemical reactions. Because the reaction rates of char gasification are much slower than that of pyrolysis, the rate of the decrease of the particle size due to chemical reactions is slower than due to pyrolysis. Particles leave the fluidized bed when the particle size reaches critical size. From Fig. 4.26 it can be seen that the particles stay in the bed for a longer time at a lower superficial gas velocity than at a higher superficial gas velocity, and the time the particles stay in the bed is close to that taken for the bed to reach steady state.

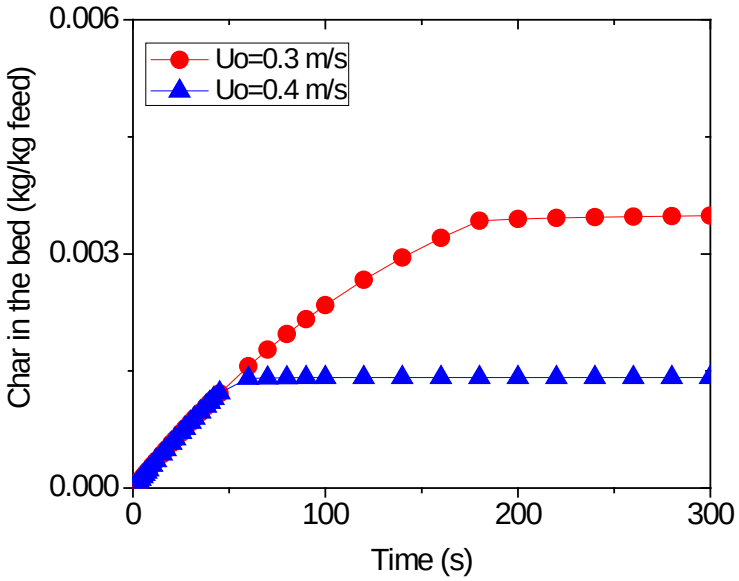

Figure 4. 25 Evolution of char in the bed with time for the one-dimensional one-phase kinetic model, T=870 ^{o}C, steam/biomass ratio=1, the particle size is 0.3 mm, and superficial velocities (U_o) are 0.3 and 0.4 m/s

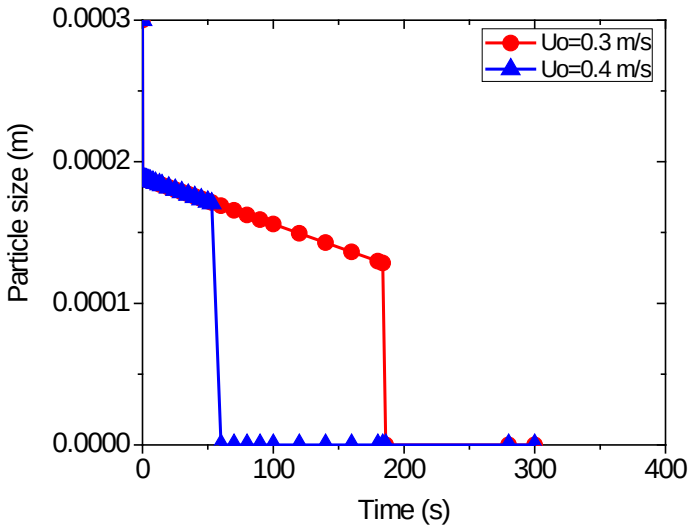

Figure 4. 26 Evolution of the size of a single particle in the bed for the one-dimensional one-phase kinetic model, T=870 ^{o}C, steam/biomass ratio=1, the particle size is 0.3 mm, and superficial velocities (U_o) are 0.3 and 0.4 m/s

4.4.2 Effect of temperature and superficial gas velocity

Four different temperatures are studied: 600 ^{o}C, 677 ^{o}C, 777 ^{o}C and 870 ^{o}C, and at each temperature five superficial gas velocities are selected: 0.12, 0.2, 0.3, 0.4 and 0.5 m/s. The particle size is 0.3 mm.

The yields of char and dry tar-free gas at different temperatures and superficial gas velocities are shown in Fig. 4.27. As the gasifier temperature increases, the amount of dry tar-free gas increases, while that of char produced decreases, which is consistent with the results obtained by other models. The reasons explaining this kind of change is the same as those in previous section for other models. Elevated temperature increases the amount of gases produced through pyrolysis and decreases that of char. In addition, elevated temperature favors the water-gas shift reaction and char-gas reactions, so more combustible gases are generated at higher temperature than at lower temperature. It can be also seen from Fig. 4.27 that the yield of dry tar-free gas decreases with increased superficial gas velocity, while that of char decreases. This is mainly because the amount of char entrained out of the bed increased with increased superficial gas velocity, so based on mass balance that of dry tar-free gas decreases.

The gas volumetric fraction at different temperatures and superficial gas velocity is shown in Fig. 4.28. First it can be noticed that although the gas volumetric fraction does not change significantly over the range of temperatures studied, the gas volumetric fraction of CO and CO_2 decreases, while that of H_2 increases. As the

temperature increases, the reaction rate of char-gas reactions increases, so more CO_2 is consumed and more CO and H_2 are generated. However, because the reaction rate of the water-gas shift reaction also increases, the consumption of CO through the water-gas shift reaction also increases. The overall result of the water-gas shift reaction and the char-gas reactions is the increase of H_2 and decrease of CO and CO_2. In addition, it can be seen that the gas volumetric fractions at 0.12 m/s and 0.2 ms/s are very close, and the gas volumetric fractions at other superficial gas velocities are also very close, which results from the values of their similar solid residence times in the bed.

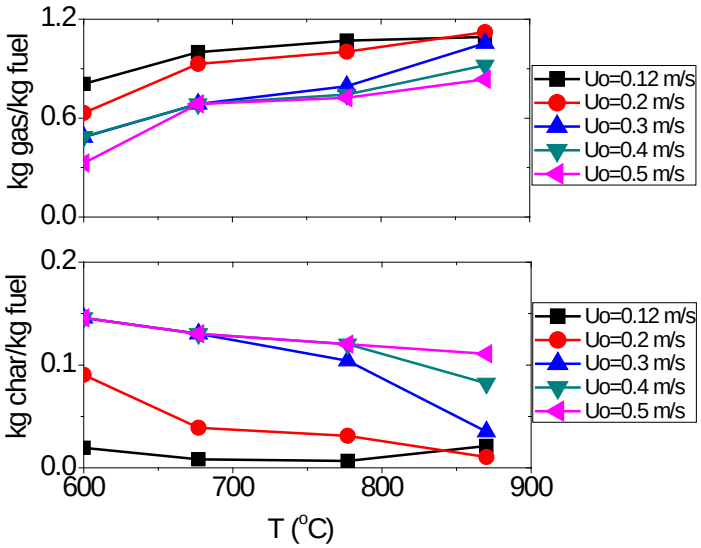

Figure 4. 27 Effect of gasifier temperature and superficial velocity (U_o) on yields of char and dry and tar-free gas for the one-dimensional one-phase kinetic model, steam/biomass ratio=1, and the particle size is 0.3 mm

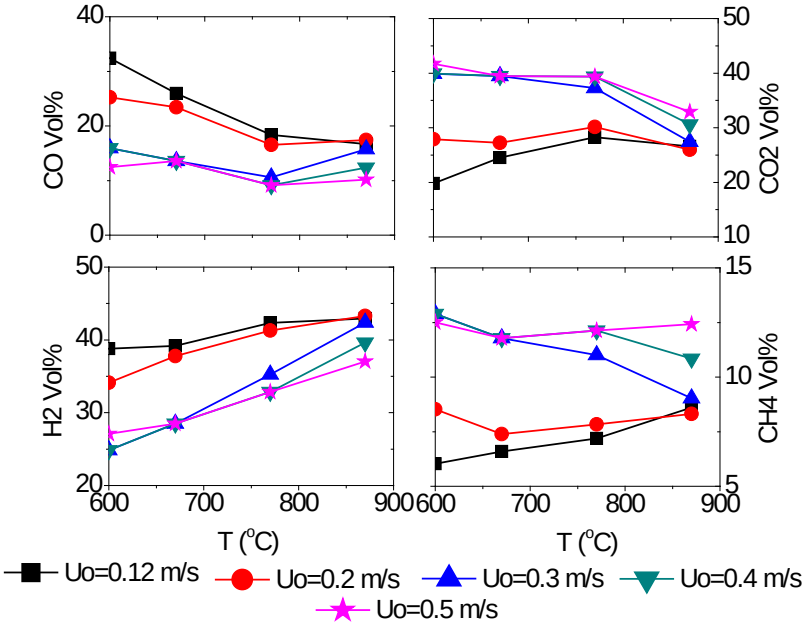

Figure 4. 28 Effect of temperature and superficial gas velocity (U_o) on the gas volumetric fraction for the one-dimensional one-phase kinetic model, steam/biomass ratio=1, and the particle size is 0.3 mm

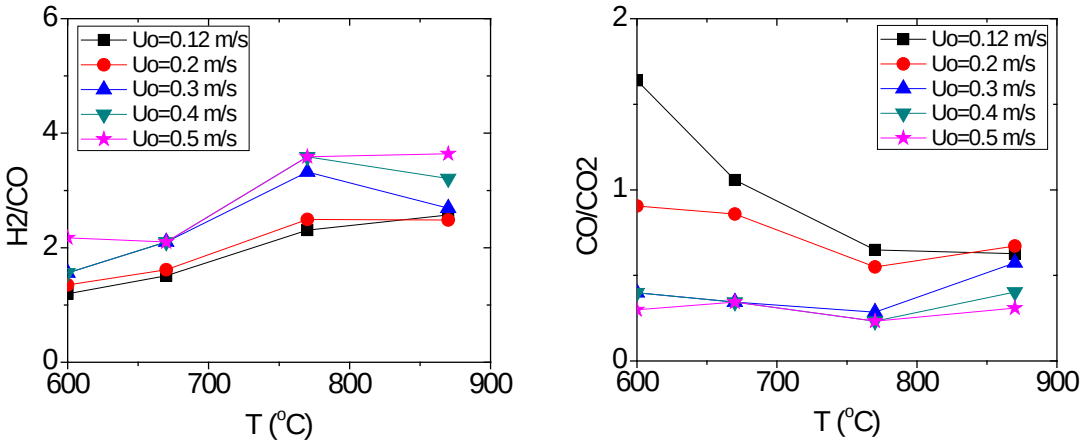

Figure 4. 29 Effect of temperature and superficial gas velocity (U_o) on H2/CO and CO/CO2 ratios for the one-dimensional one-phase kinetic model, steam/biomass ratio=1, and the particle size is 0.3 mm

The evolution of the H_2/CO ratio and the CO/CO_2 ratio with elevated temperatures and

increased superficial gas velocities is shown in Fig. 4.29. The change of H_2/CO ratio and CO/CO_2 ratio is an indication of the evolution of the gas volumetric fraction over the range of temperatures and superficial gas velocities studied.

4.4.3 Effect of superficial gas velocity and steam/biomass ratio

The effect of superficial gas velocity and steam/biomass ratio on the yields of gasification products is studied. Five superficial gas velocities are evaluated: 0.12 m/s, 0.2 m/s, 0.3 m/s, 0.4 m/s, and 0.5 m/s, and the minimum superficial gas velocity of 0.12 m/s is selected because the minimum fluidization velocity is 0.11 m/s. In addition, for each superficial gas velocity, four different steam/biomass ratios are studied: 0.25, 0.5, 1.0, and 1.5. The steam/biomass ratios are varied by varying the mass flow rate of fuel, while that of steam is constant. The temperature is 870 ^{o}C, and the initial particle size is 0.3 mm.

The yields of dry tar-free gas and char at different superficial gas velocities are shown in Fig. 4.30. It can be seen that with increased superficial gas velocity, the yield of dry tar-free gas decreases, while that of char increases. The increase of the yield of dry tar-free gas and the decrease of the yield of char is mainly due to the modeling concept of the kinetic model. The amount of char produced is calculated based on the amount of char entrained out of the bed, and the char entrainment is related to the superficial gas velocity. With an increased superficial gas velocity, char particles are entrained out of the bed with a larger particle size, so the amount of char entrained out of bed is

increased. In addition, at steady-state the amount of fuel and steam fed to the gasifier equals the amount of gas and char leaving the bed. With an elevated superficial gas velocity, while the yield of char increases, that of gas decreases based on mass balance. It can be also seen from Fig. 4.30 that as the superficial gas velocity increases, the yield of char at different steam/biomass ratios reaches a constant value, and that of dry tar-free gas at different steam/biomass ratios also reaches a constant value. This is because fuel particles sent to the bed first experience pyrolysis, then the pyrolyzed particles are evaluated whether they can be entrained out of the bed before they take part in gasification reactions. Because the initial particle size of fuel particles is smaller than 0.7 mm, all fuel particles are pyrolyzed immediately after they are sent to the reactor. As the superficial gas velocity increases, fuel particles spend less time in the bed. When the superficial gas velocity is 0.5 m/s, fuel particles at each steam/biomass ratio are entrained out of the bed immediately after they are sent to the reactor and are pyrolyzed. Therefore, the yield of char at each steam/biomass ratio reaches a constant value at 0.5 m/s, and the yield of dry tar-free gas at each steam/biomass ratio also approaches together.

In addition, as the steam/biomass ratio increases, the yield of dry tar-free gas after gasification also increases, while that of char decreases. This is because the addition of steam favors the char-steam reaction (Eqn. (2.6)) and the water-gas shift reaction (Eqn. (2.10)), so with an increased steam/biomass ratio more char is consumed and more steam is converted to other gases. In addition, the increase of the dry tar-free gas yield

and the decrease of the yield of char slow down with increased steam/biomass ratios. This is because as the steam/biomass ratio increases, the water-gas shift reaction approaches the equilibrium state. Therefore, although more steam is provided with increased steam/biomass ratios, the amount of dry tar-free gas generated decreases.

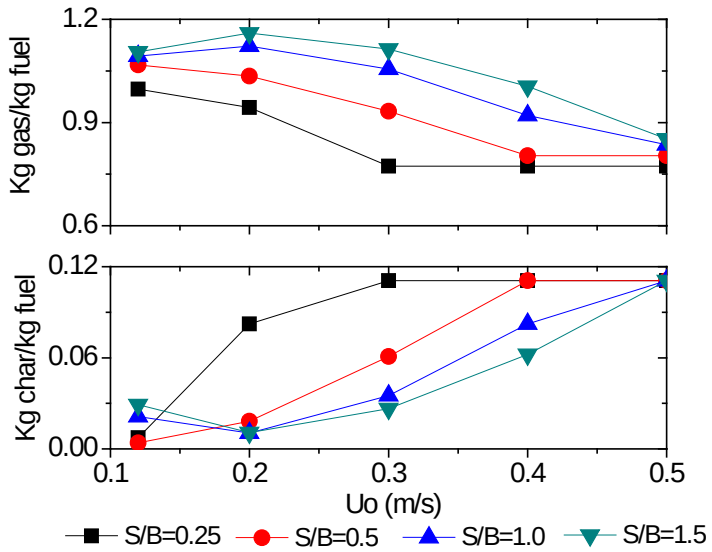

Figure 4. 30 Effect of superficial gas velocity (U_o) and steam/biomass (S/B) ratio on yields of char and dry tar-free gas for the one-dimensional one-phase kinetic model, T=870 ^oC, and the particle size is 0.3 mm

The effect of steam/biomass ratio on the gas volumetric fraction is shown in Fig. 4.31. The trend of the change of the gas volumetric fraction over the range of steam/biomass ratios and superficial gas velocities studied is similar to that obtained for the other models. With increased steam/biomass ratios, the gas volumetric fraction of CO_2 and H_2 increases, while concentrations of CO, CH_4, C_nH_m decrease. This is because the reaction rate of the water-gas shift reaction is much faster than that of char gasification reactions, thus the gas volumetric fraction of CO_2 and H_2 increases, and that of CO

decreases. As for the gas volumetric fraction of CH_4 and C_nH_m, it decreases due to the increased total gas yield. In addition, with increased superficial gas velocity, the gas volumetric fraction of CO and H_2 decreases, while that of CO_2 and CH_4 increases. This is because with increased superficial gas velocity, the reaction time of char-gas reactions decreases. Therefore, the amount of CO and H_2 generated through C-H_2O and C-CO_2 reactions decreases, leading to the increase of CO_2. When the superficial gas velocity increases to a certain value, the gas volumetric fraction reaches a constant value, which is due to the char entrainment as discussed before.

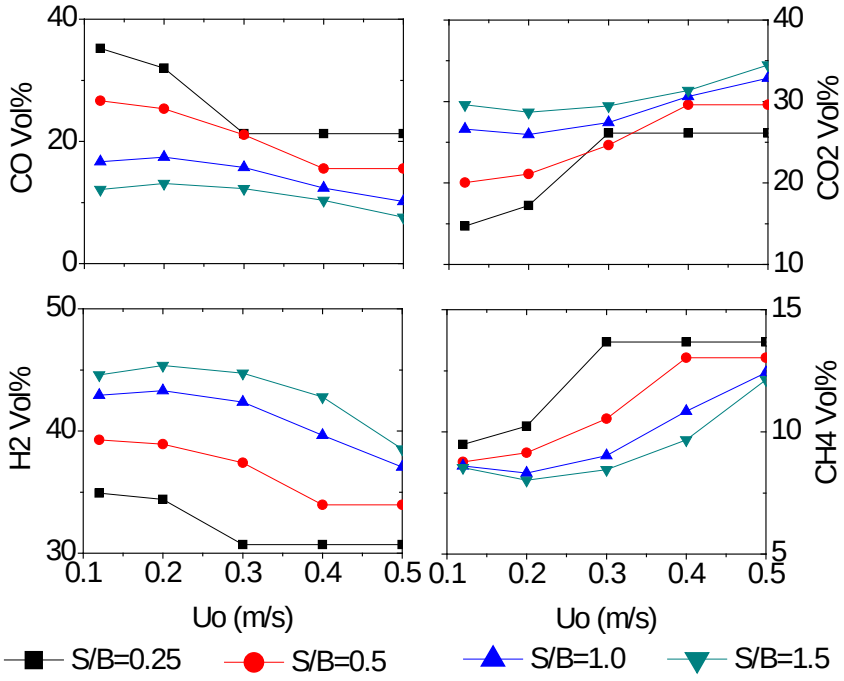

Figure 4. 31 The effect of superficial gas velocity (U_o) and steam/biomass (S/B) ratio on gas volumetric fractions for the one-dimensional one-phase kinetic model, T=870 ^oC, and the particle size is 0.3 mm

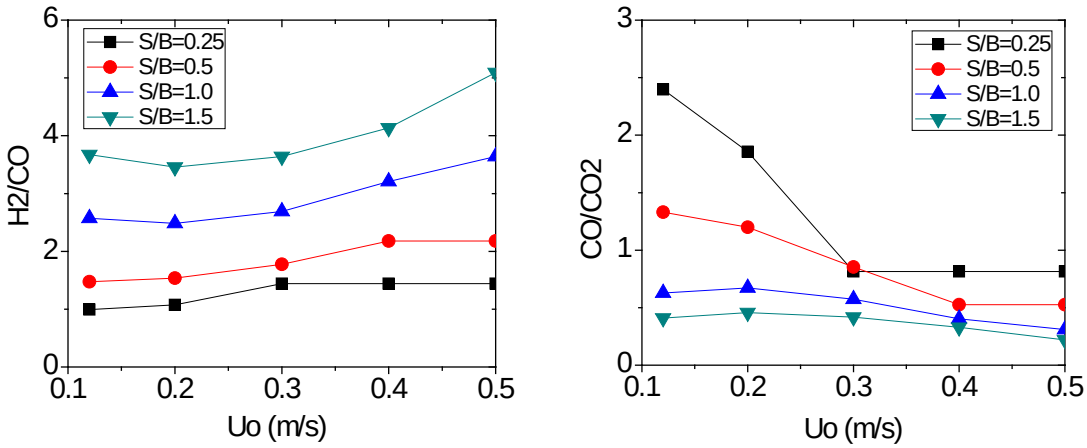

(a) H_2/CO ratio (b) CO/CO_2 ratio

Figure 4. 32 Effects of superficial gas velocity (U_o) and steam/biomass (S/B) ratio for the one-dimensional one-phase kinetic model, T=870 ^oC, and the particle size is 0.3 mm

The effect of steam/biomass ratio on the H_2/CO ratio and the CO/CO_2 ratio is shown in Fig. 4.32. It can be seen that the H_2/CO molar ratio increases and the CO/CO_2 molar ratio decreases with increased steam/biomass ratios. In addition, the H_2/CO ratio increases with an increased gas superficial velocity, while the CO/CO2 ratio decreases. The change of the H_2/CO ratio and the CO/CO_2 molar ratio can be explained by the change of the gas volumetric fraction over the range of steam/biomass ratios and superficial gas velocities studied.

4.5 One-dimensional two-phase kinetic models-all char in bed

The results of the one-dimensional two-phase kinetic model-all char in bed with particle size and the one-dimensional two-phase kinetic model-all char in bed without

considering the particle size are provided and compared together in this section. In order to facilitate making figures, these two models are represented by numbers in the figures of this section: 1- the one-dimensional two-phase kinetic model-all char in bed with particle size, and 2- the one-dimensional two-phase kinetic model-all char in bed without considering the particle size.

4.5.1 Products distribution with time and height

The concentration of gases along with the reactor height for the two models is compared. The reactor temperature is 870 ^{o}C, and the initial particle size is 0.3 mm. The gas superficial velocity is 0.4 m/s, and the steam/biomass ratio is 1. The concentration of gases is shown in Figs. 4.33-4.35. It can be seen from both figures that the concentrations of gases of these two models are the same in the fluidized bed and freeboard. In addition, from Figs. 4.33-4.35 it can be seen that as the height increases from the bottom to the top, the change of the concentrations of gases take place mainly in the bubble phase in the fluidized bed section, and the concentrations of gases remain almost constant in the emulsion phase of the fluidized bed and in the freeboard. This is because the gas in the emulsion phase of the fluidized bed is well mixed and that in the bubble phase of the fluidized bed is barely mixed due to the values selected for the gas mixing coefficients. In addition, in the freeboard, because there is only gas-gas reaction, and the gas reaches the equilibrium state very quickly, the gas concentration changes little.

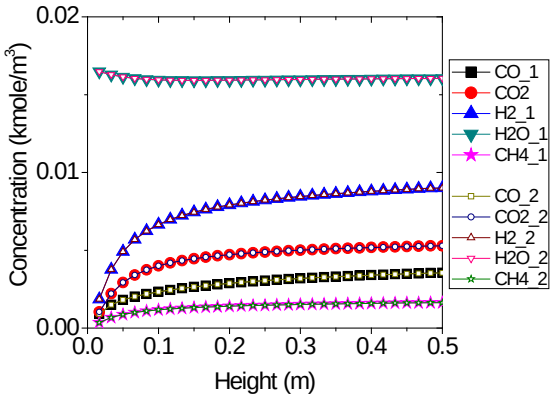

Figure 4. 33 Gas concentration in the bubble phase of the fluidized bed for the 1-D two-phase kinetic models-all char in bed, T=870 ^{o}C, steam/biomass ratio=1, the particle size is 0.3 mm, and U_o=0.4 m/s

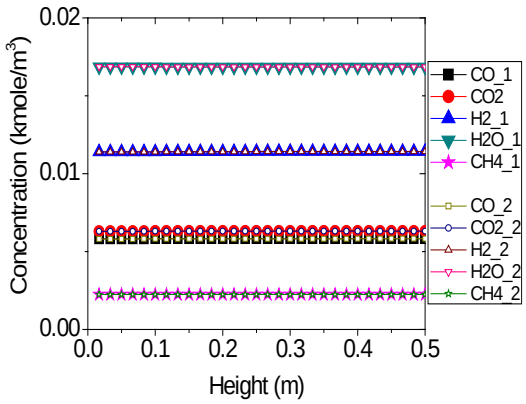

Figure 4. 34 Gas concentration in the emulsion phase of the fluidized bed for the 1-D two-phase kinetic models-all char in bed, T=870 ^{o}C, steam/biomass ratio=1, the particle size is 0.3 mm, and U_o=0.4 m/s

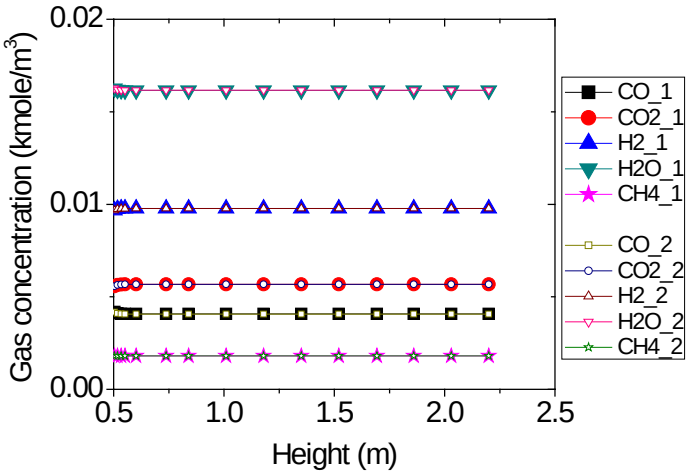

Figure 4. 35 Gas distribution in the freeboard for the 1-D two-phase kinetic model-all char in bed with particle size, T=870 ^{o}C, steam/biomass ratio=1, the particle size is 0.3 mm, and U_o=0.4 m/s

The evolution of char in the bed with time is shown in Fig. 4.36 for both models. It

can be seen that different amounts of time are required for the bed to reach steady state for these two models. In addition, at steady state, the amount of char in the bed is about 0.0042 kg/kg feed for the one-dimensional two-phase kinetic model-all char in bed with particle size, while that is 0.0007 kg/kg feed for the one-dimensional two-phase kinetic model-all char in bed without particle size. Therefore, it seems that whether the particles are dealt with in terms of the particle size or the mass affects the amount of char accumulated in the bed and the time required to reach steady state varies greatly. After extensive analysis, the reason may be because these two models used different surface areas in unit volume to calculate the reaction rates.

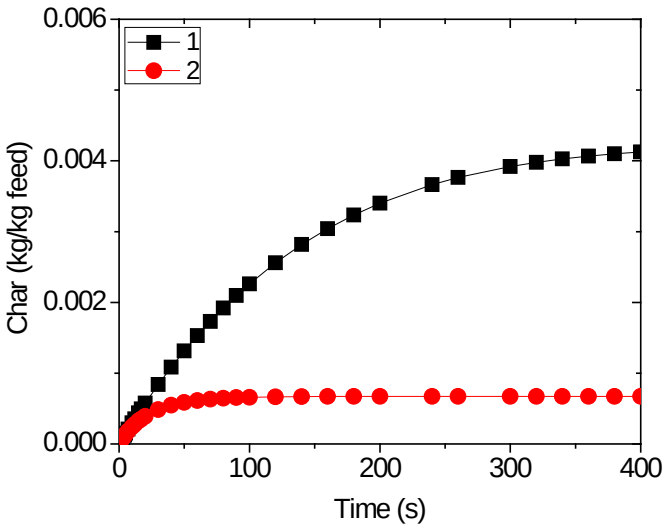

Figure 4. 36 Evolution of mass of total char in bed for the 1-D two-phase kinetic models-all char in bed, T=870 ^{o}C, steam/biomass ratio=1, the particle size is 0.3 mm, and U_o=0.4 m/s

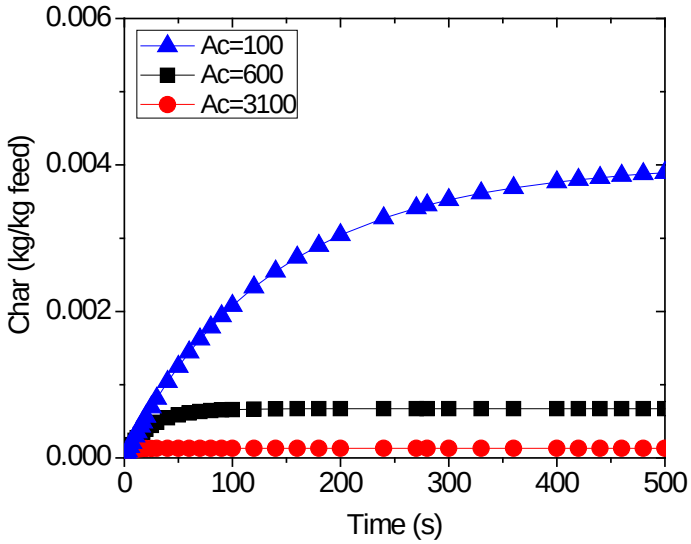

Figure 4. 37 Evolution of char in the bed with time for cases with different specific area for the 1-D two-phase kinetic model-all char in bed without particle size, T=870 ^{o}C, steam/biomass ratio=1, the particle size is 0.3 mm, and U_o=0.4 m/s

When fuel particles are dealt with in terms of the particle size (the two-phase kinetic model-all char in bed with particle size), the surface area in unit volume is calculated based on the real particle size, and a value of less than 100 m^2/kg char is obtained at steady state. However, when the fuel particles are dealt with in terms of the mass (the two-phase kinetic model-all char in bed without considering the particle size), the surface area in unit volume is calculated from the specific area (surface area of unit mass) of the corn stover char obtained directly from literature (Mullen, et al., 2010), and a value of 3100 m^2/kg char is set. All the fuel is consumed in the bed at the steady state, so the same amount of gas is produced for cases with different specific areas. For cases with different specific area, because the ratios of reaction rates of different gas-solid reactions are constant, the yields of dry tar-free gas, the concentration of gases, and the gas volumetric fraction are the same. Although the value of specific

area does not affect the ratio of reaction rates of different gas-solid reactions, it affects the absolute value of reactions rates, and thus affects the evolution of char and the amount of char accumulated in the bed. As shown in Fig. 4.37 where Ac represents the specific surface area, the evolution of char in the bed changes with the values of Ac. In addition, when Ac is 100 m^2/kg, the evolution of char in Fig. 4.37 is similar to that for the one-dimensional two-phase kinetic model-all char in bed with particle size in Fig. 4.36.

4.5.2 Effect of temperature and superficial gas velocity

The effect of gasifier temperature and superficial gas velocity on gasification results is studied. The steam/biomass ratio used is 1, and four different temperatures are selected: 600 ^oC, 677 ^oC, 777 ^oC and 870 ^oC. At each temperature, five superficial gas velocities are studied: 0.12 m/s, 0.2 m/s, 0.3 m/s, 0.4 m/s, and 0.5 m/s.

The gasification results at different temperatures and superficial gas velocities for the two models studied are shown in Figs.4.38-40. First, the gasification results at different superficial gas velocities are the same for the two models, so only one line instead of five lines exist to represent the gasification results at different superficial gas velocities. In addition, it can be seen that the two models have almost the same gasification results in terms of the yield of char and dry tar-free gas, the gas volumetric fraction, and the H_2/CO and CO/CO_2 ratios over the range of temperature studied.

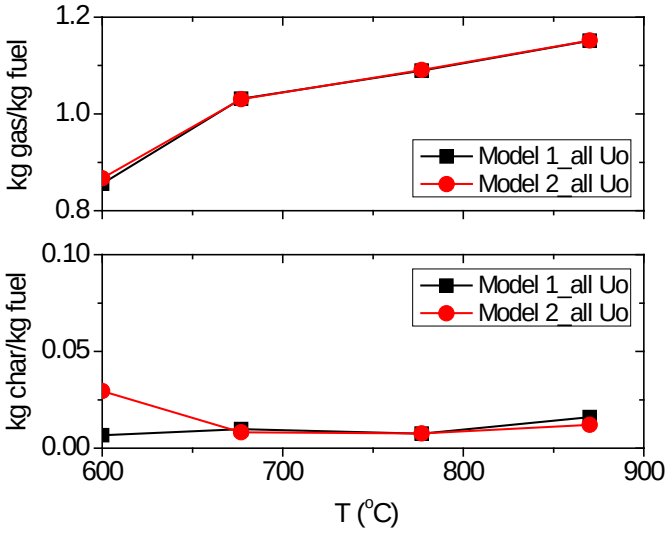

Figure 4. 38 The effect of gasifier temperature and superficial gas velocity (U_o) on the yield of char and dry tar-free gas for the 1-D two-phase kinetic models-all char in bed, steam/biomass ratio=1, and the particle size is 0.3 mm

The effect of temperature on the yield of char and dry tar-free gas is shown in Fig. 4.38. It can be seen that as the gasifier temperature increases, the amount of gas produced increases, while that of char remains almost the same. The yield of dry tar-free gas increases from 0.86 to 1.15 kg/kg feed, when the temperature increases from 600 ^{o}C to 870 ^{o}C. The yield of char for the kinetic models with all char in bed is calculated as the ratio of the total amount of char in bed to the total amount of fuel sent to the bed during the entire calculation time. After the bed reaches steady-state, which means the amount of char in the bed remains constant, the yield of char decreases due to the increased total amount of fuel sent to the bed with time, so the yield of char for these two models changes with the amount of calculation time selected. Therefore, the yield of char makes little sense for these two models, and it

will not be presented in the following section.

The effect of gasifier temperature and superficial gas velocities on the gas volumetric fractions is shown in Fig. 4.39. Although the volumetric fraction of CO, CO_2, and H_2 changes with increased temperature, the change of the gas volumetric fraction over the range of temperatures studied is very small, which is similar to that obtained from experiments (Wang, Wu and Huo, 2007).

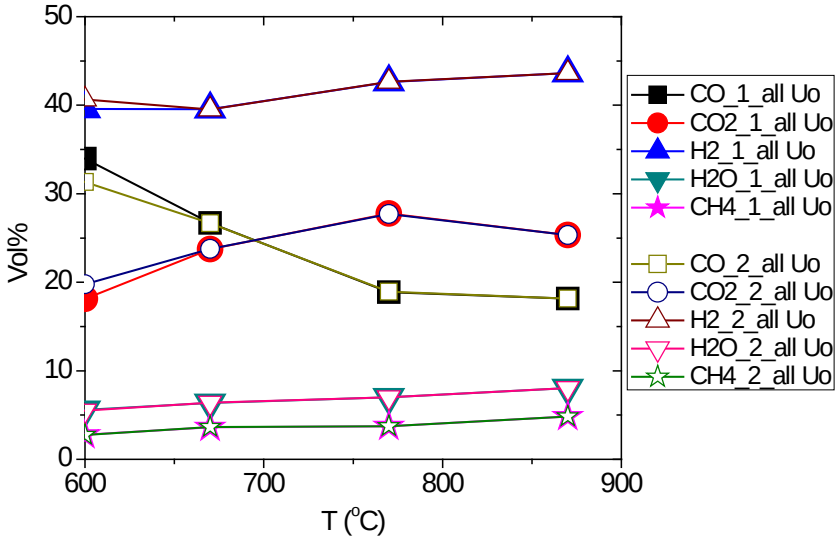

Figure 4. 39 The effect of temperature and superficial gas velocity (U_o) on the gas volumetric fraction on a dry tar-free basis for the 1-D two-phase kinetic models-all char in bed, steam/biomass ratio=1, and the particle size is 0.3 mm

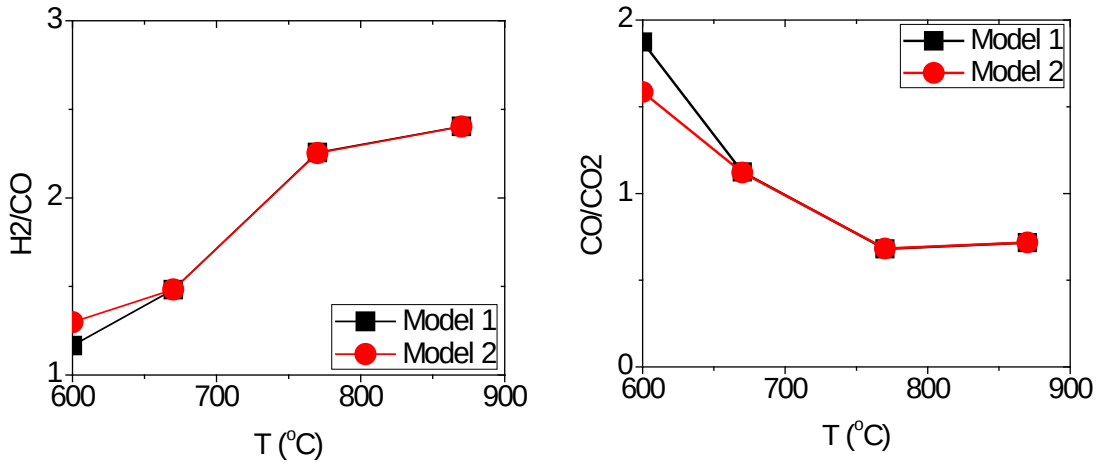

Figure 4. 40 The effect of temperature and superficial gas velocity (U_o) on the H2/CO ratio and the CO/CO2 ratio for the 1-D two-phase kinetic models-all char in bed, steam/biomass ratio=1, and the particle size is 0.3 mm

The evolution of the H_2/CO ratio and the CO/CO_2 ratio with increased temperature is shown in Fig. 4.40. The H_2/CO ratio increases with the elevated temperatures, while the CO/CO_2 ratio decreases, which is consistent with other studies (Wei, et al., 2007).

4.5.3 Effect of superficial gas velocity and steam/biomass ratio

Five different superficial gas velocities are studied: 0.12 m/s, 0.2 m/s, 0.3 m/s, 0.4 m/s, and 0.5 m/s. The minimum superficial gas velocity is set a value at 0.12 m/s because the minimum fluidization velocity calculated is 0.11 m/s. The superficial gas velocity is changed by changing the mass flow rates of both steam and fuel. At each superficial gas velocity, the mass flow rate of fuel is changed to get four different biomass ratios: 0.25, 0.5, 1.0, and 1.5. The temperature is 870 ^oC, and the initial particle size is 0.3 mm.

The gasification results at different superficial gas velocities and steam/biomass ratios for these two models are shown in Figs. 4.41, 4.42, and 4.43. First, through comparison between the gasification results for the two models studied in this section, it can be seen that these two models have the same gasification results in terms of the yield of dry tar-free gas, the gas volumetric fractions, the H_2/CO ratio, and the CO/CO_2 ratios. Therefore, it can be inferred that whether dealing with particles in the bed in terms of the particle size or mass does not affect the gasification results. Second, it can be noticed that the gasification results change little with increased superficial gas velocity at each steam/biomass ratio studied. This is because based on the modeling concepts of these two models, there is no char entrainment, and all the fuel sent to the bed is consumed in the reactor. Therefore, at different superficial gas velocities, because the amount of char needed to be consumed is the same, and because the reaction rates are the same due to the constant temperature, the gasification results are the same.

The yield of dry tar-free gas at different steam/biomass ratios and superficial gas velocities is shown in Fig. 4.41. As the steam/biomass ratio increases from 0.25 to 1.5, the yield of gas after gasification increases from 1.01 to 1.19 kg/kg fuel for both models. The increase of the yield of dry tar-free gas can be explained by the char-gas reactions and the water-gas shift reaction. In addition, the same as other models, the increase of the dry tar-free gas slows down with increased steam/biomass ratios. As

the steam/biomass ratio increases from 0.25 to 1.0, the yield of dry tar-free gas increases from 1.01 to 1.15 kg/kg feed, and it increases from 1.15 to 1.19 kg/kg feed when the steam/biomass ratio increases from 1.0 to 1.5. It is because as the steam/biomass ratio increases, the water-gas shift reaction approaches the equilibrium state; thus, although more steam is provided, it is not needed for the reaction.

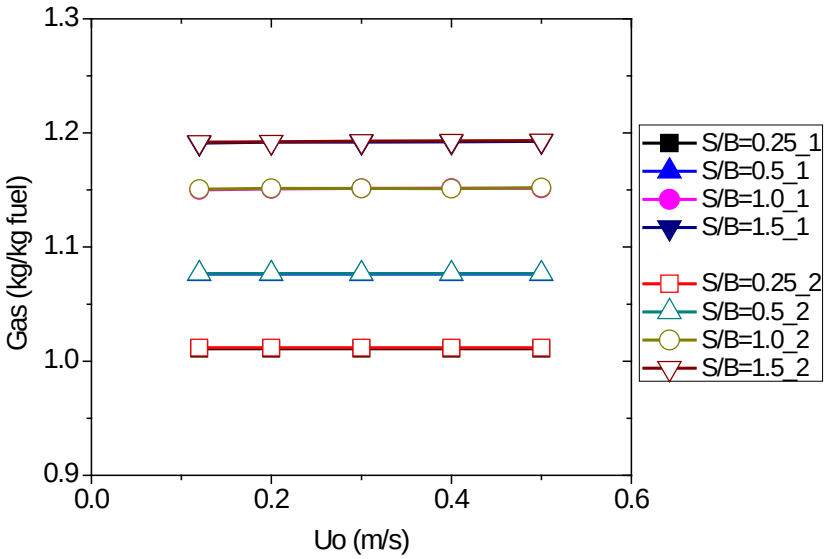

Figure 4. 41 Effect of superficial gas velocity (U_o) and steam/biomass (S/B) ratio on the yield of dry tar-free gas for the 1-D two-phase kinetic models-all char in bed, T=870 ^oC, and the particle size is 0.3 mm

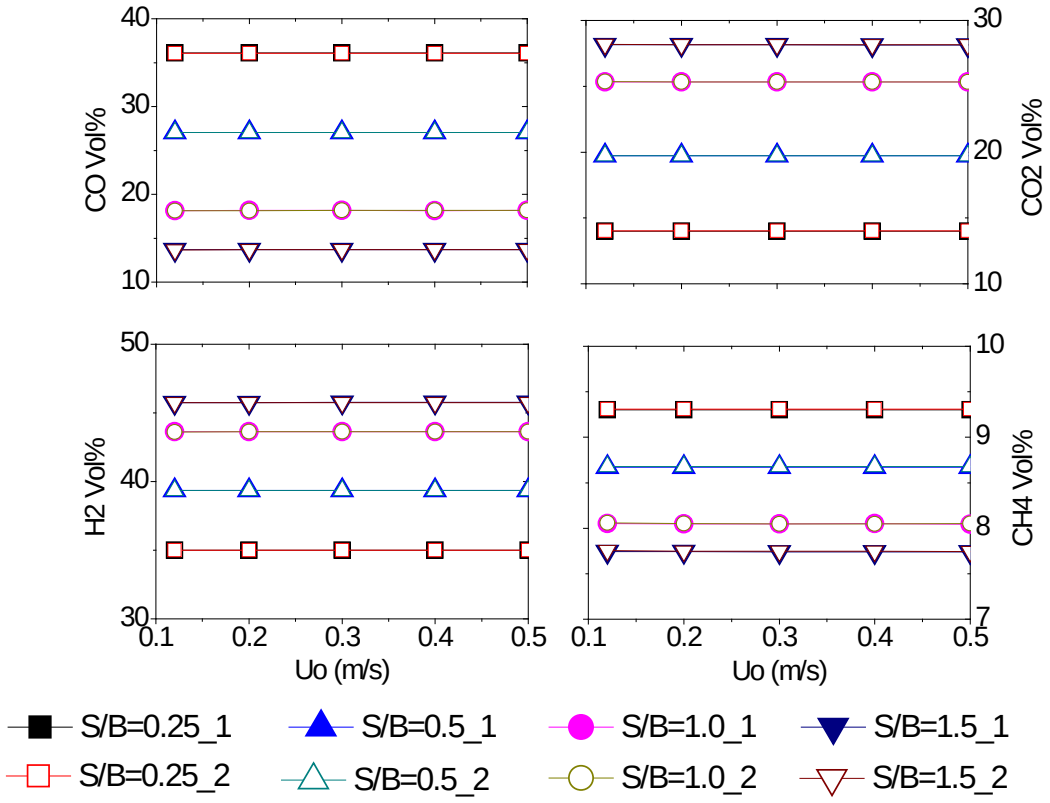

Figure 4. 42 Effect of superficial gas velocity (U_o) and steam/biomass (S/B) ratio on gas volumetric fractions for the 1-D two-phase kinetic models-all char in bed, T=870 ^oC, and the particle size is 0.3 mm

The effect of superficial gas velocity and steam/biomass ratio on the gas volumetric fraction is shown in Fig. 4.42. The trend of the change of the gas volumetric fractions over the range of steam/biomass ratios is similar to that obtained for other models. With increased steam/biomass ratios, the gas volumetric fractions of CO_2 and H_2 increase, while those of CO, CH_4, and C_nH_m decrease. This is because the reaction rate of the water-gas shift reaction is much faster than that of char gasification reactions, so the gas volumetric fraction of CO_2 and H_2 increases, and that of CO decreases. In addition, the gas volumetric fraction of CH_4 and C_nH_m decreases due to the increased

total gas yield.

The effect of steam/biomass ratio on the H_2/CO ratio and the CO/CO_2 ratio is shown in Fig. 4.43. It can be seen that with increased steam/biomass ratios the H_2/CO molar ratio increases, while the CO/CO_2 molar ratio decreases. The change of H_2/CO and CO/CO_2 molar ratios can be explained by the change of the gas volumetric fraction over the range of steam/biomass ratios.

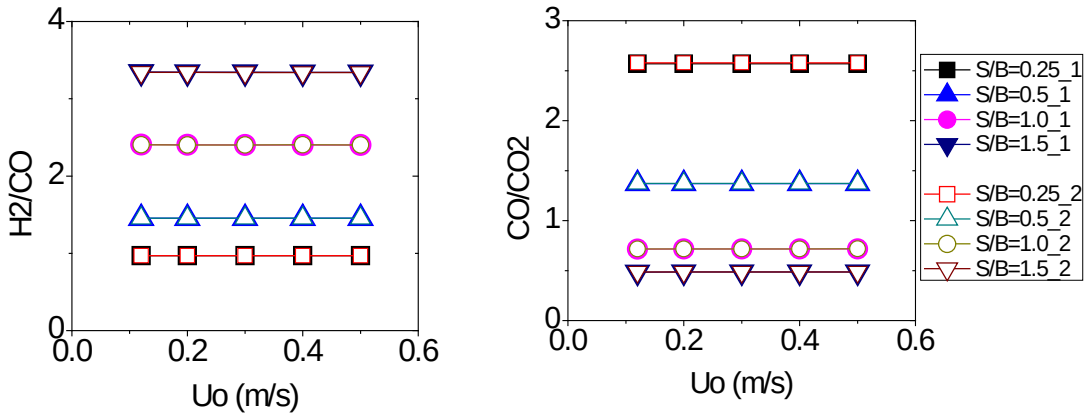

Figure 4. 43 The effect of superficial gas velocity (U_o) and steam/biomass (S/B) ratio on the H2/CO ratio and the CO/CO2 ratio for the 1-D two-phase kinetic models-all char in bed, T=870 ^oC, and the particle size is 0.3 mm

4.6 One-dimensional two-phase kinetic model

4.6.1 Evolution of fuel in the bed with time

The evolution of particles in the fluidized bed is shown in Figs. 44-45 under the following operating conditions: 1) the temperature is 870 ^oC; 3) the initial particle size is 0.3 mm; and 4) the steam/biomass ratio is 1. The mass flow rates of steam and fuel

are varied at different superficial gas velocities. It can be seen that it takes a longer time for the bed to reach steady state and particles stay in the bed for a longer time at a higher superficial gas velocity than at a lower superficial gas velocity. The bed reaches steady state when the solids consumed in the bed equals the amount of fuel sent to the bed minus the amount of particles entrained out of the bed during unit time. The amount of fuel consumed in the bed during unit time is proportional to the total fuel in the bed, and the process of reaching the steady state is a process of char accumulating in the bed. Compared to cases at a lower superficial gas velocity, cases at a higher superficial gas velocity have more char entrained out of the bed, so less solids need to be consumed during unit time at steady state. Therefore, given the similar reaction rates of gas-solid reactions at different superficial gas velocity, a smaller amount of fuel is in the bed at steady-state, and it takes less time for the bed to reach steady state at a higher superficial velocity than at a lower superficial velocity. In addition, the time required for the bed to reach steady state is close to the amount of time particles stay in the bed. Based on this model, about 320 seconds are required for the bed to reach steady-state at 870 ^{o}C when the superficial gas velocity is 0.2 m/s. Neogi (Neogi, et al., 1986) predicted a time of 1400-1600 seconds for the bed to reach steady state at 800 ^{o}C with a gas superficial velocity of 0.14-0.165 m/s. Because more time is required for the bed to reach steady state at a lower gas superficial velocity and at a higher temperature than at a higher superficial gas velocity and at a lower temperature, the difference may be due to the different temperatures and superficial gas velocities used. In addition, as discussed in the previous section, cases reach steady state earlier

with a smaller steam/biomass ratio than with a larger steam/biomass ratio. Since the steam/biomass ratio used in the literature is larger than 2, the difference may be also due to the relatively small steam/biomass ratio used. The difference may be also due to the different reaction rates are used in these two studies.

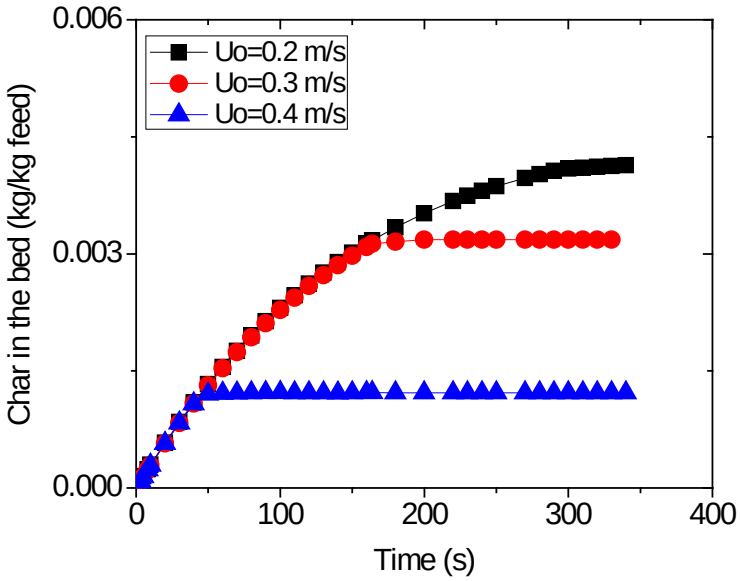

Figure 4. 44 Evolution of char in the bed with time for the 1-D two-phase kinetic model at three superficial gas velocities (U_o), T=870 ^oC, steam/biomass ratio=1, and the particle size is 0.3 mm

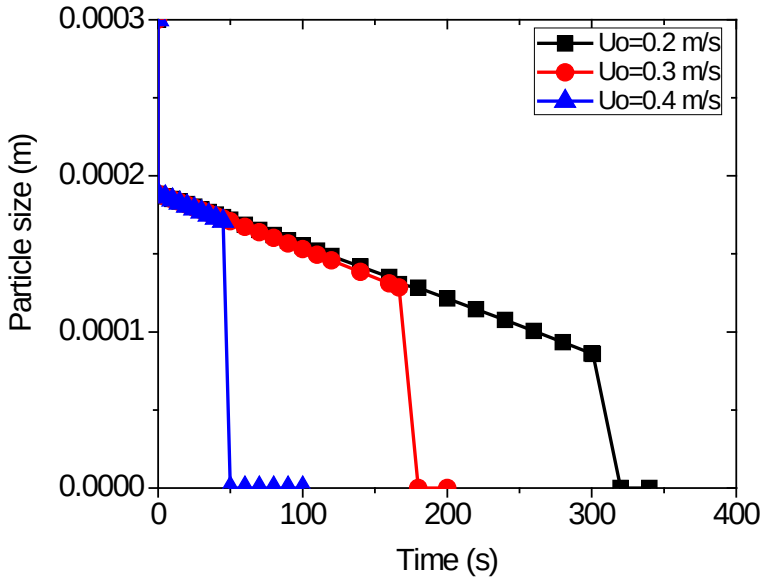

Figure 4. 45 Evolution of the size of a single particle in the bed with time for the 1-D two-phase kinetic model at three superficial gas velocities (U_o), T=870 ^oC, steam/biomass ratio=1, and the particle size is 0.3 mm

4.6.2 Effect of temperature and superficial gas velocity

The effect of gasifier temperature on gasification product yields and gas distribution was studied. The steam/biomass ratio used is 1, and four different temperatures are studied: 600 ^oC, 677 ^oC, 777 ^oC and 870 ^oC. Because the superficial gas velocity (the velocity of steam at the inlet) increases with elevated temperature when the mass flow rate of steam is constant, the mass flow rates of steam and fuel are varied to achieve a constant superficial gas velocity at different temperatures. In addition, in order to study the evolution of gasification products at different superficial gas velocities, five superficial gas velocities are evaluated: 0.12 m/s, 0.2 m/s, 0.3 m/s, 0.4 m/s, and 0.5 m/s. Because the minimum fluidization velocity calculated in this study is 0.11 m/s,

the minimum superficial gas velocity selected is 0.12 m/s.

The yields of char and dry tar-free gas at different temperatures are shown in Fig. 4.46. It can be seen that as the gasifier temperature increases the amount of dry tar-free gas produced also increases while that of char decreases. This is because as the temperature increases the yield of pyrolysis gas also increases while that of char decreases, which directly leads to the increase in the yield of gas and the decrease in the yield of char after gasification. In addition, because the chemical reaction rates of char-gas reactions increase with increased temperatures, more char is consumed and more gas is generated at elevated temperature. As indicted by some researchers, the water-gas shift reaction cannot reach equilibrium state if the temperature is not high enough and proceeds to the right hand side as temperature increases (Herguido, Corella and Gonzalez-Saiz, 1992; Rapagnà, et al., 2000; Franco, et al., 2003; Wei, et al., 2007; Carpenter, et al., 2010), which also results in the consumption of H_2O and the generation of gasification gas. Because there are no experimental results available on the values of $[H_2]$ $[CO_2]/[CO]$ $[H_2O]$ at different temperatures for corn stover, the values for wood were used for corn stover at the same temperature in this study (Herguido, Corella and Gonzalez-Saiz, 1992), which may be different from that for corn stover and thus leads to errors. In this model, tar and heavier hydrocarbon steam reforming, tar thermal cracking are not included due to lack of information, and these reactions may also contribute to the increase of gas yield in the real process. Through careful examination of Fig. 4.46, it can be found that the yield of dry tar-free gas

decreases and that of char increases when the temperature increases from 770 ^{o}C to 870 ^{o}C with a superficial gas velocity of 0.12 m/s.

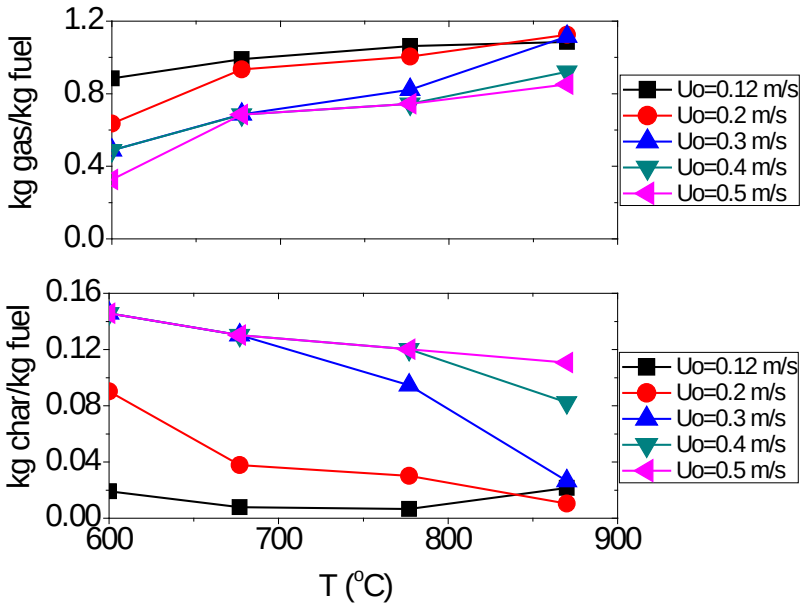

Figure 4. 46 Effect of temperature and superficial gas velocity (U_o) on yields of char and dry tar-free gas for the 1-D two-phase kinetic model, steam/biomass ratio=1, and the particle size is 0.3 mm

According to the chapter 2, different equations (Eqn. 2.65-2.68) are used to calculate the terminal velocity of particles in the bed based on the value of Reynolds number, and the terminal velocities calculated by different equations have different values. When the superficial gas velocity is 0.12 m/s, the equation used to calculate the terminal velocity at 870 ^{o}C is different from that used for other temperatures, and it calculates a smaller value than the other equations does. Based on the modeling concept, once the terminal velocity of particles is less than the superficial gas velocity, particles in the bed are entrained out of the bed immediately. Therefore, when the

superficial gas velocity is 0.12 m/s, the change in yields of char and dry tar-free gas from 770 ^{o}C to 870 ^{o}C is different from that from 600 ^{o}C to 770 ^{o}C.

Comparing the yields of char and dry tar-free gas at different superficial gas velocities in Fig. 4.46, it can be seen that with decreased superficial gas velocity the yield of dry tar-free gas increases, while that of char decreases. This is mainly because the amount of char entrained out of the bed is closely related to the superficial gas velocity. With a higher superficial gas velocity, particles are able to be entrained out of the bed at a higher terminal velocity than with a lower superficial gas velocity. The size of particles entrained out of the bed at a higher superficial gas velocity is larger than that at a lower superficial gas velocity. Given the same number of particles at different superficial gas velocities, more char is entrained out of the bed at a higher superficial gas velocity than at a lower superficial gas velocity, and less gas is produced based on the mass balance. Comparing the change of yields of char and dry tar-free gas obtained in this study to those from experiments (Corella, et al., 1991), it is found that the trend in change of char is opposite to that in literature. In the literature, the yield of char decreases with increased superficial gas velocity. The reason may be because in literature the amount of char produced includes the amount of char in the bed while in this study the amount char produced is the amount of char entrained out of bed at steady-state. The reason also may be because during the real process particle reactions are limited under low gas superficial velocity due to poor mass transfer.

The change of the gas volumetric fraction with elevated temperature is shown in Fig. 4.47, and it has a similar trend to some experimental results (Corella, et al., 1991; Herguido, Corella and Gonzalez-Saiz, 1992). With an increase of temperature from 600 ^{o}C to 870 ^{o}C, the volumetric fraction of H_2 increases, while that of CO and CO_2 decreases. As the temperature of the gasifier increases, the reactivity of reactions (C-H_2O, C-CO_2, C-H_2, and water-gas shift reaction) also increases. Because the reaction rate of C-H_2 is much slower than other reactions, the consumption of H_2 through the C-H_2 reaction is much slower than the generation of H_2 through the C-H_2O and water-gas shift reactions and pyrolysis, which results in an increased gas volumetric fraction of H_2. In addition, although CO can be generated through the C-CO_2 reaction and the C-H_2O reaction, because more CO is consumed through the water-gas shift reaction, the gas volumetric fraction of CO decreases with increased temperature, which indicates that the water-gas shift reaction plays a very important role in determining the gas volumetric fraction. As for the volumetric fraction of CO_2, although more CO_2 is generated through the water-gas shift reaction than consumed through the C-CO_2 reaction, because much less CO_2 is generated through pyrolysis at elevated temperatures (You, et al., n.d.), the volumetric fraction of CO_2 decreases as temperature increases. The increase of the gas volumetric fraction of C_nH_m is mainly due to the increase of the yield of C_nH_m during pyrolysis with increased temperature. The gas volumetric fraction of CH_4 increases slightly when the superficial gas velocity is 0.12 m/s and 0.2 m/s, while it decreases at other superficial gas velocities. This is because the increase of the yield of dry tar-free gas at lower superficial gas velocities

(0.12 m/s, and 0.2 m/s) is slower than that at higher superficial gas velocities. At lower superficial gas velocities (0.12 m/s, and 0.2 m/s), the increase of CH_4 with increased temperature is larger than the increase of total gas, so the gas volumetric fraction of CH_4 increases slightly. However, because the increase of CH_4 with increased temperature is smaller than that of total gas at other superficial velocities, the gas volumetric fraction of CH_4 decreases.

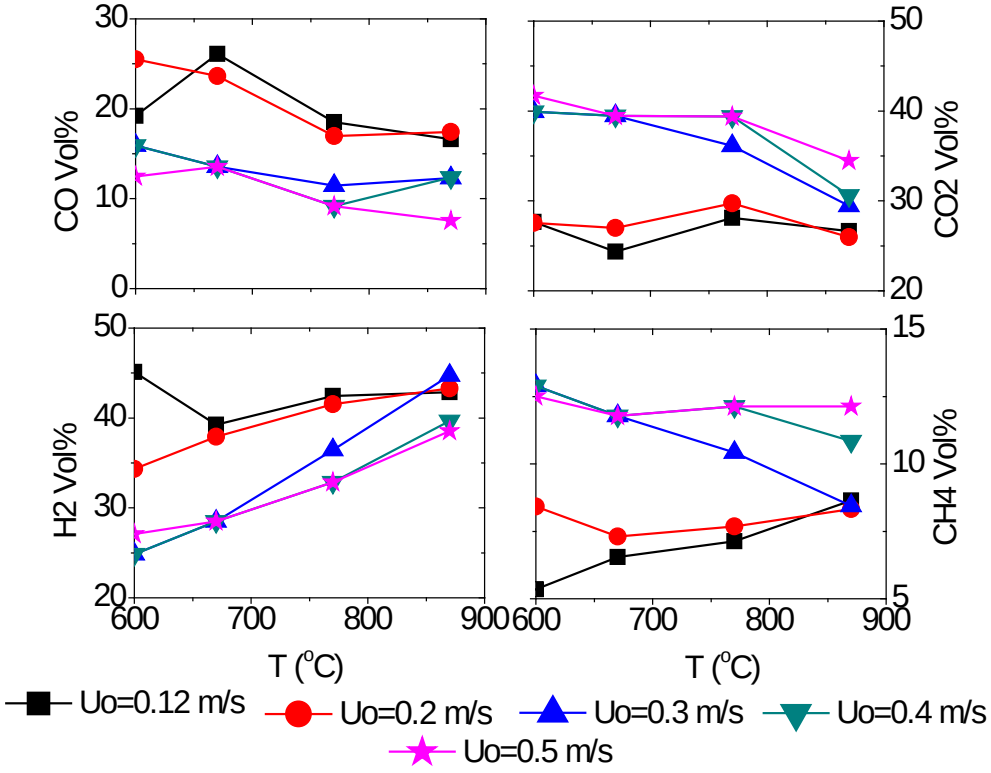

Figure 4. 47 Effect of temperature and superficial gas velocity (U_o) on the gas volumetric fraction on a dry basis for the 1-D two-phase kinetic model, steam/biomass ratio=1, and the particle size is 0.3 mm

From both Figs. 4.46 and 4.47, it can be seen that the gasification results at low superficial gas velocities (0.12 m/s and 0.2 m/s) are close, while those at high

superficial gas velocities (0.3 m/s, 0.4 m/s, and 0.5 m/s) are close. This is because particles stay in the bed for a longer time at low superficial velocities, while they are entrained out of the bed shortly after they are sent to the bed at higher superficial gas velocities, which indicates the effect of residence time on gasification results. In addition, it can be seen that with increased superficial gas velocity, the volumetric fraction of CO and H_2 decreases, while that of CO_2 and CH_4 increases. The decrease of the volumetric fractions of CO and H_2 and the increase of the volumetric fraction of CO_2 is due to the decreased gas-solid reaction time resulting from increased superficial gas velocity. With an increased superficial gas velocity, particles stay in the bed for a shorter time and are entrained out of the bed with a larger size, thus more CO_2 and H_2O remain un-reacted and less CO and H_2 are produced. In addition, because C_nH_m produced from pyrolysis remains constant, the volumetric fraction of C_nH_m increases with increased superficial gas velocity due to decreased dry tar-free gas.

The evolution of H_2/CO ratio and CO/CO_2 ratio with temperature is shown in Fig. 4.48. The H_2/CO ratio increases with an elevated temperature, while the CO/CO_2 ratio decreases, which is consistent with other studies (Wei, et al., 2007). The change of H_2/CO ratio and CO/CO_2 ratio with temperature can be explained by the change of volumetric fraction of gases.

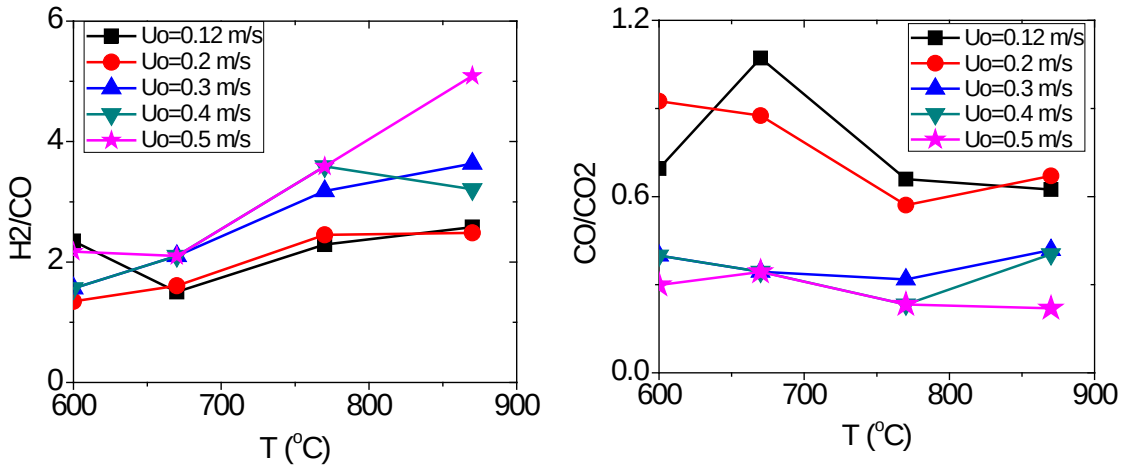

Figure 4. 48 The effect of temperature and superficial gas velocity (U_o) on H2/CO and CO/CO2 ratios for the 1-D two-phase kinetic model, steam/biomass ratio=1, and the particle size is 0.3 mm

4.6.3 Effect of superficial gas velocity and steam/biomass ratio

The effect of superficial gas velocity (defined as the velocity of steam at the reactor inlet) on gasification products is studied, and five values are selected: 0.12 m/s, 0.2 m/s, 0.3 m/s, 0.4 m/s, and 0.5 m/s. The superficial gas velocity is varied by changing the mass flow rates of steam and biomass, while maintaining a constant steam/biomass ratio. Addition of steam to the gasifier favors the production of H_2, but too much steam can dilute the gas and absorb a lot of energy. Three steam/biomass ratios are selected: 0.5, 1.0, and 1.5. Change of Steam/biomass ratio can be achieved either by changing the mass flow rate of fuel while keeping a constant mass flow rate of steam, or by changing the mass flow rate of steam while keeping a constant fuel, or by changing

both steam flow rate and fuel flow rate. The steam/biomass ratio is varied by changing the mass flow rate of fuel while that of steam is kept constant at the same superficial gas velocity. The temperature of the gasifier is 870 ^{o}C.

The yield of char and dry tar-free gas is shown in Fig. 4.49. As the steam/biomass ratio increases, the yield of dry tar-free gas also increases, while that of char decreases at the same superficial gas velocity. This is because the addition of steam favors the char-steam reaction and the water-gas shift reaction, thus more char is consumed and more steam is converted to other gases with an increased steam/biomass ratio. Due to the different gas compositions, the critical particle size at which particles can be entrained out of the bed is different at different steam/biomass ratios, and particles are entrained out of the bed with a smaller particle size at a higher steam/biomass ratio than at a lower steam/biomass ratio. Therefore, with increased steam/biomass ratio, less char is entrained out of the bed, leading to a larger yield of dry tar-free gas. This can be confirmed by the change of the yields of char and gas with a steam/biomass ratio of 0.5. When the steam/biomass ratio is 0.5, particles can be entrained out of the bed immediately after they are sent to the bed at 0.4 and 0.5 m/s, so the yields of char and dry tar-free gas are the same at the two superficial velocities. Based on the yield of char at other steam/biomass ratios, it can be concluded that a larger superficial gas velocity is required to entrain the same particles out of the bed at a larger steam/biomass ratio than at a smaller steam/biomass ratio. In addition, it can also be noticed in Fig. 4.49 that as steam/biomass ratio increases, the increase of gas yield and

the decrease of char production slow down at the same superficial gas velocity. This is because as the steam/biomass ratio increases the water-gas shift reaction approaches equilibrium state. Thus, although more steam is provided, the increase of steam consumption decreases.

The yields of char and dry tar-free gas at each steam/biomass ratio increase with increased superficial gas velocity. The reason is also due to the different residence times of char in the bed. In addition, when the superficial gas velocity increases from 0.12 m/s to 0.5 m/s, the difference among the yields of dry tar-free gas at each steam/biomass ratio first increases and reaches a maximum value at 0.4 m/s. However, after that the difference decreases, and the yields of char and dry tar-free gas at different steam/biomass ratios are almost the same when the superficial gas velocity is 0.5 m/s. At low velocity (0.12 m/s) particles stay in the bed for a large amount of time, and at high velocity (0.5 m/s) particles are entrained out of the bed shortly after they are sent to the bed. Due to similar particle residence times in the bed at different steam/biomass ratios, the yields of char and dry tar-free gas are similar. When the superficial gas velocity is in the range of 0.12 to 0.5 m/s, particles stay in the bed for different amounts of time at different steam/biomass ratio, so the yields of char and dry tar-free gas are different.

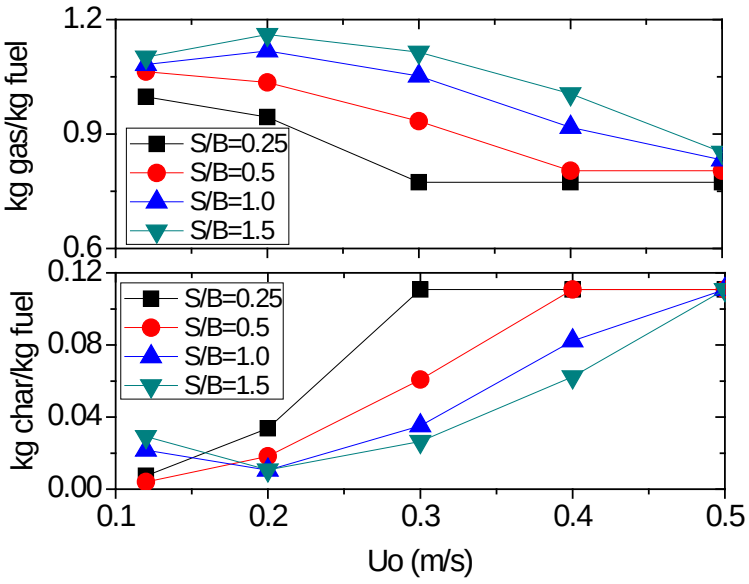

Figure 4. 49 Effect of the superficial gas velocity (U_o) and steam/biomass (S/B) ratio on yields of char and dry tar-free gas for the 1-D two-phase kinetic model, T=870 ^oC, and the particle size is 0.3 mm

The gas volumetric fractions are different steam/biomass ratios and different superficial gas velocities are shown in Fig. 4.50. As the steam/biomass ratio increases, the gas volumetric fraction of CO_2 and H_2 increase, while that of CO, CH_4, and C_nH_m decrease. The effect of the water-gas shift reaction on gas distribution overweighs that of the char-gas reactions. Because a lot of steam is available, the water-gas shift reaction proceeds to the right hand side, which leads to the production of CO_2 and H_2 and the consumption of CO. In addition, because the generation of CH_4 through the C-H_2 reaction is very slow and no gasification reactions exist to produce C_nH_m, the gas volumetric fraction of CH_4 and C_nH_m decreases a little with increased steam/biomass ratios.

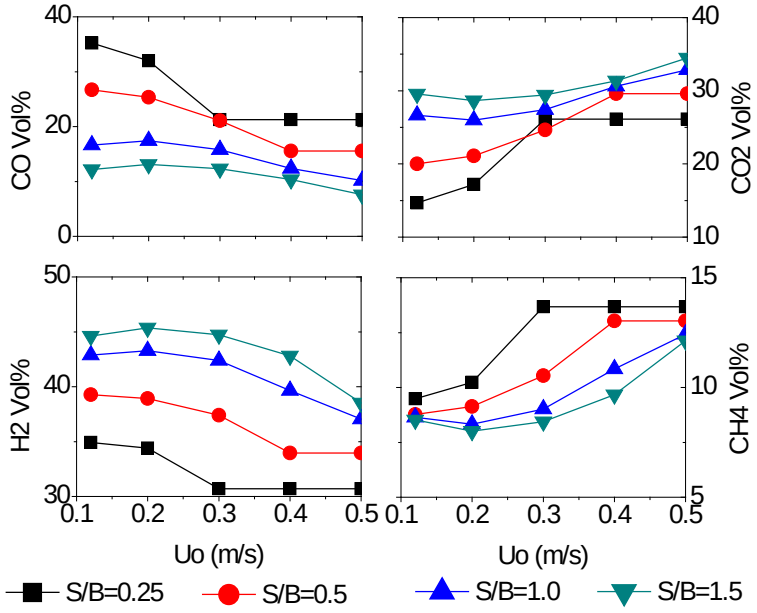

Figure 4. 50 Effect of the superficial gas velocity (U_o) and steam/biomass (S/B) ratio on the gas volumetric fraction on a dry basis for the 1-D two-phase kinetic model, T=870 ^oC, and the particle size is 0.3 mm

As the superficial gas velocity increases from 0.12 m/s to 0.5 m/s, the gas volumetric fraction of CO and H_2 decreases, while that of CO_2, CH_4 and C_nH_m increases. In addition, the change of gas volumetric fraction of all gases is slower in the range of 0.12 to 0.2 m/s than in the range of 0.3 to 0.5 m/s. With increased superficial gas velocity, the residence time of particles staying in the bed decreases, and so does the gas-solid reaction time. With increased superficial gas velocity, less CO_2 is consumed and less CO is generated through the C-CO_2 reaction, and less H_2 and CO is generated through the C-H_2O reaction. Therefore, the gas volumetric fraction of CO and H_2 decreases, and that of CO_2 increases with increased superficial gas velocity. The increase of the gas volumetric fraction of CH_4 and C_nH_m with increased superficial gas

velocity is mainly due to the decreased total gas. The rate of the change of the gas volumetric fraction with increased superficial gas velocity is due to the change of the residence time of particles staying in the bed. It can be included that at 870 ^{o}C the residence time plays a very important role in determining the gasification products.

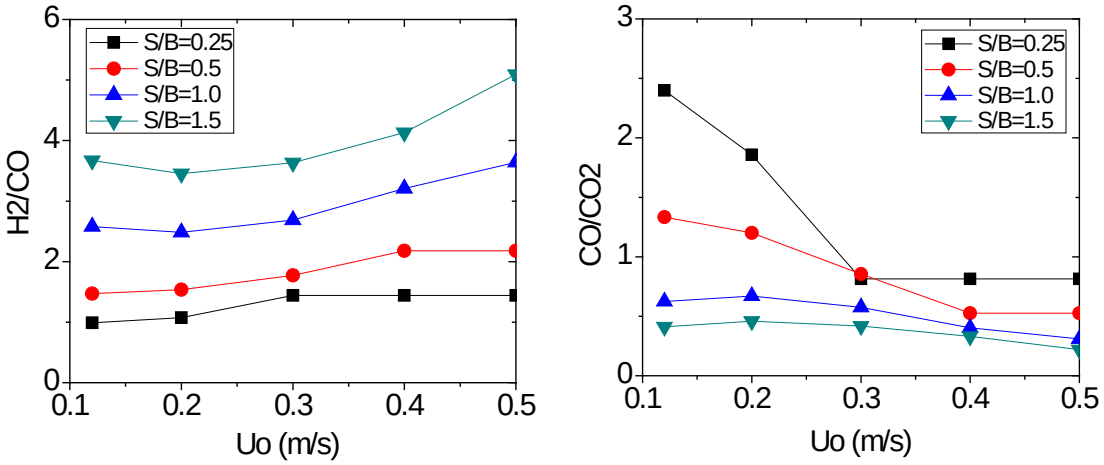

Figure 4. 51 The effect of superficial gas velocity (U_o) and steam/biomass (S/B) ratio on H2/CO and CO/CO2 ratios for the 1-D two-phase kinetic model, T=870 ^{o}C, and the particle size is 0.3 mm

The effect of two important parameters, the hydrogen-to-carbon monoxide ratio and the carbon monoxide-to-carbon dioxide ratio, are shown in Fig. 4.51 as a function of superficial gas velocity and steam/biomass ratio. It can be seen that the H_2/CO molar ratio increases with increased steam/biomass ratios, while the CO/CO_2 molar ratio decreases. As the steam/biomass ratio increases, both H_2 and CO increase due to the C-H_2O reaction. However, since CO is also consumed and H_2 is generated by the water-gas shift reaction, the H_2/CO ratio increases with increased steam/biomass ratios. The CO/CO_2 ratio decreases with increased steam/biomass ratios due to the decrease

of CO and the increase of CO_2 through the water-gas shift reaction. In addition, with increased gas superficial velocities the H_2/CO ratio increases, while the CO/CO_2 ratio decreases. This is because with increased gas superficial velocity, less char is consumed, and thus less CO, H_2 are generated through char-steam and C-CO_2 reactions, and more CO_2 is leaving the bed directly.

4.6.5 Effect of particle size

Four different particle sizes were studied: 0.3 mm, 0.5 mm, 0.8 mm, and 1.3 mm. The steam/biomass ratio is 1, and the superficial gas velocity is 0.45 m/s. The temperature is 870 ^oC. The gasification results using these four different particle sizes are shown in Figs. 4.52-54.

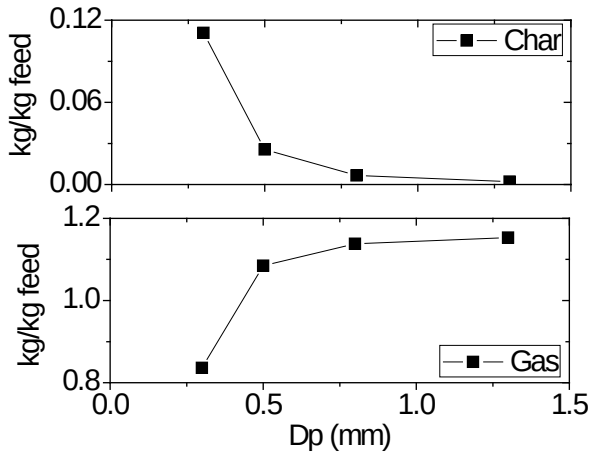

Figure 4. 52 Effect of particle size on yield of char and dry tar gas for the 1-D two-phase kinetic model, T=870 ^oC, steam/biomass ratio =1, U_o=0.45 m/s, and the particle size is 0.3 mm

Figure 4.52 shows the yields of char and dry tar gas at different particle sizes. The

yield of gas with a larger particle size is more than that with a smaller particle size. When the particle size increases from 0.3 mm to 1.3 mm, the yield of dry tar gas increases from 0.84 to 1.15 kg/kg feed. Based on the concept of this model particles can keep taking part in chemical reactions as long as there is carbon available and their terminal velocity is larger than the gas superficial velocity. Therefore, because particles do not experience segmentation, the number of particles fed into the reactor at the same time remains the same during the whole process until they are entrained out of the bed. Because the diameter of particles when they are entrained out of the bed for the same operating conditions is similar, cases with larger number of particles have more char entrained out of the bed than those with a smaller number of particles. Given the same fuel mass flow rate, cases with larger particle size have smaller number of particles, thus the amount of char entrained out of the bed for these cases are less than cases with smaller particle size .

Although the changes of yield of char and dry tar-free gas is reasonable based on the concept of the model, it is different from the experimental results. In the actual experimental process, larger particles generate more char and less gas while small particles produce less char and more gas. This difference between the simulation results and the experimental results is because char deactivation and segmentation are not modeled due to lack of related theory and experimental data. Therefore, this model is not able to predict the yield of char and gas correctly. To improve this model, char deactivation and segmentation model should be included, or some kind of critical time

which is the maximum time that particles take part in chemical reactions can be introduced. Once the particle residence time in the bed exceeds this critical time, particles will be removed out of the bed immediately. This critical time can be obtained through extensive experiments.

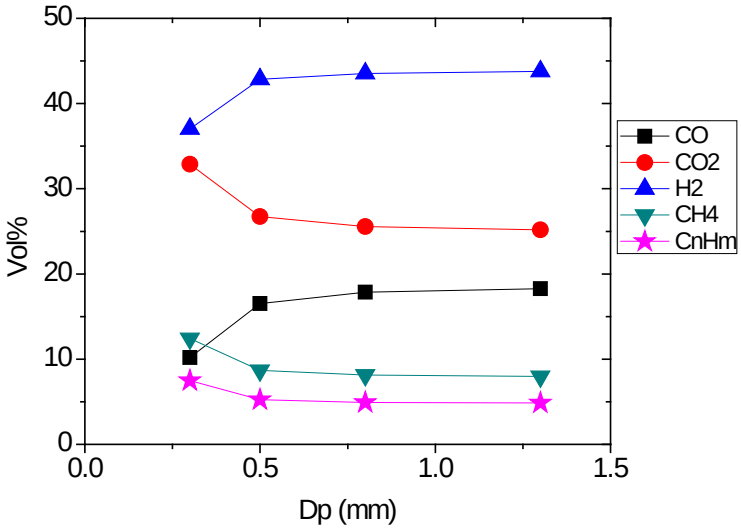

Figure 4. 53 Effect of particle size on gas volumetric fraction for the 1-D two-phase kinetic model, T=870 ^{o}C, steam/biomass ratio =1, U_o=0.45 m/s, and the particle size is 0.3 mm

The effect of particle size on gas volumetric fraction is shown in Fig. 4.53. It can be seen that the gas volumetric fraction changes significantly when particle size increases from 0.3 mm to 0.5mm, then it remains nearly constant with increased particle size. This may be because the yield of gases after pyrolysis is different for different initial particle sizes, especially for small particle sizes, which leads to different gas volumetric fractions after gasification. This may be also due to the different amounts of time particles stay in the bed. Particles of size 0.3 mm are entrained out of the bed immediately after the fuel is sent to the reactor and pyrolyzed, and there is no

additional time for char-gas reaction. However, larger particles stay in the bed and take part in char-gas reactions for a longer time. The H_2/CO and CO/CO_2 ratios are shown in Fig. 4.54.

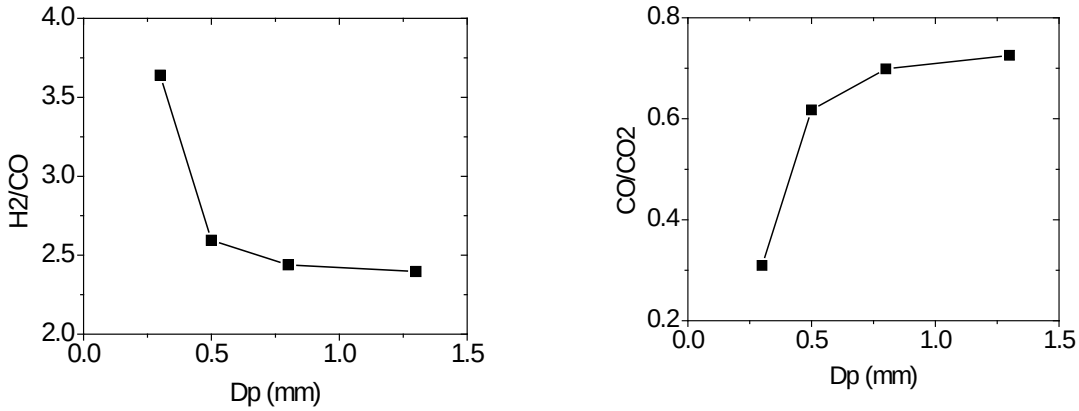

Figure 4. 54 Effect of particle size on H2/CO and CO/CO2 ratios for the 1-D two-phase kinetic model, T=870 ^{o}C, steam/biomass ratio=1, U_o=0.45 m/s, and the particle size is 0.3 mm

4.7 Model comparison

The seven models developed in this study are compared in this section. To facilitate drawing figures, the models are represented by the following numbers: 1: the zero-dimensional equilibrium model-non-stoichiometric; 2: the zero-dimensional equilibrium model-stoichiometric; 3: the zero-dimensional kinetic model; 4: the one-dimensional one-phase kinetic model; 5: the one-dimensional two-phase kinetic model; 6: the one-dimensional two-phase kinetic model-all char in bed with particle size; and 7: the one-dimensional two-phase kinetic model-without particle size. The

models developed in this studied are compared through investigation of effects of steam/biomass ratio, temperature, and superficial gas velocity on gasification products. Because the results of the zero-dimensional kinetic model (4) change with time, the results obtained at the 1st second with a particle size of 0.3mm are shown here.

4.7.1 Effect of temperature

The effect of temperature is studied with the operating conditions of: 1) the steam/biomass ratio is 1; 2) the initial particle size is 0.3 mm; 3) the superficial gas velocity is 0.4 m/s for kinetic models with fluid dynamics.

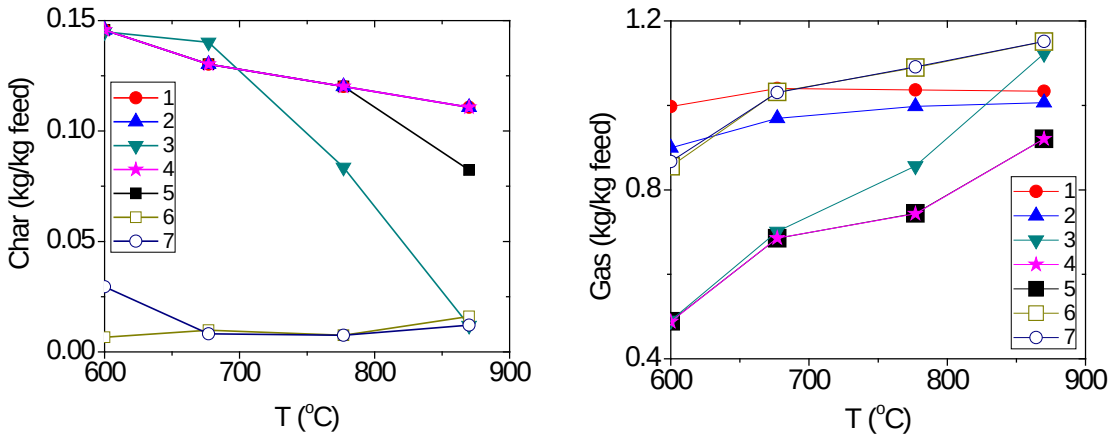

Figure 4. 55 Yields of char and dry tar-free gas at different temperatures for different models, steam/biomass ratio=1, the particle size = 0.3 mm, and U_o=0.4 m/s

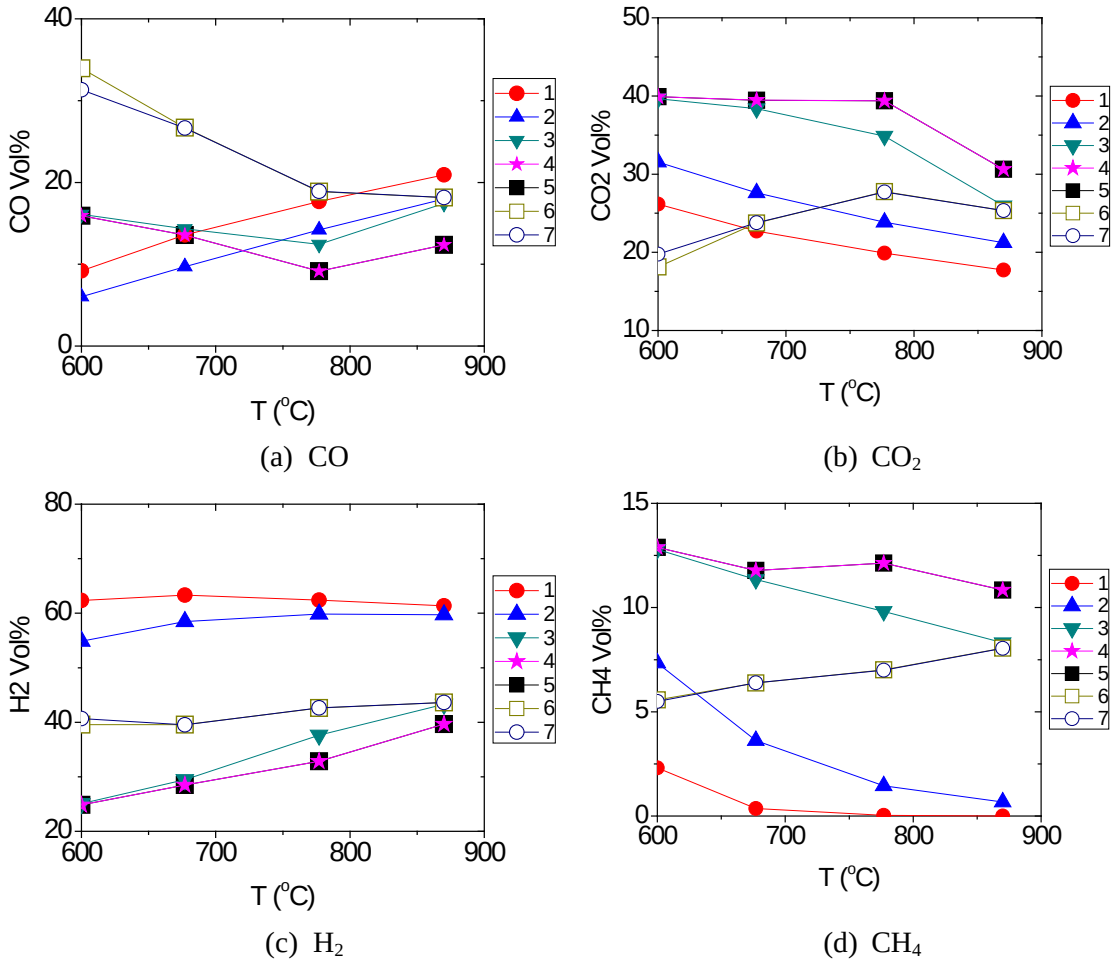

Figure 4. 56 Effect of temperature on the gas volumetric fraction for different models, steam/biomass ratio=1, the particle size = 0.3 mm, and U_o=0.4 m/s

The yields of char and dry tar-free gas, gas volumetric fraction, and higher heating values (HHVs) at different temperatures for the several models are shown in Figs. 4.55 to 4.58. First, it can be seen that there are two pairs of kinetic models, and models in the same pair have almost the same gasification results in terms of the yield of char and dry tar-free gas, gas volumetric fraction, and HHVs. One pair is the one-dimensional one-phase kinetic model (4) and the one-dimensional two-phase kinetic model (5), and the other pair is the one-dimensional two-phase kinetic

model-all char in bed with particle size (6) and the one-dimensional two-phase kinetic model-all char in bed without particle size (7). This is because each pair has similar modeling concepts. Both the one-dimensional one-phase kinetic model (4) and the one-dimensional two-phase kinetic model (5) are kinetic models including fluid dynamics and have char entrainment. Both the one-dimensional two-phase kinetic model-all char in bed with particle size (6) and the one-dimensional two-phase kinetic model-all char in bed without particle size (7) are kinetic models including fluid dynamics and do not have char entrainment.

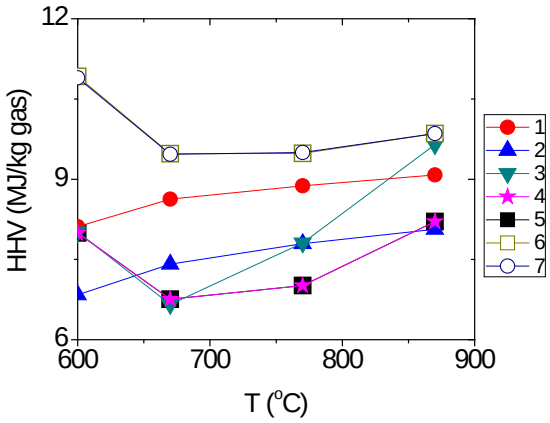

Figure 4. 57 Effects of temperature on HHV including H2O and tar for different models, steam/biomass ratio=1, the particle size = 0.3 mm, and U_o=0.4 m/s

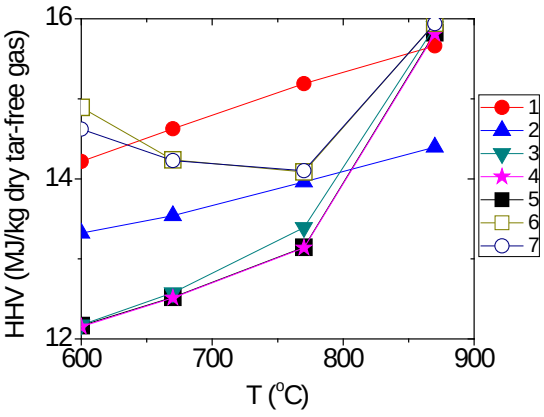

Figure 4. 58 Effects of temperature on HHV excluding H2O and tar for different models, steam/biomass ratio=1, the particle size = 0.3 mm, and U_o=0.4 m/s

In addition, although the gasification results (the yields of char and dry tar-free gas, gas volumetric fractions, and HHVs) of the non-stoichiometric equilibrium model (1) and the stoichiometric equilibrium model (2) are not as close as the above two pairs of models, they have similar patterns of evolution with increased temperatures. This is

because both of the two equilibrium models are based on the minimum Gibbs free energy theory. The yields of dry tar-free gas, gas volumetric fraction, and HHVs of the zero-dimensional kinetic model (3) are closer to those of the kinetic models with char entrainment (4 and 5), especially at low temperature (600 ^{o}C and 670 ^{o}C). However, as the temperature increases, the difference between the zero-dimensional kinetic model (3) and kinetic models including fluid dynamics with char entrainment (4 and 5) becomes larger. This may be because the gasification results of the zero-dimensional kinetic model (3) change with time due to the modeling concept, and the results presented in these figures are those obtained at 1 s. It is possible that the gasification results of the zero-dimensional kinetic model (3) at other times are closer to the results of models 4 and 5. In addition, at high temperatures, the reaction rates are fast, and there is little char left at 1 s for the zero-dimensional kinetic model (3), while there is a certain amount of char produced when using models 4 and 5, leading to different gasification results.

4.7.2 Effect of steam/biomass ratio

The yields of char and dry tar-free gas of the seven models at different steam/biomass ratios are compared over the range of steam/biomass ratio in Fig. 4.59. Through comparison it can be seen that the yields of char and dry tar-free gas of the two equilibrium models (1 and 2) are very close. This may be due to the fact that because equilibrium models (1 and 2) cannot predict the yield of char, the yield of char of the

equilibrium models (1 and 2) was fixed in advance and given the same value predicted by the one-dimensional two-phase kinetic model (5) at different steam/biomass ratios. Because the water-gas shift reaction and the C-H_2 reaction are set at equilibrium state in both equilibrium models (1 and 2), a similar amount of H_2O is consumed in both models, and thus a similar amount of gas is produced by both models based on the mass balance. In addition, the yield of dry tar-free gas of the equilibrium models (1 and 2) is higher than the other 5 models. The possible reason may be because the products of equilibrium models do not include the tar, and thus biomass which would otherwise become tar turns into low molecular gases.

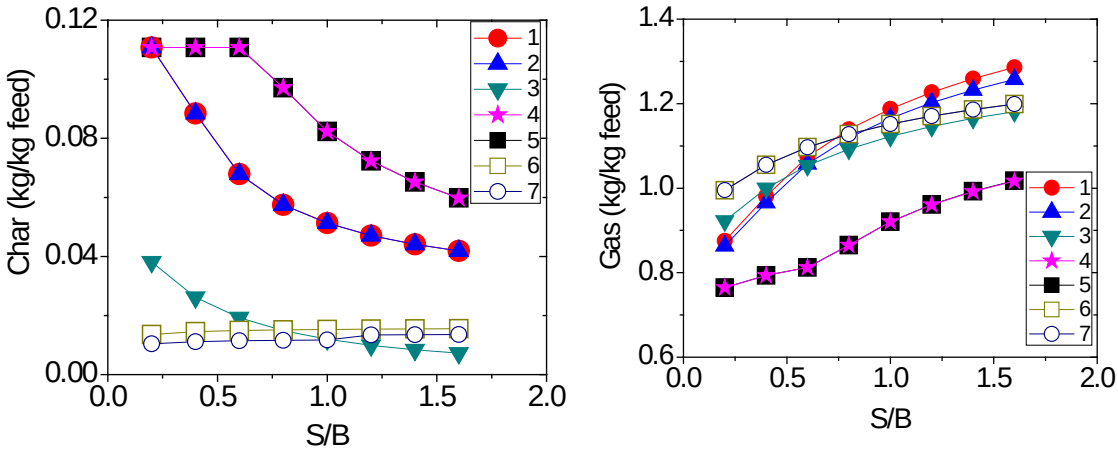

Figure 4. 59 Effects of steam/biomass ratio on yields of char and dry tar-free gas for different models, T=870 ^oC, the particle size = 0.3 mm, and U_o=0.4 m/s

It can also be seen from Fig. 4.59 that the yields of char and dry tar-free gas predicted by the one-dimensional one-phase kinetic model (4) are very close to those predicted by the one-dimensional two-phase kinetic model (5). Another pair of models that predict similar yield of char and dry tar-free gas is the one-dimensional two-phase

kinetic model-all char in bed with particle size (6) and the one-dimensional two-phase kinetic model-all char in bed without particle size (7) as discussed in the section 4.6. As for the zero-dimensional kinetic model (3), its yields are closer to the kinetic models without char entrainment (6 and 7) although the largest difference between the yield of dry tar-free gas obtained by the zero-dimensional kinetic model (3) and that of the kinetic models without char entrainment (6 and 7) is nearly 0.1 kg/kg gas.

In addition, it can be seen from Fig. 4.59 that kinetic models with char entrainment (4 and 5) predict the highest amount of char and the lowest amount of dry tar-free gas of all the seven models over the range of steam/biomass ratio studied.

The gas volumetric fractions predicted by the seven models at different steam/biomass ratios are compared over the range of steam/biomass ratios studied in Fig. 4.60. It can be seen clearly that the change of gas volumetric fractions predicted by the seven models have the same trend with increased steam/biomass ratios. With an increased steam/biomass ratio, the volumetric fractions of H_2 and CO_2 increase while those of CO and CH_4 decrease. In addition, it can be seen that equilibrium models (1 and 2) have similar gas volumetric fractions, and kinetic models with char entrainment (4 and 5) also predicts similar gas volumetric fractions. The gas volumetric fractions predicted by model 3 are close to those predicted by kinetics models without char entrainment (6 and 7). The gas volumetric fractions of H_2 and CH_4 predicted by equilibrium models (1 and 2) are different greatly from those predicted by kinetic

models (3 to 7). This may be because unlike kinetic models equilibrium models do not include C_nH_m and tar in its products, which leads to different gas volumetric fractions. In addition, equilibrium models cannot predict gases with large a Gibbs free energy such as CH_4 correctly, which affects the gas volumetric fraction of other gases. From Fig. 4.60 it can also be found that the volumetric gas fractions predicted by the seven models have great difference at low steam/biomass ratios, and the difference become smaller as the steam/biomass ratio increases.

The evolution of H_2/CO and CO/CO_2 ratios with increased steam/biomass ratio is shown in Fig. 4.61 for the seven models. It can be seen that these models have similar H_2/CO ratio over the range of steam/biomass ratio studied, but the CO/CO_2 ratio of equilibrium models (1 and 2) are somewhat different from those of other models. Moreover, the CO/CO_2 ratios predicted by the two equilibrium models are also somewhat different from each other.

The higher heating value of gases produced at different steam/biomass ratios for these models are shown in Figs. 4.62 and 4.63. It can be seen that kinetic models with char entrainment (4 and 5) have almost the same HHVs, and kinetic models without char entrainment (3, 6, and 7) also have very close HHVs. However, the HHVs predicted by equilibrium models (1, and 2) are not very close, and the largest differences is about 2 MJ/kg gas or MJ/kg dry tar-free gas. In addition, it can be seen that the

difference between the HHVs predicted by kinetic models (3, 4, 5, 6, and 7) decreases with increased steam/biomass ratio and that between the HHV of gas excluding H_2O and tar predicted by equilibrium model remain almost the same over the range of steam/biomass ratio studied.

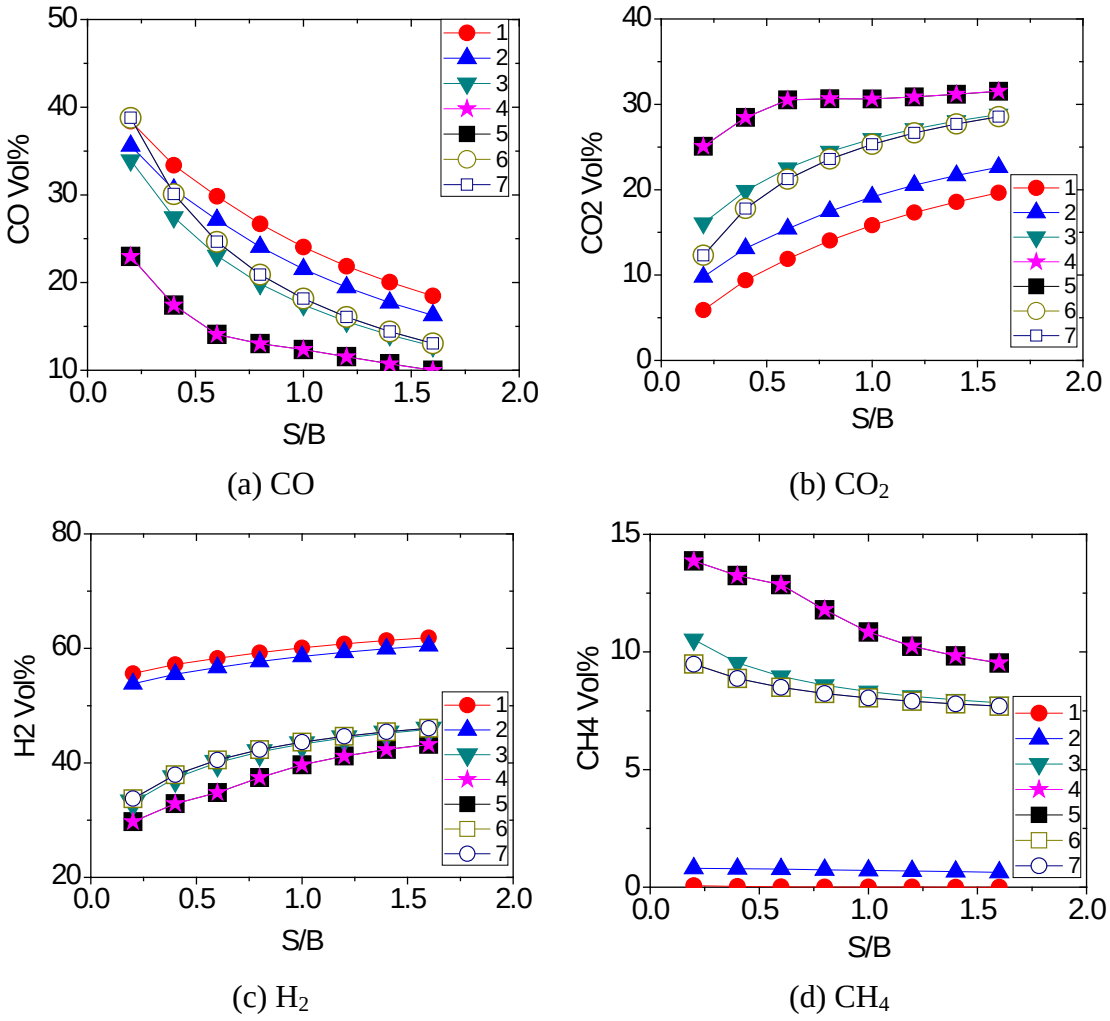

(a) CO (b) CO_2

(c) H_2 (d) CH_4

Figure 4. 60 Effects of steam/biomass ratio on gas volumetric fractions for different models, T=870 ^oC, the particle size = 0.3 mm, and U_o=0.4 m/s

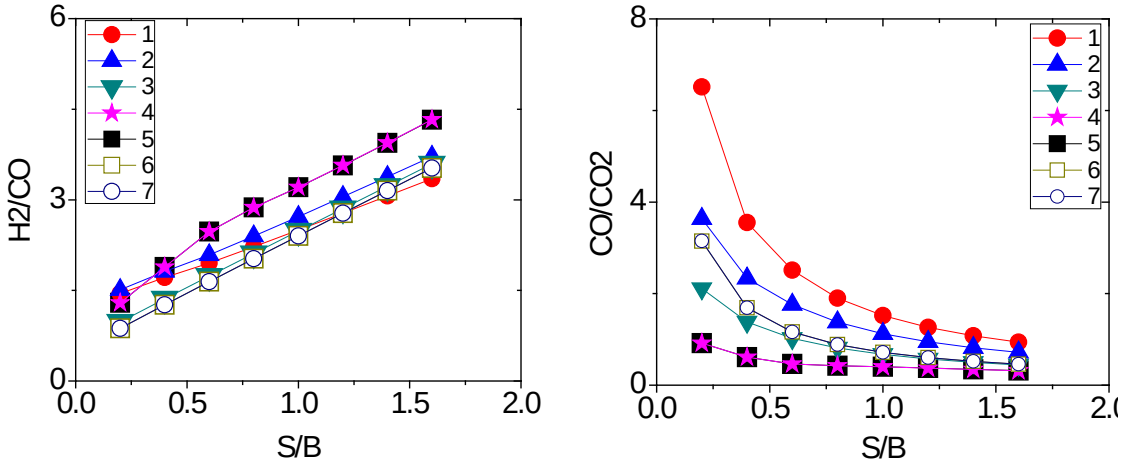

Figure 4. 61 Effects of steam/biomass ratio on H2/CO and CO/CO2 ratios for different models, T=870 ^{o}C, the particle size = 0.3 mm, and U_o=0.4 m/s

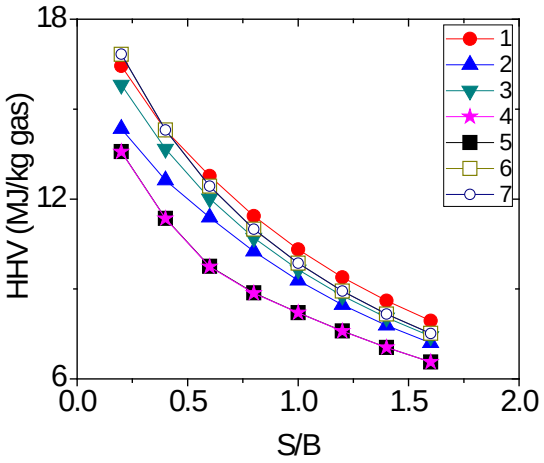

Figure 4. 62 Effects of steam/biomass ratio on HHV including H2O and tar for different models, T=870 ^{o}C, the particle size = 0.3 mm, and U_o=0.4 m/s

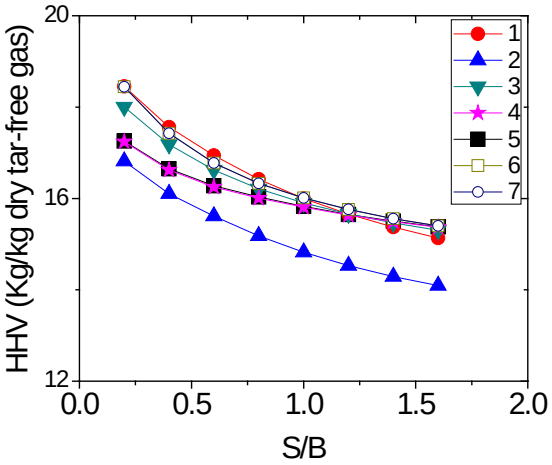

Figure 4. 63 Effects of steam/biomass ratio on HHV excluding H2O and tar for different models, T=870 ^{o}C, the particle size = 0.3 mm, and U_o=0.4 m/s

4.7.3 Effect of superficial gas velocity

The effect of superficial gas velocity is studied for kinetic models considering fluid dynamics (4, 5, 6, and 7). The temperature is 870 ^{o}C, and the steam/biomass ratio is 1. The initial particle size is 0. 3 mm.

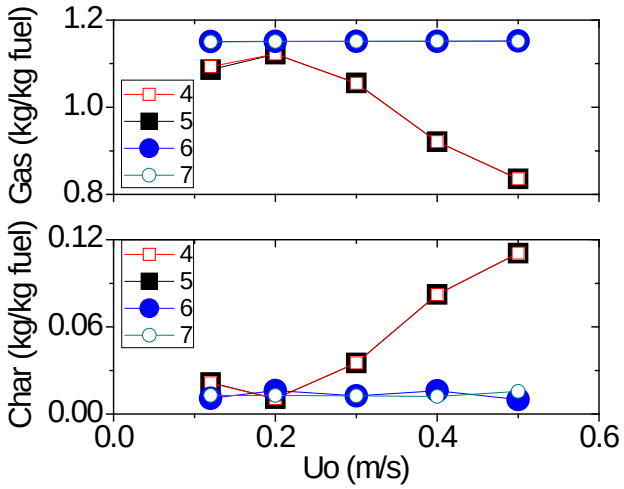

Figure 4. 64 Effects of superficial gas velocity (U_o) on yield of char and dry tar-free gas for models 4 through 7, T=870 ^{o}C, the particle size = 0.3 mm, and steam/biomass ratio=1

The gasification results are shown in Figs. 4.64 to 4.67. The one-dimensional two-phase kinetic model-all char in bed with particle size (6) and the one-dimensional two-phase kinetic model-all char in bed without particle size (7) have almost the same gasification results in terms of the yields of char and dry tar-free gas, gas volumetric fraction, H_2/CO ratio, CO/CO_2 ratio, and HHVs with increased superficial gas velocities. In addition, the one-dimensional two-phase kinetic model (5) and the one-dimensional one-phase kinetic model (4) also have the similar yields of char and

dry tar-free gas, gas volumetric fraction, H_2/CO ratio, CO/CO_2 ratio, and HHVs. This is because models belonging to the same pair have the same modeling concepts. In addition, it can be seen that there is some difference between the gasification results of these two pairs of kinetic models. The difference is small at low superficial gas velocities (0.12 m/s and 0.2 m/s), and increases with increased superficial gas velocities. This is because at low superficial gas velocities, particles of the kinetic models with char entrainment need to reduce their size to a small value in order to be entrained out of the bed. At very low superficial gas velocities, the size of particles entrained out of the bed is very small, so the amount of particles entrained out of the bed can be neglected and these two sets of kinetic models have similar gasification results. However, with increased superficial gas velocity, particles can be entrained out of the bed at an increased particle size, so an increased number of particles are entrained out of the bed, which leads to an increased difference between models with and without char entrainment. The HHV considering H_2O predicted by the kinetic models with char entrainment (4 and 5) is lower than that predicted by the kinetic models without char entrainment (6 and 7). This is because kinetic models with char entrainment (4 and 5) predict more H_2O than kinetic models without char entrainment (6 and 7), which can be proved by the similar HHVs without H_2O and tar predicted by these four models.

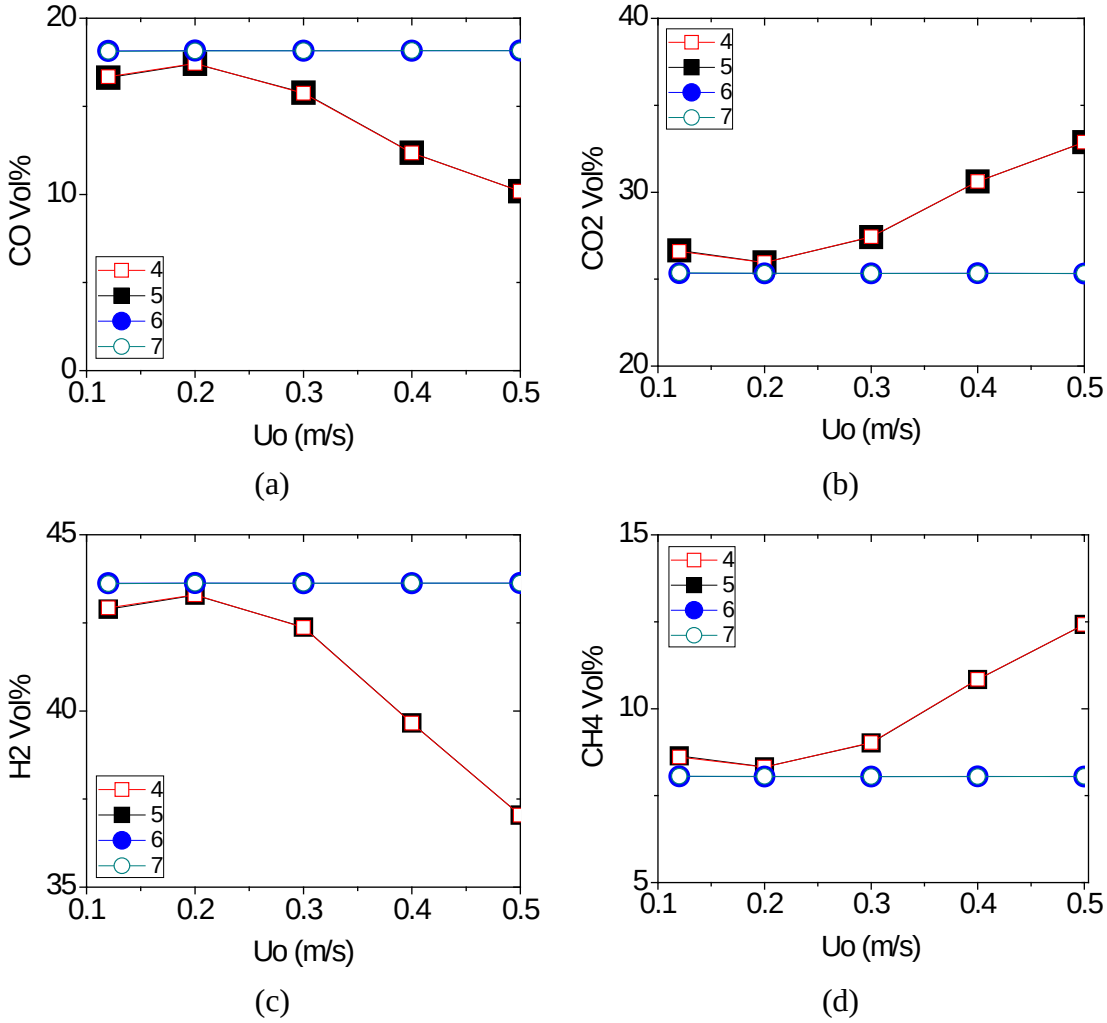

Figure 4. 65 Effects of superficial gas velocity (U_o) on gas volumetric fractions for models 4 through 7, T=870 ^oC, the particle size = 0.3 mm, and steam/biomass ratio=1

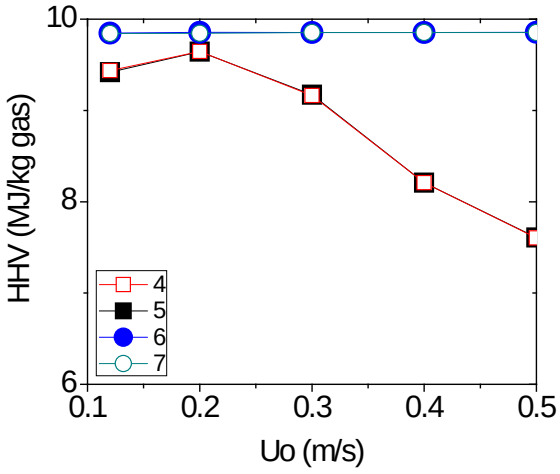

Figure 4. 66 Effects of superficial gas velocity (U_o) on HHV including H2O and tar for models 4 through 7, T=870 ^oC, the particle size = 0.3 mm, and steam/biomass ratio =1

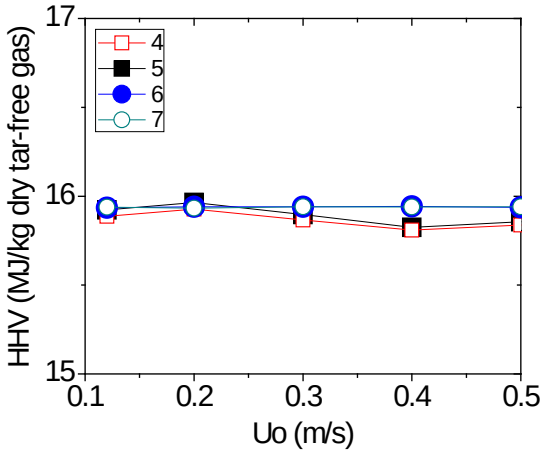

Figure 4. 67 Effects of superficial gas velocity (U_o) on HHV excluding H2O and tar for models 4 through 7, T=870 ^oC, the particle size = 0.3 mm, and steam/biomass ratio =1

4.7.4 Summary of models

In this section, an overall summary of the comparisons among these seven models is presented to assist future researchers with model selection. It will include the disadvantages and advantages of these models, the calculation time required, the application condition, and the similarities and differences between some models. Because char deactivation and segmentation are not able to be modeled due to the lack of related theories, the following conclusions are made under an assumption that char deactivation and segmentation do not happen.

The non-stoichiometric equilibrium model (1) and the stoichiometric equilibrium model (2) are summarized in Table 4.1. It can be seen that some differences between these two models exist. The one-dimensional one-phase kinetic model (4) and the one-dimensional two-phase kinetic model (5) are compared in Table 4.2 and Figs. 4.68-4.70, which indicates that these two models are almost equivalent. These two models can be used to model any fluidized bed, and the one-dimensional two-phase kinetic model-all char in bed with particle size (6) and the one-dimensional two-phase kinetic model-all char in bed without particle size (7) are their special cases. Additional qualitative model comparisons are shown in Tables 4.4 to 4.6. In Table 4.4, kinetic models (3, 4, 5, 6, and 7) are compared to equilibrium models (1 and 2). In Table 4.5, kinetic models (3, 4, 5, 6, and 7) are compared to each other. In Table 4.6, the applications of kinetic models with fluid dynamics (4, 5, 6, and 7) are compared to fuels with different ash content (low, medium, and high).

Table 4. 1 Comparison between the non-stoichiometric equilibrium model (1) and the stoichiometric equilibrium model (2)

	Non-stoichiometric equilibrium model (1)	Stoichiometric equilibrium model (2)
Yields of char	Given as input	
Yields of dry tar-free gas	Almost the same at different steam/biomass ratios Minor difference (0.012-0.079 kg/kg feed) at different temperature, and difference decreases with temperature	
Gas volumetric fraction	Some differences exist Differences over the range of steam/biomass ratio studied 2.2-2.8% for CO; 3.0-3.9% for CO_2; 1.4-1.8% for H_2; 0.6-0.8% for CH_4 Differences over the range of temperature studied: 2.5-3.3% for CO; 3.5-5.4% for CO_2 1.6-7.4% for H_2; 0.7-5.0% for CH_4	
H_2/CO and CO/CO_2 ratios	Some differences exist Differences over the range of steam/biomass ratio studied 0.06-0.37 for H_2/CO; 0.22-2.88 for CO/CO_2 Differences over the range of temperature studied: 0.31-2.04 for H_2/CO; 0.15-0.31 for CO/CO_2	
HHVs	Some differences exist Differences over the range of steam/biomass ratio studied 1.04-1.64 for HHV without H_2O and tar 0.74-2.10 for HHV including H_2O and tar Differences over the range of temperature studied: 0.90-1.26 for HHV without H_2O and tar 1.02-1.27 for HHV including H_2O and tar	
Calculation time	1 second	
Model selection	When only simple estimation is required	
Application	Gases reach equilibrium state at exit	

Table 4. 2 Comparison between kinetic models including fluid dynamics (4 and 5) with char entrainment

	1-D two-phase kinetic model (5)	1-D one-phase kinetic model (4)
Yields of char	Almost the same	
Yields of dry tar-free gas	Almost the same at different steam/biomass ratios. Small difference exists when studying the effects of superficial gas velocity and temperature: Difference is in the range of 0.05-0.07 kg/kg feed at different superficial gas velocities Difference is in the range of 0.02-0.25 kg/kg feed at different temperature Model (4) predicts more gas than model (5)	
Gas volumetric fraction	Almost the same	
H_2/CO and CO/CO_2 ratios	Almost the same	
HHVs	Almost the same	
Gas concentration in the bed	Almost the same as shown in Fig. 4.85	
The amount of char in bed	Small difference, exists (about 10% percent of the mass of model 5)	
Time needed to reach steady-state	Very close	
Calculation time	Several hours to several days	
Advantages	Detailed and accurate results.	Accurate results. Relatively shorter calculation time than model (5)
Disadvantages	Long calculation time	
Model selection	No preference	
Application	Any situation	

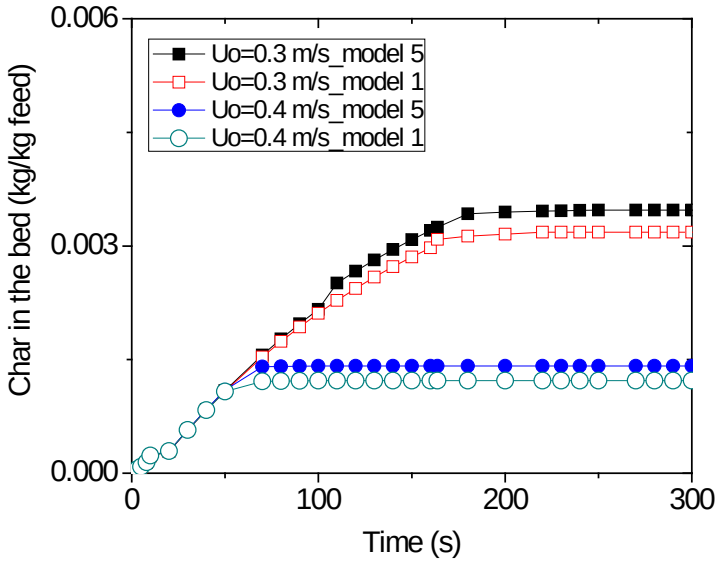

Figure 4. 68 Evolution of char in the bed with time for the 1-D one-phase kinetic model (4) and the 1-D two-phase kinetic model (5) at two superficial gas velocities (U_o), T=870 ^oC, the particle size = 0.3 mm, and steam/biomass ratio =1

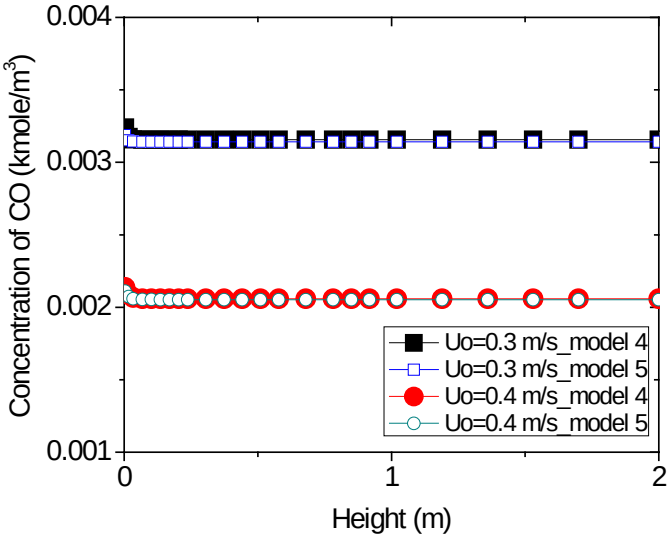

Figure 4. 69 Concentration of CO along with the height of the freeboard for the 1-D one-phase kinetic model (4) and the 1-D two-phase kinetic model (5) at two superficial gas velocities (U_o), T=870 ^oC, the particle size = 0.3 mm, and steam/biomass ratio=1

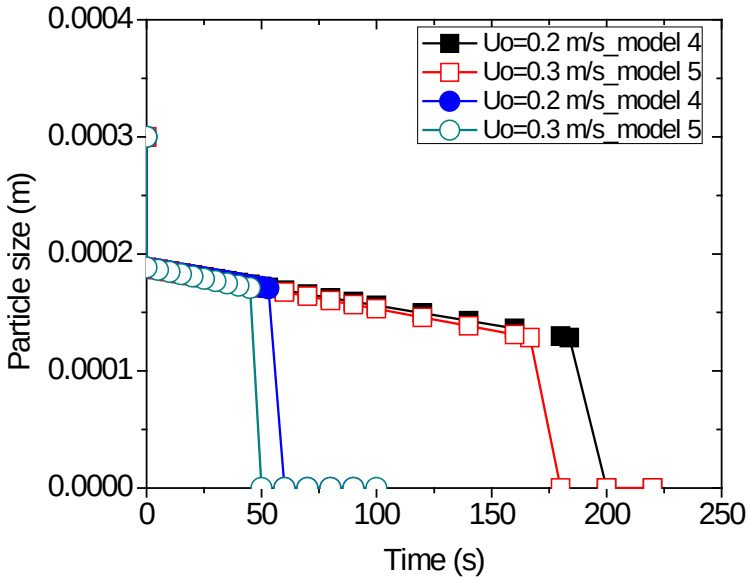

Figure 4. 70 Evolution of the size of a single particle in the bed for the 1-D one-phase kinetic model (4) and the 1-D two-phase kinetic model (5) at two superficial gas velocities (U_o), T=870 ^oC, the particle size = 0.3 mm, and steam/biomass ratio=1

Table 4. 3 Comparison between kinetic models including fluid dynamics with all char in bed (6 and 7) (S/B=1, T=870 oC, superficial gas velocity is 0.4 m/s, and particle size is 0.3 mm)

	1-D two-phase kinetic model-all char in bed with particle size (6)	1-D two-phase kinetic model-all char in bed without particle size (7)
Yields of char	Almost the same with small difference (<0.01 kg/kg feed)	
Yields of dry tar and N2-free gas	Almost the same with small difference (<0.002 kg/kg feed)	
Gas volumetric fraction	Almost the same	
H_2/CO and CO/CO_2 ratios	Almost the same	
HHVs	Almost the same	
Gas concentration in the bed	Almost the same	
The amount of char in bed	0.0042 kg/kg feed	Increase as the value of specific area decreases
Time needed to reach steady-state	400 seconds	
Calculation time	Several hours to several days	A few hours
Advantages	Detailed and accurate information	Short calculation time
Disadvantages	Long calculation time	Inaccurate information of time-related parameters and the amount of char in bed
Model selection	When time related information and the amount of char in the bed are needed	When only information of yields of char and gas, and gas distribution at the exit is require, using this model can shorten computation time.
Application	When the majority of fuel is consumed in the bed and fuel entrainment is negligible	

Table 4. 4 Comparison between kinetic models (3, 4, 5, 6, and 7) and equilibrium models (1 and 2)

	Kinetic models (3, 4, 5, 6, and 7)	Equilibrium models (1 and 2)
Information required	• Pyrolysis yields • Reaction rates • Kinetic models with fluid dynamics also requires: • Reactor geometry • Parameters of fluid dynamics	• Fuel ultimate analysis • Equilibrium constants
Information provided	• Yields of char and gas with time • Distribution of char and gas in the bed with time • Evolution of change of particle size in the bed with time • Effects of temperature, pressure, steam/biomass ratio, superficial gas velocity, particle size, and mass flow rate • Percentage of fuel consumed and entrained out of the bed (for model 4 and 5)	• Yields of char and gas • Effects of temperature, pressure, and steam/biomass ratio
Advantages	• Provides thorough information of the char and gas in the bed and with time • Reflects the effects of multiple variables • Closer to the real process	• Very easy to establish models • Calculation time is very short, about 1 second.
Disadvantages	• The process of establishing models is very complex • Requires much longer calculation time compared with equilibrium models. Calculation time varies from less than one hour to days	• Only three variables can be studied and cannot reflect the change of some operating conditions • Needs strict operating condition, most of the time results are not close to real process
When to apply	• Need thorough information of gas and char with time, char and gas distribution in the bed, etc. • Need to get the effects of multiple variables on gasification results	• The system is at equilibrium state, and just needs a rough estimation of the gasification products

Table 4. 5 Comparison between kinetic models (3, 4, 5, 6, and 7)

	Kinetic models with char entrainment (4 and 5)	Kinetic models without char entrainment (6 and 7)	Zero-dimensional kinetic model (3)
Difference	• Particles are entrained out of the bed once their terminal velocity is smaller than superficial gas velocity	• Particles stay in the bed all the time	• Both gas and solids are in the system. Modeled as a closed system
Disadvantage	• Failed to include char deactivation and particle segmentation due to lack of theories and experimental data • Not able to predict the effect of particle size correctly, due to the first disadvantage. More char and less gas is obtained for smaller particle size, which is opposite to the real process		• Cannot provide information of gasification products distribution in the reactor • Cannot reflect the change of some operating conditions • Predicts much higher gas concentration than other kinetic models due to much smaller gas volume calculated
When to apply	• A lot of particle entrainment occurs	• Gas superficial velocity is very small and the particle size is large so that almost all the particles are consumed in the bed before they can be entrained out of the bed	• Need a rough estimation of gasification products with time

Table 4. 6 Summary of the kinetic model with fluid dynamics to different fuels

Ash content	Low (<7%, such as wood)	Medium (7%-12%, such as corn stover)	High (>12% , such as manure)
Bed steady state	Reach steady state	Does not reach	Does not reach
Fragmentation	Exists. Decreases particle size and increases the number of particles. Therefore, char reactivity and the amount of char entrained out of the bed are increased	Fragmentation exists. Increases reactivity, and more particles, and more char entrained out of the bed	No, due to ash skeleton, shape and volume does not change a lot.
Attrition	Yes	Yes	Yes
Char deactivation	Unknown. Since little information is available on char deactivation for low ash content fuel. Because no char accumulation in the bed, it can be inferred that the char is still active before it can be entrained out of the bed.	Yes.	Yes.
Char accumulation	No	Yes. The percentage of carbon in the particle is unknown.	Yes. The percentage of carbon in the particle is unknown.
Disadvantage of current model	Compared to the real process, fragmentation cannot be modeled.	Compared to the real process, fragmentation and char deactivation cannot be modeled.	Compared to the real process, char deactivation cannot be modeled.
Problems of current models	Without fragmentation and char deactivation, char produced of larger particles is smaller than that of smaller particles, and the amount of gas produced is also different.		
Possible Solution	The other method is removal particles once their residence time/bed depth exceeds a certain value. Under this condition, more char will be produced for larger particles.		

5 Effect of gasification models on BIGCC system

The effects of different gasification models developed in previous chapters on overall biomass integrated gasification combined cycle (BIGCC) system performance will be evaluated in this chapter by incorporating gasification models in BIGCC models.

5.1 BIGCC system overview

A model of a 0.19 hm^3 y^{-1} (50 million gallon per year) dry-grind corn ethanol plant that uses biomass to produce process heat and generate electricity was developed (Zheng, Morey and Kaliyan, 2010). The process heat is used for the ethanol production process including co-product drying. Some of the electricity generated is used by the plant with the excess power sent to the grid.

The ethanol part of the process is based on an Aspen Plus model of a dry-grind plant obtained from the USDA Agricultural Research Service (McAloon, et al., 2000; McAloon, Taylor and Yee, 2004; Kwiatkowski, et al., 2006). This BIGCC model adds biomass gasification and combustion to produce syngas following the approach of De Kam, Morey and Tiffany (2009a). It includes syngas cleanup prior to the gas turbine as well as stack gas treatment. The power generation model is based on a combined cycle gas turbine and steam turbine. The biomass gasification/combustion and power generation comprise the power island at the biomass fueled ethanol plant.

A conventional dry-grind ethanol plant uses a direct-fired natural gas dryer for co-product drying. A thermal oxidizer destroys volatile organic compounds (VOCs) in the dryer exhaust air. To accommodate biomass fuels, either a steam tube dryer or a superheated steam dryer is substituted for the direct fired dryer. In the case of the steam tube dryer, dryer exhaust is directed to the twin fluidized bed combustor, the gas turbine, or a duct burner following the gas turbine to destroy VOCs. In the case of the superheated steam dryer, water vapor removed from the product is collected in the superheated steam. A portion of the superheated steam is removed and condensed to reduce energy use and recover water. Although Aspen Plus models were developed for both of these drying systems (Zheng, Morey and Kaliyan, 2010), in this study only the steam tube drying system is used since this system has higher system efficiency and sends more power to the grid. Schematic diagrams illustrating the overall configuration of the BIGCC systems with corn stover as fuel is shown in Fig. 5.1. The steam tube dryer schematic shows the configuration where dryer exhaust mixed with preheated air from the stack exhaust is directed to the inlet of the gas turbine.

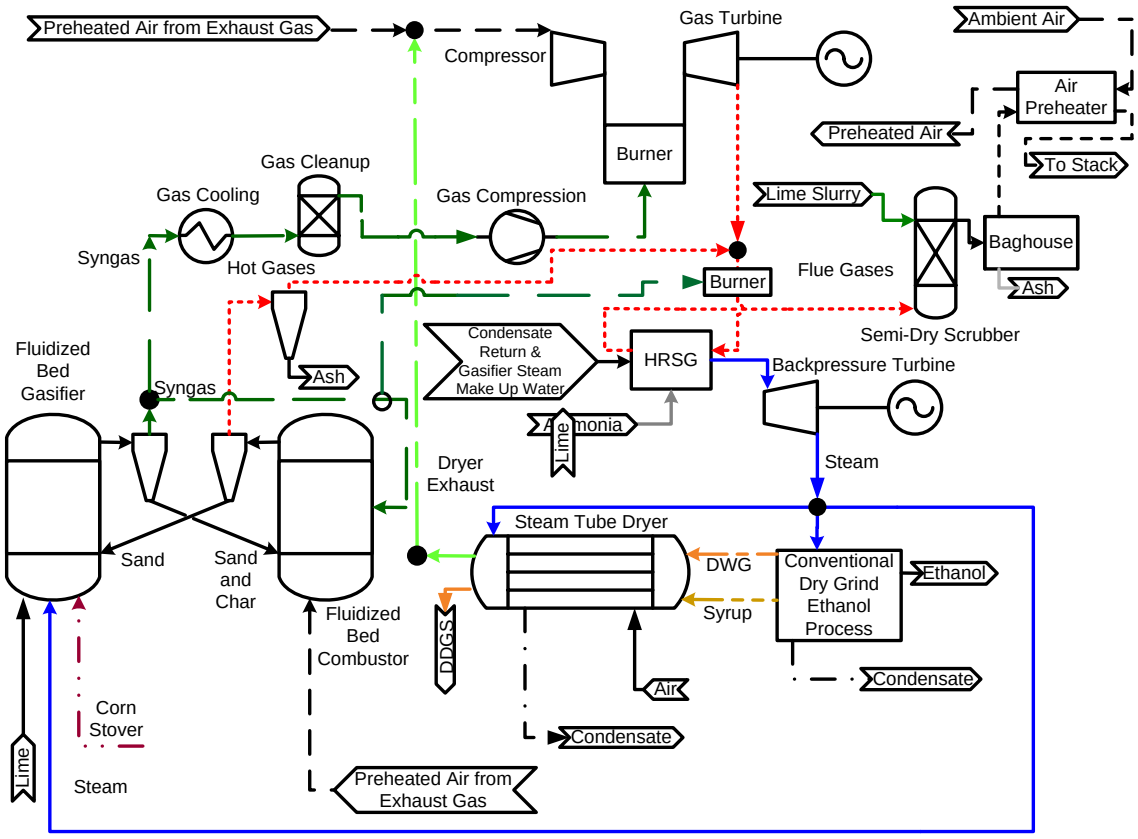

Figure 5. 1 Schematic diagram of corn stover fired steam tubing drying BIGCC system

5.2 Aspen Plus model for BIGCC system

The implementation of various components of the BIGCC systems in Aspen Plus 2006 software (AspenTech, http://www.aspentech.com) is detailed below.

5. 2.1 Biomass fuels

Although more than one kind of fuels were used for BIGCC systems in previous work Zheng, Morey and Kaliyan, 2010), since the fuel used in gasification models is corn stover, corn stover is the only fuel used in the BIGCC systems. Corn stover is defined as

solid nonconventional components in Aspen Plus models.

5. 2.2 Gasification/combustion including gas cleanup and stack gas treatment

A twin fluidized bed gasification/combustion system based on the SilvaGas® process (Paisley and Welch, 2003) is used in this study to model syngas production from biomass fuel. Different gasification models developed in previous chapters are used to predict the gasification products in the twin fluidized bed gasification/combustion system. Previously, De Kam, Morey and Tiffany (2009b) divided biomass fuels into two parts: one part goes to the gasifier to produce syngas, and the other goes to the combustor to provide heat for the gasifier (Fig. 5.2). Whereas, in this study, all of the fuel is sent to the gasifier, and the heat needed for the gasification process is produced in the combustor from char and a portion of syngas from the gasifier if needed (Fig. 5.3). Simulation results have shown similar system thermal performances for both configurations (Figs. 5.2 and 5.3), but the most important advantage of using the new configuration (Fig. 5.3) is that the size of the combustor is reduced, which can decrease the system cost significantly. In addition, the new configuration provides greater flexibility for gas cleanup, which is important especially when the fuel is herbaceous biomass such as corn stover. Fig. 5.1 illustrates the new fluidized bed gasification/combustion configuration where all biomass fuel going to the gasifier and a part of syngas sent to the combustor as needed.

A part of syngas besides char is sent to the combustor to generate heat, and the

remainder of the syngas is cooled, cleaned (impurities such as HCl, NH_3, H_2S, and C_6H_6O), and sent to gas compressors at 84 ^oC and 1 atm. Syngas compressor intercooler is used to cool the compressed syngas to 157 ^oC, and heat is recovered to preheat a part of condensate water for steam cycle.

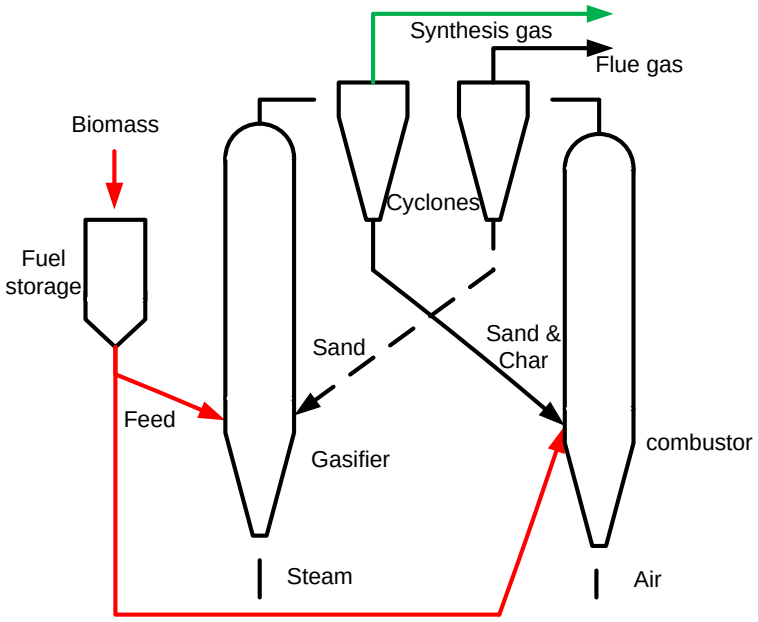

Figure 5. 2 Schematic diagram of the twin-fluidized bed gasification system used by previous researchers (De Kam, Morey and Tiffany, 2009b)

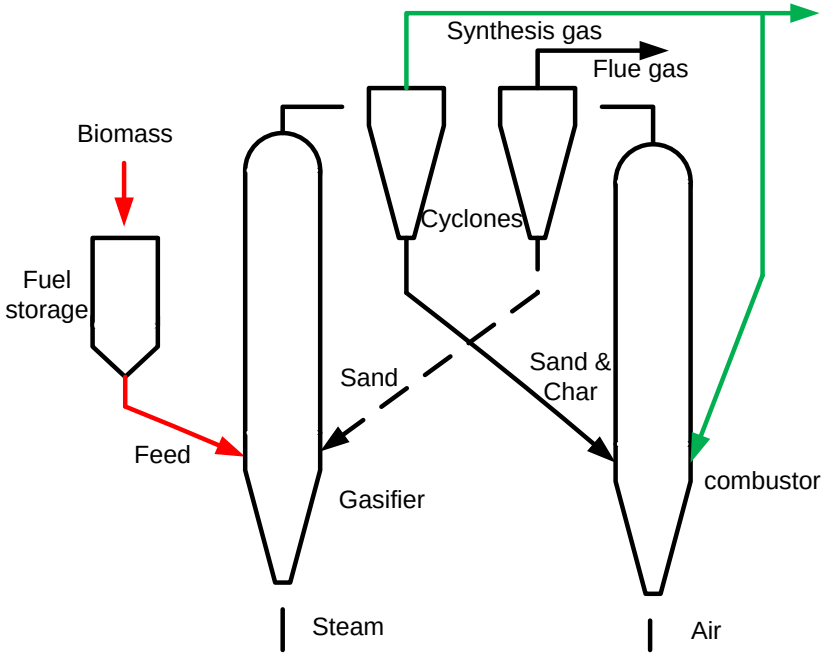

Figure 5. 3 Schematic diagram of the twin-fluidized bed gasification system used in this study

5.2.3 Power generation – gas turbine and steam turbine

The process is modeled using specifications found from references (Paisley and Welch, 2003; De Kam, Morey and Tiffany, 2009b). Compressed syngas is combusted in the burner of the gas turbine with compressed air, and then the combustion exhaust is sent to the gas turbine to generate electricity. In order to protect the gas turbine from a too high temperature, air provided is much more than that needed for complete combustion. The amount of air is calculated so that the temperature of the exhaust from the gas turbine burner is 1078 ^{o}C. The gas turbine has an isentropic efficiency of 90% and a mechanical efficiency of 98%, and its discharge pressure is 1 atm. Exhaust from the gas turbine is mixed with exhaust from the combustor, and sent to the steam generation system. A

duct-burner is used after the gas turbine (before the steam generation system) when the heat energy from the exhaust mixture could not meet the ethanol plant's process heat demand.

Steam generation system contains an economizer, an evaporator, and a superheater. Hot exhaust gas first goes through the superheater, then the evaporator, and finally the economizer. Pressure loss is assumed 700 kPa for the superheater, and 500 kPa for the evaporator. Condensate water enters the steam generation system at 7500 kPa and 149 ^{o}C, and leaves at 6300 kPa and 482 ^{o}C from superheater. A 3% of water from economizer is taken out as the blowdown water. A 5 ^{o}C temperature decrease is assumed for heat loss from the superheater to steam turbine. The steam turbine has an isentropic efficiency of 75%, and a mechanical efficiency of 97%, and its discharge pressure is 446 kPa. Certain amount of steam (steam/dry biomass ratio is 0.21 on a mass basis) is taken from steam turbine exhaust to serve as a gasification agent, and the rest is mixed with makeup water which is equal to the blowdown water and then sent to downstream usage – steam tube dryers and corn ethanol production process. The excess electricity generated from the BIGCC is sent to the grid after meeting the BIGCC parasitic power load and ethanol plant needs. Exhaust from the steam generation system is first sent to gas cleaning facilities to reduce impurities (NO_x, SO_x, and HCl), and then sent through a heat exchanger to preheat the air entering the combustor before being rejected into stack.

5.2.4 Drying

In this study, only the steam tube dryer is employed to dry co-products. Steam tube dryers used here are similar to those used in previous work (De Kam, Morey and Tiffany, 2009a; De Kam, Morey and Tiffany, 2009b). An Aspen Plus model of the steam tube dryer is shown in Fig. 5.4. The amount of steam needed for the drying process is well controlled such that the moisture content of the dried feedstock is about 10% on a wet weight basis, and the amount of ambient air is calculated so that the exhaust leaving the steam tube dryer has a humidity ratio of 0.75 kg water/kg dry air. Wet feedstock is mixed with air, and then goes through a RSTOIC block where all the nonconventional moisture (i.e., moisture in the feedstock) is converted into conventional water (Fig. 5.4). Then, the mixture of air and feedstock is sent to a counter-flow heat exchanger where liquid water is vaporized and carried away by the air. During this process wet feedstock is dried, and hot steam becomes condensate. The temperature of dried feedstock and exhaust is at 87 ^{o}C. After leaving the heat exchanger, dried feedstock is separated by a FLASH2 block from the dryer exhaust, a mixture of air, vaporized moisture, and volatile organic compounds (VOCs) produced in the process of drying. The dryer exhaust (air, water vapor, and VOCs) must be treated to destroy the VOCs (Svoboda, et al. 2009).

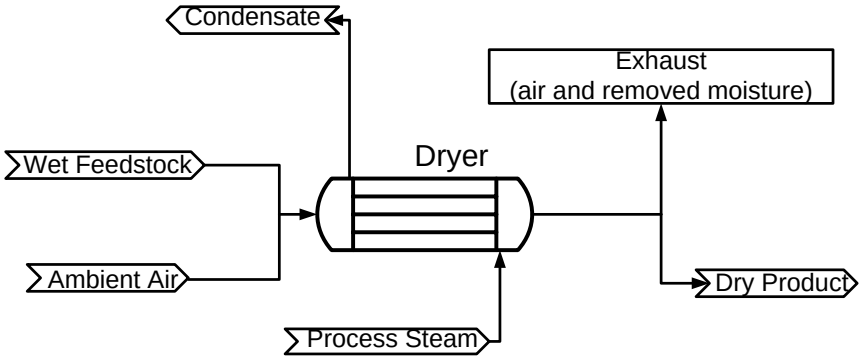

Figure 5. 4 Steam tube dryer

Three kinds of dryer exhaust treatment methods were evaluated and compared in previous studies. Because the main purpose of this study is to evaluate the effect of different gasification models on overall BIGCC system performance, only two dryer exhaust treatment methods are studied: 1) sending dryer exhaust to combustor and 2) sending dryer exhaust to the gas turbine. Since the dryer exhaust contains a large amount of water vapor, a significant amount of energy is required to heat it. BIGCC systems using the first dryer exhaust treatment method consume some syngas that could otherwise be sent to the gas turbine to generate power. Temperature reached in the gas turbine combustor (1078 ^{o}C) is sufficient to destroy VOCs in the dryer exhaust, and BIGCC systems using the second dryer exhaust treatment method have greater power production for the same fuel input. When the second dryer exhaust treatment method is used, the ambient air is preheated with stack exhaust to insure that the ambient air-dryer exhaust mixture does not drop below its dew point as it enters the gas turbine.

5.3 Effect of gasification models on BIGCC system performance

The main purpose of this chapter is to determine how different gasification models affect overall performance of BIGCC systems. The BIGCC system performance with the gasification model developed by De Kam, Morey, and Tiffany (2009b) will be compared to performance using several gasification models developed in this study. The gasification model developed by De Kam, Morey, and Tiffany (2009b) is an equilibrium model (here referred as De Kam equilibrium model). It differs from the two equilibrium models developed in this study. The yields of some gases are controlled based on experimental results when using the De Kam equilibrium model, while the yields of all gases are only determined by minimizing Gibbs free energy of the system in the other two equilibrium models developed in this study. The configuration of the BIGCC systems in this section is the same as that used in previous studies for BIGCC systems: 1) 10 bar syngas compressing pressure for the gas turbine; 2) fuel input rate of 110 MW; 3) steam tube dryer for ethanol co-product; and 4) gasifier temperature of 870 ^{o}C and steam/biomass ratio of 0.2.

Four models developed in previous chapters are selected to be integrated to the BIGCC system, and their gasification results are compared to the system using De Kam's gasification model in Table 5.1. Because the one-dimensional one-phase kinetic model has very close gasification results to the one-dimensional two-phase kinetic model in terms of gas distribution and yields of gases and char, this model is not selected, and neither is the one-dimensional two-phase kinetic model-all char in bed without particle

size. The zero-dimensional kinetic model is not selected because its gasification results changes with time.

Table 5. 1 Gasification results of different gasification models used for the BIGCC system

Gasification model	De Kam's equilibrium model	Two-phase kinetic model	Non-stoichiometric equilibrium model	Two-phase kinetic model-all char in bed	Stoichiometric Equilibrium model
Yield of char, kg/kg fuel	0.082	0.111	0.111	0.001	0.111
Yield of gas, kg /kg fuel	0.730	1.019	0.860	1.129	1.025
Gas distribution, kg/kg fuel					
CO	0.366	0.220	0.577	0.543	0.546
CO2	0.198	0.370	0.218	0.263	0.248
H2	0.013	0.02	0.064	0.033	0.062
H2O	0.311	0.236	0.160	0.115	0.161
CH4	0.090	0.075	0	0.075	0.008
CnHm	0.062	0.079	0	0.079	0
Tar	0.006	0.02	0	0.02	0
HHV, MJ/Kg gas excluding H2O and tar	18.79	17.28	17.38	18.48	17.07
HHV, MJ/Kg gas	13.28	13.58	14.65	16.84	14.38
HHV excluding tar	13.13	13.19	14.63	16.52	14.39
Gas volumetric fraction					
CO	40.7%	23.0%	35.8%	38.8%	34.4%
CO2	14.0%	25.1%	8.6%	12.3%	9.9%
H2	20.8%	29.7%	55.6%	33.7%	54.8%
CH4	17.6%	13.9%	0.04%	9.5%	0.8%
CnHm	6.9%	8.3%	35.8%	5.7%	0

Results of BIGCC systems using different gasification models with dryer exhaust sent to the gas turbine are shown in Table 5.2. It can be seen that although there are some differences between system performances of these BIGCC systems using different gasification models, these BIGCC models can be divided into three groups. BIGCC models belonging to the same group have similar system performance in terms of power generation efficiency, system thermal efficiency, and the amount of power sent to the grid. These three groups are: 1) BIGCC system using De Kam's equilibrium model and BIGCC system using the two-phase kinetic model-all char in bed; 2) BIGCC system using the non-stoichiometric equilibrium model and using the stoichiometric equilibrium model; 3) BIGCC system using the two-phase kinetic model. It can also

be seen that compared to the other four cases the BIGCC system using the two-phase kinetic model has higher power generation efficiency and system thermal efficiency, and sends more power to gird. This is mainly because the BIGCC system using the two-phase kinetic model generates more power by the gas turbine (24.5 MW compared to 23.1-23.8 MW) and consumes relatively less power for parasitic BIGCC (4.3 MW compared to 3.9-5.3MW) than the other BIGCC systems as shown in Table 5.2.

The amount of power generated by the gas turbine is affected by both syngas HHV and the syngas distribution among the gas turbine, the combustor, and the duct burner. For different gasification models, due to different syngas distribution as shown in Table 5.1 the amount of heat required for the gasification process is different as shown in Table 5.2. Because the heat required for the gasification process is generated by combusting syngas besides residual char from gasfifier, higher heat demanding requires a larger amount of syngas sent to the gasifier, and thus less syngas is left for the duct burner and the gas turbine. With a larger amount of syngas sent to the gas turbine, more power is generated, and thus the system has higher power generation efficiency. Compared with other gasification models, the two-phase kinetic model requires relatively small heat for gasification process (18.2 MW compared to 16.7 -27.1 MW), and thus more syngas is sent to the gas turbine for power generation (23.1 Mg/h compared to 18.1-22.5 Mg/h) and more power is generated by the BIGCC system using the two-phase kinetic model. In addition, the BIGCC system using the two-phase kinetic model consumes the least

amount of power for syngas compression (3.38 MW with a mass flow rate of 23.1 Mg/h) due to its syngas distribution.

Different gasification models generate syngas with different gas distributions, and different gas distributions result in different HHVs, different heat demands for gasification process, and different amounts of power required for gas compression all of which determine the overall BIGCC system performance. The effect of syngas HHV on system performance can be illustrated by comparing BIGCC system using the two-phase kinetic model-all char in bed and BIGCC system using the stoichiometric equilibrium model. It can be seen in Table 5.2 that BIGCC system using the two-phase kinetic model-all char in bed sends more power to grid and have higher system thermal efficiency than BIGCC system using the stoichiometric equilibrium model while their power generation efficiencies are the same. A certain amount of air, much more than that needed for complete combustion, is sent to the gas turbine to bring the temperature of gas from gas turbine burner to desired temperature before sending this hot gas to gas turbine for power generation. Because when the mass flow rates are the same, compared to syngas with a lower HHV syngas with a higher HHV produces a combustion product with a higher temperature, thus more air is sent to the gas turbine to cool down the combustion products, resulting in a larger mass flow rate and more power generated for the gas turbine. Syngas generated by the two-phase kinetic model-all char in bed has a HHV without tar of 16.52 MJ/kg gas while that generated by the stoichiometric equilibrium model has a HHV without tar of 14.39 MJ/kg. Therefore, compared to the

BIGCC system using the stoichiometric equilibrium model, the BIGCC system using the two-phase kinetic model-all char in bed sends less syngas (18.1 Mg/h vs 20.9 Mg/h) to gas turbine, but generates comparable amount of power (23.1 MW vs 23.1 MW).

Power generation efficiency is a ratio of the amount of total gross power generated by gas turbine and steam turbine to the total energy input rate. Because the amount of power generated by steam turbine is the same for BIGCC systems using different gasification models due to similar amount of steam entering the steam turbine, BIGCC systems generate similar amount of power by gas turbine have similar power generation efficiency (31.4% vs 31.4%). However, the system thermal efficiency is calculated using the net power excluding the amount of power consumed by parasitic BIGCC instead of total power generated by gas turbine and steam turbine. Therefore, when the amount of total gross power generated is the same, BIGCC systems having larger amount of power consumed by parasitic BIGCC have lower system thermal efficiency. Because the BIGCC system using the two-phase kinetic model-all char in bed sends less synas to the gas turbine, it consumes less power for syngas compression (2.93 MW vs 4.23 MW) than BIGCC system using stoichiometric equilibrium model, which explains the differences between thermal efficiency (73.7% vs 72.5%) and the amount of power to grid (25.9 MW vs 24.6 MW) of these two BIGCC systems. Similarly, the above reasons can be used to explain difference in system performances of BIGCC system using De Kam's equilibrium model and BIGCC system using the two-phase kinetic model-all char in bed.

Results of BIGCC systems using different gasification models with dryer exhaust sent to the combustor are shown in Table 5.3. Through comparison between Table 5.2 and Table 5.3, it can be seen that the difference between BIGCC systems using different gasification models becomes smaller when dryer exhaust is sent to the combustor instead of being sent to the gas turbine. This can be explained by the effect of dryer exhaust treatment methods on the syngas distribution between combustor, gas turbine, and the duct burner. Because dryer exhaust contains a large amount of H_2O due to the drying process, a certain amount of syngas is needed to raise the temperature of the dryer exhaust to the temperature of the combustor. Compared to BIGCC systems sending dryer exhaust to gas turbine, in BIGCC systems sending dryer exhaust to the combustor has more heat in the exhaust from combustor, and thus less or no syngas is required in the duct burner. Since the syngas distribution between combustor, gas turbine, and duct burner does not vary a lot when changing the gasification model in the BIGCC system, BIGCC systems with different gasification models have similar but not identical system performances.

Table 5. 2 BIGCC system performance for a 0.19 hm^3 y^{-1} ethanol plant with corn stover fuel at 110 MW input rate and dry exhausted sent to the gas turbine. [a]

	De Kam's equilibrium model	Two-phase kinetic model	Non-stoichiometric equilibrium model	Two-phase kinetic model-all char in bed	Sotichiometric Equilibrium model
Power generation efficiency[b]	32.1%	32.7%	31.3%	31.4%	31.4%
Thermal efficiency[b]	74.0%	74.7%	72.4%	73.7%	72.5%
Power generation, MW					
Total power by gas turbine	53.7	55.2	52.2	53.6	52.4
Gas turbine[c]	23.8	24.5	23.0	23.1	23.1
Steam turbine	11.5	11.5	11.5	11.5	11.5
Total[c]	35.3	36.0	34.4	34.6	34.6
Power Use, MW					
Ethanol process	4.7	4.7	4.7	4.7	4.7
Dryers [d]	0	0	0	0	0
Parasitic BIGCC [d]	4.3	4.3	5.3	3.9	5.3
To Grid	26.2	27.0	24.4	25.9	24.6
Total	35.3	36.0	33.6	34.6	34.6
Process Heat, MW					
Ethanol process	27.9	27.9	27.9	27.9	27.9
Dryer	22.6	22.6	22.6	22.6	22.6
Total	50.5	50.5	50.5	50.5	50.5
Synthesis Gas Split, MW					
Combustor	7.9	3.1	17.4	43.1	15.4
Gas turbine	93.2	107.2	89.5	89.6	90.2
Duct burner	7.6	7.7	6.0	4.1	6.0
Combustor Input, MW					
Char	18.0	24.2	24.2	0	24.2
Syngas	7.9	3.1	17.4	43.1	15.4
Total	25.9	27.3	41.6	43.1	39.6
Combustor Output, MW					
Heat to gasifier	16.7	18.2	27.1	26.7	25.8
Combustion exhaust	9.2	9.1	14.5	16.4	13.8
Information of some streams					
Mass flow of syngas compressors, Mg/h	22.5	23.1	20.4	18.1	20.9
Power needed for syngas compressors, MW	3.42	3.38	4.26	2.93	4.27
Mass flow of gas turbine, Mg/h	289.5	299.0	280.9	292.2	282.0
Air sent to gas turbine, Mg/h	267.0	275.9	260.5	274.1	261.1
Power consumed for air compressor for gas turbine, MW	29.6	30.7	28.3	30.6	29.3

Note: BIGCC = biomass integrated gasification combined cycle.

[a] All energy and power values are based on the fuel higher heating value (HHV). Corn stover: 110 MW (637 Mg d^{-1} at 13% moisture).

[b] Generation efficiency (%) = total power generated × 100 / fuel input rate. Thermal efficiency (%) = [(total power generated + total process heat) × 100 / fuel input rate].

[c] Gas turbine = total power by gas turbine – shaft power for gas turbine air compressor (not given). Total = gas turbine + steam turbine.

[d] Power use by superheated steam dryers or parasitic BIGCC was calculated based on power consumed by compressors, fans, and pumps with an electric motor efficiency of 95%.

Table 5. 3 BIGCC system performance for a 0.19 hm^3 y^{-1} ethanol plant with corn stover fuel at 110 MW input rate and dry exhausted sent to the combustor. [a]

	Matt's model	Two-phase kinetic model	Non-stoichiometric equilibrium model	Two-phase kinetic model-all char in bed	Stoichiometric equilibrium
Power generation efficiency[b]	27.4%	28.3%	27.0%	27.0%	27.1%
Thermal efficiency[b]	70.3%	71.2%	69.3%	70.2%	69.3%
Power generation, MW					
Total power by gas turbine	37.6	39.9	37.1	37.9	37.3
Gas turbine[c]	18.6	19.7	18.3	18.3	18.4
Steam turbine	11.5	11.5	11.5	11.5	11.5
Total[c]	30.1	31.1	29.8	29.8	29.8
Power Use, MW					
Ethanol process	4.7	4.7	4.7	4.7	4.7
Dryers [d]	0	0	0	0	0
Parasitic BIGCC [d]	3.3	3.4	4.1	3.1	4.1
To Grid	22.1	23.1	21.0	22.0	21.1
Total	30.1	31.1	29.8	29.8	2.8
Process Heat, MW					
Ethanol process	27.9	27.9	27.9	27.9	27.9
Dryer	22.6	22.6	22.6	22.6	22.6
Total	50.5	50.5	50.5	50.5	50.5
Synthesis Gas Split, MW					
Combustor	38.7	37.2	46.4	65.8	44.4
Gas turbine	70.0	80.5	66.5	70.4	66.9
Duct burner	0	0.3	0	0	0.3
Combustor Input, MW					
Char	18.0	24.2	24.2	0	24.2
Syngas	38.7	37.2	46.4	65.8	44.4
Total	56.7	61.4	70.6	65.8	68.6
Combustor Output, MW					
Heat to gasifier	16.7	18.2	27.1	26.2	25.8
Combustion exhaust	40.0	43.2	43.5	39.6	42.8

Note: BIGCC = biomass integrated gasification combined cycle.

[a] All energy and power values are based on the fuel higher heating value (HHV). Corn stover: 110 MW (637 Mg d^{-1} at 13% moisture).

[b] Generation efficiency (%) = total power generated × 100 / fuel input rate. Thermal efficiency (%) = [(total power generated + total process heat) × 100 / fuel input rate].

[c] Gas turbine = total power by gas turbine – shaft power for gas turbine air compressor (not given). Total = gas turbine + steam turbine.

[d] Power use by superheated steam dryers or parasitic BIGCC was calculated based on power consumed by compressors, fans, and pumps with an electric motor efficiency of 95%.

6 Summary and Conclusions

Biomass corn stover is a promising source of renewable energy. Fluidized bed steam gasification is one of the most widely used technologies for using biomass due to multiple advantages such as its flexibility to deal with different fuels, rapid mass and heat transfer, and the high energy-content gas produced. In this study seven gasification models are developed and compared varying from simpler equilibrium models to more complex two-phase kinetic models for steam gasification of corn stover. The seven models include a zero-dimensional non-stoichiometric equilibrium model, a zero-dimensional stoichiometric equilibrium model, a zero-dimensional kinetic model, a one-dimensional one-phase kinetic model, a one-dimensional two-phase kinetic model-all char in bed with particle size, and a one-dimensional two-phase kinetic model-all char in bed without particle size. Two of the seven models are equilibrium models and the rest are kinetic models. The five kinetic models can be further classified into kinetic models with fluid dynamics and kinetic models without fluid dynamics. Kinetic models with fluid dynamics include kinetic models without char entrainment and kinetic models with char entrainment.

An un-reacted core shrinking model is used to describe reaction kinetics. A pyrolysis model considering the effect of particle size and temperature is developed and implemented in kinetic models considering the effect of particle size. Compared to most kinetic models developed by other researchers, the one-dimensional two-phase

kinetic model can reflect the effect of the effect of particle size, ash content, mass flow rate, and superficial gas velocity as well as temperature and steam/biomass ratio. In addition, this model can provide information on gas and char in the bed and out of the bed at any time, the evolution of particles in the bed, particle size distribution in the bed, percentages of particles consumed during reactions, turned to fines by friction, or entrained out of the bed. The information provided for this reactor can help people to select optimum operating conditions and design the size of reactors.

Extensive comparisons between these models are conducted. The one-dimension two-phase kinetic model predicts almost the same results as the one-dimensional one-phase kinetic model in terms of the gas volumetric fraction, the yields of char and dry tar-free gas, the evolution of particles in the bed, the simulation time, and HHV values, which indicates that the number of phases in the fluidized bed has a small effect on the simulation results. Based on the modeling concepts of these two models, they can be used to model any fluidized bed gasification. The one-dimensional two-phase kinetic model-all char in bed with particle size also predicts almost the same gasification results as the one-dimensional two-phase kinetic model-all char in bed without particle size. However, the time required for the bed to reach steady-state, the amount of fuel in the bed at steady state, and the simulation time are different for these two models. The main reason is because these two models used different methods of calculating the surface area for the reaction. These two models are special cases of the one-dimensional two-phase kinetic model, and they can only be used

when the majority of fuel stays in the bed and fuel entrainment is negligible.

Although the two equilibrium models fail to predict the same results, the results predicted by the two equilibrium models tend to be close. The results of equilibrium models for different systems are the same as long as pressure, temperature, and mass flow rates are constant. The gasification results predicted by the zero-dimensional kinetic model is closer to that predicted by kinetic models with char entrainment than by other models.

Several gasification models developed in this study have been applied to biomass integrated gasification combined cycle (BIGCC) systems to provide heat and power at ethanol plant. Systems using different gasification models have similar but not identical system performances.

Although the complex one-dimensional two-phase kinetic model developed is able to predict much more information than most kinetic models, and the extensive comparisons done among the several models developed in this study can provide a guide for future study, this study has limitations. First, because there is a lack of theories for char deactivation and segmentation, they are not included in the kinetic models developed in this study; thus, the kinetic models developed are not able to accurately model fuels in which char deactivation and segmentation are important. Second, since experimental results for corn stove are limited, experimental results for

other biomass materials are used instead, and the results obtained by the models developed in this study may be different from the real experimental results for corn stover.

Some recommendations are provided for future studies. First, char deactivation and segmentation are very important for high ash content fuel and low ash content fuel, respectively, and some work can be done to develop related theories, so future researchers can develop more accurate models. Second, current kinetic models developed seldom consider the effect of ash content, deactivation, and segmentation, so researchers had better consider these factors in the future especially for some kind of fuels. Third, more experimental study can be conducted on the fluidized bed pyrolysis and steam gasification of corn stover, while considering the effect of particle size, to provide data for model development and validation.

7. References

Abdollahi, M., Guy, C. and Chaouki, J., 2010, Biomass gasification in rotating fluidized bed. [online] Available at: <http://dc.engconfintl.org/cgi/viewcontent.cgi?article=1083&context=fluidization_xiii> [Accessed 11 November 2012].

Ammendola, P. and Scala, F., 2012. Attrition of lignite char during fluidized bed gasification. *Experimental Thermal and Fluid Science*, 43, p. 9-12.

Aspen Plus, 2012. *Conceptual design of chemical processes*. [online] Available at: <http://www.aspentech.com/products/aspen-plus.aspx> [Accessed 11 November 2012].

Aspen Plus. *Aspen Plus user guide*.[online] Available at: <http://www.chemengr.ucsb.edu/~ceweb/courses/che184b/aspenplus/UserGuideVol1.pdf > [Accessed 11 November 2012].

Aznar, M. P., Corella, J., Delgado, J. and Lahoz, J., 1993. Improved steam gasification of lignocellulosic residues in a fluidized bed with commercial steam reforming catalysts. *Ind. Eng. Chem. Res.*, 32(1), p.1-10.

Babu, B.V. and Sheth, P. N., 2006. Modeling and simulation of reduction zone of down draft biomass gasifier: Effect of char reactivity factor. *Energy Conversion and Management*, 47(15-16), p.2602-2611.

Barea, A. G. and Ollero, P., *FLETGAS: An optimized fluidized bed gasification system for biomass and waste*. [online] Available at: < http://grupo.us.es/bioenergia/templates/jubilee/pdf/FLETGAS_resumme.pdf> [Accessed 11 November 2012].

Barrio, M., Gobel, B., Risnes, H., Henriksen, U., Hustad, J. E. and Sorensen, L.H., 2008. Steam gasification of wood char and the effect of hydrogen inhibition on the chemical kinetics. In: Bridgwater, A., ed. Progress *in Thermochemical Biomass Conversion.* Available at: <http://onlinelibrary.wiley.com/doi/10.1002/9780470694954.ch2/summary> [Accessed 11 November 2012].

Basu, P., 2006. *Combustion and Gasification in Fluidized Beds*. [online] Available at: <http://books.google.com/books?id=bFT204XDTQ0C&pg=PA116&lpg=PA116&dq=char+fragmentation+gasification&source=bl&ots=CvyuzyMld9&sig=eqgrkmFIXqWYVDoYtpVZAYB3IIA&hl=en#v=onepage&q=char%20fragmentation%20gasification&f=false> [Accessed 11 November 2012].

Basu, P. and Kaushal, P., 2009. Modeling of Pyrolysis and Gasification of Biomass in Fluidized Beds: A Review. *Chemical Product and Process Modeling*, 4(1). Available at: <http://www.bepress.com/cgi/viewcontent.cgi?article=1338&context=cppm&sei-redir=1#search=%22Modeling%20Pyrolysis%20Gasification%20Biomass%20Fluidized%20Beds%3A%20Review%22> [Accessed 11 November 2012].

Bayarsaikhan, B., Sonoyama, N., Hosokai, S., Shimada, T., Hayashi, J., Li, C. and Chiba, T., 2006. Inhibition of steam gasification of char by volatiles in a fluidized bed under continuous feeding of a brown coal. *Fuel*, 85(3), p.340-349.

Beck, S., Wang, M. J. and Hightower, J. A., 1981. Gasification of Oak Sawdust, Mesquite, Corn Stover, and Cotton Gin Trash in a Countercurrent Fluidized Bed Pilot Reactor. In: Klass, D.L., ed. *Biomass as a Nonfossil Fuel Source*. Chapter 17.

Bethie, W. W., 1996. *Gas turbine*. 2rd ed. New Jersey: Wiley.

Blasi, C. D.. 2F-1 Kinetic modeling of biomass gasification and combustion. [online] Available at: http://www.scribd.com/doc/82820752/2F-1-Kinetic-Modelling-of-Biomass-Gasification-and-Combustion > [Accessed 11 November 2012].

Blasi, C. D., 2009. Combustion and gasification rates of lignocellulosic chars. *Progress in Energy and Combustion Science*, 35(2), p.121-140.

Biba, V., Macak, J., Klose, E., and Malecha, J., 1978. Mathematical model for the gasification of coal under pressure. *Ind. Eng. Chem. Process Des. Dev.*, 17(1), p.92-98.

Brewer, C., Unger, R. and Brown, R., 2009. Characterization of chars form fast pyrolysis and gasification of switchgrass and corn stover. [online] Available at: <http://www.scribd.com/doc/89763781/Brewer-Characterization-Presentation-NACB2009> [Accessed 11 November 2012].

Brown, J. W., Dobbs, R. M., Devenish, S. and Gilmour, I. A., 2006. Biomass gasification in a 100kW fast internal circulating fluidised bed gasfier. *New Zealand Journal of Forestry*, 51(2), p.19-22. Available at: < http://www.nzjf.org/free_issues/NZJF51_2_2006/C18D8438-855C-4EF7-A945-BE15DFB5F6C7.pdf> [Accessed 11 November 2012].

Bustamante, F., Enick, R. M., Cugini, A., Killmeyer, R., Howard, B.H., Rothenberger, K. S., Ciocco, M., Morreale, B., Chattopadhyay, S. and Shi, S.. *Kinetics of the homogeneous reverse water-gas shift reaction at high temperataure*. [online] Available at:

<http://www.netl.doe.gov/technologies/hydrogen_clean_fuels/refshelf/papers/hydrogen/kinetics%20of%20the%20homogeneous%20reverse%20water-gas%20shift%20reaction.pdf> [Accessed 11 November 2012].

Carpenter, D. L., Bain, R. L., Davis, R. E., Dutta, A., Feik, C. J., Gaston, K. R., Jablonski, W., Phillips S. D. and Nimlos, M. R., 2010. Pilot-Scale Gasification of Corn Stover, Switchgrass, Wheat Straw, and Wood: 1. Parametric Study and Comparison with Literature. *Ind. Eng. Chem. Res*., 49(4), p.1859-1871.

Chattopadhyay, P., 2000. *Boiler Operation Engineering: Questions and Answers*. Available at: Google Books [Accessed 11 November 2012].

Chavarie, C., and Grace, J. R., 1975. Performance analysis of afluidized bed reactor. II. Observed reactor behavior compared with simple two-phase models. *Ind. Eng. Chem. Fundamen.*, 14 (2), p.79-86

Chejne, F. and Hernandez, J.P., 2002. Modeling and simulation of coal gasification process in fluidized bed. *Fuel*, 81(13), p.1687-1702.

Choi, J. H., Son, J. E. and Kim, S. D., Bubble size and frequency in gas fluidized beds. *J. Chem. Eng. Jpn*, 21, p.171-178.

Clift, R., Grace, J. R. and Weber, M. E., 1978. *Bubbles, Drops, and Particles*. New York: Academic Press.

Corella, J., Aznar, M. P., Delgado, J. and Aldea, E., 1991. Steam gasification of cellulosic wastes in a fluidized bed with downstream vessels. *Ind. Eng. Chem. Res.*, 30(10), p.2252-2262.

Corella, J., Toledo, J. M. and Molina, G., 2008. Steam gasification of coal at low−medium (600−800 °C) temperature with simultaneous CO2 capture in a bubbling fluidized bed at atmospheric pressure. 2. results and recommendations for scaling up. *Ind. Eng. Chem. Res.*, 47(6), p.1798-1811.

De Diego, L. F., García-Labiano, F., Abad, A., Gayán, P. and Adánez, J., 2002. Modeling of the devolatilization of nonspherical wet pine wood particles in fluidized beds. *Ind. Eng. Chem. Res*., 41(15), p.3642-3650.

De Kam, M.J., Morey, R.V. and Tiffany, D.G., 2009a. Integrating biomass to produce heat and power at ethanol plants. *Applied Eng. in Agric*, 25(2), p.227-244.

De Kam, M.J., Morey, R.V. and Tiffany, D.G., 2009b. Biomass integrated gasification combined cycle for heat and power at ethanol plants. *Energy Conversion and Management*, 50(7), p.1682-1690.

Delvosalle, C. and Vanderschuren, J., 1985. Gas-to-particles and particle-to-particle

heat transfer in fluidized beds of large particles. Chem. Eng. Sci., 40, p.769-779.

De Souza-Santos, M. L., 2004. *Solid Fuels Combustion and Gasification: Modeling, Simulation, and Equipment operation*. NewYork.

De Souza-Santos, M. L., 1989. Comprehensive modelling and simulation of fluidized bed boilers and gasifiers. *Fuel*, 68(12), p.1507-1521.

Enviro News & Business, 2009. *Biomass Pyrolysis and Gasification – Processes and Differences*. [online] Available at: <http://www.enviro-news.com/article/biomass-pyrolysis-and-gasification-processes-and-differences.html > [Accessed 11 November 2012].

Farrell, A.E., Plevin, R.J., Turner, B.T., Jones, A.D., O'Hare, M. and Kammen, D.M., 2006. Ethanol can contribute to energy and environmental goals. *Science*, 311, p.506-508. Available at: http://www.sciencemag.org/content/311/5760/506.full [Accessed 11 November 2012].

Fiaschi, D. and Michelini, M., 2001. A two-phase one-dimensional biomass gasification kinetics model. *Biomass and Bioenergy*, 21(2), p.121-132.

Flanigan, V. J. and PADISCOR (Pasig Agricultural Development and Industrial Supply Corporation), 1987. *A fluid bed gasifier/engine system using rice hulls*. [pdf] Missouri: University of Missouri-Rolla. Available at: < http://pdf.usaid.gov/pdf_docs/PNABX915.pdf> [Accessed 11 November 2012].

Fletcher, T. H., Kerstein, A. R., Pugmire, R. J. and Grant, D. M., 1990. Chemical percolation model for devolatilization. 2. Temperature and heating rate effects on product yields. Energy Fuels, 4(1), p.54-60.

Franco, C., Pinto, F., Gulyurtlu, I. and Cabrita, I., 2003. The study of reactions influencing the biomass steam gasification process. *Fuel*, 82(7), p.835-842.

Froment, G. F. and Bischoff, K. B., 1990. *Chemical Reactor Analysis and Design*. 2rd ed. New York: Wiley.

Fueyo, N. and Dopazo, C., 1995. Fluidization fundamentals. In: Cuenca, M. A. and Anthony E. J., eds. Pressurized fluidized Bed Combustion. London: Blackie Academic and Professional, pp.37-79. Available at: <http://www.unizar.es/dopazo/PUBS/Refereed%20Journals%20CD/28PresFluidiBedComb.pdf > [Accessed 11 November 2012].

Furnas, C. C., 1929. *Flow of gases through beds of broken solids*. Washington: U.S. Government Printing Office

Gabra, M., Pettersson, E., Backman, R. and Kjellström, B., 2001. Evaluation of

cyclone gasifier performance for gasification of sugar cane residue-Part 1: gasification of bagasase. *Biomass and Bioenergy*, 21(5), p.351-369

Gao, N. and Li, A., 2008. Modeling and simulation of combined pyrolysis and reduction zone for a downdraft biomass gasifier. *Energy Conversion and Management*, *Management*, 49(12), p. 3483-3490.

Gaston, K. R., Jarvis, M. W., Pepiot, P., Smith, K. M., Frederick, William J., Jr. and Nimlos, M. R., 2011. Biomass Pyrolysis and Gasification of Varying Particle Sizes in a Fluidized-Bed Reactor. *Energy Fuels*, 25(8), p.3747-3757.

Geldart, D., 1972. The effect of particle size and size distribution on the behavior of gas-fluidized beds. *Powder Technol*, 6, p.201-205.

Geldart, D., 1975. Predicting the expansion of gas fluidized beds. In: Fluidization Technology. Kearins D.L., ed. Washington,DC: Hemisphere. P.237-244.

Gil, J., Corella, J., Aznar, M. P. and Caballero, M. A., 1999. Biomass gasification in atmospheric and bubbling fluidized bed: Effect of the type of gasifying agent on the product distribution. *Biomass and Bioenergy*, 17(5), p.389-403.

Giltrap, D.L., McKibbin, R. and Barnes, G.R.G., 2003. A steady state model of gas-char reactions in a downdraft biomass gasifier. *Solar Energy*, 74(1), p.85-91.

Gordillo, E. D. and Belghit, A., 2011a. A two phase model of high temperature steam-only gasification of biomass char in bubbling fluidized bed reactors using nuclear heat. *International Journal of Hydrogen Energy*, 36(1), p.374-381.

Gordillo, E. D. and Belghit, A., 2011b. A bubbling fluidized bed solar reactor model of biomass char high temperature steam-only gasification. *Fuel Processing Technology*, 92(3), p.314-321

Graham, R. G., Bergougnou, M. A. and Freel, B. A., 1994. The kinetics of vapor-phase cellulose fast pyrolysis reactions. *Biomass and Bioenergy*, 7(1-6), p.33-47.

Granatstein, D.L.. *Gasification vs combustion of waste/biomass in fluidized bed reactors*. [online] Available at: <http://www.ieabioenergytask36.org/Publications/2001-2003/Publications/Gasification_vs_Combustion_of_Waste-Biomass_in_Fluidized_Bed_Reactors.pdf> [Accessed 11 November 2012].

Haider, A. and Levenspiel, O., 1989, Drag coefficient and terminal velocity of spherical and non-spherical particles. Powder Technol, 58, p.63-70.

Hajaligol, M. R., Howard, J. B., Longwell, J. P. and Peters, W. A., 1982. Product

compositions and kinetics for rapid pyrolysis of cellulose. *Ind. Eng. Chem. Process Des. Dev.*, 21(3), p.457-465.

Heiberg, D. D. and Eichberg, M. eds., 1982. *Chemical Engineering Series*. New York: McGraw-Hill Company, Inc.

Herguido, J., Corella, J. and Gonzalez-Saiz, J., 1992. Steam gasification of lignocellulosic residues in a fluidized bed at a small pilot scale. Effect of the type of feedstock. *Ind. Eng. Chem. Res*., 31(5), p.1274-1282.

Higman, C. and Maarten, van der B., 2003. Gasification. 2rd ed. [Elsevier]. Available at: <http://www.knovel.com/web/portal/browse/display?_EXT_KNOVEL_DISPLAY_bookid=1262&VerticalID=0> [Accessed 11 November 2012].

Hobbs, M. L., Radulovic, P. T. and Smoot, L. D., Combustion and gasification of coals in fixed-beds. *Progress in Energy and Combustion Science*, 19(6), p. 505-586.

Holder, R., 2008. A Global Reaction Mechanism for Transient Simulations of Three-Way Catalytic. [e-book] s.l.: Cuvillier Verlag. Available at: <http://books.google.com/books?id=1YsyFB0mzx8C&pg=PA49&lpg=PA49&dq=A+Global+Reaction+Mechanism+for+Transient+Simulations+of+Three-Way+Catalytic&source=bl&ots=3k0ykHV6GR&sig=TFloQAjnzuJ6VpYhcOnved3EBRw&hl=en&sa=X&ei=zBWaUPjJNeLM2AXuw4Bg&ved=0CDQQ6AEwAQ > [Accessed 11 November 2012].

Hongming, J., 1991. *A numerical simulation of a fluidized bed gasifier*, PhD. University of Minnesota-Twin Cities.

Hoveland, D. A., Walawender, W. P., Fan, L. T. and Lai, F. S., 1982. Steam gasification of grain dust in a fluidized bed reactor. Transactions of the ASAE (American Society of Agricultural Engineers), 25(4), p.1076-1080.

Hrdlicka, J., Feik, C., Carpenter, D., and Pomeroy, M., 2008. Parametric gasification of oak and pine feedstocks using the TCPDU and lipstream water-gas shift catalysis. [pdf] Golden: National Renewable Energy Laboratory. Available at: <http://libweb.anglia.ac.uk/referencing/harvard.htm> [Accessed 11 November 2012].

Huang, H. and Ramaswamy, S., 200. Modeling Biomass Gasification Using Thermodynamic Equilibrium Approach. *Applied biochemistry and Biotechnology*, 154(1-3), p.14-25.

Jand, N. and Foscolo, P. U., 2005. Decomposition of wood particles in fluidized beds. *Ind. Eng. Chem. Res*., 44(14), p.5079-5089.

Jarungthammachote, S. and Dutta, A., 2007. Thermodynamic equilibrium model and second law analysis of a downdraft waste gasifier. *Energy*, 32(9), p.1660-1669.

Jarungthammachote, S. and Dutta, A., 2008. Equilibrium modeling of gasification: Gibbs free energy minimization approach and its application to spouted bed and spout-fluid bed gasifiers. *Energy Conversion and Management*, 49(6), p.1345-1356.

Ji, P., Feng, W. and Chen, B., 2009. Comprehensive Simulation of an Intensified Process for H2 Production from Steam Gasification of Biomass. *Ind. Eng. Chem. Res.*, 48(8), p.3909-3920.

Jiang, H. and Morey, R.V., 1992. A numerical model of a fluidized bed biomass gasifier. *Biomass and Bioenergy*, 3(6), p.431-447.

Kato, K. and Wen, CY., 1969. Bubble assemblage model for fluidized bed catalytic reactors. *Chem Eng Sci*. 24, p.1351-1369.

Kersten, S. R. A., Wang, X., Prins, W. and van Swaaij, W. P. M,. 2005. Biomass Pyrolysis in a Fluidized Bed Reactor. Part 1: Literature Review and Model Simulations. Ind. Eng. Chem. Res., 44(23), p.8773-8785.

Klinghoffer, N., Castaldi, M. J. and Nzihou, A., 2011. Beneficial use of ash and char from biomass gasification. *Proceedings of the 19th Annual North American Waste-to-Energy Conference*, [online] Available at: <http://www.seas.columbia.edu/earth/wtert/sofos/nawtec/nawtec19(new)/NAWTEC19-5421.pdf> [Accessed 11 November 2012].

Krambeck, F. J., Avidan, A. A., Lee, C. K. and Lo M. N., 1987. Predicting fluid-bed reactor efficiency using adsorbing gas tracers. *AIChE Journal*, 33(10), p.1727-1734.

Krishna, R., 1988. Simulation of an industrial fluid bed reactor using a bubble growth model. Chem. Eng. Res. Des., Trans. I. Chem. E, 66, p.463-469.

Kumar, A., Wang, L., Dzenis, Y. A., Jones, D. D. and Hanna, M. A., 2008. Thermogravimetric characterization of corn stover as gasification and pyrolysis feedstock. *Biomass and Bioenergy*, 32(5), p.460-467.

Kumar, A., Noureddini, H., Demirel, Y., Jones, D. D. and Hanna, M. A., 2009. Simulation of corn stover and distillers grains gasification with Aspen Plus. Transactions of the ASABE, 52(6), p.1989-1995.

Kuznetsov, B. N. and Shchipko, M. L., 2009. Wood waste steam gasification to methane-enriched fuel gas. *Chemistry*, 2(3).

Kunii, D. and Levenspiel, O., 1969. Fluidization Engineering. New York: John Wiley.

Kwiatkowski, J.R., McAloon, A.J., Taylor, F. and Johnston, D.B., 2006. Modeling the process and costs of fuel ethanol production by the corn dry-grind process. *Ind Crops and Products*, 23(3), p.288-96.

Lavoie, J., Chaouki, J. and Drouin, G.. *Biomass gasification in a bubbling fluidized bed: bed: numerical modeling and experiments*. [online] Available at: <http://archivos.labcontrol.cl/wcce8/offline/techsched/manuscripts/jl7g22.pdf > [Accessed 11 November 2012].

Li, X., Grace, J. R., Watkinson, A. P., Lim, C. J. and Ergudenler, A., 2001. Equilibrium modeling of gasification: a free energy minimization approach and its application to a circulating fluidized bed coal gasifier. *Fuel*, 80(2), p.195-207.

Liu, H. and Gibbs, B. M., 2003. Modeling NH3 and HCN emissions from biomass circulating fluidized bed gasifiers. *Fuel*, 82(13), p.1591-1604.

Löffler, G., Kaiser, S., Bosch, K. and Hofbauer, H., 2003. Hydrodynamics of a dual fluidized-bed gasifier—Part I: simulation of a riser with gas injection and diffuser. *Chemical Engineering Science*, 58(18), p.4197-4213.

Lü, P., Kong, X., Wu, C., Yuan, Z., Ma, L. and Chang, J., 2008. Modeling and simulation of biomass air-steam gasification in a fluidized bed. *Frontiers of Chemical Engineering in China*, 2(2), p.209-213.

Loha, C., Chatterjee, P.K., Chattopadhyay, H., 2011. Performance of fluidized bed steam gasification of biomass – Modeling and experiment. *Energy Conversion and Management*, 52, p.1583-1588.

McAloon, A.J., Taylor, F., Yee, W.C., Ibsen, K. and Wooly, R., 2000. *Determining the cost of producing ethanol from corn starch and lignocellulosic feedstocks*. Colorado: National Renewable Energy Laboratory.

McAloon, A.J., Taylor, F. and Yee, W.C., 2004. A model of the production of ethanol by the dry grind process. Proceedings of the Corn Utilization & Technology Conference; Indianapolis, IN.

Malekshahian M. and Hill, J. M., 2011. Kinetic analysis of CO2 gasification of petroleum coke at high pressures. *Energy Fuels*, 25(9), p.4043-4048.

Mansaray, K. G., Al-Taweel, A. M., Ghaly, A. E., Hamdullahpur, F. and Ugursal, V. I., 2000. Mathematical Modeling of a Fluidized Bed Rice Husk Gasifier: Part I-Model Development. *Energy Sources*, 22(1), p.83-98.

Manyà, J. J., Velo, E. and Puigjaner, L., 2003. Kinetics of biomass pyrolysis: a reformulated three-parallel-reactions model. *Ind. Eng. Chem. Res*., 42(3), p.434-441.

Meijden, C.M. van der, Drift, A. van der and Vreugdenhil, B.J., 2012. *Benefits of allothermal biomass gasification for co-firing*. Copenhagen. Available at: < http://www.ecn.nl/docs/library/report/2012/m12008.pdf> [Accessed 11 November 2012].

Melgar, A., Perez, J. F., Laget, H. and Horillo, A., 2007. Thermochemical equilibrium modelling of a gasifying process. *Energy Conversion and Management*, 48(1), p.59-67.

Merrick, D. and Highley, J., 1974. Particle size reduction and elutriation in a fluidized bed process. *AIChE Symp. Ser*., 70, p.366-378.

Miccio, F., 1999. *Gasification of two biomass fuels in bubbling fluidized bed.* [online] Available at: <http://www.scribd.com/doc/7141833/Gasification-of-Two-Biomass-Fuels-in-Bubbling-Fluidized-Bed> [Accessed 11 November 2012].

Milioli, F.E. and Foster, P.J., 1995. Entrainment and elutriation modelling in bubbling fluidized beds. *Powder Technology*, 83(3), p.233-244.

Morey, R.V., Tiffany, D.G. and Hatfield, D.L., 2006. Biomass for electricity and process heat at ethanol plants. *Applied Eng. in Agric*, 22 (5), p.723-728.

Mori, S. and Wen, CY., 1975. Estimation of bubble diameter in gaseous fluidized beds. *AIChE J*, 21, p.109-115.

Mountouris, A., Voutsas, E. and Tassios, D., 2006. Solid waste plasma gasification: Equilibrium model development and energy analysis. *Energy Conversion and Management*, 47(13–14), p.1723-1737.

Mueller, S. and Cuttica, J., 2007. Research investigation for the potential use of combined heat and power at natural gas and coal fired dry mill ethanol plants. [pdf] Chicago: University of Illinois Energy Resource Center. Available at: < http://www.midwestcleanenergy.org/Archive/pdfs/EthanolStudyReport_Nov2007.pdf> [Accessed 11 November 2012].

Mullen, C. A., Boateng, A. A., Goldberg, N. M., Lima, I. M., Laird, D. A., and Hicks, K. B., 2010. Bio-oil and bio-char production from corn cobs and stover by fast pyrolysis. *Biomass and Bioenergy*, 34, p. 67-74.

Nemtsov, D. and Zabaniotou, A., 2008. Mathematical modelling and simulation approaches of agricultural residues air gasification in a bubbling fluidized bed reactor. *Chemical Engineering Journal*, 143(1-3), p.10-31.

Neogi, D., Chang, C. C., Walawender, W. P. and Fan, L. T., 1986. Study of coal gasification in an experimental fluidized bed reactor. *AIChE Journal*, 32(1), p.17-28.

NETL. *Advantages of Gasification - Feedstock Flexibility*. [online] Available at: <http://www.netl.doe.gov/technologies/coalpower/gasification/gasifipedia/7-advantages/7-3-1_coalranks.html> [Accessed 11 November 2012].

Nicklin, D. J., Wilkes, J. O. and Davidson, J.F., 1962. Two-phase flow in vertical tube. *Transaction of the Institution of Chemical Engineers*, 40, p.61-68.

Nikooa, M. B. and Mahinpey, N., 2008. Simulation of biomass gasification in fluidized bed reactor using ASPEN PLUS. *Biomass and Bioenergy*, 32(12), p.1245-1254.

Nunn, T. R., Howard, J. B., Longwell, J. P. and Peters, W. A., 1985. Product compositions and kinetics in the rapid pyrolysis of sweet gum hardwood, *Ind. Eng. Chem. Process Des. Dev*., 24(3), p.836-844.

Olazar, M., Aguado, R., J San José, M. and Bilbao, J., 2001. Kinetic study of fast pyrolysis of sawdust in a conical spouted bed reactor in the range 400–500 °C. *Journal of Chemical Technology and Biotechnology*, 76(5), p.469-476.

Okuga. A.. *Analysis and operability optimization ofan updraft gasifier unit*. [online] Available at: <http://w3.wtb.tue.nl/fileadmin/wtb/ct-pdfs/Master_Theses/finalreport_A_Okuga.pdf> [Accessed 11 November 2012].

Paisley, M.A. and Welch, M.J., 2003. Biomass gasification combined cycle opportunities using the future energy SilvaGas gasifier coupled to Alstom's industrial gas turbines. *Proceedings of ASME Turbo Expo*,1, p.211-217.

Pan, H., and Eberhardt, T. L., 2011. Characterization of fly ash from the gasification of wood and assessment for its application as a soil amendment. BioResources, [online] Available at: <http://www.srs.fs.fed.us/pubs/ja/2011/ja_2011_han_001.pdf> [Accessed 11 November 2012].

Pepiot, P., Dibble, C. J. and Foust, T. D., 2010. Computational Fluid Dynamics Modeling of Biomass Gasification and Pyrolysis. In: Nimlos, M. R. and Crowley M. F., eds. Computational Modeling in Lignocellulosic Biofuel Production. p. 273-298.

Perkins, C. M., Woodruff, B., Andrews, L., Lichty, P., Lancaster, B., Bingham, C. and Weimer, A. W., 2008. Synthesis gas production by rapid solar thermal gasification of corn stover. In: National Renewable Energy Laboratory (NREL), *2008 14th Biennial CSP SolarPACES (Solar Power and Chemical Energy Systems)*. Las Vegas, 4-7 March 2008. Golden, CO: National Renewable Energy Laboratory

Porteiro, J., Míguez, J.L., Granada, E. and Moran, J.C., 2006. Mathematical modelling of the combustion of a single wood particle. *Fuel Processing Technology*,

87(2), p.169-175.

Prabir, B., 2011. *Biomass Gasification and Pyrolysis: Practical Design and Theory*. 1st ed. Beijing: Science Press.

Pyle, D.L. and Zaror C.A., 184. Heat transfer and kinetics in the low temperature pyrolysis of solids. *Chemical Engineering Science*, 39(1), p.147-158.

Radmanesh, R., Chaouki, J. and Guy, C., 2006. Biomass gasification in a bubbling fluidized bed reactor: Experiments and modeling. *AIChE Journal*, 52(12), p.4258-4272.

Raman, K. P., Walawender, W. P. and Fan, L. T., 1980. Gasification of feedlot manure in a fluidized bed reactor. the effect of temperature. *Ind. Eng. Chem. Process Des. Dev.*, 19(4), p.623-629.

Raman, P., Walawender, W. P., Fan, L. T. and Chang, C. C., 1981. Mathematical model for the fluid-bed gasification of biomass materials. Application to feedlot manure. *Ind. Eng. Chem. Process Des. Dev.*, 20(4), p.686-692.

Ranzi, E., Cuoci, A., Faravelli, T., Frassoldati, A., Migliavacca, G., Pierucci, S. and Sommariva, S., 2008. Chemical Kinetics of Biomass Pyrolysis. *Energy Fuels*, 22(6), p.4292-4300.

Rapagnà, S., Jand, N., Kiennemann, A. and Foscolo, P.U., 2000. Steam-gasification of biomass in a fluidised-bed of olivine particles. Biomass and Bioenergy, 19(3), p.187-197.

Rapagnà, S. and Mazziotti di Celso, G., 2008. Devolatilization of wood particles in a hot fluidized bed: Product yields and conversion rates. Biomass and Bioenergy, 32(12), p.1123-1129.

Reed, T. B. and Das, A., 1988. Handbook of Biomass Downdraft Gasifier Engine Systems. [e-book] n.l.: Biomass Energy Foundation. Available at: Google Books [Accessed 11 November 2012].

Rezaiyan, J. and Cheremisinoff, N. P., 2005. *Gasification Technologies: A Primer for Engineers and Scientists*. FL: CRC Press

Rowe, P. N., 1976. Prediction of bubble size in a gasfluidized bed. *Chem Eng Sci*, 31, p.285-288.

Sadaka, S. S., Ghaly, A. E. and Sabbah, M. A., 2002. Two phase biomass air-steam gasification model for fluidized bed reactors: Part I—model development. *Biomass and Bioenergy*, 22(6), p.439-462.

Sakaguchi, M., Watkinson, A. P. and Ellis, N., 2010. Steam gasification of bio-oil and

bio-oil/char slurry in a fluidized bed reactor. *Energy Fuels*, 24(9), p.5181-5189.

Salam, P. A., Kumar, S. and Siriwardhana, M., 2010. *The status of biomass gasification gasification in Thailand and Cambodia*. [online] Available at: <http://www.eepmekong.org/_downloads/Biomass_Gasification_report_final-submitted.pdf> [Accessed 11 November 2012].

Scott, D. S., Piskorz, J., Grinshpun, A. and Graham, R. G.. *The effect of temperature on on liquid product composition from the fast pyrolysis of cellulose*. [online] Available at: at: <http://web.anl.gov/PCS/acsfuel/preprint%20archive/Files/Merge/Vol-32_2-0001.pdf> [Accessed 11 November 2012].

Seo, D., Lee, S. K., Kang, M. W., Hwang, J. and Yu, Tae-U., 2010. Gasification Reactivity of Biomass Chars with CO2. *Biomass and Bioenergy*, 34(12), p.1946-1953.

Sett, A. and Bhattacharya, S.C., 1988. Mathematical modeling of a fluidised-bed charcoal gasifier. *Applyied Energy*, 30, p.161-186.

Shapouri, H., Duffield, J.A. and Wang, M., 2002. The energy balance of corn ethanol: An update. [pdf] Washington, D.C: U.S. Department of Agriculture. Available at: <www.transportation.anl.gov/pdfs/AF/265.pdf> [Accessed 11 November 2012].

Sharma, A. K., 2008. Equilibrium modeling of global reduction reactions for a downdraft (biomass) gasifier. *Energy Conversion and Management*, 49(4), p.832-842.

Singer, S. L. and Ghoniem, A. F.. Comprehensive Gasification Modeling of Char Particles with Multi-Modal Pore structure. [online] Available at: <http://hyksos.mit.edu/rgdWebFiles/SimchaCNF.pdf> [Accessed 11 November 2012].

Sinnott, R. K. and Towler, G., 2012. Chemical Engineering Design: Principles, Practice and Economics of Plant and Process Design. 2nd ed. s.l.: Butterworth-Heinemann.

Slezak, Andrew A., Jr., 2008. Modeling of Particle Trajectories of Coal Size and Density Fractions in a Gasifier. Master. West Virginia University

Smith, K.J., Arkun, Y. and Littman, H., 1982. Studies on Modeling and Control of Spouted Bed Reactors. Part I: Reactor Modeling. *Chem. Eng. Sci*., 37(4), p.567-579.

Solomon, P. R., Hamblen, D. G., Carangelo, R. M., Serio, M. A. and Deshpande, G. V., 1988. General model of coal devolatilization. *Energy Fuels*, 2(4), p.405-422.

Srinivas, B. and Amundson, N. R., 1980. A single-particle char gasification model. *AIChE Journal*, 26(3), p.487-496.

Stringel, S. S., 2011. High temperature gasification of millimetric wood particles

between 800°C and 1400°C. PhD. Université de Toulouse.

Svoboda, K., Martinec, J., Pohorely, M. and Baxter, D., 2009. Integration of biomass drying with combustion/gasification technologies and minimization of emissions of organic compounds. *Chemical Papers*, 63(1), p.15-25.

Tojo, K., Chang, C. C. and Fan, L. T., 1981. Modelling of dynamic and steady-state shallow fluidized bed coal combustors. Effects of feeder distribution. *Ind. Eng. Chem. Process Des. Dev*, 20, p.411-416.

Toomey, R.D. and Johnstone, H.F., 1952. Gaseous Fluidization of Solid Particles. *Chem.Eng Prog*. 48, 220-226.

Tran, D. Q. and Rai, C., 1978. A kinetic model for pyrolysis of Douglas fir bark. *Fuel*, 57(5), p.293-298.

Turton, R. and Levenspiel. O., 1986. A short note on the drag correlation for spheres. Powder Technol, 47, p.83-86.

UC Davis Chem WiKi, 2010. *Pre-exponent factor*. [online] Available at: <http://chemwiki.ucdavis.edu/Physical_Chemistry/Kinetics/Reaction_Rates/Temperature_Dependence_of_Reaction_Rates/Arrhenius_Equation/Pre-exponential_factor> [Accessed 11 November 2012].

Vaezi, M., Passandideh-Fard, M., Moghiman, M., Charmchi, M., 2008. Modeling Biomass Gasification: A New approach to utilize renewable sources of Energy. *ASME International Mechanical Engineering Congress and Exposition*. Boston, 31 October – 6 November 2008. Massachusetts: ASME.

Van den Aarsen, F.G., Beenackers, A.A.C.M. and van Swaaij, W.P.M., 1986. Modeling of a fluidized bed wood gasifier. In: Ostergaard, K. and Sørensen A., eds. Proceedings of the 5th Engineering Foundation Conference on Fluidization. New York Publ.

Wang, Z., Zhang, H., Zhuang, J., 2007. Experimental study on biomass gasification in heat pipe biomass gasifier. Available at: < http://rd.springer.com/chapter/10.1007/978-3-540-75997-3_477 > [Accessed 11 November 2012].

Wang, L., Shahbazi, A. and Hanna, M. A., 2011. Characterization of corn stover, distiller grains and cattle manure for thermochemical conversion, Biomass and Bioenergy, 35(1), p.171-178.

Wang, M., Wu, M. and Huo, H., 2007. Life-cycle energy and greenhouse gas emission impacts of different corn ethanol plant types. *Environmental Research Letters*, 2(2).

Wang, Y. and Kinoshita, C.M., 1993. Kinetic model of biomass gasification. *Solar*

Energy, 51(1), p.19-25.

Wei, L., Xu, S., Zhang, L., Liu, C., Zhu, H. and Liu, S., 2007. Steam gasification of biomass for hydrogen-rich gas in a free-fall reactor. *International Journal of Hydrogen Energy*, 32(1), p.24-31.

Wen, C.Y., 1968. Non-catalytic heterogeneous solid fluid reaction models. *Ind. Eng. Chem.*, 60(9), p.34.

Wen, C. Y. and Chen, L. H., 2004. Fluidized bed freeboard phenomena: entrainment and elutriation. AIChE Journal, 28(1), p. 117-128. Available at: <http://onlinelibrary.wiley.com/doi/10.1002/aic.690280117/pdf> [Accessed 11 November 2012].

Wen, C. Y. and Yu, Y. H., 1966. A generalized method for predicting the minimum fluidization velocity. AIChE Journal,12(3), p.610-612.

Werther, J., 1978. Mathematische modellierung von Wirbelschichtreaktoren. *Chemie Ingenieur Technik*, 50(11), p. 850-860.

White III, C. W. and Seider, W. D., 1981. Computation of phase and chemical equilibrium, part IV: Approach to chemical equilibrium. *AIChE Journal*, 27(3), p.466-471.

Wu, Y., Wu S. and Gao, J., 2009. A Study on the applicability of kinetic Models for shenfu coal char gasification with CO2 at elevated temperatures. *Energies*, 2(3), p.545-555.

Wu, Y., Zhang, J., Smith, P. J., Zhang, H., Reid, C., Lv, J. and Yue, G., 2010. Three-dimensional simulation for an entrained flow coal slurry gasifier. *Energy Fuels*, 24(2), p.1156-1163.

Wurzenberger, J. C., Wallne, S., Raupenstrauch, H. and Khinast, J. G., 2002. Thermal conversion of biomass: Comprehensive reactor and particle modeling. *AIChE Journal*, 48(10), p.2398-2411.

Xiao, X., Le, D. D., Li, L., Meng, X., Cao, J., Morishita, K. and Takarada, T., 2010. Catalyticsteamgasification of biomass in fluidizedbed at lowtemperature: Conversion f rom livestockmanurecompost tohydrogen-richsyngas. *Biomass and Bioenergy*, 34(10), p.1505-1512.

Xu, Q., Pang, S. and Levi, T., 2011. Reaction kinetics and producer gas compositions of steam gasification of coal and biomass blend chars, part 1: Experimental investigation. *Chemical Engineering Science*, 66(10), p.2141-2148.

Yan, H., Heidenreich, C. and Zhang, D., 1998. Mathematical modeling of a bubbling

fluidised-bed coal gasifier and the significance of ‘net flow’. *Fuel*, 77(9-10), p.1067-1079.

Yang, W., ed., 2003. *Handbook of fluidization and fluid-particle systems*. Pittsburgh: CRC Press

Yasui, G. and Johanson, L.N., 1958. Characteristics of gas pockets in fluidized beds. *A.I.Ch.E. J*., 4, p445-452.

You, Z., You, S., Li, X., Luo, Y. and Jiao, Y.. The carbonization characteristics studies of corn stalk in a fixed bed reactor. Available at: < http://ieeexplore.ieee.org/stamp/stamp.jsp?arnumber=05517226 > [Accessed 11 November 2012].

Zainal, Z.A., Ali, R., Lean, C.H. and Seetharamu, K. N., 2001. Prediction of performance of a downdraft gasifier using equilibrium modeling for different biomass materials. *Energy Conversion and Management*, 42(12), p.1499-1515.

Zanzi, R., Sjöström, K. and Björnbom, E., 2002. Rapid pyrolysis of agricultural residues at high temperature. *Biomass and Bioenergy*, 23(5), p.357-366.

Zhang, J., 1998. Motion of Particles through Fluids. CPE 124. [online via internal VLE] Newcastle University Available at: < http://lorien.ncl.ac.uk/ming/particle/cpe124p2.html > [Accessed 11 November 2012].

Zheng, H., Morey, R. V. and Kaliyan, N., 2010. *Biomass integrated gasification combined cycle systems at corn ethanol plants*. Pittsburgh, Pennsylvania 20-23 June 2010. Michigan: the American Society of Agricultural and Biological Engineers.